Title
Nuclear Effective Theory of $\mu\rightarrow e$ Conversion

Permalink
https://escholarship.org/uc/item/2xb6m9rr

Author
Rule, Evan Johnson

Publication Date
2022

Peer reviewed|Thesis/dissertation

Nuclear Effective Theory of $\mu \to e$ Conversion

by

Evan Johnson Rule

A dissertation submitted in partial satisfaction of the

requirements for the degree of

Doctor of Philosophy

in

Physics

in the

Graduate Division

of the

University of California, Berkeley

Committee in charge:

Professor Wick Haxton, Chair
Professor Yury Kolomensky
Professor Karl A. van Bibber

Summer 2022

Nuclear Effective Theory of $\mu \to e$ Conversion

Abstract

Nuclear Effective Theory of $\mu \to e$ Conversion

by

Evan Johnson Rule

Doctor of Philosophy in Physics

University of California, Berkeley

Professor Wick Haxton, Chair

The coming decade promises exceptional experimental progress in searches for charged lepton flavor-violating (CLFV) $\mu \to e$ conversion due to efforts at Fermilab (Mu2e) and J-PARC (COMET). Branching ratio sensitivities for this process are expected to advance by four orders of magnitude, potentially extending the reach of these probes up to energies of 10^4 TeV. A pressing challenge for theorists is to extract the maximum amount of information about possible sources of CLFV from these measurements, whether or not a signal of new physics is detected.

Efforts to observe $\mu \to e$ conversion share many similarities with other experimental programs where the nucleus is treated as a laboratory in which to search for beyond-standard-model (BSM) physics. These approaches are utilized because they present certain practical advantages: In searches for CLFV, the act of trapping a muon into the Coulomb field of a nucleus allows one to control the energy of the final state electron, ensuring that it is maximal compared to the energy of background electrons originating in standard-model free muon decays. The downside of employing the nucleus as part of the apparatus is that a host of complex nuclear physics consequently intervenes between the experimentalist and the desired observable. To extract meaningful constraints, one must have a method for disentangling the nuclear physics from the underlying BSM physics.

Another experimental setting in which the nucleus is treated as a laboratory is in direct detection searches for weakly-interacting massive particle (WIMP) dark matter, where one aims to discern the mass, spin, and fundamental interactions of WIMP dark matter through scattering off of atomic nuclei. Again, to access the sought-after information about BSM physics, one must be able to separate it cleanly from the nuclear physics. In the case of dark matter direct detection, this separation has been achieved through the development of an effective theory formulated at the nuclear scale, which factorizes the nuclear physics from the BSM dark matter physics, sequestering the latter quantity into unknown low-energy constants (LECs) that are probed directly by experiment. As the effective theory describes the most general coupling between the WIMPs and the nucleus, the LECs that specify the effective theory represent the maximum information about the nature of dark matter that can be obtained from scattering off of nuclei.

In this thesis, we introduce an analogous effective theory for the problem of $\mu \to e$

conversion. In order to adapt the existing framework to the problem at hand, several significant modifications are required, primarily stemming from the differing nature of the particles that couple to the nucleus in each scenario: non-relativistic plane-wave dark matter must be replaced by a bound muon in the initial state and an ultra-relativistic electron in the final state. We focus primarily on the case of elastic $\mu \to e$ conversion, wherein the nucleus remains in its ground state (as this ensures that the energy of the outgoing electron is maximal).

The three-momentum transferred from the leptons to the nucleus $q \approx m_\mu$ is comparable to the inverse nuclear size, allowing significant angular momentum to be transferred between the leptons and the nucleus. As a result, the nuclear multipole expansion cannot be truncated at any order. This decomposition is complicated by the fact that the outgoing electron interacts with the nuclear charge through the Coulomb potential. Nonetheless, the nuclear multipole expansion can be performed in a straightforward manner by replacing the Coulomb-distorted electron wave function with a plane-wave form parameterized by a suitable local momentum.

The effective theory is then specified by a controlled expansion in terms of the relevant velocity operators for the nucleons $\vec{v}_N$ and the bound muon $\vec{v}_\mu$. (The electron velocity is, in essence, "integrated out" of the theory by the assumption that it is ultra-relativistic.) The construction of the nucleon-scale effective theory proceeds in two steps: First, we specify a complete set (through a given order in power-counting) of CLFV operators that couple the leptons to single-nucleon charges and currents. Next, after performing the nuclear multipole decomposition, the resulting nucleon-level theory is embedded into the target nucleus, where the approximate parity and time-reversal symmetries of the nuclear ground state restrict the operators that can contribute to elastic $\mu \to e$ conversion.

A valid effective theory can be constructed at three distinct degrees of complexity: The most basic theory is generated by including neither $\vec{v}_N$ nor $\vec{v}_\mu$. Relativistic corrections to the muon wave function and effects stemming from nuclear compositeness are completed ignored, and the CLFV amplitude depends on just three nuclear response functions, those of a point-like nucleus. Next, we extend the theory by considering $\vec{v}_N$ to first order, and consequently the set of nuclear responses is enlarged by the addition of three velocity-dependent response functions. Finally, we formulate the most complete effective theory, including both velocity operators, $\vec{v}_N$ and $\vec{v}_\mu$, to first order. This corresponds to the inclusion of relativistic muon effects, in the form of the muon's lower Dirac component, and introduces six additional nuclear responses. The muon's lower component always appears as a correction to the upper-component contribution, and therefore we consider the second of these constructions—containing $\vec{v}_N$ but not $\vec{v}_\mu$—to be the prototypical effective theory, complete through leading order in the nuclear response.

The various nuclear responses can be understood as the "nuclear dials" that an experimentalist can tune through nuclear target selection in order to access different regions of CLFV parameter space. The nucleus ^{27}Al, the target of the Mu2e and COMET experiments, has ground-state angular momentum $J = 5/2$ and provides good sensitivity across a range of responses that are spin- and velocity-dependent/independent. On the other hand, a target such as Ca, whose natural abundance consists (almost) entirely of isotopes with ground-state angular momentum $J = 0$, will not couple to non-scalar operators. A detailed understanding of the interplay between the various nuclear responses is prerequisite to carrying out an experimental program—across a multitude of targets—in order to fully constrain the unknown

CLFV parameters of the nuclear-scale effective theory.

Much of the previous literature has focused on a narrow special case in which the leading operator that mediates $\mu \to e$ conversion couples equally to protons and neutrons and is spin- and velocity-independent. Such an operator sums coherently in the conversion amplitude and receives an enhancement by the atomic mass number A relative to incoherent operators, thereby dominating the CLFV response in cases where it is present. The primary advantage of working in this limited case is that the nuclear physics, which is a source of significant complication in general, becomes exceedingly simple. In fact, the coherent nuclear response is governed entirely by the scalar nucleon density, a quantity that is accurately determined by experiments. When considering specific extensions of the standard model that yield a leading coherent response, the $\mu \to e$ branching ratio can be predicted with a well-understood uncertainty. However, in the initial discovery phase of CLFV searches, one should not assume anything about the underlying nature of flavor-violating operators. The proper approach, which we pursue in this thesis, is to constrain the most general interaction as specified by the effective theory.

In memory of my mother, Janice Mary Rule, and my brother, Dr. Seth Michael Rule.

Contents

List of Figures

List of Tables

Acknowledgments

I would like to thank my advisor Wick Haxton for suggesting the problem of $\mu \to e$ conversion as an ideal setting for a nuclear-scale effective theory. Wick's patient guidance was essential not only to the development of the ideas presented in this thesis but to my own maturation as a physicist to be capable of undertaking this work. His example is one to which I will always aspire.

I would like to express my appreciation to the other members of my thesis committee, Yury Kolomensky and Karl van Bibber, for their critical review of this manuscript.

I would also like to acknowledge Michael Ramsey-Musolf for providing valuable direction on several aspects of this work, especially the treatment of two-nucleon operators, and for broadening my understanding of $\mu \to e$ conversion beyond the nuclear scale. I am similarly indebted to my collaborators Vincenzo Cirigliano and Kaori Fuyuto, having learned so much about the high-energy aspects of $\mu \to e$ conversion from our work together.

Special recognition is also due to the members of the extended Haxton group, whose valuable feedback and insightful questions have helped to shape my own understanding of this material. In particular, I am grateful to Ken McElvain and Katherine Hambleton for many informal but productive discussions on this problem and many others.

Finally, I would like to thank my family for their enthusiastic support and unwavering belief in me. It is much easier to accomplish a difficult task when the people who are closest to you are certain that you can do it. I want to express special appreciation for my parents, who worked so hard to give me a life that is full of opportunity. I am forever grateful to my wife Valerie for providing me with constant inspiration to continue this endeavor, punctuated with well-timed reminders to take a much-needed break. Her loving support—as well as her thoughtful advice on word choice and syntax—has been instrumental to this work achieving its final form.

Chapter 1

Introduction

Throughout the modern history of particle physics, tests of lepton flavor violation have played a crucial role in advancing theoretical understanding. When it was first hypothesized that the weak interaction is mediated by charged bosons, only a single neutrino flavor was known to exist. Based on this assumption, Feinberg [1] in 1958 noted that the proposed charged bosons of the weak force would induce $\mu^+ \to e^+ + \gamma$ at the level of 10^{-4}, a branching ratio already excluded by the upper limit of 2×10^{-5} on this process set in 1955 by the Columbia University Nevis cyclotron [2]. The work of Feinberg immediately led to the two-neutrino hypothesis [3], where separate neutrinos couple to the muon and electron, respectively, thereby forbidding (in the absence of neutrino flavor violation) the $\mu^+ \to e^+ + \gamma$ decay. When the two-neutrino hypothesis was confirmed at Brookhaven National Laboratory [4] in 1965, it was the first indication of a conserved quantum number associated with lepton flavor, extending to both the charged and neutral leptons[1]. To this day, lepton flavor is enshrined in the Lagrangian of the standard model of particle physics as a conserved quantity.

On the other hand, the modern philosophy of particle physics advocates that global symmetries that are not the consequence of an underlying gauge symmetry are "accidental" and ultimately violated, though perhaps to a highly suppressed degree. This is commonly the expectation for the apparently accidental standard-model symmetries of baryon and lepton number conservation: many extensions of the standard model, including supersymmetry (SUSY) and other Grand Unified Theories (GUTs), lead to the violation of baryon and lepton number at high energies, permitting, for example, a free proton to decay on an extremely long timescale.

From the observation of neutrino oscillations [5, 6], it is presently known that lepton flavor is not exactly conserved in nature, and some modification of the standard model is required to account for this phenomenon. Given that neutrinos oscillate between flavor eigenstates as they propagate and that charged leptons interact with neutrinos through the electroweak force, one can immediately envision processes, for example that shown in Fig. 1.1, by which charged lepton flavor is violated at one-loop level. The rate for such reactions, however, is suppressed by $(m_\nu/m_W)^4$, leading to an overall branching ratio that is roughly 40 orders of magnitude below current experimental sensitivities. This implies that any observation of charged lepton flavor violation (CLFV) is an unambiguous sign of physics beyond the

---

[1]This progress also contributed to the eventual recognition that the "μ meson", as it was known at the time of Feinberg's seminal work, is not associated with the strong nuclear force and is, in fact, a lepton.
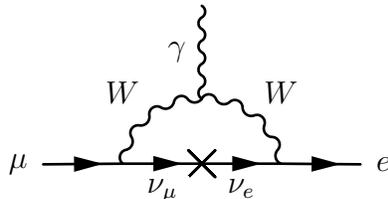
Figure 1.1: Example of CLFV induced by neutrino flavor oscillations. The CLFV rate that results from this source alone is unobservably small.

standard model (BSM).

In fact, observable rates of CLFV are a consequence of many proposed BSM theories including, among others, extensions that generate neutrino masses [7, 8], account for the muon $g - 2$ anomaly [9, 10], exploit supersymmetry [11–14] or other mechanisms [15–17] for unification, and explain the observed matter/antimatter asymmetry [18, 19]. Since Feinberg first considered the $\mu \to e\gamma$ reaction, an immense variety of CLFV processes—many involving the tau lepton as well—have been identified as probes of new physics, and in recent years a number of important constraints on flavor-violating operators have been obtained from colliders, especially the Large Hadron Collider (LHC). In particular, searches at A Toroidal LHC Apparatus (ATLAS), Compact Muon Solenoid (CMS) and Large Hadron Collider beauty (LHCb) have constrained the branching ratios of CLFV processes including the Z boson decays $Z \to e\tau$ and $Z \to \mu\tau$ [20, 21], the Higgs boson decays $h \to e\mu$, $h \to \mu\tau$, and $h \to e\tau$ [22–24], the B meson decays $B^+ \to K^+\mu^-\tau^+$ [25], $B^+ \to K^+\mu^\pm e^\mp$ [26], $B_s^0 \to \tau^\pm\mu^\mp$, and $B^0 \to \tau^\pm\mu^\mp$ [27], and the purely leptonic decay $\tau \to 3\mu$ [28–30].

In the next few years, the Belle II experiment [31] at the High Energy Accelerator Research Organization (KEK) in Japan is expected to produce competitive limits on a range of CLFV processes including $\tau \to e\gamma$, $\tau \to e\ell^+\ell^-$, and $B^0 \to K^{*0}\ell^+\ell^-$, and the future Electron-Ion Collider (EIC) [32] at Brookhaven National Laboratory (BNL) is expected to further strengthen constraints on CLFV τ decays [33]. The existing limits on $\tau \to e$ transitions are typically much weaker than those on $\mu \to e$ decays. On the other hand, specific UV models, including the SUSY seesaw model [34], may lead to an enhanced rate for CLFV processes involving the tau lepton.

Such enhancements notwithstanding, the muonic sector provides a particularly favorable landscape in which to search for CLFV. Apparent violations of lepton flavor universality in B meson decays [35] and the muon $g - 2$ anomaly [36] may each be interpreted as hints of new muonic physics, potentially with a flavor-violating component. Independent of these considerations, the CLFV processes of $\mu \to e$ conversion in nuclei and $\mu \to 3e$ are among the most sensitive tests of new physics beyond the standard model, yielding, in particular, a more general constraint on supersymmetric grand unification than either proton decay or neutrino masses [37]. In contrast to the collider constraints summarized above, these muon decays represent relatively low-energy probes of CLFV, accessible at dedicated experiments.

In this work, our primary focus is the process of $\mu \to e$ conversion where a muon is

captured into the Coulomb field of an atomic nucleus. Once bound, the muon quickly de-excites to the $1s$ ground state of the nuclear Coulomb field. The timescale for transition to the ground state (within 10^{-9} to 10^{-12} seconds) is much faster than standard-model muon decay processes ($\approx 10^{-6}$ seconds), and therefore one may describe the muon as residing in the $1s$ state. There are two primary standard-model processes through which the muons then decay: decay in orbit

$$\mu^- \to e^- + \bar{\nu}_e + \nu_\mu, \tag{1.1}$$

and standard muon capture

$$\mu^- + A(Z, N) \to \nu_\mu + A(Z - 1, N + 1), \tag{1.2}$$

where Z is the nuclear charge and N the number of neutrons. Both of these processes conserve total lepton number as well as lepton flavor; the former produces a continuous spectrum of electrons that constitutes the primary experimental background in searches for CLFV $\mu \to e$ conversion. We are interested in the process

$$\mu^- + A(Z, N) \to e^- + A(Z, N), \tag{1.3}$$

which conserves total lepton number but violates lepton flavor by converting a muon into an electron with no neutrino byproducts. The relevant quantity that is constrained by experiments is the branching ratio

$$B(\mu^- + (A, Z) \to e^- + (A, Z)) \equiv \frac{\Gamma(\mu^- + (A, Z) \to e^- + (A, Z))}{\Gamma(\mu^- + (A, Z) \to \nu_\mu + A(Z - 1, N + 1))}, \tag{1.4}$$

where the numerator is the rate for the CLFV conversion process, and the denominator is the rate of standard muon capture.

The earliest limit on the neutrinoless conversion of captured muons was obtained in 1952 from the cosmic-ray experiments of Lagarrigue & Peyrou [38], who constrained the conversion process by counting the number of electron tracks produced by cosmic-ray muons stopped in copper and tin plates of a cloud chamber. Accounting for electrons produced in free muon decays, they were able to determine a CLFV branching ratio consistent with zero, $B(\mu \to e) = 0.04 \pm 0.05$. In 1955, the same year that Lokanathan & Steinberger obtained a pioneering limit on $\mu \to e\gamma$, the Nevis cyclotron was also the setting for the first $\mu \to e$ conversion collider experiment. Employing a copper target to trap roughly 400 muons—produced from the decay of cyclotron pions—in 20 hours of running time, Steinberger & Wolfe were able to obtain an upper limit of $B(\mu \to e) \lesssim 2 \times 10^{-4}$ (90% confidence level) [39].

In the decades since the first constraints were obtained, improving detector technology and increasingly intense muon beams have allowed experimentalists to extend the reach of conversion searches by nearly ten orders of magnitude: The current best limit on the $\mu \to e$ conversion branching ratio is $B(\mu \to e) < 7 \times 10^{-13}$ (90% CL), set by the SINDRUM II collaboration [40] using Au as the target nucleus. The next generation of experiments, Mu2e at Fermilab [41] and the COherent Muon to Electron Transition (COMET) experiment [42] at Japan Proton Accelerator Research Complex (J-PARC), are expected to improve this limit by four orders of magnitude, potentially probing new physics scales up to 10^4 TeV. Both of

these experiments have chosen ^{27}Al as the target nucleus, and in this work we will frequently specialize to this case. Beyond the initial run, it is a high priority for both experiments to explore different target nuclei.

Among a number of experimental advances contributing to the anticipated exceptional improvement in CLFV sensitivity, one primary source is the shear number of muons that can be captured onto the nuclear target [43, 44]. Mu2e in particular will benefit from a pulsed muon beam that is $\approx 10,000$ times more intense than the previous generation of conversion experiments. Over their respective primary lifetimes, Mu2e and COMET are each expected to stop $\approx 10^{18}$ muons. An evolution of the Mu2e experiment has recently been proposed that aims to leverage future beamline upgrades at Fermilab in order to progress the sensitivity by a further order of magnitude [45].

Significant advances in the sensitivity of searches for $\mu \to e\gamma$ and $\mu \to 3e$ are also soon expected with the advent, respectively, of the Mu to E Gamma (MEG) II and Mu3e experiments, both located at the Paul Scherrer Institute (PSI). The branching ratios for these two processes are measured relative to the dominant free-muon decay mode; that is

$$B(\mu \to e\gamma) \equiv \frac{\Gamma\left(\mu \to e + \gamma\right)}{\Gamma\left(\mu \to e + 2\nu\right)}, \quad B(\mu \to 3e) \equiv \frac{\Gamma\left(\mu \to 3e\right)}{\Gamma\left(\mu \to e + 2\nu\right)}. \tag{1.5}$$

The existing branching ratio limits for $\mu \to e$ conversion, $\mu \to e\gamma$, and $\mu \to 3e$ are shown in Table 1.1. The corresponding limits expected at the next-generation experiments are shown in Table 1.2.

The expected limits from $\mu \to e$ conversion experiments are considerably more stringent than those obtained from either of the free CLFV muon decays. This advantage is largely due to the favorable kinematics of the decay of a captured muon: if the nucleus remains in its ground state throughout the conversion process then the outgoing electron will have an energy at the very endpoint of the spectrum of background electrons emitted in standard-model $\mu \to e + 2\nu$ decays. Restricting to the case without nuclear excitation—which we refer to as *elastic* $\mu \to e$ conversion—limits the operators that can contribute due to the approximate parity and time-reversal symmetries of the nuclear ground state.

Depending on the underlying CLFV physics, these three processes may be strongly interconnected. For example, an operator that mediates $\mu \to e\gamma$ can be embedded in a nucleus—the photon is virtual and exchanged with the nuclear charge—and thereby induce $\mu \to e$ conversion. Particular UV models of CLFV should provide unambiguous predictions for the branching ratios $B(\mu \to e\gamma)$, $B(\mu \to 3e)$, and $B(\mu \to e)$ in various target nuclei. If these quantities can be computed with well-understood uncertainties, then measurements of CLFV processes can be used to exclude candidate BSM theories. Relating the low-energy $\mu \to e$ conversion process to an underlying UV theory of CLFV, however, is a formidable theoretical challenge, due in part to the considerable range of energy scales that the problem spans.

The modern paradigm for treating problems with large scale separations is effective theory. In these scenarios, one typically encounters a small dimensionless quantity, such as the ratio of two energy scales: one large, associated perhaps with the mass of a heavy degree of freedom, and one small, say the energy at which one intends to probe the system. Effective theory permits one to remove, or "integrate out", the heavy particle from the description while retaining its effect on the low-energy physics. A complete basis, consistent

Process	Limit	Experiment/Lab	Year	Reference
$\mu^- + Cu \to e^- + Cu$	$< 1.6 \times 10^{-8}$	SREL	1972	[46]
$\mu^- + {}^{32}S \to e^- + {}^{32}S$	$< 7 \times 10^{-11}$	SIN	1981	[47]
$\mu^- + Pb \to e^- + Pb$	$< 4.6 \times 10^{-11}$	SINDRUM II	1996	[48]
$\mu^- + Ti \to e^- + Ti$	$< 6.1 \times 10^{-13}$	SINDRUM II	1998	[49]
$\mu^- + Au \to e^- + Au$	$< 7.0 \times 10^{-13}$	SINDRUM II	2006	[50]
$\mu^+ \to e^+ \gamma$	$< 4.2 \times 10^{-13}$	MEG at PSI	2016	[51]
$\mu^+ \to e^+ e^- e^+$	$< 1.0 \times 10^{-12}$	SINDRUM	1988	[52]

Table 1.1: Existing branching ratio limits on the CLFV processes $\mu \to e$, $\mu \to e\gamma$, and $\mu \to 3e$. All limits correspond to 90% confidence level.

Process	Limit	Experiment/Lab	Reference
$\mu^- + {}^{27}Al \to e^- + {}^{27}Al$	$< 8 \times 10^{-17}$	Mu2e at Fermilab	[53]
$\mu^- + {}^{27}Al \to e^- + {}^{27}Al$	$< 7 \times 10^{-15}$	COMET (Phase I) at J-PARC	[42]
$\mu^- + {}^{27}Al \to e^- + {}^{27}Al$	$< 7 \times 10^{-17}$	COMET (Phase II) at J-PARC	[42]
$\mu^+ \to e^+ \gamma$	$< 6 \times 10^{-14}$	MEG II at PSI	[54]
$\mu^+ \to e^+ e^- e^+$	$< 6 \times 10^{-15}$	Mu3e at PSI (Phase I)	[55]
$\mu^+ \to e^+ e^- e^+$	$< 4 \times 10^{-16}$	Mu3e at PSI (Phase II)	[55]

Table 1.2: Expected limits on CLFV branching ratios at next-generation experiments. All limits correspond to 90% confidence level.

with the prescribed symmetries, is constructed from the remaining degrees of freedom. Each term appears at a particular order in the small dimensionless quantity, which acts as a power-counting parameter. The full effective theory basis contains an infinite number of operators with unknown coefficients that encode the relevant physics, including the impact of the integrated-out heavy particle. In order to restore predictive power, one truncates the basis at finite order in the power-counting, at the cost of incurring some error in the calculation of observables. A proper effective theory improves systematically at each higher order.

The landscape of effective theories relevant to $\mu \to e$ conversion is illustrated in Fig. 1.2. The CLFV physics is associated with an energy scale Λ_{CLFV}—typically well above the electroweak scale—at which the dimensionless CLFV couplings (potentially to new degrees of freedom) are order one. In the spirit of effective theory, at energies below Λ_{CLFV} we may integrate out any heavy BSM particles, generating a set of effective operators in terms of standard-model degrees of freedom.

Two major theoretical hurdles arise as one attempts to extract from the standard-model
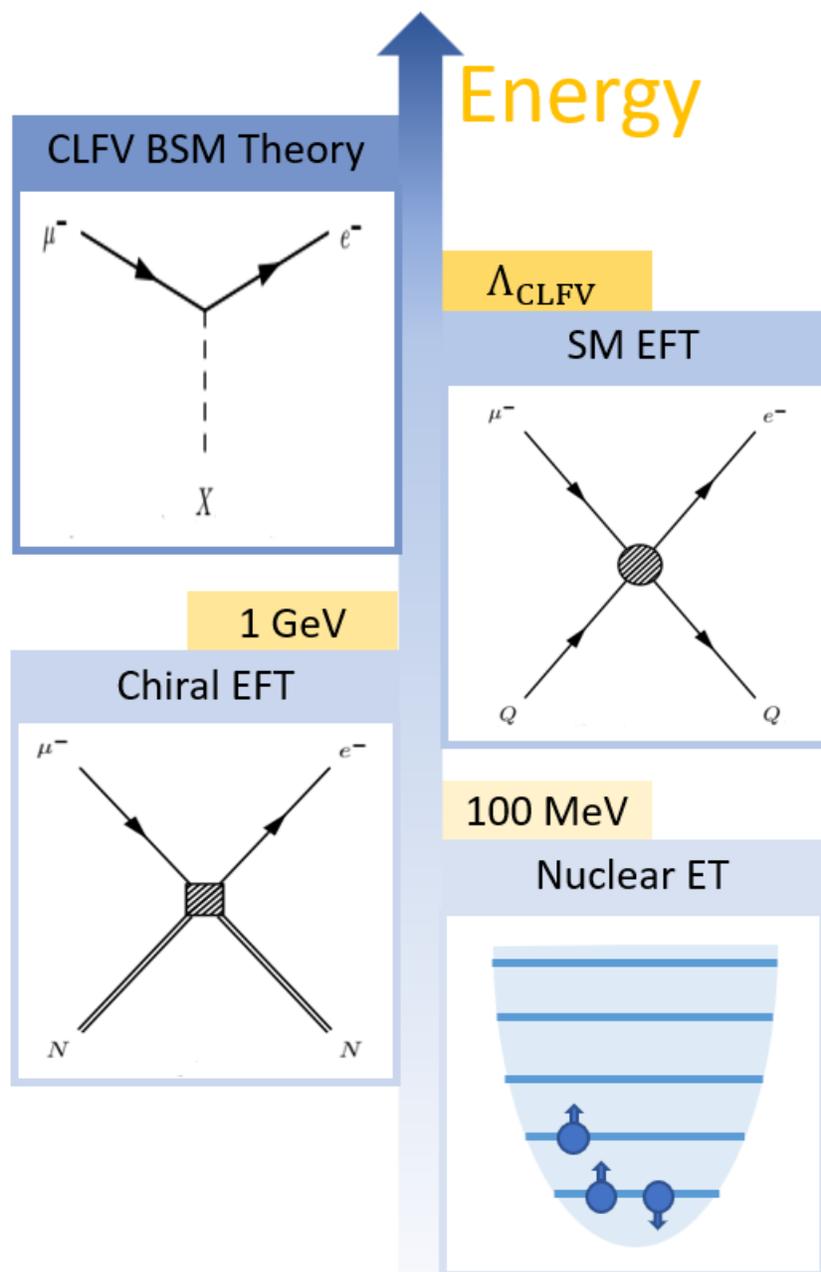
Figure 1.2: Sketch of the various energy scales that are relevant to $\mu \to e$ conversion and the effective theories that can be employed in each regime.

effective theory a prediction for the $\mu \to e$ conversion branching ratio: At energies $\gtrsim 1$ GeV, the strong-force physics is well described by a perturbative treatment of the theory of quantum chromodynamics (QCD) in terms of quark and gluon degrees of freedom. The conversion experiments, on the other hand, are performed at sufficiently low energies that the quarks hadronize into nucleons. Although QCD remains the correct fundamental theory in this regime, it is strongly coupled and essentially intractable. Instead, one must undertake a non-perturbative matching between quark and hadron degrees of freedom that requires input from either experiment or lattice QCD calculations. Fortunately, we are entering an era where precision lattice QCD calculations make it possible to quantify the errors associated with this matching procedure.

The nucleon-level operators thus obtained must ultimately be embedded in a nucleus, where the form of the response is constrained by the angular momentum, isospin, parity, and time-reversal symmetries of the nuclear ground state. This is the second major theoretical hurdle in connecting the UV theory to experiment, due to the complex nuclear many-body physics required to evaluate the relevant response functions. In order to construct a many-body wave function for a nucleus like ^{27}Al in the nuclear shell-model, one relies upon phenomenological interactions that have been tuned to reproduce low-energy nuclear observables, such as charge radii and low-lying spectra. At present, the errors associated with these treatments are not rigorously quantified and can certainly be significant.

These difficulties can be circumvented if one restricts focus to the case of coherent $\mu \to e$ conversion, in which the only nuclear operator under consideration is the isoscalar monopole charge operator. The term "coherent" refers to the fact that this operator sums constructively over every nucleon in the nucleus, and therefore the amplitude is enhanced by roughly a factor of $A = N + Z$ relative to the incoherent process. Specializing to the coherent case results in a dramatic simplification of the nuclear physics: rather than relying on difficult and imprecise modeling of the nuclear many-body wave function, the coherent amplitude can be computed from an experimentally determined quantity, the scalar nucleon density. Thus, if one connects the coherent nucleon operator to its quark-level counterparts—relying on lattice QCD to quantify the associated matching errors—it is possible to complete the chain of effective theories from the scale of $\mu \to e$ conversion up to the high-energy realm of candidate UV CLFV theories, yielding a prediction for the coherent conversion branching ratio with well-understood uncertainties. This construction was recently completed though next-to-leading order in the quark/hadron matching [56, 57], providing a valuable tool for discriminating among BSM theories.

On the other hand, this "top-down" approach is not general and can only be used to exclude those particular UV models that yield a leading coherent operator. At present, there is no reason to expect that nature has been so kind as to concentrate sources of CLFV into such a narrow response. Indeed, one should consider the problem in general, including all operators allowed by the relevant symmetries through a given order in some small parameter(s). Of course, each of the various effective theories represented in Fig. 1.2 provides a complete description of the physics within its domain of applicability, and if one were to, say, begin from the most general effective theory of CLFV at the level of standard-model degrees of freedom and proceed downward to the nuclear scale, then one must recover the most general nuclear-level effective theory. In doing so, however, it is highly likely that one has horribly obscured the underlying CLFV physics, convoluting it with the nuclear physics.

The $\mu \to e$ conversion experiments have the advantage that the nuclear target can be varied, potentially providing additional complementary measurements. As such, a formalism that factorizes the part of the response that depends on the choice of nuclear target from the CLFV physics is highly desirable. Furthermore, being the scale at which the relevant measurements are conducted, the nuclear scale is the most natural setting for an effective theory of $\mu \to e$ conversion, allowing one to identify those quantities that are directly probed by experiment. In this sense, the nuclear-scale effective theory represents the most general constraint that elastic $\mu \to e$ conversion can place on underlying CLFV operators.

The bulk of this thesis is dedicated to the development and application of a nuclear effective theory for the elastic $\mu \to e$ conversion process. This formalism was first introduced in Refs. [58, 59]. The development of the effective theory is mirrored in the structure of this thesis, which we now outline:

Chapter 2 describes the treatment of the leptonic fields. We demonstrate how accurate wave functions for both the bound muon and outgoing electron can be obtained by numerical solution of the Dirac equation with potential given by the nuclear Coulomb field. Although these solutions can be fruitfully employed in the case of coherent conversion—as has been done extensively in the existing literature—they are very tedious to extend to the general case, obscuring what is actually rather simple physics. In contrast, by introducing an approximate form for the electron wave function, we are able to achieve a dramatically simplified expression for the most general CLFV amplitude without compromising the accuracy. Previous investigators who have attempted to extend beyond the coherent case have employed a naïve plane-wave form for the electron and, as a result, incurred significant errors. Our treatment retains both the simplicity of the plane wave solution and the accuracy of the numerical solution.

We further abridge the effective theory by introducing several approximations for the bound muon. Particularly in light nuclei, one can neglect altogether the lower component of the muon's Dirac wave function, which arises only as a relativistic correction. (Later, in Chapter 7, we demonstrate that, even in heavy nuclei where relativistic effects become significant, the muon's lower component provides little new physics information, amounting in essence to a shift in the nuclear form factors and, correspondingly, a renormalization of the associated operator coefficients. The basic structure of the nuclear-scale effective theory is unchanged.) In addition, we argue that the slowly varying radial wave function of the muon's upper component can be well-approximated by a constant value, eliminating the need to compute cumbersome numerical integrals and, to a large extent, decoupling the muon from the nucleus. Significant attention is dedicated to understanding the errors associated with these simplifications when applied to a range of nuclear targets.

In Chapter 3, we identify the six basic Hermitian operators from which the effective theory is constructed. When combined through first order in the relevant power-counting parameters, these building-block operators yield the 16 independent CLFV operators that constitute the basis of the nucleon-level effective theory. Performing a multipole decomposition of the resulting nuclear charges and currents, we identify 11 independent nuclear responses that govern the conversion amplitude. However, the approximate parity and time-reversal symmetries of the nuclear ground state limit the operators that can contribute to the elastic $\mu \to e$ conversion process to just 6 allowed responses.

The rate for $\mu \to e$ conversion is then expressed in terms of the six allowed responses

and two interference terms. Each term is factorized into a product of leptonic and nuclear response functions. The leptonic responses represent the most general constraint on CLFV operators that can be obtained from elastic $\mu \to e$ conversion—only 8 independent quantities are probed. (Accounting for operators that couple distinctly to protons and neutrons, the number of independent responses is doubled to 16.)

Chapter 4 explores the properties of each of the six allowed nuclear response functions, which correspond to "nuclear dials" that can be tuned through target selection in order to probe different combinations of CLFV parameters. In some cases, the essential behavior of the nuclear responses depends only on macroscopic nuclear quantities like charge, spin, and isospin. In other situations, the results are sensitive to subtle details of nuclear structure, including correlations that are properly described by nuclear shell-model calculations. We compare the strength of various spin- and velocity-dependent/independent responses across a range of nuclei in order to assess the sensitivity of different targets to CLFV operators.

In Chapter 5, we obtain constraints on the low-energy constants of the nuclear effective theory from existing and future $\mu \to e$ conversion experiments. To simplify the analysis, we consider the case in which a single nucleon-level CLFV operator is active. We obtain an upper limit on the magnitude of the associated coupling constant and translate this limit into an approximate scale of new physics that the operator probes.

Chapter 6 discusses the relationship between $\mu \to e$ conversion, $\mu \to e\gamma$, and $\mu \to 3e$. We highlight a few potential mechanisms by which these processes may be interrelated and explore possible detection scenarios across all three probes at the next generation of experiments.

In Chapter 7, we restore the muon's lower component to the effective theory, representing its impact in terms of the action of the muon velocity operator. Six novel nuclear responses are required in order to fully describe the coupling to the muon's p-wave lower component. We derive an expression for the decay rate including the relativistic muon effects and discuss the impact of these corrections on the interpretation of $\mu \to e$ conversion experiments.

In Chapter 8, we explicitly perform the matching required to connect experimental CLFV constraints directly to BSM parameters for the particular scenario of coherent $\mu \to e$ conversion mediated by a heavy scalar particle. We demonstrate how—within this special case—CLFV branching ratios can be computed with controlled uncertainties, allowing one to rigorously exclude candidate UV models that fall within this category. The matching between quark and nucleon degrees of freedom is performed through next-to-leading order in chiral power-counting, including the effect of two-nucleon operators. We apply this formalism to the case in which $\mu \to e$ conversion is induced by flavor-violating Yukawa couplings to the standard-model Higgs boson.

Chapter 9 describes in greater detail the treatment of the two-nucleon operator that contributes to scalar-mediated coherent conversion at next-to-leading order. After transforming to position-space, we evaluate the two-nucleon operator using nuclear shell-model wave functions. We discuss the limitations of this approach and comment on the broader impact of two-nucleon contributions upon efforts to interpret $\mu \to e$ conversion limits.

In Chapter 10, we conclude with a summary of the progress reported in this thesis and introduce two directions for future work. First, we describe an extension of the effective theory formalism to include the inelastic conversion process in which the nucleus transitions to an excited state. The inelastic process circumvents the constraints imposed by nuclear parity and time-reversal symmetries and allows one to probe operators that are otherwise forbidden

by the elastic process. Significant collaboration with experimentalists will be required in order to more fully understand the feasibility of such a measurement.

Finally, we outline the work that remains in matching the nuclear-scale effective theory to higher-scale effective theories. Once complete, this program will allow us to connect general constraints obtained from conversion experiments to candidate BSM theories. We note a few related works in the literature that will aid in these efforts.

Striving to maintain a clear and concise narrative, we have relegated the details of many calculations to a series of appendices:

Appendix A introduces some of the basic conventions for spinors that we adopt in this work and provides details related to the expansion of the nucleon and lepton Dirac currents in terms of Pauli spinors.

Appendix B provides an introduction to spherical tensor operators. Particular attention is devoted to the vector spherical harmonics, which arise frequently in the nuclear multipole decomposition.

Appendix C introduces the one- and two-body density matrices that are used to efficiently compute many-body nuclear matrix elements of few-body operators.

Appendix D contains detailed expressions required in the evaluation of harmonic oscillator matrix elements of the single-nucleon response functions.

Appendix E provides the details of the Fermi gas averaging procedure that we employ in order to reduce the two-nucleon operator to an effective single-nucleon operator. Results are reported for both the spin-dependent and spin-independent effective operators.

Appendix F contains the details of the Fourier transform of the two-nucleon operator, including the full momentum-transfer-dependent result in position space.

Chapter 2

Treatment of the Leptonic Fields

In comparison to the nuclear physics, the leptonic physics of $\mu \to e$ conversion is relatively straightforward and can be computed to high accuracy. In particular, it is known that the muon occupies the $1s$ state of the nuclear Coulomb field. Nuclear charge distributions have been determined from electron scattering experiments, and so one may (numerically) solve the Dirac equation for the captured muon in the field of a realistic nuclear Coulomb potential. This procedure yields the wave function and determines the binding energy of the muon. Conservation of energy then dictates the energy of the outgoing electron, and again one may solve the Dirac equation for the electron in the Coulomb field of the nucleus. The resulting wave functions account for relativistic effects and the finite extent of the nuclear charge. The downside of this approach is that one is now burdened with numerical solutions for the lepton wave functions, which can make subsequent calculations exceedingly complicated.

In this chapter, we describe in detail how to obtain the Dirac solutions for the muon and electron. We highlight the special cases where the precise numerical solutions can be employed with minimal overhead and then demonstrate the difficulties that one encounters when attempting to incorporate these solutions into a fully general approach. Finally, based on careful study of the Dirac solutions, we introduce approximate lepton wave functions that dramatically simply the formalism and illuminate the underlying physics.

2.1 Solutions of the Dirac Equation for a Spherically Symmetric Potential

The Dirac equation for a particle of mass m in a spherically symmetric potential $V(r)$ may be written as

$$E\psi = \left[-i\gamma_5\sigma_r \left(\partial_r + \frac{1}{r} - \frac{\gamma_0}{r}K \right) + V(r) + \bar{m}\gamma_0 \right] \psi, \qquad (2.1)$$

with

$$\gamma_5 = \begin{pmatrix} 0 & I_2 \\ I_2 & 0 \end{pmatrix}, \qquad \gamma_0 = \begin{pmatrix} I_2 & 0 \\ 0 & -I_2 \end{pmatrix}, \qquad (2.2)$$

and

$$\sigma_r = \begin{pmatrix} \vec{\sigma} \cdot \hat{r} & 0 \\ 0 & \vec{\sigma} \cdot \hat{r} \end{pmatrix}, \qquad K = \begin{pmatrix} \vec{\sigma} \cdot \vec{L} + I_2 & 0 \\ 0 & -\left(\vec{\sigma} \cdot \vec{L} + I_2 \right) \end{pmatrix}. \tag{2.3}$$

In the above, E is the energy of the lepton, $\vec{L} = -i\vec{r} \times \vec{\nabla}$ is the orbital angular momentum operator, and I_2 is the two-dimensional identity matrix. The mass $\bar{m}$ is the reduced mass of the lepton

$$\bar{m} = \frac{mM_T}{m + M_T}, \tag{2.4}$$

where m is the lepton mass and M_T is the nuclear target mass.

The solutions can be expressed as eigenfunctions of the operators J^2, J_z, and K. Letting the corresponding eigenvalues be represented by j, m, and κ, respectively, the Dirac wave functions have the generic form

$$\psi_m^\kappa(\vec{r}) = \begin{pmatrix} \frac{G_\kappa(r)}{r} \, \Omega_{jm}^\ell(\hat{r}) \\ i\frac{F_\kappa(r)}{r} \, \Omega_{jm}^{\ell'}(\hat{r}) \end{pmatrix}, \tag{2.5}$$

where Ω_{jm}^ℓ is a spinor spherical harmonic

$$\Omega_{jm}^\ell(\hat{r}) = \sum_{m_\ell m_s} \langle \ell \, m_\ell \, \tfrac{1}{2} \, m_s | j \, m \rangle \, Y_{\ell m_\ell}(\hat{r}) \, \xi_{m_s}, \tag{2.6}$$

and ξ_{m_s} is a Pauli spinor. The spinor spherical harmonics satisfy the following properties:

$$\begin{aligned} L^2 \Omega_{jm}^\ell &= \ell(\ell+1)\Omega_{jm}^\ell, \\ J^2 \Omega_{jm}^\ell &= j(j+1)\Omega_{jm}^\ell, \\ J_z \Omega_{jm}^\ell &= m\Omega_{jm}^\ell, \\ \left(\vec{\sigma} \cdot \vec{L} + I_2 \right) \Omega_{jm}^\ell &= -\kappa\Omega_{jm}^\ell. \end{aligned} \tag{2.7}$$

The Dirac solutions are indexed by $\kappa = ..., -3, -2, -1, 1, 2, 3, ...$ where $j = |\kappa| - \frac{1}{2}$ and

$$\kappa = \begin{cases} -(\ell+1), & \kappa < 0 \\ \ell, & \kappa > 0 \end{cases}. \tag{2.8}$$

In the case of $\mu \to e$ conversion, the muon is known to be in the $\kappa = -1$ state. In principle, the electron can be produced in any partial wave, limited by the fact that it must couple together with the $j = 1/2$ muon to the nucleus. The radial wave functions are obtained by solving the coupled differential equations

$$\begin{aligned} \frac{dG}{dr} &= -\frac{\kappa}{r}G + (E - V(r) + \bar{m}) \, F, \\ \frac{dF}{dr} &= \frac{\kappa}{r}F - (E - V(r) - \bar{m}) \, G. \end{aligned} \tag{2.9}$$

The Coulomb potential that we employ is based on a two-parameter Fermi model of the proton density

$$\rho_p(r) = \frac{\rho_0}{1 + e^{(r-c)/\beta}}, \tag{2.10}$$

where the parameters c and β are fit to electron scattering data, and the normalization constant ρ_0 is determined by our convention

$$\int_0^\infty dr \, r^2 \rho_p(r) = Z. \tag{2.11}$$

In fact, ρ_0 can be determined analytically in terms of the polylogarithm function $\text{Li}_n(z)$,

$$\rho_0 = -\frac{Z}{2\beta^3 \text{Li}_3\left(-\exp\left[c/\beta\right]\right)}, \tag{2.12}$$

as can the associated Coulomb potential

$$V_C(r) = -\frac{\alpha Z}{r} \left\{ 1 + \frac{\rho_0 \beta^3}{Z} \left[\frac{r}{\beta} \text{Li}_2\left(-e^{(c-r)/\beta}\right) + 2\text{Li}_3\left(-e^{(c-r)\beta}\right) \right] \right\}. \tag{2.13}$$

The values of c and β that we employ for the nuclei of interest are given in Table 2.1, along with the implied values of the root-mean-square (RMS) charge radius $\sqrt{\langle r^2 \rangle}$, which can also be expressed analytically for the two-parameter Fermi model

$$\begin{aligned} \sqrt{\langle r^2 \rangle} &\equiv \left(\frac{1}{Z} \int dr \, r^4 \rho_p(r) \right)^{1/2} \\ &= \sqrt{12} \beta \left[\frac{\text{Li}_5\left(-\exp[c/\beta]\right)}{\text{Li}_3\left(-\exp[c/\beta]\right)} \right]^{1/2}. \end{aligned} \tag{2.14}$$

The Dirac solutions obtained from these potentials for the nuclei ^{27}Al and ^{48}Ti are shown for the muon in Fig. 2.4 and for the electron in Fig. 2.1 and Fig. 2.2, respectively. With the prescription outlined here, one may obtain Dirac solutions for the $\kappa = -1$ bound muon, determine the muon binding energy and hence the energy of the outgoing electron and then solve for electron radial wave functions for any κ.

2.2 The Coherent Case and its Limitations

The downside of utilizing the Dirac solutions directly in calculations of the $\mu \to e$ branching ratio lies in the fact that the lepton current must be integrated against the nuclear current, which, given the numerical nature of the lepton solutions, precludes a simplified expression for all but the most trivial operators. In general, the effective interaction Hamiltonian consists of terms of the form

$$H_i = c_i \int d^3x \, \bar{\psi}_e(\vec{x}) \mathcal{O}_L \psi_\mu(\vec{x}) \bar{\psi}_N(\vec{x}) \mathcal{O}_N \psi_N(\vec{x}), \tag{2.15}$$

where c_i is a low-energy constant (LEC), and the operators $\mathcal{O}_L$, $\mathcal{O}_N$ may carry Lorentz indices, in which case they couple to an overall scalar. To some extent, one may factorize

the leptonic and nuclear currents by introducing an auxiliary coordinate $\vec{y}$ and inserting an intermediate delta function

$$\delta(\vec{x} - \vec{y}) = \int \frac{d^3q}{(2\pi)^3} e^{i\vec{q}\cdot(\vec{x}-\vec{y})}, \tag{2.16}$$

to obtain

$$H_i = c_i \int \frac{d^3q}{(2\pi)^3} \int d^3x \, e^{i\vec{q}\cdot\vec{x}} \, \bar{\psi}_e(\vec{x})\mathcal{O}_L\psi_\mu(\vec{x}) \int d^3y \, e^{-i\vec{q}\cdot\vec{y}} \, \bar{\psi}_N(\vec{y})\mathcal{O}_N\psi_N(\vec{y}). \tag{2.17}$$

In this form, we may carry out separate multipole decompositions for the leptons and the nucleons by expanding the respective plane wave factors in partial waves as

$$e^{i\vec{q}\cdot\vec{x}} = 4\pi \sum_{L=0}^{\infty} \sum_{M=-L}^{L} i^L j_L(qx) Y^*_{LM}(\hat{q}) Y_{LM}(\hat{x}). \tag{2.18}$$

As a simple example, let us specialize to the case of a scalar-scalar coupling of the leptons to the nucleons

$$\mathcal{O}_L = 1_L, \; \mathcal{O}_N = 1_N. \tag{2.19}$$

Performing the integral $d\Omega_q$ identifies the angular momenta of the leptonic and nuclear partial waves, yielding

$$\begin{aligned}
H = \frac{2}{\pi} c \int_0^\infty dq \, q^2 \sum_{L=0}^\infty \sum_{M=-L}^L & \int d^3x \, j_L(qx) Y^*_{LM}(\hat{x}) \, \bar{\psi}_e(\vec{x})\psi_\mu(\vec{x}) \\
& \times \int d^3y \, j_L(qy) Y_{LM}(\hat{y}) \, \bar{\psi}_N(\vec{y})\psi_N(\vec{y}).
\end{aligned} \tag{2.20}$$

In practice, the summation over L is truncated by the requirement that L must couple to the total angular momentum of the nuclear ground state. Focusing on the leptonic multipoles, the muon is known to occupy the $\kappa = -1$ state, whereas the electron can be in any state that couples together with the muon to total angular momentum L. Labeling the electron state by κ, j, and m_e, we expand the lepton wave functions in Dirac partial waves as

$$\begin{aligned}
\int d^3x \, j_L(qx)Y^*_{LM}(\hat{x})\bar{\psi}_e(\vec{x})\psi_\mu(\vec{x}) = \int d^3x \, j_L(qx)Y^*_{LM}(\hat{x})\frac{1}{x^2} & \left(G^{(e)}_\kappa(x)G^{(\mu)}_{-1}(x)\Omega^{\dagger\ell}_{jm_e}(\hat{x})\Omega^0_{\frac{1}{2}m_\mu}(\hat{x}) \right. \\
& \left. - F^{(e)}_\kappa(x)F^{(\mu)}_{-1}(x)\Omega^{\dagger\ell'}_{jm_e}(\hat{x})\Omega^1_{\frac{1}{2}m_\mu}(\hat{x}) \right).
\end{aligned} \tag{2.21}$$

In principle, the angular integral $d\Omega_x$ can be computed by recoupling the spinor spherical harmonics in terms of a single ordinary spherical harmonic

$$\begin{aligned}
\Omega^{\dagger\ell_1}_{j_1m_1}(\hat{x})\Omega^{\ell_2}_{j_2m_2}(\hat{x}) = \sum_L (-1)^{j_1+m_1+j_2+L+\frac{1}{2}} & \begin{Bmatrix} \ell_1 & \ell_2 & L \\ j_2 & j_1 & \frac{1}{2} \end{Bmatrix} \\
& \times \sqrt{\frac{(2j_1+1)(2j_2+1)(2\ell_1+1)(2\ell_2+1)}{4\pi(2L+1)}} C^{L0}_{\ell_10\ell_20}C^{LM}_{j_1-m_1j_2m_2}Y_{LM}(\hat{x}).
\end{aligned} \tag{2.22}$$

We can already see that if one wants to retain generic L multipoles while considering all relevant electron partial waves, the calculation becomes quite cumbersome. On the other hand, the lowest multipole $L = 0$ is relatively simple to compute. In this case, the only electron state that contributes is $\kappa = -1$, and the angular integration is trivial:

$$\int d^3x \; j_0(qx) Y_{00}^*(\hat{x}) \; \bar{\psi}_e(\vec{x}) \psi_\mu(\vec{x})$$
$$= \frac{1}{2\sqrt{\pi}} \int_0^\infty dx \; j_0(qx) \left(G_{-1}^{(e)}(x) G_{-1}^{(\mu)}(x) - F_{-1}^{(e)}(x) F_{-1}^{(\mu)}(x) \right) \xi_{m_e}^\dagger \xi_{m_\mu}. \tag{2.23}$$

The evaluation of the nuclear wave functions also simplifies dramatically for the $L = 0$ multipole

$$\int d^3y \; j_0(qy) Y_{00}(\hat{x}) \; \bar{\psi}_N(\vec{y}) \psi_N(\vec{y}) = \frac{1}{2\sqrt{\pi}} \int_0^\infty dy \; y^2 \; j_0(qy) \rho_N(y), \tag{2.24}$$

where $\rho_N(r) = \rho_p(r) + \rho_n(r)$ is the isoscalar nuclear density. Conveniently, $\rho_p(r)$ and $\rho_n(r)$ have each been determined experimentally in a wide range of nuclei: the former is known from measurements of elastic electron scattering off of nuclei [60] whereas the latter is constrained, for example, by experiments on pionic atoms [61]. Recombining the leptonic and nuclear expressions, we may perform the integral over q to recover a radial delta function $\delta(x - y)$, allowing us to write

$$H_{L=0} = \frac{c}{4\pi} \int_0^\infty dx \; \left(G_{-1}^{(e)}(x) G_{-1}^{(\mu)}(x) - F_{-1}^{(e)}(x) F_{-1}^{(\mu)}(x) \right) \rho_N(x). \tag{2.25}$$

The remaining integration over the radial coordinate is straightforward to perform numerically. Thus, by restricting to the $L = 0$ multipole of the scalar-scalar interaction, we arrive at a very simple expression for the effective Hamiltonian, with all of the nuclear physics captured by a measured quantity, $\rho_N(x)$. In what circumstances is this simplification justified? In the case considered above, the underlying nuclear operator is the isoscalar nucleon density

$$\bar{\psi}_N(\vec{x}) \psi_N(\vec{x}) \rightarrow \hat{\rho}(\vec{x}) = \sum_{i=1}^A \delta(\vec{x} - \vec{x}_i), \tag{2.26}$$

which admits the multipole decomposition

$$M_{LM}(q) = \int d^3x \; j_L(qx) Y_{LM}(\hat{x}) \; \hat{\rho}(\vec{x})$$
$$= \sum_{i=1}^A j_L(qx_i) Y_{LM}(\hat{x}_i). \tag{2.27}$$

The $\mu \rightarrow e$ conversion amplitude involves a summation over all multipoles allowed by the restriction that they must be able to couple to the nuclear ground state. In ^{27}Al, the ground state carries angular momentum $J = 5/2$, permitting contributions from multipoles up to $L = 5$. Odd charge multipoles are forbidden by parity, leaving M_0, M_2, and M_4 as the allowed operators that must be included in the conversion amplitude. When these operators are evaluated between nuclear ground state wave functions, the $L = 0$ multipole is unique in that it sums coherently over every nucleon in the nucleus; operators with $L > 0$ can only couple

to certain subsets of nucleons. Therefore, one expects a relative enhancement of roughly a factor of A in the amplitude for the coherent operator compared to incoherent operators. This enhancement provides the justification for retaining only the $L = 0$ multipole in Eq. (2.20): the error induced in the conversion rate should be below 1% for the nuclei of interest.

It is crucial that the only nuclear operator under consideration is the nucleon density $\hat{\rho}(\vec{x})$. This argument cannot be extended to other nuclear charges or currents, as they do not give rise to coherent multipole operators and therefore provide no justification for truncating the multipole expansion. In Section 3.7, we demonstrate—by explicit calculation—the need to retain higher-order multipoles in the general case. To avoid these complications, many studies in the literature restrict their attention to the coherent conversion process. The fact that the nuclear physics then depends only on a measured quantity is a significant advantage of this approach, completely avoiding the major theoretical hurdle of embedding the single-nucleon operators into the nucleus. In Chapter 8, we consider coherent conversion in detail, demonstrating how it can be used to rigorously exclude certain UV models of CLFV.

On the contrary, the nature of CLFV physics is yet entirely unknown—depending on the underlying BSM model, coherent conversion may not constitute the leading response. Therefore one should construct the most general CLFV interaction between the leptons and the nuclear target, relying on experiment to constrain the coefficients of the effective operators. In order to consider these additional, incoherent nuclear operators while retaining a simple form for the conversion amplitude, we now proceed to introduce approximate forms for the muon and electron wave functions. Ultimately, we will replace the complicated numerical solutions by, for the muon, the simplest possible wave function: a constant value in the upper component, and for the electron, perhaps the second-simplest wave function: a free Dirac plane wave.

2.3 Approximate Treatment of the Outgoing Electron

When the $\mu \to e$ conversion process occurs without nuclear excitation, the energy of the outgoing electron E_e is given by

$$E_e = m_\mu - E_\mu^{\text{bind}} - \frac{\vec{q}^{\,2}}{2M_T}, \tag{2.28}$$

where $\vec{q}$ is the three-momentum transferred from the nucleus to the electron, m_μ and M_T are, respectively, the muon and nuclear target masses, and E_μ^{bind} is the muon's binding energy, defined here as a positive quantity. The final term on the right-hand side of Eq. (2.28) accounts for the recoil energy of the target nucleus. Working to first order in m_μ/M_T and ignoring terms subleading in $1/M_T$, we find

$$\vec{q}^{\,2} = \frac{M_T}{m_\mu + M_T} \left[\left(m_\mu - E_\mu^{\text{bind}} \right)^2 - m_e^2 \right]. \tag{2.29}$$

As shown in Table 2.1, the muon binding energy is small compared to its rest mass—even for very heavy nuclei. Therefore, the outgoing electron receives nearly all of the muon's rest

Target	c (fm)	β (fm)	$\sqrt{\langle r^2 \rangle}$ (fm)	E_μ^{bind} (MeV)	Z_{eff}	R	q (MeV)	q_{eff} (MeV)
$^{12}_{6}$C	2.215	0.491	2.505	0.1000	5.703	0.8587	105.07	108.40
$^{16}_{8}$O	2.534	0.514	2.739	0.1775	7.421	0.7982	105.11	109.16
$^{19}_{9}$F	2.580	0.567	2.904	0.2242	8.230	0.7646	105.12	109.44
$^{23}_{11}$Na	2.760	0.543	2.940	0.3337	9.855	0.7190	105.07	110.25
$^{27}_{13}$Al	3.070	0.519	3.062	0.4630	11.309	0.6583	104.98	110.81
$^{28}_{14}$Si	3.140	0.537	3.146	0.5346	12.001	0.6299	104.91	111.03
$^{32}_{16}$S	3.161	0.578	3.239	0.6924	13.184	0.5595	104.78	111.56
$^{40}_{20}$Ca	3.621	0.563	3.499	1.0585	15.692	0.4830	104.45	112.28
$^{48}_{22}$Ti	3.843	0.588	3.693	1.2615	16.656	0.4340	104.28	112.43
$^{56}_{26}$Fe	4.111	0.558	3.800	1.7182	18.603	0.3363	103.84	113.16
$^{63}_{29}$Cu	4.218	0.596	3.947	2.0885	19.856	0.3210	103.48	113.50
$^{184}_{74}$W	6.51	0.535	5.421	9.0812	33.629	0.0939	96.55	114.93

Table 2.1: Input parameters and output quantities for the muon and electron Dirac solutions: c and β are the parameters of the Fermi function that describes the nuclear density profile, $\sqrt{\langle r^2 \rangle}$ is the nuclear root-mean-square charge radius, E_μ^{bind} is the muon binding energy, Z_{eff} is the effective charge that parameterizes the constant muon approximation, R is the corresponding reduction factor, q is the physical momentum of the outgoing electron, and q_{eff} is the effective momentum that accounts for the interaction of the electron with the nuclear charge.

mass as kinetic energy and is ultra-relativistic. In this limit, the electron's wave function may be reasonably approximated as a free Dirac plane wave

$$\psi_e(\vec{r}) = \sqrt{\frac{m_e}{E_e}} u(q)\, e^{i\vec{q}\cdot\vec{r}}, \tag{2.30}$$

where the basis spinor is defined in the convention of Bjorken & Drell [62]

$$u(q) = \sqrt{\frac{E+m}{2m}} \begin{pmatrix} \xi \\ \frac{\vec{\sigma}\cdot\vec{q}}{E+m}\xi \end{pmatrix}. \tag{2.31}$$

The plane-wave form admits a partial-wave expansion, from which we make the identifications

$$G_\kappa(r) = qr j_\ell(qr),$$
$$F_\kappa(r) = \sqrt{\frac{E_e - m_e}{E_e + m_e}} \begin{cases} qr j_{\ell-1}(qr), & \kappa > 0 \\ -qr j_{\ell+1}(qr), & \kappa < 0, \end{cases} \tag{2.32}$$

where in the limit of an ultra-relativistic electron, we may take $\sqrt{(E_e - m_e)/(E_e + m_e)} \approx 1$. Although they capture the general qualitative behavior of the outgoing electron, the free Dirac solutions differ significantly from the exact numerical Coulomb solutions, as shown in Figures 2.1, 2.2, and 2.3. The outgoing electron is not free but interacts with the nuclear charge through the Coulomb potential, leading to worsening disagreement between the two solutions with increasing Z.

We can improve the agreement with the numerical solutions by employing the effective momentum approximation (EMA) [63, 64], which retains the plane-wave form but attempts to account for the Coulomb distortion of the electron wave function by replacing the physical three-momentum $\vec{q}$ with an effective momentum $\vec{q}_{\text{eff}}$. The attractive Coulomb potential produces two physical effects on the electron wave function relative to the free plane wave: First, the wavelength is shortened. Second, the probability near the origin (i.e., close to the nuclear charge) is increased. Both of these effects can be captured by replacing the Coulomb potential of Eq. (2.13), which is computed for a finite charge distribution and therefore rather complicated in form, by a constant potential well whose depth is equated with the average of the nuclear Coulomb potential over the nuclear charge density

$$\bar{V}_C \equiv \frac{\int dr\; r^2 \rho(r) V_C(r)}{\int dr\; r^2 \rho(r)}. \tag{2.33}$$

Locally in this constant potential, the momentum of the electron is the effective momentum

$$\vec{q}_{\text{eff}}^{\,2} = \frac{M_T}{M_T + m_\mu} \left[\left(m_\mu - E_\mu^{\text{bind}} - \bar{V}_C \right)^2 - m_e^2 \right]. \tag{2.34}$$

The values of the physical momentum q and effective momentum q_{eff} for various nuclear targets are given in Table 2.1. The effective momentum approximation is implemented by replacing the free Dirac plane wave by

$$u(q) e^{i\vec{q}\cdot\vec{r}} \rightarrow \frac{q_{\text{eff}}}{q} \sqrt{\frac{E_e}{2m_e}} \begin{pmatrix} \xi \\ \vec{\sigma}\cdot\hat{q}\,\xi \end{pmatrix} e^{i\vec{q}_{\text{eff}}\cdot\vec{r}}, \tag{2.35}$$
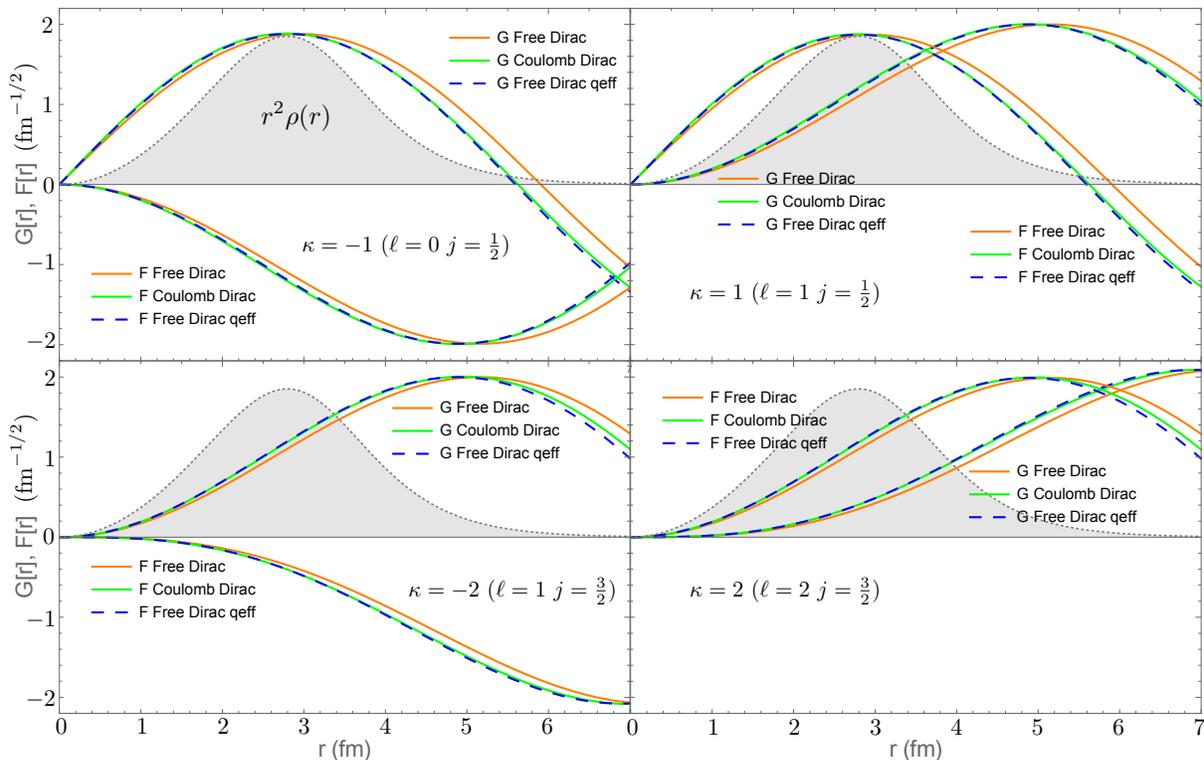
Figure 2.1: The Dirac Coulomb solutions $G(r)$ and $F(r)$ for the highly-relativistic outgoing electron produced in $\mu \to e$ conversion in ^{27}Al (green line) are compared to the free solution (orange) and to the free solution evaluated with q_{eff} (blue dashed), for low partial waves. The nuclear charge distribution is indicated by the shaded region (arbitrary normalization). The agreement between the Coulomb and free solutions evaluated with q_{eff} is quite good.

which—noting that $q_{\text{eff}} > q$ for an attractive potential—achieves the desired shortening of wavelength and increase in amplitude near the origin. As before, the partial waves can be identified as

$$G_\kappa(r) = q_{\text{eff}} r j_\ell(q_{\text{eff}} r),$$

$$F_\kappa(r) = \begin{cases} q_{\text{eff}} r j_{\ell-1}(q_{\text{eff}} r), & \kappa > 0 \\ -q_{\text{eff}} r j_{\ell+1}(q_{\text{eff}} r), & \kappa < 0. \end{cases} \tag{2.36}$$

Figures 2.1, 2.2, and 2.3 show the resulting effective momentum wave functions in various partial waves in the target nuclei ^{27}Al, ^{48}Ti, and ^{184}W, respectively. Visually, the EMA wave functions match the numerical Coulomb solutions quite well, particularly over the scale of the nuclear density. As the $\mu \to e$ transition amplitude generically depends on the integral of the CLFV lepton current over a specific nuclear transition density, it is most important that the EMA wave functions agree with the numerical reference solution in regions where the nuclear density is highest. Even in the very heavy nucleus ^{184}W, the agreement between the EMA wave functions and the Coulomb solutions over the scale of the nucleus is visually quite good, especially compared to the free Dirac plane wave.
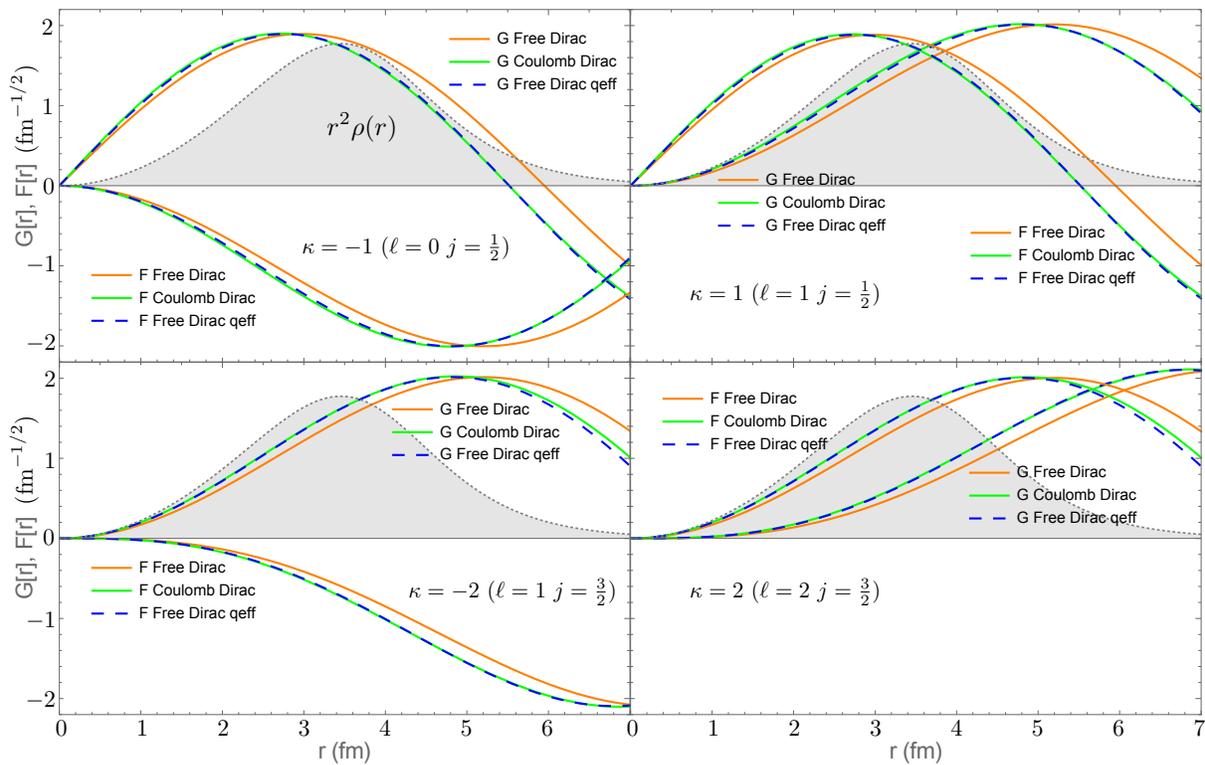
Figure 2.2: Same as Fig. 2.1 but for ^{48}Ti.
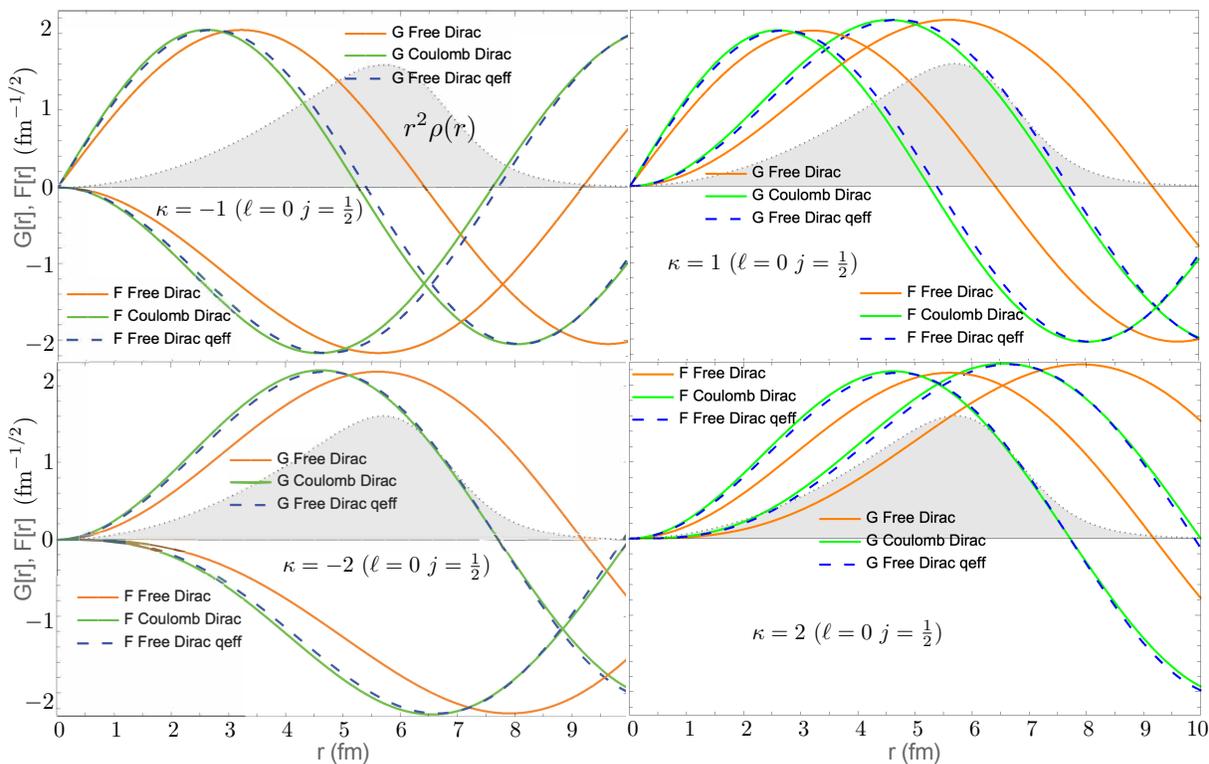
Figure 2.3: Same as Fig. 2.1 but for ^{184}W.

More quantitatively, we can assess the validity of the effective momentum approximation by computing the relative RMS error

$$\langle \delta G^2 \rangle_{\mathrm{RMS}} \equiv \left(\frac{\int dr \; \rho(r) \left(G(r) - G_{\mathrm{eff}}(r) \right)^2}{\int dr \; \rho(r) G(r)^2} \right)^{1/2}, \tag{2.37}$$

where $G(r)$ is the numerical Coulomb solution and $G_{\mathrm{eff}}(r)$ is the effective momentum plane-wave solution given by Eq. (2.36). An analogous definition can be made for $\langle \delta F^2 \rangle_{\mathrm{RMS}}$. This quantity should provide a reliable estimate of the error incurred in generic $\mu \to e$ transition matrix elements. The results for all of our nuclei of interest are shown in Table 2.2. For the light- and medium-mass targets of primary interest, the relative errors in the EMA wave function are at or below the level of 2% in each partial wave considered. Even in our fiducial heavy nucleus ^{184}W, the effective momentum approximation continues to perform very well, with errors consistently below the 10% level. Also shown in Table 2.2 is the relative RMS error of the free Dirac plane wave solution at the physical momentum q relative to the numerical Coulomb solution. Even in the lightest targets, the uncorrected plane wave suffers $\approx 5\%$ errors that quickly grow with A to exceed 10%. The EMA results in systematic improvement, reducing the RMS error by roughly a factor of 5-10 across the various nuclei and partial waves. In particular, the EMA reduces the average RMS deviation from $8\% \to 1\%$ in ^{27}Al, $14\% \to 2\%$ in ^{63}Cu, and $33\% \to 5\%$ in ^{184}W.

When considering the most general effective theory of $\mu \to e$ conversion, we must rely on many-body nuclear physics calculations that—even at the present state-of-the-art—do not have rigorous uncertainty quantification, especially for the medium-mass nuclei of primary interest. In our approach, we rely on nuclear shell-model wave functions obtained from phenomenological interactions that have been tuned to reproduce nuclear charge radii and low-lying spectra. The errors that result when such interactions are used to compute generic nuclear response functions are not well understood. Certainly, errors at least at the level of 10% would not be unexpected. For this reason, we are able to tolerate the few-percent error in the electron wave functions introduced through the EMA. As we shall demonstrate, the dramatic simplifications that this approximation enables are very much worth the associated errors, particularly considering that searches for $\mu \to e$ conversion are presently in the initial discovery phase.

2.4 Approximate Treatment of the Bound Muon

Muons that are trapped by the target quickly de-excite to the $1s$ ($\kappa = -1$) orbital of the nuclear Coulomb field. As discussed above, it is possible to obtain a highly accurate wave function for the bound muon by numerical solution of the Dirac equation. Despite the complexity of these solutions, the physics of the captured muon can be understood rather simply.

First, for light- to medium-mass nuclei, the muon is essentially non-relativistic. Figure 2.4 shows the upper and lower components of the muon's Dirac wave function, as well as the corresponding Schrödinger solution in the nuclei ^{27}Al and ^{48}Ti. For both targets, the Schrödinger solution is an excellent approximation to the upper component of the Dirac solution. Furthermore, we can appraise the relative importance of the muon's lower component

Target	\% RMS Error							
	G_{-1}	F_{-1}	G_{+1}	F_{+1}	G_{-2}	F_{-2}	G_{+2}	F_{+2}
^{12}C	0.34\%	0.44\%	0.72\%	0.24\%	1.05\%	1.78\%	1.32\%	1.53\%
^{12}C	2.22\%	4.87\%	5.29\%	1.99\%	3.68\%	5.90\%	6.32\%	3.23\%
^{16}O	0.47\%	0.61\%	0.95\%	0.23\%	0.90\%	1.60\%	1.16\%	1.37\%
^{16}O	2.86\%	5.83\%	6.24\%	2.58\%	4.56\%	7.39\%	7.80\%	4.13\%
^{19}F	0.54\%	0.72\%	1.07\%	0.27\%	0.78\%	1.44\%	1.02\%	1.22\%
^{19}F	3.19\%	6.13\%	6.53\%	2.94\%	4.89\%	7.85\%	8.25\%	4.46\%
^{23}Na	0.64\%	0.91\%	1.27\%	0.34\%	0.81\%	1.48\%	1.07\%	1.25\%
^{23}Na	3.79\%	7.29\%	7.69\%	3.56\%	5.85\%	9.53\%	9.93\%	5.43\%
^{27}Al	0.70\%	1.05\%	1.42\%	0.41\%	0.66\%	1.27\%	0.90\%	1.08\%
^{27}Al	4.35\%	8.02\%	8.41\%	4.17\%	6.60\%	10.92\%	11.31\%	6.18\%
^{28}Si	0.74\%	1.13\%	1.50\%	0.46\%	0.60\%	1.17\%	0.83\%	0.98\%
^{28}Si	4.72\%	8.31\%	8.69\%	4.57\%	6.91\%	11.42\%	11.80\%	6.50\%
^{32}S	0.84\%	1.33\%	1.70\%	0.57\%	0.61\%	1.10\%	0.83\%	0.91\%
^{32}S	5.52\%	9.11\%	9.47\%	5.39\%	7.63\%	12.51\%	12.88\%	7.24\%
^{40}Ca	0.95\%	1.51\%	1.87\%	0.76\%	0.60\%	0.85\%	0.84\%	0.64\%
^{40}Ca	7.24\%	9.98\%	10.33\%	7.19\%	8.69\%	14.46\%	14.82\%	8.31\%
^{48}Ti	1.04\%	1.57\%	1.92\%	0.91\%	0.76\%	0.87\%	1.02\%	0.61\%
^{48}Ti	8.47\%	10.13\%	10.46\%	8.47\%	8.99\%	14.91\%	15.27\%	8.63\%
^{56}Fe	1.23\%	1.73\%	2.07\%	1.16\%	0.93\%	1.05\%	1.30\%	0.67\%
^{56}Fe	10.54\%	11.17\%	11.49\%	10.57\%	10.08\%	16.90\%	17.25\%	9.74\%
^{63}Cu	1.46\%	1.89\%	2.22\%	1.42\%	1.16\%	1.30\%	1.60\%	0.85\%
^{63}Cu	12.35\%	11.95\%	12.24\%	12.39\%	10.85\%	17.87\%	18.21\%	10.53\%
^{184}W	6.64\%	4.39\%	4.38\%	6.67\%	2.60\%	3.43\%	3.76\%	2.40\%
^{184}W	47.79\%	28.17\%	28.13\%	47.91\%	25.77\%	26.60\%	26.86\%	25.76\%

Table 2.2: Relative root-mean-square error $\langle \delta G^2 \rangle_{\mathrm{RMS}}$, $\langle \delta F^2 \rangle_{\mathrm{RMS}}$ between the numerical Coulomb solutions G, F and the free Dirac plane wave solutions G_q, F_q. For each target, the top line corresponds to the effective momentum plane-wave solutions with momentum q_{eff} whereas the bottom line corresponds to the plane wave solutions with the physical momentum q.
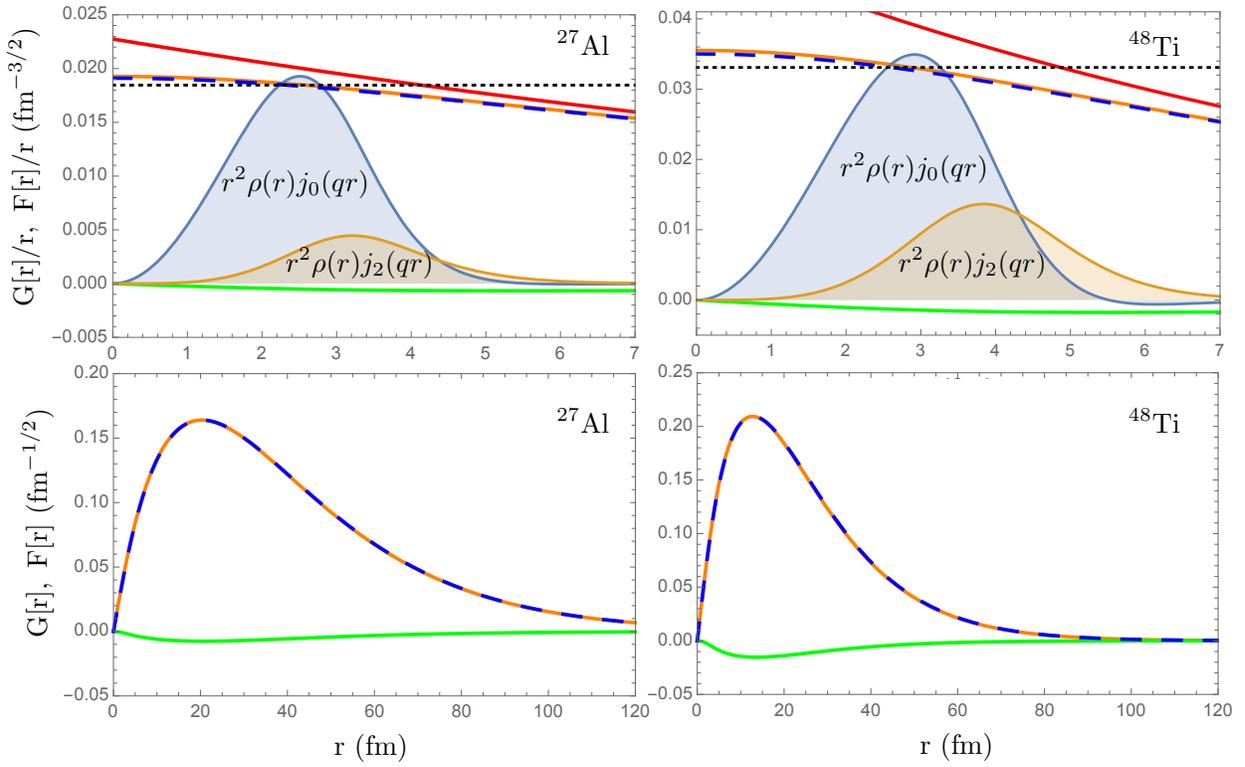
Figure 2.4: Lower panels: muon $\kappa = -1$ bound-state Dirac solutions $G(r)/r$ (orange line) and $F(r)/r$ (green) are shown for ^{27}Al (left) and ^{48}Ti (right), along with the Schrödinger solutions (blue dashed). These solutions are computed for extended nuclear charges, using the parameterizations of Table 2.1, and are properly normalized. Upper panels: the $G(r)$ (orange), $F(r)$ (green), and Schrödinger (red) solutions; also shown are the volume-weighted charge distributions $r^2\rho(r)j_0(qr)$ and $r^2\rho(r)j_2(qr)$ (shaded). The overall normalization (but not the relative normalization) of the two densities is arbitrary. As the muon wave function varies slowly over the extent of the nucleus, it is appropriate to use an average value: the black dotted line is the value obtained by averaging over $r^2\rho(r)j_0(qr)$.

by evaluating the ratio $F(r)/G(r)$. As the behavior of the muon wave functions is most important over the extent of the nucleus, a natural radius at which to measure this ratio is the radius R_0 at which the nuclear density $r^2\rho(r)$ peaks. Table 2.3 shows the ratio $|F(R_0)/G(R_0)|$ evaluated in several nuclei of interest, ranging from the very light ^{12}C to the very heavy ^{184}W. In the nucleus ^{27}Al, the lower component amounts to roughly a 3% correction to the $\mu \to e$ conversion amplitude. For sufficiently heavy nuclei, relativistic effects exceed the 10% level.

More concretely, we can assess the importance of the muon's lower component in the evaluation of a particular matrix element contributing to the $\mu \to e$ conversion amplitude. Substituting the EMA form of the electron wave function into the coherent interaction of Eq. (2.25), the relevant transition operator is

$$\hat{M} = q_{\text{eff}} \int_0^\infty dr\, r \left(j_0(q_{\text{eff}}r)G_{-1}^{(\mu)}(r) + j_1(q_{\text{eff}}r)F_{-1}^{(\mu)}(r) \right) \rho_N(r). \tag{2.38}$$

We can compute the relative contribution of the muon's lower component by defining

$$\delta \langle \hat{M} \rangle \equiv \frac{\int dr\, r j_1(q_{\text{eff}}r)\rho_N(r)F_{-1}^{(\mu)}(r)}{\int dr\, r \left(j_0(q_{\text{eff}}r)G_{-1}^{(\mu)}(r) + j_1(q_{\text{eff}}r)F_{-1}^{(\mu)}(r) \right) \rho_N(r)}. \tag{2.39}$$

The resulting values of $\delta \langle \hat{M} \rangle$ are shown in Table 2.3. In ^{27}Al, the muon's lower component contributes $\approx 2\%$ of the conversion amplitude, roughly in line with the more general estimate based on $|F(R_0)/G(R_0)|$. In ^{184}W, the lower component contributes approximately $1/4$ of the total coherent amplitude, twice the value obtained by evaluating the radial wave functions at the peak of the nuclear density.

Effectively, the lower component is generated by the action of the muon velocity operator $\vec{v}_\mu$ on the upper component, and therefore one can interpret the relative suppression of the lower component as reflecting the fact that the muon velocity is small; indeed, in ^{27}Al $\sqrt{\langle \vec{v}_\mu^2 \rangle} \approx 0.05$. As the electron is ultra-relativistic—with upper and lower components always contributing significantly—the muon's lower component consistently appears in conjunction with its upper component, permitting one to view the lower component as a correction.

Based on these appraisals, we shall at present entirely neglect the lower component of the muon's Dirac wave function. Correspondingly, in our initial formulation of the nuclear effective theory, we will overlook the impact of the muon velocity operator. These omissions are rectified in Chapter 7, where we extend the nuclear effective theory to include the muon velocity operator (and hence the lower component). The essential structure of the effective theory—as well as the insights obtained from it—are not significantly altered by this generalization, and so we now proceed with the construction of the effective theory sans lower component.

Having dispensed with the lower component of the muon's Dirac wave function, we now aim to replace the upper component by an approximate form. Focusing on ^{27}Al, the muonic Bohr radius $a_\mu^0 \approx 19.7$ fm is large compared to either the nuclear radius $r_N^{\text{rms}} = \sqrt{\langle r^2 \rangle} \approx 3.1$ fm or the scale over which the outgoing electron wave function varies, which is given by the first zero of the Bessel function $j_0(qr)$, $r_e \approx \frac{\pi}{q} \approx \frac{\pi}{m_\mu} \approx 5.9$ fm. Adopting the EMA plane-wave form for the electron, the muon wave function will be folded with ground-state

Target	$\left\|\frac{F(R_0)}{G(R_0)}\right\|$	$\delta\langle\hat{M}\rangle$	Target	$\left\|\frac{F(R_0)}{G(R_0)}\right\|$	$\delta\langle\hat{M}\rangle$	Target	$\left\|\frac{F(R_0)}{G(R_0)}\right\|$	$\delta\langle\hat{M}\rangle$
^{12}C	0.013	0.007	^{27}Al	0.030	0.019	^{48}Ti	0.049	0.039
^{16}O	0.018	0.010	^{28}Si	0.032	0.021	^{56}Fe	0.057	0.048
^{19}F	0.020	0.012	^{32}S	0.036	0.024	^{63}Cu	0.062	0.056
^{23}Na	0.025	0.015	^{40}Ca	0.045	0.033	^{184}W	0.13	0.26

Table 2.3: Two measures of the importance of the muon's lower component: $|F(R_0)/G(R_0)|$, the ratio of the lower $F(r)$ to upper $G(r)$ components of the muon's Dirac wave function evaluated at the radius R_0 where the nuclear density $r^2\rho(r)$ peaks. $\delta\langle\hat{M}\rangle$, the contribution of the muon's lower component to the coherent amplitude.

matrix elements of local nuclear operators as

$$\int d^3r\ e^{-i\vec{q}_{\mathrm{eff}}\cdot\vec{r}}\phi_{1s}^\mu(\vec{r})\,\langle g.s.|\sum_{i=1}^A\mathcal{O}(i)\delta(\vec{r}-\vec{r}_i)|g.s.\rangle\,. \tag{2.40}$$

It is instructive to consider the case of a point-like nucleus. In this limit, two simplifications arise: First, the Coulomb potential of the nucleus is that of a point-like charge, and the resulting wave function of the muon has a known analytic form. Second, as the nuclear density is concentrated entirely at the origin, the only relevant part of the muon wave function is the value at $\vec{r}=0$. Explicitly,

$$\int d^3r\ e^{-i\vec{q}_{\mathrm{eff}}\cdot\vec{r}}\phi_{1s}^\mu(\vec{r})\,\langle g.s.|\sum_{i=1}^A\mathcal{O}(i)\delta(\vec{r}-\vec{r}_i)|g.s.\rangle \to \phi_{1s}^Z(\vec{0})\,\langle g.s.|\sum_{i=1}^A\mathcal{O}(i)|g.s.\rangle\,, \tag{2.41}$$

where it is known from the point-like Schrödinger solution that

$$\phi_{1s}^Z(\vec{0})=\frac{1}{\sqrt{\pi}}\left[\frac{Z\alpha\mu c}{\hbar}\right]^{3/2}. \tag{2.42}$$

Returning to the case of an extended nuclear charge distribution, as the upper component of the muon wave function varies slowly over the extent of the nuclear density, we may replace the complicated numerical solution by a constant value

$$\int d^3r\ e^{-i\vec{q}_{\mathrm{eff}}\cdot\vec{r}}\phi_{1s}^\mu(\vec{r})\,\langle g.s.|\sum_{i=1}^A\mathcal{O}(i)\delta(\vec{r}-\vec{r}_i)|g.s.\rangle$$
$$=\phi_{1s}^{\mathrm{avg}}\int d^3r\ e^{-i\vec{q}_{\mathrm{eff}}\cdot\vec{r}}\,\langle g.s.|\sum_{i=1}^A\mathcal{O}(i)\delta(\vec{r}-\vec{r}_i)|g.s.\rangle\,. \tag{2.43}$$

Of course, there are many inequivalent—but physically reasonable—ways to define the average value ϕ_{1s}^{avg}. When it is present, the isoscalar monopole operator

$$M_{00;0}(q)=\sum_{i=1}^A j_0(qr_i)Y_{00}(\hat{r}_i), \tag{2.44}$$

is expected to dominate the elastic $\mu \to e$ transition amplitude, we define the average muon value as

$$\phi_{1s}^{\mathrm{avg}} \equiv \frac{\langle g.s.| \sum_i j_0(q_{\mathrm{eff}} r_i) Y_{00}(\hat{r}_i) \phi_{1s}^{\mu}(\vec{r}_i)|g.s.\rangle}{\langle g.s.| \sum_i j_0(q_{\mathrm{eff}} r_i) Y_{00}(\hat{r}_i)|g.s.\rangle}$$
$$= \frac{1}{\sqrt{4\pi}} \frac{\int dr\ r\rho(r) j_0(q_{\mathrm{eff}} r) G(r)}{\int dr\ r^2 \rho(r) j_0(q_{\mathrm{eff}} r)}, \tag{2.45}$$

so that the $M_{00;0}$ transition amplitude is exactly reproduced. In analogy with the point-like limit, we can parameterize the average muon value in terms of the point-like Schrödinger solution with an effective nuclear charge Z_{eff}

$$\phi_{1s}^{\mathrm{avg}} = \phi_{1s}^{Z_{\mathrm{eff}}}(\vec{0}) = \frac{1}{\sqrt{\pi}} \left[\frac{Z_{\mathrm{eff}} \alpha \mu c}{\hbar} \right]^{3/2}. \tag{2.46}$$

An alternative parameterization that is common in the muon capture literature (see e.g., Ref. [65]) is to write the average wave function in terms of a reduction factor $R < 1$ defined by

$$|\phi_{1s}^{\mathrm{avg}}(\vec{0})|^2 \equiv R|\phi_{1s}^{Z}(\vec{0})|^2, \tag{2.47}$$

from which it follows that R is given by the cube of the ratio of the effective charge to the physical charge

$$R = \left(\frac{Z_{\mathrm{eff}}}{Z} \right)^3. \tag{2.48}$$

The values of R and Z_{eff} for our nuclear targets of interest are shown in Table 2.1. It is clear from these results that the finite nuclear size is crucial to the physics of $\mu \to e$ conversion; even for the relatively light nucleus ^{27}Al (with a charge radius $\sqrt{\langle r^2 \rangle} = 3.062$ fm) the coherent conversion rate is reduced by $\approx 35\%$ compared to the point-like nucleus result.

As discussed above, we have chosen to define the average muon value in order to exactly reproduce the matrix element of the isoscalar monopole operator. Therefore, errors will only be incurred when this constant value is employed in the calculation of other transition amplitudes. For example, consider the *isovector* monopole operator

$$M_{00;1}(q) = \sum_{i=1}^{A} j_0(q r_i) Y_{00}(\hat{r}_i) \tau_3(i), \tag{2.49}$$

which depends on the isovector nuclear density $\rho_p(r) - \rho_n(r)$. In ^{27}Al, the isovector density is approximately that of a single $1d_{5/2}$ proton hole in a ^{28}Si core. We see from Table 2.4 that one incurs an error of $\approx 2\%$ in the $\mu \to e$ decay rate by using the value of R (Z_{eff}) defined for the operator $M_{00;0}$ to compute matrix elements of $M_{00;1}$. By a similar token, the ground state of ^{27}Al carries total angular momentum $J = 5/2$, and therefore the nuclear charge generates contributions not just from the monopole (M_0) but also the quadrupole (M_2) and hexadecapole (M_4) operators as well. Figure 2.4 illustrates the difference in nuclear transition densities between the monopole and quadrupole operators—not including the additional effects of nuclear structure. As shown in Table 2.4, the inclusion of the $J > 0$ charge multipole operators alters the computed value of R (and hence the $\mu \to e$ rate) by

Target	R and % variation					
	$W_{M_0}^{00}$	W_M^{00}	$W_{M_0}^{pp}$	W_M^{pp}	$W_{M_0}^{11}$	W_M^{11}
^{27}Al	0.6566	0.6565	0.6570	0.6569	0.6434	0.6417
	0.00%	-0.01%	0.07%	0.06%	-2.01%	-2.26%
^{63}Cu	0.3204	0.3204	0.3200	0.3199	0.3287	0.3281
	0.00%	-0.01%	-0.15%	-0.16%	2.58%	2.38%
	$W_{\Sigma_1'}^{00}$	$W_{\Sigma'}^{00}$	$W_{\Sigma_1'}^{pp}$	$W_{\Sigma'}^{pp}$	$W_{\Sigma_1'}^{11}$	$W_{\Sigma'}^{11}$
^{27}Al	0.6475	0.6463	0.6513	0.6495	0.6561	0.6533
	-1.38%	-1.56%	-0.81%	-1.08%	-0.07%	-0.49%
^{63}Cu	0.3689	0.3141	0.3673	0.3085	0.3655	0.3026
	15.11%	-1.99%	14.62%	-3.72%	14.05%	-5.58%
	$W_{\Sigma_1''}^{00}$	$W_{\Sigma''}^{00}$	$W_{\Sigma_1''}^{pp}$	$W_{\Sigma''}^{pp}$	$W_{\Sigma_1''}^{11}$	$W_{\Sigma''}^{11}$
^{27}Al	0.6345	0.6339	0.6338	0.6332	0.6331	0.6323
	-3.36%	-3.45%	-3.46%	-3.56%	-3.58%	-3.69%
^{63}Cu	0.3275	0.2951	0.3228	0.2921	0.3182	0.2891
	2.20%	-7.92%	0.74%	-8.85%	-0.71%	-9.77%

Table 2.4: Variation in the constant muon approximation that results from averaging over transition densities other than the isoscalar monopole. The exact transition probability containing the muon wave function $G(r)/r$ has been computed for the odd-proton targets ^{27}Al and ^{63}Cu, for the charge M, transverse spin Σ', and longitudinal spin Σ'' operators, and for isoscalar (00), isovector (11), and proton (pp) couplings. The probability is then re-expressed with an effective constant Coulomb density proportional to the point-nucleus Schrödinger density, $R|\phi_{1s}^Z(\vec{0})|^2$, where R is a parameter adjusted to reproduce the exact result. For cases in which the operator appears with a subscript 0 (e.g., M_0), this exercise was performed by retaining only the leading multipole ($J_0 = 0$ for M, and $J_0 = 1$ for Σ' and Σ''). Otherwise, it was done using the full structure function. The second row of entries shows the percent deviation in the resulting value of R compared to the standard value, that obtained by averaging over the isoscalar monopole M_0.

$\approx 0.01\%$ in ^{27}Al. This effect is so small primarily because of the coherent enhancement of the monopole contribution.

We also consider the error incurred by employing the constant muon value in the calculation of the spin-dependent operators Σ' and Σ'', which correspond, respectively, to the transverse and longitudinal components of the nuclear spin current. In ^{27}Al, the typical size of these errors—as a variation in the determined value of R—is $\lesssim 3\%$. As R corresponds to a probability, the use of a fixed R across all responses in this target nucleus will affect limits derived on CLFV parameters at the level of $\lesssim 1\%$.

2.5   Comparison to Other Works

Not long after Feinberg's original work on $\mu \to e\gamma$, Weinberg & Feinberg [66] considered the analogous process in a muonic atom, wherein the photon is virtual and exchanged with the nuclear charge (see Fig. 6.1). This was the first calculation of $\mu \to e$ conversion in nuclei. In their formulation, the outgoing electron is treated as a free Dirac plane wave, and the bound muon is taken to be a constant parameterized by an effective charge Z_{eff}. Weinberg & Feinberg adopted the following definition of Z_{eff}, employed first by Wheeler [67]—and later by Primakoff [68]—in the study of standard muon capture:

$$
\begin{aligned}
\langle \phi_{1s}^{\tilde{Z}_{\text{eff}}}(\vec{0}) \rangle^2 &\equiv \frac{1}{\pi} \left(\frac{\alpha \mu c}{\hbar} \right)^3 \frac{\tilde{Z}_{\text{eff}}^4}{Z} \\
&\equiv \frac{\int d^3r \; \rho_p(r) |\phi_{1s}^\mu(\vec{r})|^2}{\int d^3r \; \rho_p(r)},
\end{aligned}
\tag{2.50}
$$

where we have introduced the notation $\tilde{Z}_{\text{eff}}$ to distinguish this definition of the effective charge from that which we adopted in the previous section. Two important differences should be noted: First, $\tilde{Z}_{\text{eff}}$ is computed by averaging the muon *probability* over the nuclear proton density $\rho_p(r)$ whereas Z_{eff} is computed by averaging the muon *amplitude* over the isoscalar monopole transition density $j_0(q_{\text{eff}}r)\rho(r)$. The latter quantity has the advantage that it exactly reproduces the leading coherent operator contributing to elastic $\mu \to e$ conversion. On the other hand, $\tilde{Z}_{\text{eff}}$ is more appropriate for the inclusive process of standard muon capture in which no single transition is expected to dominate. Indeed, the rate for standard muon capture obeys

$$
\begin{aligned}
\Gamma_{\text{capture}} &\propto \sum_f F(E_f) |\langle i|\Omega \, \phi_{1s}^\mu(\vec{r})|f\rangle|^2 \\
&\approx F(\bar{E}_f) \sum_f |\langle i|\Omega \phi_{1s}^\mu(\vec{r})|f\rangle|^2 \\
&\approx F(\bar{E}_f) \langle i|\Omega^\dagger \Omega |\phi_{1s}^\mu(\vec{r})|^2|i\rangle \\
&\approx \frac{\int d^3r \; \rho(r) |\phi_{1s}^\mu(\vec{r})|^2}{\int d^3r \; \rho(r)} F(\bar{E}_f) \langle i|\Omega^\dagger \Omega|i\rangle,
\end{aligned}
\tag{2.51}
$$

where Ω is a nuclear operator, and, after replacing the final-state phase space factor $F(E_f)$ by an average value, the sum over final states has been completed by the closure approximation.

Therefore, in the case of muon capture, the appropriate average value of the muon wave function is, in fact, the ground-state average of the muon probability.

The second significant difference between the two definitions of the effective charge is the fact that $Z_{\text{eff}}^3 \propto |\phi_{1s}^\mu|^2$ whereas $\tilde{Z}_{\text{eff}}^4 \propto |\phi_{1s}^\mu|^2$. Where does the extra power of the effective charge in the latter expression originate? Once again, the answer lies in the inclusive nature of standard muon capture, which is typically dominated by first-forbidden nuclear transitions. Consequently, rather than the naïve closure approximation invoked in Eq. (2.51), the rate for standard muon capture is governed by a modified Thomas-Reiche-Kuhn sum rule [69], leading to an additional dependence $\propto Z/2$. Thus, the effective charge in muon capture reflects a subtle combination of Coulomb and nuclear structure effects whereas the effective charge in $\mu \to e$ conversion is meant only to account for the softening of the Coulomb potential due to the finite nuclear extent. Unfortunately, this distinction has frequently been overlooked in the $\mu \to e$ conversion literature, with many authors adopting the definition appropriate to muon capture. Table 2.5 provides an incomplete survey of the $\mu \to e$ conversion literature. Beginning with the work of Shanker, studies of coherent conversion frequently retain the full Dirac forms of the muon and electron wave functions, avoiding altogether the issue of the effective charge.

The majority of the existing literature on $\mu \to e$ conversion is specialized to the coherent case, where the only nuclear operator under consideration is the charge monopole M_0. A few limited works exist concerning incoherent contributions to the elastic conversion process. These investigations of so-called "spin-dependent" conversion augment the spin-independent charge operator with the nuclear spin operator. To our knowledge, the general effective theory has never been constructed, as the nucleon velocity has always been neglected. Several authors have attempted to estimate the strength of inelastic contributions in various target nuclei.

2.6   The Nuclear Diffraction Minimum

One may wonder why the next-generation experiments have chosen a relatively light target, ^{27}Al, rather than opting for a very heavy nucleus (like W, Au, or Pb) that could maximize the coherent enhancement. Naïvely, one expects the coherent nuclear form factor

$$F_0(q_{\text{eff}}) \equiv \int_0^\infty dr \; r^2 j_0(q_{\text{eff}} r) \rho(r), \tag{2.52}$$

to grow proportionally with A. This is certainly true at zero momentum-transfer, as $F_0(0) = A$. However, as is apparent for W^{184} in Fig. 2.3, in heavier nuclei the first zero of the Bessel function $j_0(q_{\text{eff}} r)$ leads to a cancellation and a reduction in the strength of the F_0 form factor. For a given nuclear density, there exists some value of q_{eff} such that the cancellation is exact, resulting in a zero in the form factor. This is the first nuclear diffraction minimum. In ^{184}W, this minimum occurs at a momentum of $q = 133.52$ MeV. The effective momentum $q_{\text{eff}} = 114.93$ is sufficiently close to the minimum to significantly depress the coherent contribution. On the other hand, the first diffraction minimum in ^{27}Al occurs at $q = 270.93$ MeV—quite far from the effective momentum $q_{\text{eff}} = 110.81$ MeV—and the resulting cancellation is relatively small. In Table 2.6, we report the value of the coherent form factor evaluated at the relevant

Author(s)	Year [Ref]	Target(s)	Operator(s)	ψ_e	ψ_μ
Weinberg & Feinberg[†]	1959 [66]	Many	$M_{0;p}$	Plane wave	$\langle|\psi_\mu|^2\rangle_\rho$
Marciano & Sanda	1977 [70]	Many	$M_{0;\tau}$	Plane wave	$\langle|\psi_\mu|^2\rangle_\rho$
Shanker	1979 [71]	Many	$M_{0;\tau}$	Dirac	Dirac
Kosmas & Vergados[†]	1990 [72]	Many	$M_{0;\tau}$	Plane wave	$\langle|\psi_\mu|^2\rangle_\rho$
Chiang et al.[†]	1993 [73]	Many	$M_{0;\tau}$	Plane wave	$\langle|\psi_\mu|^2\rangle_\rho$
Kosmas et al.[†]	1993 [74]	^{48}Ti	$M_{0;\tau}$	Plane wave	$\langle|\psi_\mu|^2\rangle_\rho$
Czarnecki, Marciano, & Melnikov	1998 [75]	^{27}Al, ^{48}Ti, ^{208}Pb	$M_{0;\tau}$	Dirac	Dirac
Siiskonen, Suhonen, & Kosmas[†]	2000 [76]	^{27}Al, ^{48}Ti	$M_{J;\tau}\ \Sigma'_{J;\tau}\ \Sigma''_{J;\tau}$	Plane wave	$\langle|\psi_\mu|^2\rangle_\rho$
Kosmas[†]	2001 [77]	^{48}Ti, ^{208}Pb	$M_{J;\tau}\ \Sigma'_{J;\tau}\ \Sigma''_{J;\tau}$	Plane wave	$\langle|\psi_\mu|^2\rangle_\rho$
Kitano, Koike, & Okada	2002 [78]	Many	$M_{0;\tau}$	Dirac	Dirac
Kosmas	2003 [79]	Many	$M_{0;\tau}$	Plane wave	Dirac
Cirigliano et al.	2009 [80]	Many	$M_{0;\tau}$	Dirac	Dirac
Crivellin et al.	2017 [81]	^{27}Al, ^{197}Au	$M_{0;\tau}$	Dirac	Dirac
Bartolotta & Ramsey-Musolf	2018 [56]	^{27}Al	$M_{0;\tau}$	Dirac	Dirac
Cirigliano, Davidson, & Kuno	2018 [82]	^{27}Al	$M_{0;\tau}\ \Sigma'_{J;\tau}\ \Sigma''_{J;\tau}$	Plane wave	$|\phi_{1s}^Z(\vec{0})|^2$
Davidson, Kuno, & Saporta	2018 [83]	^{27}Al, Ti	$M_{0;\tau}\ \Sigma'_{J;\tau}\ \Sigma''_{J;\tau}$	Plane wave	$|\phi_{1s}^Z(\vec{0})|^2$
Civitarese & Tarutina[†]	2019 [84]	^{208}Pb	$M_{0;\tau}$	Plane wave	$|G(R_N)|^2$
Heeck, Szafron, & Uesaka	2022 [85]	Many	$M_{0;\tau}$	Dirac	Dirac
Cirigliano et al.	2022 [57]	^{27}Al,^{48}Ti,^{197}Au,^{208}Pb	$M_{0;\tau}$	Dirac	Dirac

Table 2.5: An incomplete survey of elastic $\mu \to e$ conversion studies including the nuclear targets considered, the nuclear multipole operators evaluated, and the form of the lepton wave functions employed. $\mathcal{O}_{J;\tau}$ means that both isospin structures and all allowed J were included. For the Dirac electron, all of the references surveyed restrict attention to the lowest partial waves $\kappa = \pm 1$. Besides the Dirac solution, the remaining forms of the muon wave function are all constant approximations: $\langle|\psi_\mu|^2\rangle_\rho$ is obtained by averaging the probability of the Dirac solution over the nuclear density, $|\phi_{1s}^Z(\vec{0})|^2$ is the probability of the point-like Schrödinger solution evaluated at the origin, $|G(R_N)|^2$ is the upper component of the muon's Dirac wave function evaluated at the nuclear radius. Superscript † indicates that the reference considers the inelastic process as well, although the information in the table reflects only the treatment of the elastic process.

	^{12}C	^{16}O	^{19}F	^{23}Na	^{27}Al	^{28}Si
$F_0(q_{\text{eff}})$	8.748	10.880	12.312	14.582	16.281	16.380
$\bar{\Gamma}(A)/\bar{\Gamma}(27)$	0.08	0.21	0.31	0.62	1.00	1.17
	^{32}S	^{40}Ca	^{48}Ti	^{56}Fe	^{63}Cu	^{184}W
$F_0(q_{\text{eff}})$	17.952	20.04	22.032	23.968	25.011	18.142
$\bar{\Gamma}(A)/\bar{\Gamma}(27)$	1.64	2.80	3.39	4.84	5.73	5.15

Table 2.6: The value of the coherent form factor $F_0(q_{\text{eff}})$ and the coherent decay rate per target nucleon $\bar{\Gamma}(A) = \Gamma(A)/A$ (normalized by the corresponding value for ^{27}Al) are computed for each target nucleus.

momentum q_{eff} in order to demonstrate the impact of the nuclear diffraction minimum. As A increases towards the medium-mass nuclei ^{48}Ti and ^{56}Fe, the coherent enhancement begins to diminish. Somewhere just beyond ^{63}Cu, the coherent form factor peaks and begins to decrease with increasing A.

In addition to the form factor F_0, the coherent $\mu \to e$ conversion rate Γ is a function of the target-dependent quantities q_{eff} and $|\phi_{1s}^{Z_{\text{eff}}}(\vec{0})|$. In particular,

$$\Gamma \propto q_{\text{eff}}^2 |\phi_{1s}^{Z_{\text{eff}}}(\vec{0})|^2 F_0(q_{\text{eff}})^2. \tag{2.53}$$

Assuming a fixed target mass[1], the optimal nucleus for observing the coherent process is the one that maximizes the rate per target nucleon $\bar{\Gamma}(A) \equiv \Gamma(A)/A$, which we report in Table 2.6 (normalized by the value in ^{27}Al). For light- and medium-mass nuclei, the rate per nucleon increases steadily with A due to the coherent enhancement as well as the strengthening of the nuclear Coulomb potential, which brings the peak of the muon wave function closer to the nucleus. The coherent form factor peaks just beyond ^{63}Cu; for heavier nuclei, the coherent enhancement is outweighed by the reduction from the diffraction minimum, ultimately leading to a diminishing rate per target nucleon. Thus, no advantage is gained by employing a very heavy target. (In this discussion, we have neglected the effect of the muon's lower component, which, depending on the character of the CLFV interaction, may significantly increase or decrease the coherent amplitude in heavy nuclei. Nonetheless, as the underlying nature of CLFV is yet unknown, it is probably unwise to choose a heavy nuclear target based on the tenuous assumption that some considerable relativistic enhancement will occur.)

---

[1]Here, we assume a pure target, whereas typically in conversion experiments natural targets are employed. Considering natural targets would alter the numbers in Table 2.6 somewhat but would not change the conclusion that beyond a certain point the coherent rate per nucleon begins to decrease with increasing A.

Chapter 3

Nuclear Effective Theory

In the previous chapter, we demonstrated that the essential physical behavior of the bound muon and the outgoing electron can be captured by approximate wave functions that dramatically simplify the description of the leptons in $\mu \to e$ conversion. In this chapter, our primary focus is the nucleon degrees of freedom. After performing a standard non-relativistic reduction of the nucleon currents, we demonstrate that when these results are combined with the approximate lepton wave functions, a simplified effective theory emerges that is built from four basic Hermitian vector operators acting between Pauli spinors.

The construction of an effective theory involves the enumeration of all operators that respect the chosen symmetries. The complete effective theory basis is generally an infinite set of operators, each with an unknown coupling coefficient. In order for the theory to have predictive power, we must reduce this basis to a finite number of operators by imposing a power-counting scheme, allowing us to identify and retain all operators through a given order in the (hopefully) small power-counting parameter(s). This truncation should translate to a modest error in the calculation of observables. In a proper effective theory, the accuracy improves systematically as one progresses to higher-order in the power-counting.

In elastic $\mu \to e$ conversion, the dimensionless parameters that govern the power-counting are the three velocities: the average single-nucleon velocity $\vec{v}_N$, the muon velocity $\vec{v}_\mu$, and the nuclear recoil velocity $\vec{v}_T$. In Section 2.4, we argued that the muon velocity can be neglected in our initial formulation of the effective theory. For calculations performed in the target rest frame, the center-of-mass velocity of the recoiling nucleus is quite small, $|\vec{v}_T| \approx q/M_T \approx 0.004$ in ^{27}Al, and therefore this operator can be excluded as well. The average single-nucleon velocity does contribute significantly: Treating ^{27}Al as a single unpaired $1d_{5/2}$ proton, we find $\sqrt{\langle \vec{v}_N^2 \rangle} \approx 0.21$. To achieve better than 10–20% accuracy in the effective theory, we must construct the operator basis through first order in the nucleon velocity. Beyond first order in v_N/c, ambiguities arise in the non-relativistic reduction of the nucleon currents [86].

In similar formulations, such as the effective theory of dark matter direct detection, one identifies a power-counting parameter that has the form of the three-momentum transfer divided by some mass scale, typically q/m_N. While this combination does enter into the present construction, we cannot treat it as a *fundamental* small quantity in our theory because—due to the ultra-relativistic nature of the electron—the alternate dimensionless quantity $\hat{q}$ arises naturally in our approach. Thus, operator structures such as $\hat{q} \cdot \vec{\sigma}_L \hat{q} \cdot \vec{\sigma}_N$, which would be heavily suppressed in dark matter effective theory where we must replace

$\hat{q} \to \vec{q}/m_N$, are not necessarily suppressed by any small quantity in the present case.

3.1 Single-nucleon Effective Operator Basis

The available scalar Hermitian operators are those that can be constructed from the lepton and nucleon identity operators 1_L and 1_N and from the four dimensionless three-vectors

$$i\hat{q} = i\frac{\vec{q}}{|\vec{q}|}, \ \vec{v}_N, \ \vec{\sigma}_L, \ \vec{\sigma}_N. \tag{3.1}$$

Here $\hat{q}$ is the unit vector along the direction of the three-momentum transfer to the leptons (or alternatively the velocity of the outgoing ultra-relativistic electron). The average nucleon velocity operator is defined as

$$\vec{v}_N = \frac{1}{2m_N}\left(\vec{p}_i + \vec{p}_f\right), \tag{3.2}$$

where $\vec{p}_i$ and $\vec{p}_f$ are the initial and final nucleon momenta, respectively. Our aim is to combine these six Hermitian "building-block" operators to form new scalar operators that will constitute our effective theory basis. The construction is limited by two constraints: (1) We work to first-order in the average single-nucleon velocity $\vec{v}_N$. (2) The nucleon spin operator can be combined with $\vec{v}_N$ as $\vec{v}_N \cdot \vec{\sigma}_N$ and $\vec{v}_N \times \vec{\sigma}_N$, but not as the rank-two tensor $[\vec{v}_N \otimes \vec{\sigma}_N]_2$, which would not triangulate between spin-$\frac{1}{2}$ nucleon states. We identify a total of 16 independent operators:

$$\begin{aligned}
\mathcal{O}_1 &= 1_L \, 1_N \\
\mathcal{O}_2' &= 1_L \, i\hat{q} \cdot \vec{v}_N \\
\mathcal{O}_3 &= 1_L \, i\hat{q} \cdot [\vec{v}_N \times \vec{\sigma}_N] \\
\mathcal{O}_4 &= \vec{\sigma}_L \cdot \vec{\sigma}_N \\
\mathcal{O}_5 &= \vec{\sigma}_L \cdot (i\hat{q} \times \vec{v}_N) \\
\mathcal{O}_6 &= i\hat{q} \cdot \vec{\sigma}_L \, i\hat{q} \cdot \vec{\sigma}_N \\
\mathcal{O}_7 &= 1_L \, \vec{v}_N \cdot \vec{\sigma}_N \\
\mathcal{O}_8 &= \vec{\sigma}_L \cdot \vec{v}_N \\
\mathcal{O}_9 &= \vec{\sigma}_L \cdot (i\hat{q} \times \vec{\sigma}_N) \\
\mathcal{O}_{10} &= 1_L \, i\hat{q} \cdot \vec{\sigma}_N \\
\mathcal{O}_{11} &= i\hat{q} \cdot \vec{\sigma}_L \, 1_N \\
\mathcal{O}_{12} &= \vec{\sigma}_L \cdot [\vec{v}_N \times \vec{\sigma}_N] \\
\mathcal{O}_{13}' &= \vec{\sigma}_L \cdot (i\hat{q} \times [\vec{v}_N \times \vec{\sigma}_N]) \\
\mathcal{O}_{14} &= i\hat{q} \cdot \vec{\sigma}_L \, \vec{v}_N \cdot \vec{\sigma}_N \\
\mathcal{O}_{15} &= i\hat{q} \cdot \vec{\sigma}_L \, i\hat{q} \cdot [\vec{v}_N \times \vec{\sigma}_N] \\
\mathcal{O}_{16}' &= i\hat{q} \cdot \vec{\sigma}_L \, i\hat{q} \cdot \vec{v}_N
\end{aligned} \tag{3.3}$$

We note that 12 of the 16 operators arise from scalar and vector exchanges whereas $\mathcal{O}_3, \mathcal{O}_{12}, \mathcal{O}_{13}'$ and $\mathcal{O}_{15}$ arise from higher-spin mediators. The 16 Pauli-reduced operators can also be obtained from a complete basis of Lorentz-invariant amplitudes (see Section 3.9).

The operators in Eq. (3.3) form the basis of our effective theory; that is, we may write our effective Lagrangian density as

$$\mathcal{L}_{\text{eff}} = \sum_{\alpha=n,p} \sum_{i=1}^{16} c_i^\alpha \mathcal{O}_i^\alpha, \tag{3.4}$$

where the c_i are the unknown low-energy constants (LECs) of the effective theory, which must be determined from experiment or by matching to a predictive UV theory. We have allowed for each operator to couple distinctly to protons and neutrons. Equivalently, we can transform to the isospin basis, writing

$$\mathcal{L}_{\text{eff}} = \sum_{\tau=0,1} \sum_{i=1}^{16} c_i^\tau \mathcal{O}_i t^\tau, \tag{3.5}$$

where $c_i^0 = \frac{1}{2}(c_i^p + c_i^n)$ and $c_i^1 = \frac{1}{2}(c_i^p - c_i^n)$, and the isospin matrices are $t^0 = 1$ and $t^1 = \tau_3$. Therefore, the effective theory contains a total of 32 unknown parameters associated with 16 space/spin operators each of which can have distinct couplings to protons and neutrons. If we exclude operators that are not associated with spin-0 or spin-1 mediators, 12 space/spin operators and 24 couplings remain. In general, the LECs are complex-valued.

So far, the effective theory is specified at the level of single-nucleon operators. Once these operators are properly embedded in the target nucleus, we will find that the nuclear-level effective theory is more restrictive—although the individual nucleons appear to have 32 independent CLFV responses, the same is not true of the total nuclear system. Our aim is to determine the specific constraints that a program of elastic $\mu \to e$ conversion measurements can place on the single-nucleon LECs.

As defined in Eq. (3.5), the low-energy constants carry dimensions of $1/(\text{mass})^2$. Because experimental results are conventionally expressed as a ratio with respect to the rate of a standard-model muon process, it is convenient to introduce a set of dimensionless LECs $\tilde{c}_i$ defined with respect to the weak scale

$$c_i \equiv \tilde{c}_i/v^2 = \sqrt{2} G_F \tilde{c}_i, \tag{3.6}$$

where $v = 246.2$ GeV is the Higgs vacuum expectation value, and $G_F = 1.166 \times 10^{-5}$ GeV^{-2} is the Fermi constant. Alternatively, given an experimental measurement (or limit) on an LEC, one can define a typical energy scale associated with the CLFV physics

$$\Lambda_i^\tau \equiv \frac{1}{\sqrt{|c_i^\tau|}} = \frac{v}{\sqrt{|\tilde{c}_i^\tau|}}. \tag{3.7}$$

In fact, we may characterize the sensitivity of a particular experimental search in terms of the reach in energy scale Λ_i^τ (which is operator-dependent).

Having specified the effective Lagrangian, it is relatively straightforward to obtain an expression for the $\mu \to e$ conversion rate. In order to arrive at a simple expression that factorizes the nuclear physics from the CLFV physics, we proceed by performing a multipole expansion of the nuclear charges and currents.

3.2 One-Body Nuclear Charges and Currents

The nucleon-level effective operators of Eq. (3.3) contain two single-nucleon charges: scalar 1_N and axial $\vec{v}_N \cdot \vec{\sigma}_N$, and three single-nucleon currents: spin $\vec{\sigma}_N$, velocity $\vec{v}_N$, and spin-velocity $\vec{\sigma}_N \times \vec{v}_N$. These charges and currents naturally arise in the non-relativistic expansion of Lorentz-covariant nucleon currents (see Appendix A.1). In order to embed these single-nucleon operators in a many-nucleon system, we define the total nuclear charge $J_0(\vec{x})$ and axial charge $J_0^A(\vec{x})$ operators as

$$
\begin{aligned}
J_0(\vec{x}) &\equiv \sum_{i=1}^{A} \delta(\vec{x} - \vec{x}_i), \\
J_0^A(\vec{x}) &\equiv \sum_{i=1}^{A} \frac{1}{2m_N} \left[-\frac{1}{i} \overleftarrow{\nabla}_i \cdot \vec{\sigma}_N(i) \delta(\vec{x} - \vec{x}_i) + \delta(\vec{x} - \vec{x}_i) \vec{\sigma}_N(i) \cdot \frac{1}{i} \overrightarrow{\nabla}_i \right],
\end{aligned}
\tag{3.8}
$$

and the total nuclear velocity current $\vec{J}_c(\vec{x})$, spin current $\vec{J}_A(\vec{x})$ and spin-velocity current $\vec{J}_M(\vec{x})$ operators as

$$
\begin{aligned}
\vec{J}_c(\vec{x}) &\equiv \sum_{i=1}^{A} \frac{1}{2m_N} \left[-\frac{1}{i} \overleftarrow{\nabla}_i \delta(\vec{x} - \vec{x}_i) + \delta(\vec{x} - \vec{x}_i) \frac{1}{i} \overrightarrow{\nabla}_i \right], \\
\vec{J}_A(\vec{x}) &\equiv \sum_{i=1}^{A} \vec{\sigma}_N(i) \delta(\vec{x} - \vec{x}_i), \\
\vec{J}_M(\vec{x}) &\equiv \sum_{i=1}^{A} \frac{1}{2m_N} \left[\overleftarrow{\nabla}_i \times \vec{\sigma}_N(i) \delta(\vec{x} - \vec{x}_i) + \delta(\vec{x} - \vec{x}_i) \vec{\sigma}_N(i) \times \overrightarrow{\nabla}_i \right].
\end{aligned}
\tag{3.9}
$$

Defining the corresponding leptonic charges and currents

$$
\begin{aligned}
l_0^\tau &\equiv c_1^\tau 1_L + c_{11}^\tau i\hat{q} \cdot \vec{\sigma}_L \\
l_0^{A\,\tau} &\equiv c_7^\tau 1_L + c_{14}^\tau i\hat{q} \cdot \vec{\sigma}_L \\
\vec{l}_5^\tau &\equiv c_4^\tau \vec{\sigma}_L + c_6^\tau i\hat{q} \cdot \vec{\sigma}_L i\hat{q} - c_9^\tau i\hat{q} \times \vec{\sigma}_L + c_{10}^\tau i\hat{q} 1_L \\
\vec{l}_M^\tau &\equiv c_2^\tau i\hat{q} 1_L - c_5^\tau i\hat{q} \times \vec{\sigma}_L + c_8^\tau \vec{\sigma}_L + c_{16}^\tau i\hat{q} \cdot \vec{\sigma}_L i\hat{q} \\
\vec{l}_E^\tau &\equiv -c_3^\tau \hat{q} 1_L + c_{12}^\tau i\vec{\sigma}_L + c_{13}^\tau \hat{q} \times \vec{\sigma}_L - ic_{15}^\tau \hat{q} \cdot \vec{\sigma}_L \hat{q},
\end{aligned}
\tag{3.10}
$$

we may write our effective Hamiltonian density as

$$
\begin{aligned}
\mathcal{H}_{\text{eff}}(\vec{x}) = & \sqrt{\frac{E_e}{2m_e}} |\phi_{1s}^{Z_{\text{eff}}}(\vec{0})| \frac{q_{\text{eff}}}{q} e^{-i\vec{q}_{\text{eff}} \cdot \vec{x}} \sum_{\tau=0,1} \left[l_0^\tau \sum_{i=1}^{A} \delta(\vec{x} - \vec{x}_i) \right] \\
& + l_0^{A\,\tau} \sum_{i=1}^{A} \frac{1}{2m_N} \left(-\frac{1}{i} \overleftarrow{\nabla}_i \cdot \vec{\sigma}_N(i) \delta(\vec{x} - \vec{x}_i) + \delta(\vec{x} - \vec{x}_i) \vec{\sigma}_N(i) \cdot \frac{1}{i} \overrightarrow{\nabla} \right) \\
& + \vec{l}_5^\tau \cdot \sum_{i=1}^{A} \vec{\sigma}_N(i) \delta(\vec{x} - \vec{x}_i) + \vec{l}_M^\tau \cdot \sum_{i=1}^{A} \frac{1}{2m_N} \left(-\frac{1}{i} \overleftarrow{\nabla}_i \delta(\vec{x} - \vec{x}_i) + \delta(\vec{x} - \vec{x}_i) \frac{1}{i} \overrightarrow{\nabla}_i \right) \\
& + \vec{l}_E^\tau \cdot \sum_{i=1}^{A} \frac{1}{2m_N} \left(\overleftarrow{\nabla}_i \times \vec{\sigma}_N(i) \delta(\vec{x} - \vec{x}_i) + \delta(\vec{x} - \vec{x}_i) \vec{\sigma}_N(i) \times \overrightarrow{\nabla}_i \right) \Bigg]_{int} t^\tau(i).
\end{aligned}
\tag{3.11}
$$

Here the subscript *int* denotes that technically the A single-nucleon velocities appearing in the expression should be replaced by the $A - 1$ relative (or Jacobi) velocities. There are techniques for addressing this issue connected with, for example, shell-model techniques that employ single-nucleon coordinates but nevertheless create wave functions where the nuclear center-of-mass is in a definite state, thereby removing the extra degrees of freedom. More commonly, though, this issue is ignored.

Note that if one sets $\vec{v}_N = 0$, l_0^τ and $\vec{l}_5^{\vec{\tau}}$ are unchanged, while $l_0^{A\,\tau}$, $\vec{l}_M^{\vec{\tau}}$, and $\vec{l}_E^{\vec{\tau}}$ all vanish. In this limit—that of a point-like nucleus—the only surviving operators are those associated with the macroscopic nuclear properties of charge and spin.

3.3   The Nuclear Multipole Decomposition

The effective Hamiltonian now has the form of a plane wave multiplying either a nuclear charge as $e^{i\vec{q}\cdot\vec{x}} J_0(\vec{x})$ or current as $e^{i\vec{q}\cdot\vec{x}} \vec{J}(\vec{x})$. In both cases, we may expand the exponential plane-wave factor into partial waves and thereby perform a multipole decomposition of the corresponding nuclear charge/current. Orienting our coordinate system along the direction of three-momentum transfer ($\hat{q} = \hat{e}_0$), the plane-wave factor may be expanded in partial waves as

$$e^{i\vec{q}\cdot\vec{x}} = \sum_{J=0}^{\infty} \sqrt{4\pi(2J+1)} i^J j_J(qx) Y_{J0}(\hat{x}). \tag{3.12}$$

It immediately follows that any local charge density $J_0(\vec{x})$ can be decomposed into multipole operators with good angular momentum quantum numbers J, M as

$$\mathcal{M}_{JM}(q) = \int d^3x \left[j_J(qx) Y_{JM}(\hat{x}) \right] J_0(\vec{x}). \tag{3.13}$$

When the plane wave factor multiplies a vector current, then we may expand the vector current in the spherical basis as

$$\vec{J} = \sum_\lambda J_\lambda \hat{e}_\lambda^*, \tag{3.14}$$

and then use the fact that

$$\hat{e}_\lambda Y_{lm}(\hat{x}) = \sum_{JM} \langle l\, m\, 1\, \lambda | J\, M \rangle \vec{Y}_{J\,l\,M}(\hat{x}) \tag{3.15}$$

to write

$$\hat{e}_\lambda e^{i\vec{q}\cdot\vec{x}} = -\frac{i}{q} \sum_{J=0}^{\infty} \sqrt{4\pi(2J+1)} i^J \vec{\nabla} \left(j_J(qx) Y_{J0}(\hat{x}) \right), \text{ for } \lambda = 0$$

$$= -\sum_{J\geq 1} \sqrt{2\pi(2J+1)} i^J \left[\lambda j_J(qx) \vec{Y}_{JJ\lambda}(\hat{x}) + \frac{1}{q} \vec{\nabla} \times \left(j_J(qx) \vec{Y}_{JJ\lambda}(\hat{x}) \right) \right], \text{ for } \lambda = \pm 1.$$

$$\tag{3.16}$$

Three unique tensor structures arise, reflecting the fact that each vector current can be decomposed into longitudinal, transverse-magnetic, and transverse-electric components. The

corresponding multipole projections are

$$\mathcal{L}_{JM}(q) = \frac{i}{q} \int d^3x \left[\vec{\nabla} \left(j_J(qx) Y_{JM}(\hat{x}) \right) \right] \cdot \vec{J}(\vec{x}),$$

$$\mathcal{T}_{JM}^{\text{mag}}(q) = \int d^3x \left[j_J(qx) \vec{Y}_{JJM}(\hat{x}) \right] \cdot \vec{J}(\vec{x}), \tag{3.17}$$

$$\mathcal{T}_{JM}^{\text{el}}(q) = \frac{1}{q} \int d^3x \left[\vec{\nabla} \times \left(j_J(qx) \vec{Y}_{JJM}(\hat{x}) \right) \right] \cdot \vec{J}(\vec{x}).$$

The multipole projections defined in this section are valid for any local nuclear charge $J_0(\vec{x})$ or current $\vec{J}(\vec{x})$. In the next section, we will construct these projections explicitly for the two nuclear charges and three nuclear currents that appear in the effective theory of elastic $\mu \to e$ conversion.

3.4 Projections of Nuclear Currents and Charges

The two nuclear charges and three nuclear currents that arise in the effective theory of $\mu \to e$ conversion admit a total of eleven distinct multipole response operators, corresponding to one projection of each charge and three independent projections of each current. Indeed, we find the following projections of J_0, J_0^A, $\vec{J}_c$, $\vec{J}_A$, and $\vec{J}_M$:

$$\mathcal{M}_{JM}(J_0) = \sum_{i=1}^{A} M_{JM}(q\vec{x}_i)$$

$$\mathcal{M}_{JM}(J_0^5) = -i\frac{q}{m_N} \sum_{i=1}^{A} \left[\Omega_{JM}(q\vec{x}_i) + \frac{1}{2}\Sigma_{JM}''(q\vec{x}_i) \right]$$

$$\mathcal{L}_{JM}(\vec{J}_A) = i\sum_{i=1}^{A} \Sigma_{JM}''(q\vec{x}_i),$$

$$\mathcal{T}_{JM}^{\text{el}}(\vec{J}_A) = i\sum_{i=1}^{A} \Sigma_{JM}'(q\vec{x}_i),$$

$$\mathcal{T}_{JM}^{\text{mag}}(\vec{J}_A) = \sum_{i=1}^{A} \Sigma_{JM}(q\vec{x}_i)$$

$$\mathcal{L}_{JM}(\vec{J}_c) = \frac{q}{m_N} \sum_{i=1}^{A} \left[\Delta_{JM}''(q\vec{x}_i) - \frac{1}{2}M_{JM}(q\vec{x}_i) \right] \tag{3.18}$$

$$\mathcal{T}_{JM}^{\text{el}}(\vec{J}_c) = \frac{q}{m_N} \sum_{i=1}^{A} \Delta_{JM}'(q\vec{x}_i)$$

$$\mathcal{T}_{JM}^{\text{mag}}(\vec{J}_c) = -i\frac{q}{m_N} \sum_{i=1}^{A} \Delta_{JM}(q\vec{x}_i)$$

$$\mathcal{L}_{JM}(\vec{J}_M) = \frac{q}{m_N} \sum_{i=1}^{A} \Phi_{JM}''(q\vec{x}_i)$$

$$\mathcal{T}_{JM}^{\text{el}}(\vec{J}_M) = \frac{q}{m_N} \sum_{i=1}^{A} \left[\Phi_{JM}'(q\vec{x}_i) + \frac{1}{2}\Sigma_{JM}(q\vec{x}_i) \right]$$

$$\mathcal{T}_{JM}^{\mathrm{mag}}(\vec{J}_M) = -i\frac{q}{m_N}\sum_{i=1}^{A}\left[\Phi_{JM}(q\vec{x}_i) - \frac{1}{2}\Sigma'_{JM}(q\vec{x}_i)\right],$$

where the single-nucleon multipole operators that we obtain are those familiar from the study of semi-leptonic weak interactions [87, 88]. Adding a label to denote isospin, the single-nucleon response functions are

$$M_{JM;\tau}(q) \equiv \sum_{i=1}^{A} M_{JM}(q\vec{x}_i)\, t^\tau(i)$$

$$\Omega_{JM;\tau}(q) \equiv \sum_{i=1}^{A} M_{JM}(q\vec{x}_i)\vec{\sigma}_N(i)\cdot\frac{1}{q}\vec{\nabla}_i\, t^\tau(i)$$

$$\Delta_{JM;\tau}(q) \equiv \sum_{i=1}^{A} \vec{M}_{JJM}(q\vec{x}_i)\cdot\frac{1}{q}\vec{\nabla}_i\, t^\tau(i)$$

$$\Delta'_{JM;\tau}(q) \equiv -i\sum_{i=1}^{A} \left\{\frac{1}{q}\vec{\nabla}_i\times\vec{M}_{JJM}(q\vec{x}_i)\right\}\cdot\frac{1}{q}\vec{\nabla}_i\, t^\tau(i)$$

$$\Delta''_{JM;\tau}(q) \equiv \sum_{i=1}^{A} \left(\frac{1}{q}\vec{\nabla}_i M_{JM}(q\vec{x}_i)\right)\cdot\frac{1}{q}\vec{\nabla}_i\, t^\tau(i)$$

$$\Sigma_{JM;\tau}(q) \equiv \sum_{i=1}^{A} \vec{M}_{JJM}(q\vec{x}_i)\cdot\vec{\sigma}_N(i)\, t^\tau(i) \qquad (3.19)$$

$$\Sigma'_{JM;\tau}(q) \equiv -i\sum_{i=1}^{A} \left\{\frac{1}{q}\vec{\nabla}_i\times\vec{M}_{JJM}(q\vec{x}_i)\right\}\cdot\vec{\sigma}_N(i)\, t^\tau(i)$$

$$\Sigma''_{JM;\tau}(q) \equiv \sum_{i=1}^{A} \left\{\frac{1}{q}\vec{\nabla}_i M_{JM}(q\vec{x}_i)\right\}\cdot\vec{\sigma}_N(i)\, t^\tau(i)$$

$$\Phi_{JM;\tau}(q) \equiv i\sum_{i=1}^{A} \vec{M}_{JJM}(q\vec{x}_i)\cdot\left(\vec{\sigma}_N(i)\times\frac{1}{q}\vec{\nabla}_i\right)\, t^\tau(i)$$

$$\Phi'_{JM;\tau}(q) \equiv \sum_{i=1}^{A} \left(\frac{1}{q}\vec{\nabla}_i\times\vec{M}_{JJM}(q\vec{x}_i)\right)\cdot\left(\vec{\sigma}_N(i)\times\frac{1}{q}\vec{\nabla}_i\right)\, t^\tau(i)$$

$$\Phi''_{JM;\tau}(q) \equiv i\sum_{i=1}^{A} \left(\frac{1}{q}\vec{\nabla}_i M_{JM}(q\vec{x}_i)\right)\cdot\left(\vec{\sigma}_N(i)\times\frac{1}{q}\vec{\nabla}_i\right)\, t^\tau(i),$$

where we have defined the basic multipole projections

$$M_{JM}(q\vec{x}) \equiv j_J(qx)Y_{JM}(\hat{x}),$$
$$\vec{M}_{JLM}(q\vec{x}) \equiv j_L(qx)\vec{Y}_{JLM}(\hat{x}), \qquad (3.20)$$

and $\vec{Y}_{JLM}$ is a vector spherical harmonic (see Appendix B.2).

In addition to carrying angular momentum (J, M) each multipole operator has a well-defined transformation under parity $\vec{x} \to -\vec{x}$. The operators M, Δ', Δ'', Σ, Φ', and Φ'' are *normal parity* operators that transform with a phase $(-1)^J$ under parity whereas Ω, Δ, Σ', Σ'', and Φ are *abnormal parity* operators that transform with a phase $(-1)^{J+1}$ under parity.

Matrix elements of the above multipole operators evaluated between harmonic oscillator states can be expressed analytically in terms of the dimensionless quantity $y = (qb/2)^2$, where b is the parameter that sets the length scale of the harmonic oscillator states. In particular, letting $T_J(q\vec{r})$ represent any of the 11 single-particle operators, we have

$$\langle n' \, (\ell' \, 1/2) \, j' || T_J(q\vec{r}) || n \, (\ell \, 1/2) \, j \rangle = \frac{1}{\sqrt{4\pi}} y^{(J-K)/2} e^{-y} p(y), \qquad (3.21)$$

where $K = 2$ for the normal parity operators M, Δ', Δ'', Σ, Φ', and Φ'', and where $K = 1$ for the abnormal parity operators Ω, Δ, Σ', Σ'', and Φ. The function $p(y)$ is a finite-degree polynomial in y. See Appendix D for a detailed derivation of Eq. (3.21) and other properties of the single-nucleon response functions. For the choices of phase conventions in our definitions, all of the matrix elements are real. In order to discuss time-reversal symmetry, we define the transformed operators

$$\begin{aligned}
\tilde{\Omega}_{JM}(q) &\equiv \Omega_{JM}(q) + \frac{1}{2}\Sigma''_{JM}(q), \\
\tilde{\Delta}''_{JM}(q) &\equiv \Delta''_{JM}(q) - \frac{1}{2}M_{JM}(q), \\
\tilde{\Phi}_{JM}(q) &\equiv \Phi_{JM}(q) - \frac{1}{2}\Sigma'_{JM}(q), \\
\tilde{\Phi}'_{JM}(q) &\equiv \Phi'_{JM}(q) + \frac{1}{2}\Sigma_{JM}(q),
\end{aligned} \qquad (3.22)$$

which have well-defined transformations under the exchange of initial and final single-particle states

$$\langle n \, (\ell \, 1/2) \, j || T_J(q\vec{r}) || n' \, (\ell' \, 1/2) \, j' \rangle = (-1)^\lambda \, \langle n' \, (\ell' \, 1/2) \, j' || T_J(q\vec{r}) || n \, (\ell \, 1/2) \, j \rangle, \qquad (3.23)$$

with $\lambda = j' - j$ for the operators M, Δ, Σ', Σ'', $\tilde{\Phi}'$, and Φ'', and $\lambda = j' + j$ for the operators $\tilde{\Omega}$, Δ', $\tilde{\Delta}''$, Σ, and $\tilde{\Phi}$.

The parity and time-reversal properties of the 11 single-nucleon response functions are summarized in Table 3.1. The restriction of the nucleus to remain in the ground state (which is approximately an eigenstate of P and T) throughout the $\mu \to e$ conversion process now has profound consequences for the form of the nuclear response: only those multipole operators that are even under both parity and time-reversal can contribute to the elastic conversion process. The five operators for which $\lambda = j' + j$ under exchange of initial and final states always have opposite P and T transformations for a given J. Therefore $\tilde{\Omega}$, Δ', $\tilde{\Delta}''$, Σ, and $\tilde{\Phi}$ are entirely excluded from the elastic response. For the remaining multipole operators, we are restricted to either even J for normal parity operators and odd J for abnormal parity operators. Thus, the nuclear response is limited to the six allowed response functions: even multipoles of M, $\tilde{\Phi}'$, and Φ'', and odd multipoles of Δ, Σ', and Σ''. We will now derive an expression for the $\mu \to e$ conversion rate in terms of these six response functions.

3.5   The Elastic $\mu \to e$ Decay Rate

Knowing the multipole decomposition of the relevant nuclear charges and currents, as well as the parity and time-reversal transformation properties of the resulting single-nucleon operators,

Projection	Charge/Current	Operator	Even J	Odd J	LECs Probed
Charge	1_N	M_{JM}	E-E	O-O	c_1, c_{11}
Charge	$\vec{v}_N \cdot \vec{\sigma}_N$	$\tilde{\Omega}_{JM}$	O-E	E-O	c_7, c_{14}
Longitudinal	$\vec{\sigma}_N$	Σ''_{JM}	O-O	E-E	c_4, c_6, c_{10}
Transverse magnetic	"	Σ_{JM}	E-O	O-E	c_4, c_9
Transverse electric	"	Σ'_{JM}	O-O	E-E	c_4, c_9
Longitudinal	$\vec{v}_N$	$\tilde{\Delta}''_{JM}$	E-O	O-E	c_2, c_8, c_{16}
Transverse magnetic	"	Δ_{JM}	O-O	E-E	c_5, c_8
Transverse electric	"	Δ'_{JM}	E-O	O-E	c_5, c_8
Longitudinal	$\vec{v}_N \times \vec{\sigma}_N$	Φ''_{JM}	E-E	O-O	c_3, c_{12}, c_{15}
Transverse magnetic	"	$\tilde{\Phi}_{JM}$	O-E	E-O	c_{12}, c_{13}
Transverse electric	"	$\tilde{\Phi}'_{JM}$	E-E	O-O	c_{12}, c_{13}

Table 3.1: Characteristics of the 11 single-nucleon response functions including the charge/current projection from which they arise, their parity and time-reversal transformation properties, and the LECs of the nucleon-level effective theory that are associated with each response. Based on these results, the elastic $\mu \to e$ conversion amplitude can depend only on even multipoles of M, $\tilde{\Phi}'$, and Φ'', and odd multipoles of Δ, Σ', and Σ''.

we now proceed to compute the $\mu \to e$ decay rate. Beginning from the Hamiltonian density in Eq. (3.11) and letting $j_i = j_f = j_N$ be the total nuclear angular momentum, m_i, m_f the initial and final magnetic quantum numbers of the nuclear state, and s_i, s_f the initial and final magnetic quantum numbers of the leptons, we compute the decay amplitude

$$\mathcal{M} = \langle \tfrac{1}{2} s_f; j_N m_f | \int d^3x \, \mathcal{H}(\vec{x}) \, | \tfrac{1}{2} s_i; j_N m_i \rangle , \tag{3.24}$$

by performing the multipole decomposition of the nuclear charges and currents. The result is

$$\mathcal{M} = \sqrt{\frac{E_e}{2m_e}} |\phi_{1s}^{Z_{\text{eff}}}(\vec{0})| \frac{q_{\text{eff}}}{q} \sum_{\tau=0,1} \langle \tfrac{1}{2} s_f; j_N m_f |$$

$$\left\{ \sum_{J=0,2,\ldots}^{\infty} \sqrt{4\pi(2J+1)}(-i)^J \left[l_0^\tau M_{J0;\tau}(q_{\text{eff}}) + \frac{q_{\text{eff}}}{m_N} l_{E0}^\tau \Phi''_{J0;\tau}(q_{\text{eff}}) \right] \right.$$

$$+ \sum_{J=1,3,\ldots}^{\infty} \sqrt{2\pi(2J+1)}(-i)^J \sum_{\lambda=\pm 1} \left[-i l_{5\lambda}^\tau \Sigma'_{J-\lambda;\tau}(q_{\text{eff}}) + i \frac{q_{\text{eff}}}{m_N} l_{M\lambda}^\tau \lambda \Delta_{J-\lambda;\tau}(q_{\text{eff}}) \right] \tag{3.25}$$

$$+ \sum_{J=2,4,\ldots}^{\infty} \sqrt{2\pi(2J+1)}(-i)^J \sum_{\lambda=\pm 1} \left[-\frac{q_{\text{eff}}}{m_N} l_{E\lambda}^\tau \tilde{\Phi}'_{J-\lambda;\tau}(q_{\text{eff}}) \right]$$

$$\left. + \sum_{J=1,3,\ldots}^{\infty} \sqrt{4\pi(2J+1)}(-i)^J \left[i l_{50}^\tau \Sigma''_{J0;\tau}(q_{\text{eff}}) \right] \right\} | \tfrac{1}{2} s_i; j_N m_i \rangle ,$$

where we note that the leptonic current $l_0^{A\,\tau}$ does not appear because the nuclear axial charge operator (which generates the response $\tilde{\Omega}$) is excluded from the elastic conversion process by

P and T symmetry. Next, we write the amplitude in terms of reduced matrix elements of the nuclear multipole operators using the Wigner-Eckart theorem

$$\langle j_N m_f | T_{JM} | j_N m_i \rangle = (-1)^{j_N - m_f} \begin{pmatrix} j_N & J & j_N \\ -m_f & M & m_i \end{pmatrix} \langle j_N || T_J || j_N \rangle, \tag{3.26}$$

which allows us to compute the nuclear spin-averaged amplitude squared

$$\frac{1}{2j_N + 1} \sum_{m_f, m_i} |\mathcal{M}|^2, \tag{3.27}$$

using the completeness relation for the Wigner 3-j symbols

$$\frac{1}{2j_N + 1} \sum_{m_f, m_i} \begin{pmatrix} j_N & J & j_N \\ -m_f & M & m_i \end{pmatrix} \begin{pmatrix} j_N & J' & j_N \\ -m_f & M' & m_i \end{pmatrix} = \delta_{JJ'} \delta_{MM'} \frac{1}{2J+1} \frac{1}{2j_N+1}. \tag{3.28}$$

The resulting expression is

$$\frac{1}{2j_N + 1} \sum_{m_f, m_i} |\mathcal{M}|^2 = \frac{E_e}{2m_e} |\phi_{1s}^{Z_{\text{eff}}}(\vec{0})|^2 \frac{q_{\text{eff}}^2}{q^2} \frac{4\pi}{2j_N + 1} \sum_{\tau=0,1} \sum_{\tau'=0,1}$$

$$\Bigg\{ \sum_{J=0,2,\ldots}^{\infty} \Bigg(\langle l_0^\tau \rangle \langle l_0^{\tau'} \rangle^* \langle j_N || M_{J,\tau}(q_{\text{eff}}) || j_N \rangle \langle j_N || M_{J,\tau'}(q_{\text{eff}}) || j_N \rangle$$

$$+ \frac{\vec{q}_{\text{eff}}}{m_N} \cdot \langle \vec{l}_E^\tau \rangle \frac{\vec{q}_{\text{eff}}}{m_N} \cdot \langle \vec{l}_E^{\tau'} \rangle^* \langle j_N || \Phi''_{J,\tau}(q_{\text{eff}}) || j_N \rangle \langle j_N || \Phi''_{J,\tau'}(q_{\text{eff}}) || j_N \rangle$$

$$+ \frac{2\vec{q}_{\text{eff}}}{m_N} \cdot \text{Re}\left[\langle \vec{l}_E^\tau \rangle \langle l_0^{\tau'} \rangle^* \right] \langle j_N || \Phi''_{J,\tau}(q_{\text{eff}}) || j_N \rangle \langle j_N || M_{J,\tau'}(q_{\text{eff}}) || j_N \rangle \Bigg)$$

$$+ \sum_{J=2,4,\ldots}^{\infty} \frac{1}{2} \left(\frac{q_{\text{eff}}^2}{m_N^2} \langle \vec{l}_E^\tau \rangle \cdot \langle \vec{l}_E^{\tau'} \rangle^* - \frac{\vec{q}_{\text{eff}}}{m_N} \cdot \langle \vec{l}_E^\tau \rangle \frac{\vec{q}_{\text{eff}}}{m_N} \cdot \langle \vec{l}_E^{\tau'} \rangle^* \right) \langle j_N || \tilde{\Phi}'_{J,\tau}(q_{\text{eff}}) || j_N \rangle \langle j_N || \tilde{\Phi}'_{J,\tau'}(q_{\text{eff}}) || j_N \rangle$$

$$+ \sum_{J=1,3,\ldots}^{\infty} \Bigg(\hat{q} \cdot \langle \vec{l}_5^\tau \rangle \, \hat{q} \cdot \langle \vec{l}_5^{\tau'} \rangle^* \langle j_N || \Sigma''_{J,\tau}(q_{\text{eff}}) || j_N \rangle \langle j_N || \Sigma''_{J,\tau'}(q_{\text{eff}}) || j_N \rangle$$

$$+ \frac{1}{2} \left(\langle \vec{l}_5^\tau \rangle \cdot \langle \vec{l}_5^{\tau'} \rangle^* - \hat{q} \cdot \langle \vec{l}_5^\tau \rangle \, \hat{q} \cdot \langle \vec{l}_5^{\tau'} \rangle^* \right) \langle j_N || \Sigma'_{J,\tau}(q_{\text{eff}}) || j_N \rangle \langle j_N || \Sigma'_{J,\tau'}(q_{\text{eff}}) || j_N \rangle$$

$$+ \frac{1}{2} \left(\frac{q_{\text{eff}}^2}{m_N^2} \langle \vec{l}_M^\tau \rangle \cdot \langle \vec{l}_M^{\tau'} \rangle^* - \frac{\vec{q}_{\text{eff}}}{m_N} \cdot \langle \vec{l}_M^\tau \rangle \frac{\vec{q}_{\text{eff}}}{m_N} \cdot \langle \vec{l}_M^{\tau'} \rangle^* \right) \langle j_N || \Delta_{J,\tau}(q_{\text{eff}}) || j_N \rangle \langle j_N || \Delta_{J,\tau'}(q_{\text{eff}}) || j_N \rangle$$

$$+ \frac{\vec{q}_{\text{eff}}}{m_N} \cdot \text{Re}\left[i \langle \vec{l}_M^\tau \rangle \times \langle \vec{l}_5^{\tau'} \rangle^* \right] \langle j_N || \Delta_{J,\tau}(q_{\text{eff}}) || j_N \rangle \langle j_N || \Sigma'_{J,\tau'}(q_{\text{eff}}) || j_N \rangle \Bigg) \Bigg\}, \tag{3.29}$$

where we have introduced the shorthand $\langle l \rangle \equiv \langle \frac{1}{2} s_f | l | \frac{1}{2} s_i \rangle$ for the leptonic matrix elements. The sum over lepton spins can now be computed in a straightforward way by performing the

traces over the leptonic currents. For example,

$$
\begin{aligned}
\frac{1}{2}\sum_{s_f,s_i}\langle l_0^\tau\rangle\langle l_0^{\tau'}\rangle^* &= \frac{1}{2}\sum_{s_f,s_i}\xi_{s_f}^\dagger\left(c_1^\tau 1_L + c_{11}^\tau i\hat{q}\cdot\vec{\sigma}_L\right)\xi_{s_i}\xi_{s_i}^\dagger\left(c_1^{\tau'*}1_L - c_{11}^{\tau'*}i\hat{q}\cdot\vec{\sigma}_L\right)\xi_{s_f} \\
&= \frac{1}{2}\mathrm{Tr}\left[\left(c_1^\tau 1_L + c_{11}^\tau i\hat{q}\cdot\vec{\sigma}_L\right)\left(c_1^{\tau'*}1_L - c_{11}^{\tau'*}i\hat{q}\cdot\vec{\sigma}_L\right)\right] \\
&= c_1^\tau c_1^{\tau'*} + c_{11}^\tau c_{11}^{\tau'*},
\end{aligned}
\tag{3.30}
$$

where the final result depends only on the LECs of the nucleon-level CLFV operators. Performing the spin summation for the remaining leptonic currents yields

$$
\begin{aligned}
\frac{1}{2}\frac{1}{2j_N+1}\sum_{\text{spins}}|\mathcal{M}|^2 = {} & \frac{E_e}{2m_e}|\phi_{1s}^{Z_{\text{eff}}}(\vec{0})|^2\frac{q_{\text{eff}}^2}{q^2}\frac{4\pi}{2j_N+1}\sum_{\tau=0,1}\sum_{\tau'=0,1} \\
& \left\{\sum_{J=0,2,\ldots}^{\infty}\left[R_M^{\tau\tau'}\langle j_N||M_{J;\tau}(q_{\text{eff}})||j_N\rangle\langle j_N||M_{J;\tau'}(q_{\text{eff}})||j_N\rangle\right.\right. \\
& + \frac{q_{\text{eff}}^2}{m_N^2}R_{\Phi''}^{\tau\tau'}\langle j_N||\Phi''_{J;\tau}(q_{\text{eff}})||j_N\rangle\langle j_N||\Phi''_{J;\tau'}(q_{\text{eff}})||j_N\rangle \\
& \left.- \frac{2q_{\text{eff}}}{m_N}R_{\Phi''M}^{\tau\tau'}\langle j_N||\Phi''_{J;\tau}(q_{\text{eff}})||j_N\rangle\langle j_N||M_{J;\tau'}(q_{\text{eff}})||j_N\rangle\right] \\
& + \sum_{J=2,4,\ldots}^{\infty}\left[\frac{q_{\text{eff}}^2}{m_N^2}R_{\tilde{\Phi}'}^{\tau\tau'}\langle j_N||\tilde{\Phi}'_{J;\tau}(q_{\text{eff}})||j_N\rangle\langle j_N||\tilde{\Phi}'_{J;\tau'}(q_{\text{eff}})||j_N\rangle\right] \\
& + \sum_{J=1,3,\ldots}^{\infty}\left[R_{\Sigma''}^{\tau\tau'}\langle j_N||\Sigma''_{J;\tau}(q_{\text{eff}})||j_N\rangle\langle j_N||\Sigma''_{J;\tau'}(q_{\text{eff}})||j_N\rangle\right. \\
& + R_{\Sigma'}^{\tau\tau'}\langle j_N||\Sigma'_{J;\tau}(q_{\text{eff}})||j_N\rangle\langle j_N||\Sigma'_{J;\tau'}(q_{\text{eff}})||j_N\rangle \\
& + \frac{q_{\text{eff}}^2}{m_N^2}R_{\Delta}^{\tau\tau'}\langle j_N||\Delta_{J;\tau}(q_{\text{eff}})||j_N\rangle\langle j_N||\Delta_{J;\tau'}(q_{\text{eff}})||j_N\rangle \\
& \left.\left.- \frac{2q_{\text{eff}}}{m_N}R_{\Delta\Sigma'}^{\tau\tau'}\langle j_N||\Delta_{J;\tau}(q_{\text{eff}})||j_N\rangle\langle j_N||\Sigma'_{J;\tau'}(q_{\text{eff}})||j_N\rangle\right]\right\},
\end{aligned}
\tag{3.31}
$$

where we have defined the following combinations of the LECs:

$$
\begin{aligned}
R_M^{\tau\tau'} &\equiv c_1^\tau c_1^{\tau'*} + c_{11}^\tau c_{11}^{\tau'*} \\
R_{\Phi''}^{\tau\tau'} &\equiv c_3^\tau c_3^{\tau'*} + (c_{12}^\tau - c_{15}^\tau)\left(c_{12}^{\tau'*} - c_{15}^{\tau'*}\right) \\
R_{\Phi''M}^{\tau\tau'} &\equiv \mathrm{Re}\left[c_3^\tau c_1^{\tau'*} - (c_{12}^\tau - c_{15}^\tau)c_{11}^{\tau'*}\right] \\
R_{\tilde{\Phi}'}^{\tau\tau'} &\equiv c_{12}^\tau c_{12}^{\tau'*} + c_{13}^\tau c_{13}^{\tau'*} \\
R_{\Sigma''}^{\tau\tau'} &\equiv (c_4^\tau - c_6^\tau)(c_4^{\tau'*} - c_6^{\tau'*}) + c_{10}^\tau c_{10}^{\tau'*} \\
R_{\Sigma'}^{\tau\tau'} &\equiv c_4^\tau c_4^{\tau'*} + c_9^\tau c_9^{\tau'*} \\
R_{\Delta}^{\tau\tau'} &\equiv c_5^\tau c_5^{\tau'*} + c_8^\tau c_8^{\tau'*} \\
R_{\Delta\Sigma'}^{\tau\tau'} &\equiv \mathrm{Re}\left[c_5^\tau c_4^{\tau'*} + c_8^\tau c_9^{\tau'*}\right].
\end{aligned}
\tag{3.32}
$$

The R coefficients defined above are in terms of the dimensionful LECs c_i^τ. If we consider instead the analogous dimensionless leptonic tensors $\tilde{R}$ defined in terms of $\tilde{c}_i^\tau$, then the elastic $\mu \to$ decay rate can be expressed as

$$
\Gamma = \frac{G_F^2}{\pi} \frac{q_{\text{eff}}^2}{1 + \frac{q}{M_T}} |\phi_{1s}^{Z_{\text{eff}}}(\vec{0})|^2 \sum_{\tau=0,1} \sum_{\tau'=0,1} \left\{ \left[\tilde{R}_M^{\tau\tau'} W_M^{\tau\tau'}(q_{\text{eff}}) + \tilde{R}_{\Sigma''}^{\tau\tau'} W_{\Sigma''}^{\tau\tau'}(q_{\text{eff}}) + \tilde{R}_{\Sigma'}^{\tau\tau'} W_{\Sigma'}^{\tau\tau'}(q_{\text{eff}}) \right] \right.
$$
$$
+ \frac{q_{\text{eff}}^2}{m_N^2} \left[\tilde{R}_{\Phi''}^{\tau\tau'} W_{\Phi''}^{\tau\tau'}(q_{\text{eff}}) + \tilde{R}_{\tilde{\Phi}'}^{\tau\tau'} W_{\tilde{\Phi}'}^{\tau\tau'}(q_{\text{eff}}) + \tilde{R}_\Delta^{\tau\tau'} W_\Delta^{\tau\tau'}(q_{\text{eff}}) \right]
$$
$$
\left. - \frac{2q_{\text{eff}}}{m_N} \left[\tilde{R}_{\Phi''M}^{\tau\tau'} W_{\Phi''M}^{\tau\tau'}(q_{\text{eff}}) + \tilde{R}_{\Delta\Sigma'}^{\tau\tau'} W_{\Delta\Sigma'}^{\tau\tau'}(q_{\text{eff}}) \right] \right\},
$$
(3.33)

where the factor $(1 + q/M_T)^{-1}$ accounts for the distortion of phase space by nuclear recoil, and where we have defined the nuclear response functions

$$
W_O^{\tau\tau'}(q) \equiv \frac{4\pi}{2j_N + 1} \sum_{J=0,2,\ldots}^\infty \langle j_N || O_{J;\tau}(q) || j_N \rangle \langle j_N || O_{J;\tau'}(q) || j_N \rangle \text{ for } O = M, \Phi''
$$
$$
W_O^{\tau\tau'}(q) \equiv \frac{4\pi}{2j_N + 1} \sum_{J=1,3,\ldots}^\infty \langle j_N || O_{J;\tau}(q) || j_N \rangle \langle j_N || O_{J;\tau'}(q) || j_N \rangle \text{ for } O = \Sigma', \Sigma'', \Delta
$$
$$
W_{\tilde{\Phi}'}^{\tau\tau'}(q) \equiv \frac{4\pi}{2j_N + 1} \sum_{J=2,4,\ldots}^\infty \langle j_N || \tilde{\Phi}'_{J;\tau}(q) || j_N \rangle \langle j_N || \tilde{\Phi}'_{J;\tau'}(q) || j_N \rangle \tag{3.34}
$$
$$
W_{\Phi''M}^{\tau\tau'}(q) \equiv \frac{4\pi}{2j_N + 1} \sum_{J=0,2,\ldots}^\infty \langle j_N || \Phi''_{J;\tau}(q) || j_N \rangle \langle j_N || M_{J;\tau'}(q) || j_N \rangle
$$
$$
W_{\Delta\Sigma'}^{\tau\tau'}(q) \equiv \frac{4\pi}{2j_N + 1} \sum_{J=1,3,\ldots}^\infty \langle j_N || \Delta_{J;\tau}(q) || j_N \rangle \langle j_N || \Sigma'_{J;\tau'}(q) || j_N \rangle .
$$

Both the nuclear response functions W and the leptonic response functions $\tilde{R}$ are dimensionless. If all dimensionful prefactors in Eq. (3.33) are evaluated in GeV units, rates in 1/sec will be obtained by dividing by $\hbar$.

As expected from considerations of parity and time-reversal symmetry, the $\mu \to e$ conversion rate can be expressed in terms of the six allowed single-nucleon response functions, as well as two interference terms. Each nuclear response function W is multiplied by a corresponding leptonic response function R. This is precisely the factorization between nuclear physics and CLFV physics that we hoped to achieve in formulating an effective theory of $\mu \to e$ conversion at the nuclear scale. As one varies the choice of nuclear target, the nuclear response functions W vary depending on the details of nuclear structure. The parameters of the lepton approximations, q_{eff} and Z_{eff}, also change depending on the target. Crucially, the low-energy constants of the single-nucleon CLFV operators, the c_i^τ, should not depend on the nuclear target, and therefore the leptonic response functions R will inherit this target-independence. By performing an ensemble of measurements of $\mu \to e$ conversion in a range of nuclear targets, an experimentalist can, in principle, use Eq. (3.33) to constrain and/or determine the values of the R coefficients. As we have formulated the most general

nuclear-scale effective theory, such a determination would extract the maximum amount of information that can be obtained about CLFV operators from observations of elastic $\mu \to e$ conversion. One cannot determine the values of individual operator coefficients c_i^τ, only the particular combinations specified by the leptonic response functions R. In Section 3.8, we discuss situations in which the assumed target-independence of the CLFV LECs is (weakly) violated.

Of the 16 low-energy constants describing the nucleon-level effective theory, there are 4 that do not appear in the leptonic response functions: c_2, c_7, c_{14}, and c_{16}. Consequently, the operators associated with these LECs are not probed in elastic $\mu \to e$ conversion. The reason that these operators are excluded from the elastic process is that they correspond to projections of nuclear charges and currents whose multipole projections always have opposite parity and time-reversal properties. For example, $\mathcal{O}_7 = \vec{v}_N \cdot \vec{\sigma}_N$ is the nuclear axial charge operator, which generates the $\widetilde{Omega}_J$ family of multipole operators that are even (odd) under parity and odd (even) under time-reversal for odd (even) J. Thus, the approximate P and T symmetries of the nuclear ground state preclude these operators from contributing. If nature conspires to sequester CLFV within these operators, measurements of the elastic process will be completely blind to the flavor violation.

The four excluded operators can, however, be probed by the *inelastic* process where the nucleus transitions to an excited state, thereby avoiding the rather severe parity and time-reversal constraints of the ground-state process. The inelastic process is sensitive to CLFV operators that otherwise cannot be probed, and therefore one would like to ensure that $\mu \to e$ conversion experiments can set limits on this mode. The challenge is that the energy for the nuclear excitation is subtracted from the energy of the outgoing electron, resulting in substantially higher backgrounds in the relevant region of the electron spectrum. Nonetheless, the sensitivity of next-generation $\mu \to$ conversion experiments is so impressive that interesting limits can likely be set on the inelastic process, and it is a high priority for our own future theoretical work to generalize the nuclear-scale effective theory to the inelastic case (see Section 10.1).

Returning to the elastic case, in order to utilize our formalism to place constraints on the CLFV parameters, we must be able to evaluate the nuclear response functions for the chosen nuclear target. We will now demonstrate how this can be done within the paradigm of the nuclear shell model (NSM).

3.6 Shell-model Evaluation of Nuclear Responses

Calculation of the nuclear response functions defined in Eq. (3.34) requires the evaluation of the matrix elements

$$\langle j_N || T_{J;\tau}(q_{\text{eff}}) || j_N \rangle , \tag{3.35}$$

where $|j_N\rangle$ is a wave function for the nuclear ground state, and $T_{J;\tau}$ is any of the basic single-nucleon operators in Eq. (3.19). Here, the isospin of the nuclear states has been suppressed. We will demonstrate how to compute these matrix elements using the nuclear shell model. Restoring isospin explicitly, we may write the desired matrix element in terms

of one that has been doubly-reduced in total angular momentum J and total isospin τ

$$\langle j_N; TM_T||T_{J;\tau 0}(q)||j_N; TM_T\rangle = (-1)^{T-M_T} \begin{pmatrix} T & \tau & T \\ -M_T & 0 & M_T \end{pmatrix} \langle j_N; T \stackrel{::}{:} T_{J;\tau}(q) \stackrel{::}{:} j_N; T\rangle. \tag{3.36}$$

Each nuclear operator is a sum of single-nucleon operators

$$T_{J;\tau}(q) = \sum_{i=1}^{A} T_{J;\tau}(q\vec{x}_i), \tag{3.37}$$

and therefore the doubly-reduced total nuclear matrix element can be expressed in terms of the doubly-reduced one-body density matrix $\rho_{ab}^{J;\tau}$ (see Appendix C.1) as

$$\langle j_N; T \stackrel{::}{:} T_{J;\tau}(q) \stackrel{::}{:} j_N; T\rangle = \sum_{a,b} \rho_{ab}^{J;\tau} \langle n_a\,(\ell_a\,1/2)\,j_a; 1/2 \stackrel{::}{:} T_{J;\tau}(q) \stackrel{::}{:} n_b\,(\ell_b\,1/2)\,j_b; 1/2\rangle, \tag{3.38}$$

where the sum extends over all single-particle *orbits*, labeled by harmonic oscillator quantum numbers n, ℓ, and j but not m_j. As $T_{J;\tau}(q_{\text{eff}}) = T_J(q_{\text{eff}})t^\tau$, the single-particle isospin matrix elements are readily evaluated

$$\langle 1/2||t^\tau||1/2\rangle = \begin{cases} \sqrt{2}, & \tau = 0 \\ \sqrt{6}, & \tau = 1. \end{cases} \tag{3.39}$$

From Section 3.4 (and Appendix D), we know how to evaluate the matrix elements of T_J between single-particle harmonic oscillator states in terms of the dimensionless quantity $y = (q_{\text{eff}}b/2)^2$. All that remains is to obtain the density matrix, which requires us to construct the nuclear shell-model wave function.

As an example, we model the nucleus ^{27}Al using the $2s$-$1d$ valence space above an inert ^{16}O core; that is, we assume that the 8 lowest-energy protons and neutrons are fixed in their orbitals whereas the remaining 5 protons and 6 neutrons can occupy any of the 12 states (for each species) in the $1d_{5/2}$-$2s_{1/2}$-$1d_{3/2}$ valence space, while respecting Pauli exclusion. The core, although trivial to model, is crucial to include as it contributes significantly to the coherent response. In total, 80,115 basis states are required to describe the state of the 11 valence nucleons. The ground-state configuration is determined by diagonalizing an effective Hamiltonian in the valence space. Table 3.2 reports the model spaces employed and the effective interactions available for the nuclear targets considered in this work. In addition to the shell structure, the harmonic oscillator model space is only fully specified once the oscillator length scale b has been chosen. To this end, one may employ the well-known empirical formula

$$b = \sqrt{\frac{41.467}{45\bar{A}^{-1/3} - 25\bar{A}^{-2/3}}} \text{ fm}, \tag{3.40}$$

where $\bar{A}$ is the isotope-averaged nucleon number. In many cases, the effective shell-model interactions have been tuned to reproduce nuclear charge radii as well as low-lying nuclear spectra. Alternative to the empirical formula, one may also determine a value of b that, in combination with the nuclear density obtained from the shell-model, accurately reproduces the

known nuclear charge radius. These independent determinations of the oscillator parameter b are compared in Table 3.2. The agreement is generally quite good.

As the size of the shell-model basis grows combinatorially in the number of states and particles—the basis size for ^{56}Fe is 501,113,392—it quickly becomes infeasible to diagonalize the Hamiltonian directly. Fortunately, one can obtain a converged result for the ground-state wave function using the iterative Lanczos algorithm. In particular, we employ the massively-parallel Lanczos-algorithm code BIGSTICK [89, 90] in order to obtain the ground-state of the chosen effective interaction within the model space.

The one-body density matrix is particularly useful due to the size of the basis required to model the nuclei of interest. Technically, one may obtain the many-body matrix element of a nuclear operator by expressing the total nuclear wave function in terms of a basis of Slater determinants. As mentioned, in some cases that we are interested in this basis contains over half a billion many-body states, resulting in more than 10^{17} unique matrix elements that would have to be evaluated in this naïve approach. In the present case, the nuclear operators that we wish to evaluate are all one-body operators, acting only on a single nucleon at a time while leaving the remaining $A - 1$ nucleons unchanged; one-body operators can only alter the nuclear state by one nucleon at a time. The one-body density matrix is constructed to reflect this fact, containing exactly that information about nuclear structure that is required to evaluate the total nuclear matrix element of a one-body operator of total angular momentum J and isospin τ.

In practice, $\rho_{ab}^{J,\tau}$ is obtained by evaluating the second-quantized one-body operator $\left[c_a^\dagger \otimes \tilde{c}_b \right]_{J,\tau}$ between the initial and final nuclear wave functions. For large model spaces, this calculation can still be computationally intensive (although various symmetry arguments can be utilized in order to minimize this cost). The primary advantage is that this calculation only needs to be performed once for each J and τ, and the resulting density matrix can then be used to evaluate nuclear matrix elements of any one-body operator of the same total angular momentum and isospin. BIGSTICK has built-in functionality to construct and output the one-body density matrices that are required in the evaluation of the nuclear response functions.

3.7 Nuclear Multipole Power Counting

Frequently when one performs a multipole decomposition, the expansion converges rapidly enough that the desired accuracy can be achieved by retaining only the first few leading multipoles. In this section, we demonstrate that this is explicitly *not* the case in elastic $\mu \to e$ conversion. As demonstrated by Eq. (3.21), the parameter $y = (bq_{\text{eff}}/2)^2$ governs the convergence of the nuclear multipole expansion. For $\mu \to e$ conversion in the nuclei of interest, the effective three-momentum transfer is of order the muon mass $q_{\text{eff}} \approx m_\mu$ and the nuclear oscillator parameter $b \approx 2$ fm, and therefore $y \approx 0.3$. The exact value of y for each nuclear target may be found in Table 3.2.

Not only is the dimensionless parameter y large enough to warrant the inclusion of terms beyond the leading multipole, but it turns out that any truncation scheme in y is an uncontrolled approximation. Eq. (3.21) describes the dependence on y of single-particle matrix elements. As discussed in the previous section, the total nuclear matrix elements can

Target	Isotopes	SM Space	Interactions	b (fm)	$y = (q_{\text{eff}}b/2)^2$
C	12,13	$1p$	[91]	1.67/1.70	0.21/0.22
O	16,18	$2s$-$1d$	[92, 93]	1.73/1.83	0.23/0.26
		$4\hbar\omega$	[94]	1.73/1.80	0.23/0.25
F	19	$2s$-$1d$	[92, 93]	1.76/1.88	0.24/0.27
Na	23	$2s$-$1d$	”	1.80/1.83	0.25/0.26
Al	27	$2s$-$1d$	”	1.84/1.85	0.27/0.27
Si	28-30	$2s$-$1d$	”	1.85/1.89	0.27/0.28
S	32-34	$2s$-$1d$	”	1.88/1.91	0.28/0.29
Ca	40,42,44	$2p$-$1f$	[95–97]	1.94/2.02	0.30/0.33
Ti	46-50	$2p$-$1f$	”	1.99/2.09	0.32/0.35
Fe	54,56-58	$2p$-$1f$	”	2.03/2.08	0.34/0.36
Cu	63,65	$1f_{5/2}$-$2p$-$1g_{9/2}$	[98–100]	2.07/2.12	0.35/0.37

Table 3.2: Nuclear shell-model spaces employed and available effective interactions. The first entry for the oscillator parameter b is calculated from the empirical formula Eq. (3.40). The second entry is the value of b that reproduces the measured nuclear charge radius. These values of b are then used in calculation of the corresponding value of y.

be decomposed into a sum of single-particle matrix elements multiplied by the corresponding one-body density matrix factor. The details of nuclear structure that are encoded in the density matrix determine the overall y dependence of the nuclear response functions $W(y)$ and may significantly enhance or suppress contributions from higher-J multipoles. One frequently-exploited example of this is the coherent enhancement of the isoscalar monopole operator $M_{0;0}$. Let us specialize, for the moment, to ^{27}Al. At the level of single-particle matrix elements, one naïvely expects the quadrupole operator $M_{2;0}$ to be suppressed by $y \approx 0.27$ relative to the monopole. Due to coherent enhancement of the monopole, however, the total nuclear matrix element of $M_{2;0}$ is suppressed by an additional order of magnitude relative to the monopole

$$\frac{\langle j_N || M_{2;0}(q_{\text{eff}}) || j_N \rangle}{\langle j_N || M_{0;0}(q_{\text{eff}}) || j_N \rangle} \approx 0.027. \tag{3.41}$$

Thus, in the case of coherent conversion, one is justified in retaining only the leading multipole; the resulting error in the $\mu \to e$ rate is less than 0.1%.

The isoscalar charge operator is very much a special case. Let us repeat the previous exercise with the corresponding isovector operators. Now there is no coherent enhancement, and the quadrupole operator $M_{2;1}$ is suppressed by roughly the expected factor of y:

$$\frac{\langle j_N || M_{2;1}(q_{\text{eff}}) || j_N \rangle}{\langle j_N || M_{0;1}(q_{\text{eff}}) || j_N \rangle} \approx -0.23. \tag{3.42}$$

Truncating the multipole expansion at leading order then introduces a 4.8% error in the conversion rate. A point of caution should therefore be made in regard to calculations of coherent $\mu \to e$ conversion in the literature: Many works that specialize to coherent conversion (e.g., [56, 57, 71, 78, 80, 81, 85, 101]) retain the isovector operator even though the multipole expansion is truncated at leading order. The neglect of higher multipoles should be justified when the isoscalar component is significant enough to provide a coherent enhancement—for example, if the coupling is purely to either protons or neutrons. However, in cases where the nuclear ground state carries sufficient angular momentum $j_N \geq 1$, one should not necessarily trust the result of these calculations when the coupling becomes dominantly isovector. In such a scenario, the coherent enhancement diminishes and contributions from higher multipoles become significant.

The impact of higher-order multipoles is also significant for spin-dependent nuclear operators. Among the 11 targets that we focus on in this work, there are three—Na, Al, and Cu—with only odd isotopes, an unpaired proton, and a ground-state angular momentum $j_N \geq \frac{3}{2}$ so that more than one multipole operator contributes to the total response function. Consider the spin-dependent interaction $\mathcal{O}_4 = \vec{\sigma}_L \cdot \vec{\sigma}_N$, which generates the Σ'_J and Σ''_J response functions comprised of odd J multipoles, and suppose that the isospin coupling is $(1 + \tau_3)/2$ so that the operator couples only to the unpaired proton. Evaluating the $\mu \to e$ decay rate first retaining only the leading $J = 1$ multipoles and then with all contributing multipoles, we find rate increases of 22.4% in Na, 4.7% in Al, and 65.4% in Cu. In Al, the truncation of the multipole expansion has produced only a modest error in the decay rate, whereas in Cu the error is nearly $o(1)$. It is therefore essential that one retain all allowed multipole operators in the general effective theory.

3.8 Form Factors and LEC Independence

The effective theory is constructed from single-nucleon operators and does not contain the pion, other mesons, or baryonic resonances as explicit degrees of freedom. As the three-momentum transfer in elastic $\mu \to e$ conversion satisfies $q = |\vec{q}| \approx m_\mu \approx m_\pi$, pionic contributions to single-nucleon form factors are expected to be significant. On the other hand, these form factors are evaluated at fixed q^2, and, as the magnitude of the three-momentum transfer varies by only a few percent across the light- and medium-mass nuclei of primary interest, the effect of these form factors can be absorbed into the LECs. More generally, the momentum-transfer-squared q^2 is an invariant scalar quantity (in the non-relativistic effective theory), and so for every operator $\mathcal{O}$ that is allowed by symmetries, then so is $q^{2n}\mathcal{O}$ for any $n \geq 0$. We can group all such operators using a form factor

$$c^{(0)}\mathcal{O} + c^{(2)}q^2\mathcal{O} + c^{(4)}q^4\mathcal{O} + ... = F_\mathcal{O}\left(\frac{q^2}{M^2}\right)\mathcal{O}, \tag{3.43}$$

where M is some mass scale characterizing the form factor. Massless mediators, such as a virtual photon, can be included by the addition of $1/q^2$ terms. The form factor associated with one-pion exchange is the pion propagator

$$F_\pi(q^2) = \frac{1}{q^2 + m_\pi^2}, \tag{3.44}$$

where $m_\pi = 138.039$ MeV is the isospin-averaged pion mass. Evaluating this form factor at the appropriate effective momentum, we find a variation of $\approx 5\%$ between ^{12}C and ^{184}W. For a massless mediator, the variation is slightly more than 10% across the same range of targets. In practice, the single-nucleon LECs associated with these interactions will be forced to absorb the q dependence of these form factors, thereby violating the assumed target-independence of the resulting leptonic response functions. This does not reduce the utility of the nuclear effective theory: The target-dependence of the LECs is expected to be relatively weak, and in the initial discovery phase of searches for CLFV, one can overlook the $\approx 10\%$ errors introduced by the single-nucleon form factors. When greater accuracy is required, one can match the single-nucleon effective theory to, say, chiral effective theory in order to identify the relevant form factors. The LECs of the nuclear effective theory can then be related to the corresponding momentum-independent parameters of the higher-scale effective theory. Thus, one obtains a theory in which the unknown parameters are genuinely target-independent and can be faithfully constrained by an ensemble of measurements on different nuclear targets.

One can adopt a similar attitude towards the effect of multi-nucleon interactions. As discussed in detail in Chapters 8 and 9, at next-to-leading order in chiral effective theory there is a two-nucleon diagram [see Fig. 8.1 (c)] that contributes to coherent $\mu \to e$ conversion in the case of a heavy scalar mediator. This operator is fundamentally incompatible with the structure of our effective theory, which is comprised only of single-nucleon operators. We can attempt to capture the impact of this operator by reducing it to an effective single-nucleon operator by, for example, averaging the two-nucleon operator over a degenerate Fermi gas model of the target nucleus, as done in Appendix E.

We expect that a generic two-nucleon operator can be reduced to an effective single-nucleon operator as

$$\mathcal{O}^{(2)} \to \sum_{\tau=0,1} \sum_{i=1}^{16} f_i^\tau \mathcal{O}_i t^\tau, \tag{3.45}$$

where the effective couplings f_i^τ depend on the relevant kinematic quantities as well as the nuclear density of the target. In analogy with the treatment of propagator effects, the impact of two-nucleon operators can thus be absorbed into the LECs of the single-nucleon effective theory, introducing a dependence of the LECs on the nuclear target that we anticipate will be weak as long as the higher-body terms enter at higher orders. An important aspect of matching the nuclear effective theory to higher-scale effective theories will be understanding the order at which multi-nucleon interactions become relevant.

3.9 Connection to Relativistic Amplitudes

The effective theory of $\mu \to e$ conversion was developed in terms of non-relativistic operators, assuming no underlying Lorentz-invariance. Of course, we know that the 16 operators of the effective theory must embed into Lorentz-invariant contractions of lepton and nucleon spinor currents. Defining the basic lepton

$$\chi_e \equiv \begin{pmatrix} \xi \\ \vec{\sigma}_L \cdot \hat{q}\, \xi \end{pmatrix}, \quad \chi_\mu \equiv \begin{pmatrix} \xi \\ 0 \end{pmatrix}, \tag{3.46}$$

and nucleon

$$N \equiv \begin{pmatrix} \xi \\ \frac{\vec{\sigma}_N \cdot \vec{v}_N}{2}\, \xi \end{pmatrix}, \tag{3.47}$$

spinors, the relativistic interactions are constructed from the available leptonic scalar

$$\bar{\chi}_e \chi_\mu, \quad \bar{\chi}_e i\gamma^5 \chi_\mu, \tag{3.48}$$

and four-vector

$$\bar{\chi}_e \gamma^\mu \chi_\mu, \quad \bar{\chi}_e i\sigma^{\mu\nu} \frac{q_\nu}{m_L} \chi_\mu, \quad \bar{\chi}_e \gamma^\mu \gamma^5 \chi_\mu, \quad \bar{\chi}_e \sigma^{\mu\nu} \frac{q_\nu}{m_L} \gamma^5 \chi_\mu, \tag{3.49}$$

amplitudes, contracting these with their nucleon counterparts to form all possible bilinear scalars. Here, m_L is some (not necessarily heavy) scale associated with the leptons. The Pauli reductions of the Lorentz-covariant nucleon and lepton currents are given in Appendices A.1 and A.2, respectively. The nuclear expansion neglects terms of order $\vec{v}_N^2 \approx \frac{1}{100}$ and $\frac{q^2}{m_N^2} \approx \frac{1}{100}$. The leptonic expansion includes first-order terms in the muon velocity $\vec{v}_\mu$, which we have so far neglected but will consider in Chapter 7. The relationships between the relativistic amplitudes and the Pauli-reduced operators are summarized in Table 3.3.

In this reduction, four of our effective Pauli operators—$\mathcal{O}_3$, $\mathcal{O}_{12}$, $\mathcal{O}'_{13}$, and $\mathcal{O}_{15}$—do not appear. These are the interactions associated with the nuclear spin-velocity three-current $\vec{v}_N \times \vec{\sigma}_N$, which cannot be generated by scalar or vector couplings to the nucleus, but will arise for more general mediators. For example, the pseudotensor interaction

$$\bar{\chi}_e i\sigma^{\mu\nu} \gamma^5 \chi_\mu \bar{N} i\sigma_{\mu\nu} \gamma^5 N, \tag{3.50}$$

reduces to the Pauli form

$$
\begin{aligned}
&\frac{q}{m_N} 1_L 1_N + 2i\hat{q} \cdot [\vec{v}_N \times \vec{\sigma}_N] - 2\vec{\sigma}_L \cdot \vec{\sigma}_N - 2\vec{\sigma}_L \cdot (\hat{q} \times [\vec{v}_N \times \vec{\sigma}_N]) \\
&= \frac{q}{m_N} \mathcal{O}_1 + 2\mathcal{O}_3 - 2\mathcal{O}_4 + 2i\mathcal{O}_{13}',
\end{aligned}
\tag{3.51}
$$

generating $\mathcal{O}_3$ and $\mathcal{O}_{13}'$. The four operators associated with $\vec{v}_N \times \vec{\sigma}_N$ should be retained to ensure that the EFT formulation is general. On the other hand, the 20 covariant interactions reduce to linear combinations of only 12 Pauli operators; significant redundancies exist in the covariant description, owing to the non-relativistic nature of the muon and nucleons and the ultra-relativistic nature of the electron. Although one may employ either description as a starting point, the Pauli-reduced form is more natural in the sense that it has already taken account of this overcompleteness.

j	$\mathcal{L}_{\mathrm{int}}^{j}$	Pauli Reduction	$\sum_i c_i \mathcal{O}_i$
1	$\bar{\chi}_e \chi_\mu \bar{N} N$	$1_L 1_N$	$\mathcal{O}_1$
2	$\bar{\chi}_e \chi_\mu \bar{N} i\gamma^5 N$	$1_L \left(i\frac{\vec{q}}{2m_N} \cdot \vec{\sigma}_N \right)$	$\frac{q}{2m_N} \mathcal{O}_{10}$
3	$\bar{\chi}_e i\gamma^5 \chi_\mu \bar{N} N$	$(-i\hat{q} \cdot \vec{\sigma}_L) 1_N$	$-\mathcal{O}_{11}$
4	$\bar{\chi}_e i\gamma^5 \chi_\mu \bar{N} i\gamma^5 N$	$(-i\hat{q} \cdot \vec{\sigma}_L) \left(i\frac{\vec{q}}{2m_N} \cdot \vec{\sigma}_N \right)$	$-\frac{q}{2m_N} \mathcal{O}_6$
5	$\bar{\chi}_e \gamma^\mu \chi_\mu \bar{N} \gamma_\mu N$	$1_L 1_N$	$\mathcal{O}_1$
		$-(\hat{q}1_L - i\hat{q} \times \vec{\sigma}_L) \cdot \left(\vec{v}_N + i\frac{\vec{q}}{2m_N} \times \vec{\sigma}_N \right)$	$+i\mathcal{O}_2' - \mathcal{O}_5 - \frac{q}{2m_N}(\mathcal{O}_4 + \mathcal{O}_6)$
6	$\bar{\chi}_e \gamma^\mu \chi_\mu \bar{N} i\sigma_{\mu\alpha} \frac{q^\alpha}{m_N} N$	$-(\hat{q}1_L - i\hat{q} \times \vec{\sigma}_L) \cdot \left(-i\frac{\vec{q}}{m_N} \times \vec{\sigma}_N \right)$	$\frac{q}{m_N}(\mathcal{O}_4 + \mathcal{O}_6)$
7	$\bar{\chi}_e \gamma^\mu \chi_\mu \bar{N} \gamma_\mu \gamma^5 N$	$1_L (\vec{v}_N \cdot \vec{\sigma}_N) - (\hat{q}1_L - i\hat{q} \times \vec{\sigma}_L) \cdot \vec{\sigma}_N$	$\mathcal{O}_7 + i\mathcal{O}_{10} - \mathcal{O}_9$
8	$\bar{\chi}_e \gamma^\mu \chi_\mu \bar{N} \sigma_{\mu\alpha} \frac{q^\alpha}{m_N} \gamma^5 N$	$1_L \left(-i\frac{\vec{q}}{m_N} \cdot \vec{\sigma}_N \right)$	$-\frac{q}{m_N} \mathcal{O}_{10}$
9	$\bar{\chi}_e i\sigma^{\mu\nu} \frac{q_\nu}{m_L} \chi_\mu \bar{N} \gamma_\mu N$	$-\frac{q}{m_L} 1_L 1_N$	$-\frac{q}{m_L} \mathcal{O}_1$
		$-\left(-i\frac{\vec{q}}{m_L} \times \vec{\sigma}_L \right) \cdot \left(\vec{v}_N + i\frac{\vec{q}}{2m_N} \times \vec{\sigma}_N \right)$	$-\frac{q}{m_L} \left(\mathcal{O}_5 + \frac{q}{2m_N}(\mathcal{O}_4 + \mathcal{O}_6) \right)$
10	$\bar{\chi}_e i\sigma^{\mu\nu} \frac{q_\nu}{m_L} \chi_\mu \bar{N} i\sigma_{\mu\alpha} \frac{q^\alpha}{m_N} N$	$-\left(-i\frac{\vec{q}}{m_L} \times \vec{\sigma}_L \right) \cdot \left(-i\frac{\vec{q}}{m_N} \times \vec{\sigma}_N \right)$	$\frac{q}{m_L} \frac{q}{m_N}(\mathcal{O}_4 + \mathcal{O}_6)$
11	$\bar{\chi}_e i\sigma^{\mu\nu} \frac{q_\nu}{m_L} \chi_\mu \bar{N} \gamma_\mu \gamma^5 N$	$\left(-\frac{q}{m_L} 1_L \right) \vec{v}_N \cdot \vec{\sigma}_N - \left(-i\frac{\vec{q}}{m_L} \times \vec{\sigma}_L \right) \cdot \vec{\sigma}_N$	$-\frac{q}{m_L}(\mathcal{O}_7 + \mathcal{O}_9)$
12	$\bar{\chi}_e i\sigma^{\mu\nu} \frac{q_\nu}{m_L} \chi_\mu \bar{N} \sigma_{\mu\alpha} \frac{q^\alpha}{m_N} \gamma^5 N$	$\left(-\frac{q}{m_L} 1_L \right) \left(-i\frac{\vec{q}}{m_N} \cdot \vec{\sigma}_N \right)$	$\frac{q}{m_L} \frac{q}{m_N} \mathcal{O}_{10}$
13	$\bar{\chi}_e \gamma^\mu \gamma^5 \chi_\mu \bar{N} \gamma_\mu N$	$(\hat{q} \cdot \vec{\sigma}_L) 1_N - \vec{\sigma}_L \cdot \left(\vec{v}_N + i\frac{\vec{q}}{2m_N} \times \vec{\sigma}_N \right)$	$-i\mathcal{O}_{11} - \mathcal{O}_8 - \frac{q}{2m_N} \mathcal{O}_9$
14	$\bar{\chi}_e \gamma^\mu \gamma^5 \chi_\mu \bar{N} i\sigma_{\mu\alpha} \frac{q^\alpha}{m_N} N$	$-\vec{\sigma}_L \cdot \left(-i\frac{\vec{q}}{m_N} \times \vec{\sigma}_N \right)$	$\frac{q}{m_N} \mathcal{O}_9$
15	$\bar{\chi}_e \gamma^\mu \gamma^5 \chi_\mu \bar{N} \gamma_\mu \gamma^5 N$	$(\hat{q} \cdot \vec{\sigma}_L)(\vec{v}_N \cdot \vec{\sigma}_N) - \vec{\sigma}_L \cdot \vec{\sigma}_N$	$-i\mathcal{O}_{14} - \mathcal{O}_4$
16	$\bar{\chi}_e \gamma^\mu \gamma^5 \chi_\mu \bar{N} \sigma_{\mu\alpha} \frac{q^\alpha}{m_N} \gamma^5 N$	$(\hat{q} \cdot \vec{\sigma}_L) \left(-i\frac{\vec{q}}{m_N} \cdot \vec{\sigma}_N \right)$	$i\frac{q}{m_N} \mathcal{O}_6$
17	$\bar{\chi}_e \sigma^{\mu\nu} \frac{q_\nu}{m_L} \gamma^5 \chi_\mu \bar{N} \gamma_\mu N$	$\left(-i\frac{\vec{q}}{m_L} \cdot \vec{\sigma}_L \right) 1_N$	$-\frac{q}{m_L} \mathcal{O}_{11}$
		$-i\frac{q}{m_L} (\vec{\sigma}_L - \hat{q}\hat{q} \cdot \vec{\sigma}_L) \cdot \left(\vec{v}_N + i\frac{\vec{q}}{2m_N} \times \vec{\sigma}_N \right)$	$-\frac{q}{m_L} \left(i\mathcal{O}_8 + i\frac{q}{2m_N} \mathcal{O}_9 + i\mathcal{O}_{16}' \right)$
18	$\bar{\chi}_e \sigma^{\mu\nu} \frac{q_\nu}{m_L} \gamma^5 \chi_\mu \bar{N} i\sigma_{\mu\alpha} \frac{q^\alpha}{m_N} N$	$-i\frac{q}{m_L} (\vec{\sigma}_L - \hat{q}\hat{q} \cdot \vec{\sigma}_L) \cdot \left(-i\frac{\vec{q}}{m_N} \times \vec{\sigma}_N \right)$	$i\frac{q}{m_L} \frac{q}{m_N} \mathcal{O}_9$
19	$\bar{\chi}_e \sigma^{\mu\nu} \frac{q_\nu}{m_L} \gamma^5 \chi_\mu \bar{N} \gamma_\mu \gamma^5 N$	$\left(-i\frac{\vec{q}}{m_L} \cdot \vec{\sigma}_L \right) (\vec{v}_N \cdot \vec{\sigma}_N)$	$-\frac{q}{m_L} \mathcal{O}_{14}$
		$-i\frac{q}{m_L} (\vec{\sigma}_L - \hat{q}\hat{q} \cdot \vec{\sigma}_L) \cdot \vec{\sigma}_N$	$-\frac{q}{m_L} (i\mathcal{O}_4 + i\mathcal{O}_6)$
20	$\bar{\chi}_e \sigma^{\mu\nu} \frac{q_\nu}{m_L} \gamma^5 \chi_\mu \bar{N} \sigma_{\mu\alpha} \frac{q^\alpha}{m_N} \gamma^5 N$	$\left(-i\frac{\vec{q}}{m_L} \cdot \vec{\sigma}_L \right) \left(-i\frac{\vec{q}}{m_N} \cdot \vec{\sigma}_N \right)$	$\frac{q}{m_L} \frac{q}{m_N} \mathcal{O}_6$

Table 3.3: Relativistic $\mu \to e$ conversion amplitudes $\mathcal{L}_{\mathrm{int}}^{j}$ and the corresponding linear combinations of the $\mathcal{O}_i$ resulting from the Pauli reduction.

Chapter 4

Nuclear Response Function Properties

The factorized form of the conversion rate presents a clear path to extracting all of the information about CLFV operators that can be probed in elastic $\mu \to e$ conversion. Indeed, the nuclear response functions W can be interpreted as the "nuclear dials" available to an experimentalist—dials that can be tuned through nuclear target selection in order to probe different linear combinations of the CLFV response functions. To aid in this endeavor, one would like to understand the general properties of the 6 (12, accounting for isospin) allowed nuclear response functions, including their dependence on macroscopic nuclear quantities such as charge and spin.

Broadly, we may distinguish three of the allowed nuclear responses, M, Σ', and Σ'', as velocity-*independent* and the remaining three, Δ, $\tilde{\Phi}'$, and Φ'', as velocity-*dependent*. The velocities in question—consistent with our definition of the effective interaction in terms of intrinsic nuclear coordinates—are the relative (or Jacobi) velocities of the nucleons. As these quantities are purely internal to the nuclear system, the velocity-dependent operators must vanish in the limit of a point-like nucleus. One way of approaching the point-like limit is to consider that the nucleus is probed by a very long wavelength operator; that is, $q_{\text{eff}} \to 0$. We note that in the expression for the $\mu \to e$ decay rate, Eq. (3.33), each of the velocity-dependent operators is accompanied by a factor q_{eff}^2/m_N^2, reflecting the fact that these responses vanish in the point-like limit.

On the other hand, the velocity-independent operators survive in the point-like limit; indeed, the leading multipoles have rather simple forms at $q_{\text{eff}} = 0$

$$M_{00}(0) = \frac{1}{\sqrt{4\pi}} \sum_{i=1}^{A} 1(i)$$

$$\Sigma'_{1M}(0) = \frac{1}{\sqrt{6\pi}} \sum_{i=1}^{A} \sigma_{1M}(i) \tag{4.1}$$

$$\Sigma''_{1M}(0) = \frac{1}{\sqrt{12\pi}} \sum_{i=1}^{A} \sigma_{1M}(i).$$

These are the total charge and total spin operators for the nucleus—macroscopic quantities that do not depend on any internal structure. The transverse-electric Σ'_1 and longitudinal Σ''_1 projections of the spin current are proportional in the long-wavelength limit, though they are distinct at finite q_{eff}. If a target with total ground-state angular momentum $j_N = 0$ is

selected, then only the coherent operator M_{00} will contribute; the spin-dependent operators require a nuclear state with $j_N \geq \frac{1}{2}$.

Although the prefactor q_{eff}^2/m_N^2 causes their response functions to vanish in the limit of zero momentum-transfer, the velocity-dependent operators can be expanded for long wavelengths as

$$\Delta_{1M}(0) = -\frac{1}{\sqrt{24\pi}} \sum_{i=1}^{A} \ell_{1M}(i)$$

$$\tilde{\Phi}'_{2M}(0) = -\frac{1}{\sqrt{20\pi}} \sum_{i=1}^{A} \left[\vec{x}(i) \otimes \left(\vec{\sigma}(i) \times \frac{1}{i}\vec{\nabla}(i) \right)_1 \right]_{2M} \tag{4.2}$$

$$\Phi''_{JM}(0) = \begin{cases} -\frac{1}{6\sqrt{\pi}} \sum_{i=1}^{A} \vec{\sigma}(i) \cdot \vec{\ell}(i), & J = 0 \\ -\frac{1}{\sqrt{30\pi}} \sum_{i=1}^{A} \left[\vec{x}(i) \otimes \left(\vec{\sigma}(i) \times \frac{1}{i}\vec{\nabla} \right)_1 \right]_{2M}, & J = 2 \end{cases},$$

where $\vec{\ell}$ is the orbital angular momentum operator, and $\otimes$ denotes a spherical tensor product whereas $\times$ denotes the conventional cross product. The lowest multipole of the transverse-electric projection of the spin-velocity current is $J = 2$, and therefore $\tilde{\Phi}'$ can only contribute if $j_N \geq 1$.

The momentum-dependence of the nuclear response functions $W_{\mathcal{O}}^{\tau\tau}(q)$ for ^{27}Al is shown in Fig. 4.1. In Fig. 4.2, we show the corresponding results for Cu—a case analogous to Al, as the only stable isotopes, ^{63}Cu and ^{65}Cu, have an unpaired nucleon. The nuclear responses for Al were computed by diagonalizing the USDB interaction in the $2s$-$1d$ shell-model space, whereas for Cu we employed the GCN2850 interaction in the $1f_{5/2}$-$2p$-$1g_{9/2}$ valence space. The ground state of ^{27}Al has total angular momentum $j_N = \frac{5}{2}$, and both isotopes of Cu have ground-state angular momentum $j_N = \frac{3}{2}$. The angular momentum selection rules therefore allow all six response functions to contribute. The nuclei ^{27}Al, ^{63}Cu, and ^{65}Cu carry total isospin $T = \frac{1}{2}$, $T = \frac{5}{2}$, and $T = \frac{7}{2}$, respectively, thereby permitting a coupling to isovector operators in all cases.

The isoscalar nuclear response is dominated, unsurprisingly, by the charge operator, particularly the coherent contribution of M_{00}. Quite remarkable is the strength of the Φ'' response. In the long-wavelength limit, Φ''_{00} reduces to the spin-orbit operator, which satisfies (for spin $s = 1/2$ nucleons)

$$\vec{\sigma} \cdot \vec{\ell} = \vec{j}^{\,2} - \vec{\ell}^{\,2} - \vec{s}^{\,2}$$
$$= j(j+1) - \ell(\ell+1) - \frac{3}{4}. \tag{4.3}$$

There are $2(\ell+1)$ states where $j = \ell + \frac{1}{2}$, for which the spin-orbit term evaluates to ℓ, and 2ℓ states where $j = \ell - \frac{1}{2}$, for which the spin-orbit term evaluates to $-(\ell+1)$. In nuclei, the strong nuclear spin-orbit force breaks the degeneracy between the $j = \ell \pm \frac{1}{2}$ subshells and moves the spin-aligned subshell $j = \ell + \frac{1}{2}$ to lower energy. As this subshell is progressively filled with nucleons, the spin-orbit response of Φ''_0 sums coherently. Once the spin-anti-aligned $j = \ell - \frac{1}{2}$ subshell starts to be filled, the spin-orbit contribution begins to cancel against that from the spin-aligned subshell. When both subshells are completely occupied, the total spin-orbit contribution is identically zero.

^{27}Al is an ideal nucleus for exploiting the semi-coherence of Φ_0'': in the extreme single-particle picture, all five states of the spin-aligned $1d_{5/2}$ subshell are occupied, while the anti-aligned $1d_{3/2}$ subshell is entirely vacant. Even after accounting for the additional momentum suppression factor—not included in the figures—$q_{\text{eff}}^2/m_N^2 W_{\Phi''}^{00}(q_{\text{eff}}) \approx 0.16$ is larger than either of the spin responses $W_{\Sigma'}^{00}(q_{\text{eff}}) \approx 0.09$, $W_{\Sigma''}^{00}(q_{\text{eff}}) \approx 0.11$.

Cu also shows a strong semi-coherent response from the operator Φ_0''. Protons completely fill the $1f_{7/2}$ subshell, leaving the anti-aligned counterpart vacant. In ^{63}Cu (^{65}Cu), neutrons completely fill the $1f_{7/2}$ and $2p_{3/2}$ subshells with two (four) neutrons occupying the anti-aligned $1f_{5/2}$ subshell, partially negating the coherence of the spin-orbit operator. Nonetheless, we find that the semi-coherence significantly enhances the response: $q_{\text{eff}}^2/m_N^2 W_{\Phi''}^{00}(q_{\text{eff}}) \approx 0.78$ is larger than either of the spin responses $W_{\Sigma'}^{00}(q_{\text{eff}}) \approx 0.15$, $W_{\Sigma''}^{00}(q_{\text{eff}}) \approx 0.12$.

Consequently, in the targets Al and Cu, we identify a hierarchy of isoscalar response functions

$$W_M^{00} \gg \left\{ W_{\Sigma'}^{00}, W_{\Sigma''}^{00}, \frac{q_{\text{eff}}^2}{m_N^2} W_{\Phi''}^{00} \right\} \gg \left\{ \frac{q_{\text{eff}}^2}{m_N^2} W_{\Delta}^{00}, \frac{q_{\text{eff}}^2}{m_N^2} W_{\tilde{\Phi}'}^{00} \right\}, \tag{4.4}$$

that is contrary to the naïve picture in which the velocity-dependent operators are generically subleading. As Φ'' is associated with the spin-velocity current $\vec{v}_N \times \vec{\sigma}_N$, which arises for tensor and other more exotic mediator, targets like Al and Cu have a special sensitivity to velocity-dependent couplings associated with such interactions.

In the case of isovector couplings, an isospin-symmetric core makes no contribution, and consequently in light targets with no appreciable neutron excess like ^{27}Al, one finds a hierarchy

$$\left\{ W_M^{11}, W_{\Sigma'}^{11}, W_{\Sigma''}^{11} \right\} \gg \left\{ \frac{q_{\text{eff}}^2}{m_N^2} W_{\Delta}^{11}, \frac{q_{\text{eff}}^2}{m_N^2} W_{\tilde{\Phi}'}^{11}, \frac{q_{\text{eff}}^2}{m_N^2} W_{\Phi''}^{11} \right\}, \tag{4.5}$$

that is fully dictated by velocity-suppression. To an extent, this picture is altered in heavier nuclei, where the excess of neutrons restores some of the coherence from the $M_{00;1}$ and $\tilde{\Phi}_{00;1}''$ responses. This effect is readily observed in Fig. 4.2 in the case of Cu.

Figure 4.3 shows the strength of the various velocity-independent response functions across 11 different nuclear targets, ranging in mass from the lightest, C, to the heaviest, Cu. One can plainly see how the coherent response increases with nucleon number A, though it is also somewhat dampened by the nuclear diffraction minimum for heavier nuclei. The isovector charge response function W_M^{11} also generally exhibits the expected behavior and is roughly proportional to the isospin asymmetry $|Z - N|$. Examining the spin-dependent responses, the targets that are composed primary of odd-nucleon isotopes—F, Na, Al, and Cu—provide the strongest response. The minor impurities of ^{13}C, ^{29}Si, ^{33}S, ^{47}Ti/^{49}Ti, and ^{57}Fe are not sufficient to produce an appreciable spin-dependent response in their respective targets. It is interesting to note how strong the Σ' and Σ'' responses are in ^{19}F.

Turning to the velocity-dependent response functions in Fig. 4.4, the trends are more difficult to discern. It is clear that $\tilde{\Phi}'$, the transverse-electric projection of the spin-velocity current, is consistently the weakest nuclear response, owing to the fact that it is velocity-suppressed and its leading multipole is $J = 2$. The transverse-magnetic projection of convective current Δ is also generally suppressed, though it is worth noting that ^{27}Al shows the strongest Δ response in both isospin channels of all nuclei considered. Finally, as discussed above, the longitudinal projection of the spin-velocity current Φ'' sums coherently over spin-aligned $j = \ell + \frac{1}{2}$ and spin-anti-aligned $j = \ell - \frac{1}{2}$ subshells but vanishes when both subshells
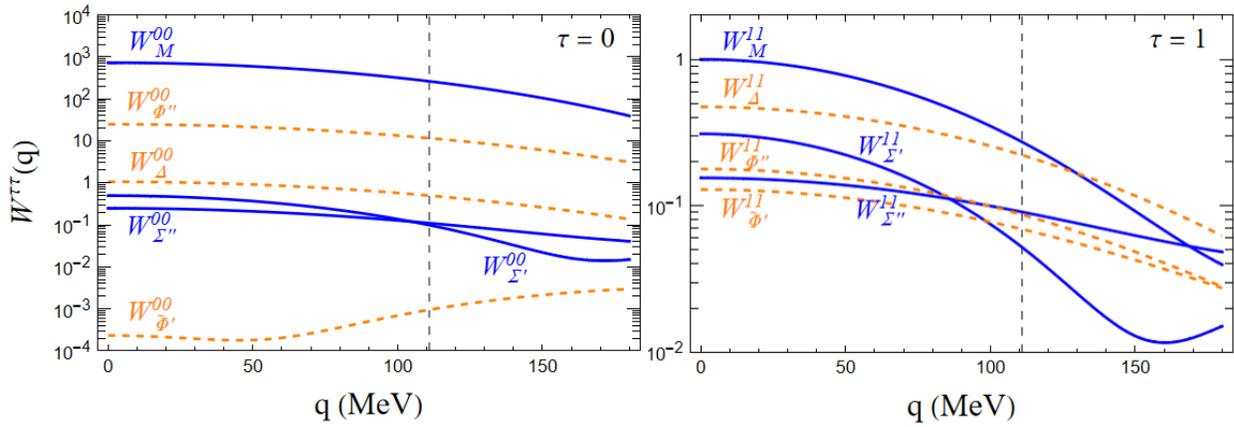
Figure 4.1: The nuclear response functions $W_{\mathcal{O}}^{\tau\tau}(q_{\text{eff}})$ for the six operators contributing to elastic $\mu \to e$ conversion in ^{27}Al. The left (right) panel gives the results for the isoscalar (isovector) coupling. The response functions are needed at the three-momentum transfer q_{eff} indicated by the dashed line. The results in blue correspond to charge and spin couplings, while those in orange correspond to the velocity-dependent operators where the response functions are accompanied by the additional factor $q_{\text{eff}}^2/m_N^2 \approx 0.014$.
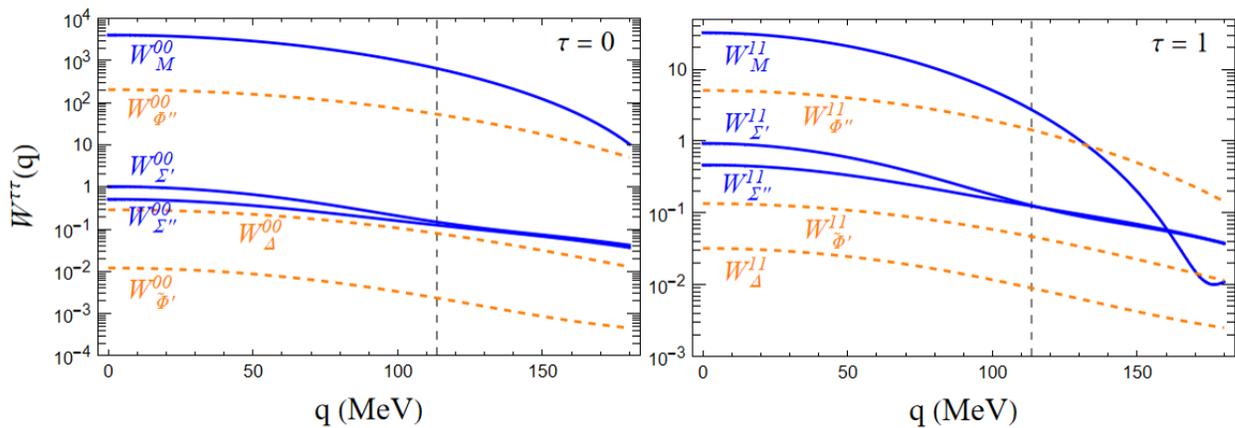
Figure 4.2: As in Fig. 4.1 but for Cu.

are fully occupied. As such, this contribution vanishes entirely for the doubly-magic nuclei ^{16}O and ^{40}Ca (though the response for the natural targets O and Ca is nonzero due to valence neutrons in the non-magic isotopes). The spin-orbit response is strongest when the lower-energy spin-aligned subshells are filled and the anti-aligned subshells are vacant. In Ti especially, we see how the response is primarily driven by neutrons filling the $1f_{7/2}$ shell, leading to a strong isovector response.

Comparing across all 12 allowed response functions, it appears that ^{27}Al is quite a good choice of initial nuclear target for the next-generation experiments, with competitive sensitivities to coherent, spin-dependent, and velocity-dependent operators. The interplay between nuclear target selection and the resulting nuclear response functions provides the blueprint for determining the nature of CLFV through an ensemble of measurements on various target nuclei. For example, if a $\mu \to e$ conversion signal were observed with an Al target but not with a Ca target, it would be good evidence that the underlying CLFV operators are not coherent, but either nuclear spin- or velocity-dependent. One might then attempt an experiment on Ti, which is typically weak in spin-dependent responses but rather sensitive to the majority of velocity-dependent couplings.

Finally, we may consider the limit $\vec{v}_N \to 0$, in which case only the three velocity-independent response functions M, Σ', and Σ'' contribute to the conversion amplitude. The resulting formalism is a valid effective theory in its own right, corresponding to the limit of a point-like nucleus. Accordingly, the operators of the nucleon-level theory that survive in the point-nucleus limit are $\mathcal{O}_1$, $\mathcal{O}_4$, $\mathcal{O}_6$, $\mathcal{O}_9$, $\mathcal{O}_{10}$, and $\mathcal{O}_{11}$, representing the most general set of single-nucleon operators that probe only the macroscopic nuclear quantities of charge and spin. Although the spin-dependent response has been considered previously in the literature (see Table 2.5), the only spin operator included in those works is the Gamow-Teller $\mathcal{O}_4 = \vec{\sigma}_L \cdot \vec{\sigma}_N$, which generates a specific linear combination of the longitudinal Σ'' and transverse-electric Σ' responses. In fact, these responses are entirely independent, and therefore, to our knowledge, our work is the first time that even the relatively simple point-nucleus response has been considered in full generality.
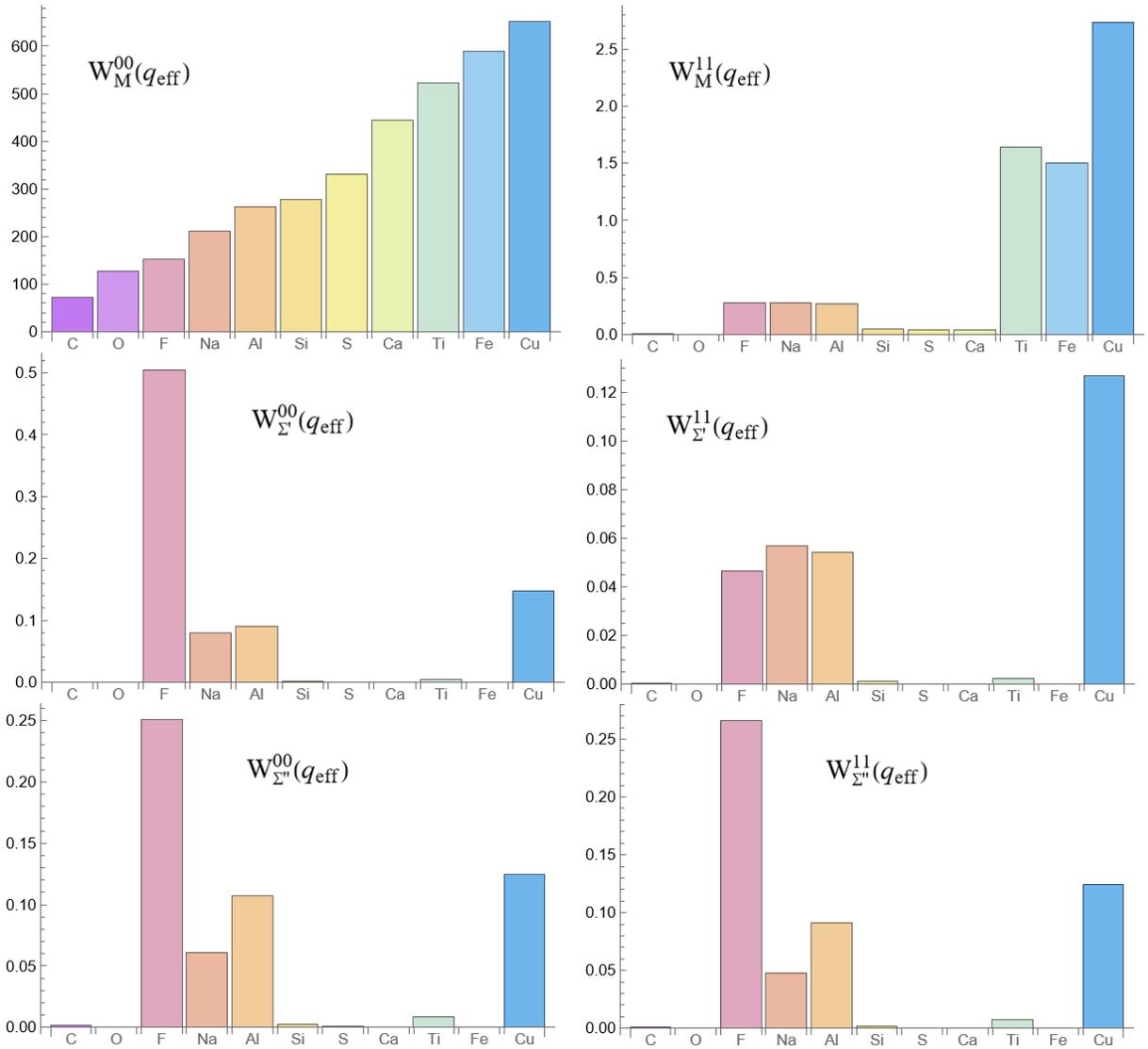
Figure 4.3: Velocity-independent response functions computed for the 11 nuclear targets of interest.
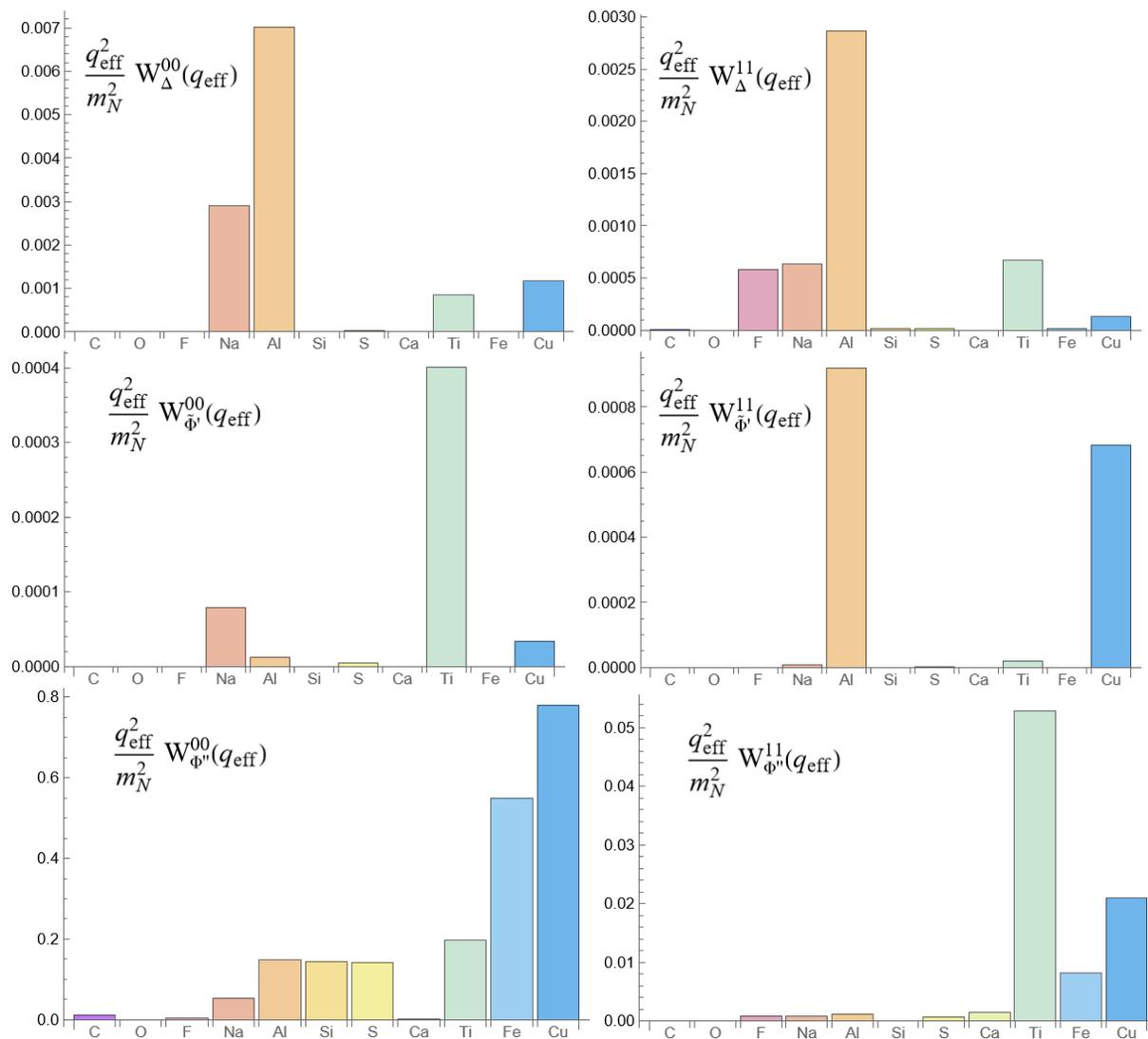
Figure 4.4: Velocity-dependent response functions computed for the 11 nuclear targets of interest and multiplied by the corresponding momentum suppression factor q_{eff}^2/m_N^2.

Chapter 5

LEC Analysis

Having demonstrated how the nuclear response functions can be computed for a specified target using nuclear many-body techniques, the only unknowns that remain in our expression for the decay rate $\Gamma(\mu \to e)$ are the CLFV low-energy constants $\tilde{c}_i^\tau$. Of course, our primary objective is to constrain these quantities through experimental measurements of the branching ratio

$$B(\mu \to e) = \frac{\Gamma(\mu \to e)}{\Gamma(\mu \to \nu_\mu)}, \tag{5.1}$$

where $\Gamma(\mu \to \nu_\mu)$ is the rate of standard muon capture.

Over the next five years, new experiments employing high-intensity pulsed muon beams should lead to substantial improvement in $\mu \to e$ conversion limits. The COMET experiment at J-PARC is expected to reach a branching ratio sensitivity $B(\mu \to e) < 7 \times 10^{-15}$ (90% CL) in Phase I and, ultimately, $B(\mu \to e) \lesssim 7 \times 10^{-17}$ in Phase II. The Mu2e experiment at Fermilab is expected to reach a branching ratio sensitivity of 8×10^{-17} (90% CL), and a proposed followup experiment Mu2e II, which will take advantage of future beam upgrades at Fermilab, could improve this limit by another order of magnitude. Both COMET and Mu2e will employ Al targets. A second J-PARC experiment has been proposed by the DeeMe collaboration [102] and aims to achieve a $\mu \to e$ branching ratio limit of 1×10^{-13} for a graphite target. A followup experiment, hoping to achieve a branching ratio sensitivity 2×10^{-14} with a silicon carbide target, has also been discussed.

With the exception of the SIN experiment on ^{32}S, all past and planned experiments have employed natural targets; therefore, we carry out shell-model calculations for each isotope with natural abundance $> 0.2\%$ and compute the total $\mu \to e$ conversion rate as a sum over the isotopes weighted by their abundance. To convert the CLFV decay rate to a branching ratio, we normalize by the corresponding rate for standard muon capture, adopting the values

$$\Gamma(\mu \to \nu_\mu) = \begin{Bmatrix} 0.0378 & \text{C} \\ 0.703 & \text{Al} \\ 0.865 & \text{Si} \\ 1.351 & \text{S} \\ 2.592 & \text{Ti} \\ 5.673 & \text{Cu} \end{Bmatrix} \times 10^6 \text{ s}^{-1}, \tag{5.2}$$

which were obtained by computing weighted averages of the measurements compiled in Ref. [103]. For the capture of muons onto the compound SiC, the capture probability is proportional to Z [104], and therefore 70% of muons capture onto Si and 30% capture onto C.

We estimate the impact of these proposed new experiments on CLFV bounds in the following way: We isolate the impact of individual effective theory operators by setting all of the single-nucleon LECs equal to zero except for one, say $\tilde{c}_i^\tau$. For a given branching ratio bound, there is an implied upper limit on the magnitude of the non-zero CLFV coupling $|\tilde{c}_i^\tau| \leq y_i^\tau$. Larger couplings would yield observable rates of $\mu \to e$ conversion. Table 5.1 shows the maximum magnitude of each LEC that is consistent with the specified branching ratio limit.

More physically, assuming that the LEC under consideration is natural at the scale of CLFV physics, one may convert the dimensionless LEC limit into an approximate scale probed by the given operator

$$\Lambda_i^\tau = \frac{v}{\sqrt{y_i^\tau}}. \tag{5.3}$$

The corresponding values of Λ_i^τ are shown in Table 5.2. The operators that generate the coherent response, $\tilde{c}_1^0$ and $\tilde{c}_{11}^0$, probe the highest scale of new physics—up to 10^4 TeV in ^{27}Al at a branching ratio sensitivity $\approx 10^{-17}$. By this same measure, the existing limit in Ti provides a constraint up to ≈ 900 TeV; the next-generation experiments will improve the reach in energy scale by more than an order of magnitude. The isovector operators $\tilde{c}_1^1$ and $\tilde{c}_{11}^1$, which do not benefit from the coherent enhancement, are still capable of probing up to $\approx 2,000$ TeV. The Mu2e/COMET design sensitivity is so impressive that even the weakest probe, $\tilde{c}_{13}^\tau$, associated only with the highly-suppressed $\tilde{\Phi}'$ response function, is capable of probing new physics up to ≈ 200 TeV in the isoscalar case and ≈ 500 TeV in the isovector. The fact that the Mu2e and COMET measurements in ^{27}Al will provide much stricter individual operator limits does not render previous (or planned but less ambitious, e.g., DeeMe) experiments obsolete, as different nuclear targets constrain different combinations of the underlying leptonic response functions. The single-source scenario considered here is only meant to illustrate the relative sensitivity of each CLFV operator; in practice, we must retain all allowed operators, which are then constrained by the available measurements.

Target	Al	C	SiC	^{32}S	Ti	Cu
Branching Ratio	$10^{-17\dagger}$	$10^{-13\dagger}$	$2 \times 10^{-14\dagger}$	7×10^{-11}	6.1×10^{-13}	1.6×10^{-8}
$\tilde{c}_1^0, \tilde{c}_{11}^0$	4.0E-10	5.1E-8	1.8E-8	1.0E-6	7.4E-8	1.2E-5
$\tilde{c}_1^1, \tilde{c}_{11}^1$	1.2E-8	6.3E-6	1.4E-6	-	1.3E-6	1.9E-4
$\tilde{c}_3^0, \tilde{c}_{15}^0$	1.6E-8	4.0E-6	7.3E-7	4.5E-5	3.8E-6	3.5E-4
$\tilde{c}_3^1, \tilde{c}_{15}^1$	1.9E-7	1.3E-4	4.0E-5	-	7.3E-6	2.1E-3
$\tilde{c}_4^0$	1.4E-8	9.4E-6	4.1E-6	-	1.5E-5	5.9E-4
$\tilde{c}_4^1$	1.7E-8	1.1E-5	4.9E-6	-	1.7E-5	6.1E-4
$\tilde{c}_5^0, \tilde{c}_8^0$	7.8E-8	9.6E-5	7.1E-5	-	5.8E-5	9.0E-3
$\tilde{c}_5^1, \tilde{c}_8^1$	1.2E-7	1.6E-4	7.3E-5	-	6.5E-5	2.7E-2
$\tilde{c}_6^0, \tilde{c}_{10}^0$	2.0E-8	1.1E-5	5.5E-6	-	1.8E-5	8.7E-4
$\tilde{c}_6^1, \tilde{c}_{10}^1$	2.2E-8	1.2E-5	6.1E-6	-	2.0E-5	8.7E-4
$\tilde{c}_9^0$	2.1E-8	1.9E-5	6.2E-6	-	2.8E-5	8.0E-4
$\tilde{c}_9^1$	2.8E-8	2.2E-5	8.1E-6	-	3.4E-5	8.7E-4
$\tilde{c}_{12}^0$	1.6E-8	4.0E-6	7.3E-7	4.5E-5	3.8E-6	3.5E-4
$\tilde{c}_{12}^1$	1.4E-7	1.3E-4	4.0E-5	-	7.3E-6	2.1E-3
$\tilde{c}_{13}^0$	1.8E-6	-	-	-	8.4E-5	5.3E-2
$\tilde{c}_{13}^1$	2.1E-7	-	-	-	3.7E-4	1.2E-2

Table 5.1: Limits on the CLFV LECs imposed by $\mu \to e$ conversion branching ratios. Given the specified branching ratio limits, the allowed values of the dimensionless LECs are given by $|\tilde{c}_i^\tau| \lesssim y_i^\tau$, where the y_i^τ are the column entries. The $\dagger$'s indicate branching ratios achievable in planned experiments. E-$x \equiv 10^{-x}$.

Target	Al	C	SiC	^{32}S	Ti	Cu
Branching Ratio	$10^{-17\,\dagger}$	$10^{-13\,\dagger}$	$2 \times 10^{-14\,\dagger}$	7×10^{-11}	6.1×10^{-13}	1.6×10^{-8}
$\tilde{c}_1^0, \tilde{c}_{11}^0$	1.2E4	1.1E3	1.9E3	2.4E2	9.1E2	7.1E1
$\tilde{c}_1^1, \tilde{c}_{11}^1$	2.2E3	9.8E1	2.1E2	-	2.1E2	1.8E1
$\tilde{c}_3^0, \tilde{c}_{15}^0$	1.9E3	1.2E2	2.9E2	3.7E1	1.3E2	1.3E1
$\tilde{c}_3^1, \tilde{c}_{15}^1$	5.7E2	2.1E1	3.9E1	-	9.1E1	5.3E0
$\tilde{c}_4^0$	2.1E3	8.0E1	1.2E2	-	6.3E1	1.0E1
$\tilde{c}_4^1$	1.9E3	7.6E1	1.1E2	-	5.9E1	9.9E0
$\tilde{c}_5^0, \tilde{c}_8^0$	8.8E2	2.5E1	2.9E1	-	3.2E1	2.6E0
$\tilde{c}_5^1, \tilde{c}_8^1$	7.2E2	2.0E1	2.9E1	-	3.0E1	1.5E0
$\tilde{c}_6^0, \tilde{c}_{10}^0$	1.8E3	7.5E1	1.1E2	-	5.9E1	8.3E0
$\tilde{c}_6^1, \tilde{c}_{10}^1$	1.7E3	7.1E1	9.9E1	-	5.5E1	8.3E0
$\tilde{c}_9^0$	1.7E3	5.7E1	9.9E1	-	4.7E1	8.7E0
$\tilde{c}_9^1$	1.5E3	5.2E1	8.7E1	-	4.2E1	8.4E0
$\tilde{c}_{12}^0$	1.9E3	1.2E2	2.9E2	3.7E1	1.3E2	1.3E1
$\tilde{c}_{12}^1$	6.6E2	2.1E1	3.9E1	-	9.1E1	5.4E0
$\tilde{c}_{13}^0$	1.8E2	-	-	-	2.7E1	1.1E0
$\tilde{c}_{13}^1$	5.4E2	-	-	-	1.3E1	2.3E0

Table 5.2: Approximate energy scale $\tilde{\Lambda}_i^\tau = \Lambda_i^\tau/\text{TeV}$ probed by the effective CLFV operators at a given $\mu \to e$ conversion branching ratio limit. The †s indicate branching ratios achievable in planned experiments. E-$x \equiv 10^{-x}$.

Chapter 6

Relationship to $\mu \to e\gamma$ and $\mu \to 3e$

The process of $\mu \to e$ conversion in nuclei is just one probe of possible CLFV physics. There is significant theoretical and experimental interest in CLFV processes involving the tau lepton, in addition to the muon and electron, as well as non-leptonic particles in the initial and/or final states. Flavor-violating decays of relatively heavy particles such as the Higgs, Z boson, B mesons, and τ lepton are currently constrained by proton-proton collider experiments including ATLAS, CMS, and LHCb. Competitive limits on select CLFV processes—especially τ decays—are anticipated in the near future from e^+e^- collisions at the Belle II experiment and from collisions at the Electron-Ion Collider of electrons with either protons or heavy atomic nuclei. Dedicated experiments MEG II and Mu3e are designed to search, respectively, for the relatively low-energy CLFV processes $\mu \to e\gamma$ and $\mu \to 3e$.

Many of the above-mentioned processes are interrelated. For example, if the CLFV vertex that mediates $h \to e\mu$ exists, then it will induce both $\mu \to e$ conversion through the exchange of a virtual Higgs and $\mu \to e\gamma$ through one- and two-loop diagrams. (This scenario is considered in detail in Section 8.6.) Thus, a combination of measurements from colliders and dedicated decay experiments will play a complementary role in distinguishing among candidate UV theories of CLFV. In this chapter, limiting our discussion to CLFV muon decays, we explore the relationship between $\mu \to e$ conversion, $\mu \to e\gamma$, and $\mu \to 3e$. We explore the limits that can be placed on operator coefficients if Mu2e/COMET, MEG II, and Mu3e achieve their design sensitivity and comment on the wide range of possible detection scenarios at these next-generation experiments.

The most general CLFV electromagnetic vertex coupling a photon to the leptons is

$$
\begin{aligned}
\Gamma^\mu_{\mu \to e} = {} & \frac{1}{\Lambda^2} \left(q^2 \gamma^\mu - q^\mu \slashed{q} \right) \left[\tilde{f}_R(q^2) + i \tilde{f}_A(q^2) \gamma_5 \right] \\
& + i \frac{m_\mu}{\Lambda^2} \sigma^{\mu\nu} q_\nu \left[\tilde{f}_M(q^2) + i \tilde{f}_E(q^2) \gamma_5 \right],
\end{aligned}
\tag{6.1}
$$

where Λ is the scale of CLFV physics, and the subscripts R, A, M, and E denote the induced (dimensionless) CLFV charge radius, anapole, magnetic dipole, and electric dipole form factors, respectively. In the case of on-shell photon production, shown in Fig. 6.1 (a), the four-momentum transfer satisfies $q^2 = 0$, and the charge radius and anapole form factors do not contribute. The resulting $\mu \to e\gamma$ decay rate has the simple form

$$
\Gamma \left(\mu \to e\gamma \right) = \frac{1}{2} \alpha \frac{m_\mu^5}{\Lambda^4} \left(|\tilde{f}_M(0)|^2 + |\tilde{f}_E(0)|^2 \right).
\tag{6.2}
$$

Figure 6.1: (a) On-shell $\mu \to e\gamma$ decay mediated by CLFV vertex. (b) Conversion process induced by the $\mu \to e\gamma$ vertex. The photon is virtual and exchanged with the nuclear charge.

To arrive at the branching ratio, we normalize by the rate of standard model $\mu \to e + 2\nu$ decay. The result is exceedingly simple:

$$B(\mu \to e\gamma) = 192\alpha\pi^3 \left(\frac{v}{\Lambda}\right)^4 \left(|\tilde{f}_M(0)|^2 + |\tilde{f}_E(0)|^2\right). \tag{6.3}$$

In comparison to $\mu \to e$ conversion, the on-shell $\mu^+ \to e^+\gamma$ process—the focus of the MEG and MEG-II experiments—is a relatively clean probe of CLFV physics, as it does not depend on any nuclear physics. The drawback is that one must detect both the positron and the photon, with backgrounds primarily coming from radiative muon decay $\mu^+ \to e^+\nu\bar{\nu}\gamma$ and from accidental coincidence of a positron from Michel decay $\mu^+ \to e^+\nu\bar{\nu}$ with a photon originating from either radiative muon decay, bremsstrahlung, or $e^+e^- \to \gamma\gamma$ annihilation. Consequently, the expected branching ratio sensitivity at the next-generation MEG II experiment, $B(\mu \to e\gamma) < 6 \times 10^{-14}$ (90% CL), is roughly three orders of magnitude less sensitive than the corresponding limits on $\mu \to e$ conversion expected at Mu2e and COMET.

If $\mu \to e$ conversion proceeds through exchange of a virtual photon, as in Fig. 6.1 (b), then all four CLFV electromagnetic form factors in Eq. (6.1) contribute. The photon couples directly to the nuclear Coulomb charge, and therefore the $\mu \to e$ conversion amplitude is

$$\frac{4\pi\alpha}{q^2}\bar{\chi}_e\Gamma^\mu_{\mu\to e}(q^2)\chi_\mu \; \bar{N}\gamma_\mu \left(\frac{1+\tau_3}{2}\right) N. \tag{6.4}$$

Retaining only the dominant coherent contribution and approximating the fixed four-momentum of the photon propagator as $q^2 \approx -m_\mu^2$, we find the following values for the nucleon-level effective theory LECs:

$$\tilde{c}_1^0 = \tilde{c}_1^1 = 2\pi\alpha\frac{v^2}{\Lambda^2}\left[\tilde{f}_R(-m_\mu^2) + \tilde{f}_M(-m_\mu^2)\right]$$
$$\tilde{c}_{11}^0 = \tilde{c}_{11}^1 = 2\pi\alpha\frac{v^2}{\Lambda^2}\left[\tilde{f}_A(-m_\mu^2) - \tilde{f}_E(-m_\mu^2)\right]. \tag{6.5}$$

If we assume that the momentum dependence of the form factors is mild $\tilde{f}(-m_\mu^2) \approx \tilde{f}(0)$, then the rates for $\mu \to e$ conversion and $\mu \to e\gamma$ will be correlated through their dependence

on the dipole form factors $\tilde{f}_M$ and $\tilde{f}_E$. We can explore this relationship further by setting $\tilde{f}_A = \tilde{f}_E = 0$ and assuming that $|\tilde{f}_R| + |\tilde{f}_M| = 1$. This latter condition corresponds to the requirement that at least one of the non-zero form factors is approximately natural at the scale of CLFV physics Λ. Figure 6.2 shows the regions of parameter space in Λ and $|\tilde{f}_R/\tilde{f}_M|$ that are excluded by current and future experiments. As expected, we see that the on-shell process provides no constraint in the limit $\tilde{f}_R \gg \tilde{f}_M$.

For the conversion process, two cases must be distinguished: If $\tilde{f}_R$ and $\tilde{f}_M$ have the same sign, then the total rate is independent of the ratio $|\tilde{f}_R/\tilde{f}_M|$, as we have assumed $|\tilde{f}_R| + |\tilde{f}_M| = 1$. If, however, the charge radius and magnetic dipole form factors are opposite sign, then they interfere destructively, leading to a total cancellation when $|\tilde{f}_R/\tilde{f}_M| = 1$. (In actuality, the cancellation is not exact—only the leading coherent contribution is zero, and the typically suppressed spin- and velocity-dependent operators constitute the leading response. We can infer from Table 5.2 that the limits on Λ in this case are at least a factor of five weaker.) In the cancellation scenario, it is possible to observe a $\mu \to e\gamma$ signal at MEG II without a corresponding $\mu \to e$ conversion signal at Mu2e/COMET Phase II. Otherwise, one generically expects the conversion experiments to provide a more stringent constraint on electromagnetic CLFV couplings than the on-shell photon experiments, despite the fact that the rate for virtual-photon-mediated $\mu \to e$ conversion is suppressed by a factor of α relative to the on-shell process—the conversion experiments aim to achieve roughly six-thousand times better sensitivity.

To get some sense of the relationship of these processes to $\mu \to 3e$, we consider the effective Lagrangian

$$\mathcal{L} = \frac{1}{\Lambda^2} \left(C_{\mu eee}^L \bar{e}_L^c \mu_L \bar{e}_L e_L^c + C_{\mu eee}^R \bar{e}_R^c \mu_R \bar{e}_R e_R^c \right), \tag{6.6}$$

where $e_L^c = -i\sigma_2 e_R^*$ and $e_R^c = i\sigma_2 e_L^*$ are charge-conjugated electron spinors. $C_{\mu eee}^L$ and $C_{\mu eee}^R$ are (dimensionless) Wilson coefficients. The branching ratio is then given by

$$B(\mu \to 3e) = \frac{1}{2} \left(\frac{v}{\Lambda} \right)^4 \left(|C_{\mu eee}^L|^2 + |C_{\mu eee}^R|^2 \right). \tag{6.7}$$

In general, there are dimension-six operators that mediate $\mu \to 3e$ beyond those included in Eq. (6.6). We have restricted to those operators unique in that at one-loop order [see Fig. 6.3 (a)] they generate an effective $\mu \to e\gamma$ vertex that is enhanced by a large logarithm. The resulting electromagnetic couplings are [105–107]

$$\begin{aligned}
\tilde{f}_R &= -\frac{1}{(4\pi)^2} \frac{2}{3} \left(C_{\mu eee}^L + C_{\mu eee}^R \right) \ln\frac{-q^2}{\Lambda^2}, \\
\tilde{f}_A &= -i\frac{1}{(4\pi)^2} \frac{2}{3} \left(C_{\mu eee}^L - C_{\mu eee}^R \right) \ln\frac{-q^2}{\Lambda^2},
\end{aligned} \tag{6.8}$$

where we have retained only the large logarithm contributions. Assuming that these are the only contributions to the charge radius and anapole form factors, these relations can be inverted to write the $\mu \to 3e$ branching ratio in terms of the induced couplings

$$B(\mu \to 3e) = \left(\frac{v}{\Lambda} \right)^4 \left(\frac{12\pi^2}{\ln\left(m_\mu^2/\Lambda^2\right)} \right)^2 \left(|\tilde{f}_R(-m_\mu^2)|^2 + |\tilde{f}_A(-m_\mu^2)|^2 \right). \tag{6.9}$$
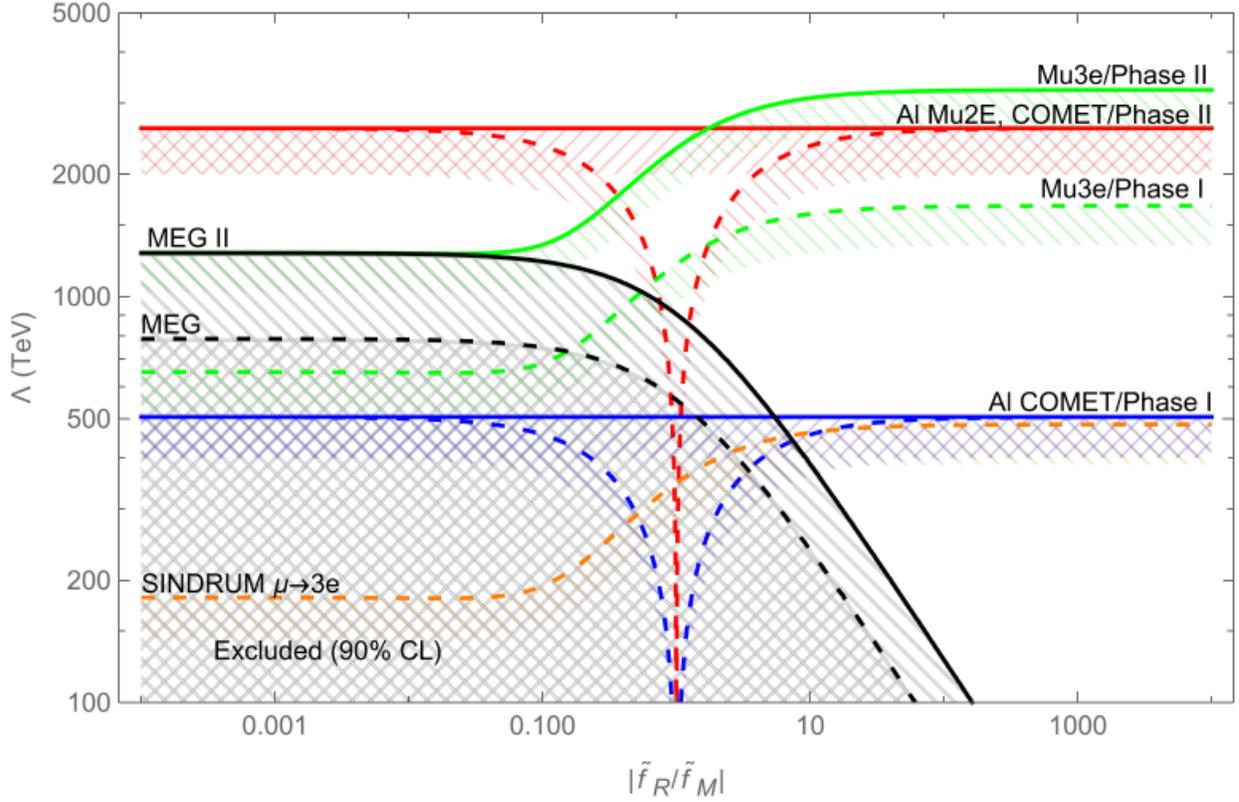
Figure 6.2: Exclusion curves for the CLFV electromagnetic coupling considered in Eq. (6.1) for the case $\tilde{f}_A = \tilde{f}_E = 0$ and $|\tilde{f}_R| + |\tilde{f}_M| = 1$. The dashed (solid) black curve shows the (expected) limit for on-shell $\mu \to e\gamma$ obtained from MEG (MEG II). The branching ratio limits are $B(\mu \to e\gamma) < 4.2 \times 10^{-13}$ for the MEG experiment and 6×10^{-14} for MEG II. The dashed (solid) green curve shows the (expected) limit for $\mu \to 3e$ obtained from Mu3e Phase I (Phase II). The branching ratio limit is $B(\mu \to 3e) < 6 \times 10^{-15}$ (4×10^{-16}) for Phase I (II) of Mu3e. The orange curve corresponds to the existing limit $B(\mu \to 3e) < 1.0 \times 10^{-12}$ obtained by SINDRUM. The solid red (blue) curve corresponds to a $\mu \to e$ branching ratio limit $B(\mu \to e) < 10^{-17}$ (7×10^{-15}) for the case where $\tilde{f}_R$ and $\tilde{f}_M$ contribute with the same sign. The dashed red (blue) curve is analogous to the solid red (blue) curve for the case where $\tilde{f}_R$ and $\tilde{f}_M$ are opposite sign. In this case, the charge radius and magnetic dipole contributions to the coherent conversion on nuclei cancel when $|\tilde{f}_R/\tilde{f}_M| = 1$.
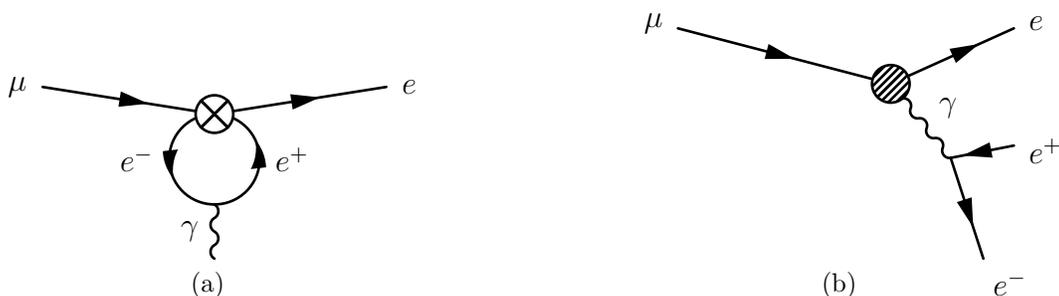
Figure 6.3: (a) One-loop diagram in which an underlying $\mu \to 3e$ vertex [that of Eq. (6.6)] generates $\mu \to e\gamma$. This contribution is only nonzero for off-shell photons. (b) Tree-level diagram in which $\mu \to e$ induces $\mu \to 3e$ via pair production.

This expression describes the $\mu \to 3e$ process when the CLFV is dominated by the charge radius (or anapole) coupling but vanishes in the limit where the magnetic (or electric) dipole moment coupling becomes large. In the latter case, the strong dipole interaction mediates $\mu \to e\gamma$, and the $\mu \to 3e$ process then proceeds through a virtual photon decaying to an electron/positron pair, as in Fig. 6.3 (b). In this limit, the branching ratios satisfy a simple relation [108]

$$B(\mu \to 3e) \approx \frac{\alpha}{3\pi} \left(\ln\frac{m_\mu^2}{m_e^2} - 2 \right) B(\mu \to e\gamma). \tag{6.10}$$

We may now interpret the $\mu \to 3e$ exclusion curves in Fig. 6.2: When $|\tilde{f}_R| \gg |\tilde{f}_M|$, $\mu \to 3e$ proceeds through the four-fermion interaction of Eq. (6.6), and $\mu \to e$ conversion is induced by the large-logarithm-enhanced loop diagram. Despite the logarithmic enhancement, the α suppression of the virtual photon process is significant enough that—assuming final phase sensitivities—Mu3e will provide a stronger constraint on the charge-radius-dominated region of parameter space. In contrast, when $|\tilde{f}_R| \ll |\tilde{f}_M|$, then both $\mu \to e$ conversion and $\mu \to 3e$ are suppressed by α, and consequently the advantage in sensitivity of Mu2e and COMET over Mu3e translates into a stronger constraint on dipole-dominated couplings.

We reiterate that the scenario discussed here is not general. Although Eq. (6.1) is the most general CLFV electromagnetic coupling describing the $\mu \to e\gamma$ process, additional (non-photonic) sources of $\mu \to 3e$ and $\mu \to e$ conversion will alter the interplay between these three processes. Nonetheless, it is worth taking a moment to survey the landscape of Fig. 6.2 to get a scope of the rich variety of experimental outcomes that are possible in the next generation. If we consider the charge-radius-dominated scenario $|\tilde{f}_R/\tilde{f}_M| \gg 1$, then it is extremely unlikely that we will detect the on-shell process at MEG II. Depending on the scale of CLFV physics, it may be possible to detect CLFV at both Mu2e/COMET and Mu3e or only at Mu3e (or, of course, a null result at all experiments). At the other extreme, the magnetic-dipole-dominated scenario $|\tilde{f}_R/\tilde{f}_M| \ll 1$, the sensitivities of Mu3e and MEG II are quite comparable but fall short of the conversion experiments. Depending on the scale Λ, we may observe one of three possible outcomes: (1) detection at all experiments (2) detection at

Mu2e/COMET but not Mu3e or MEG II (3) no detection.

Finally, if the source of CLFV is such that the charge radius and magnetic dipole couplings are roughly equal $|\tilde{f}_R/\tilde{f}_M| \approx 1$, then we must also consider the possible cancellation in the $\mu \to e$ conversion rate. Without cancellation, the sensitivity of Mu3e is roughly on par with the conversion experiments, and we could observe one of four possible outcomes: (1) detection at all experiments (2) detection at Mu2e/COMET and Mu3e but not MEG II (3) detection only at either Mu3e or Mu2e/COMET (4) no detection. If the cancellation is significant, then we don't expect any signal from the conversion experiments. One particularly interesting possibility is that we may observe a CLFV signal at MEG II and Mu3e but not Mu2e/COMET. Such a result could be interpreted as good evidence for the cancellation scenario, though a more general analysis would be warranted.

Chapter 7

Relativistic Muon Corrections

In our initial formulation of the nuclear effective theory of $\mu \to e$ conversion, we argued that for light- and medium-mass nuclei it is an acceptable approximation to neglect contributions proportional to the lower component of the muon wave function (see Section 2.4). This stands in contrast to many previous authors, who—typically focusing only on the case of coherent conversion—retain the complete numerical Dirac solution for the lower component. In that restricted setting, such a treatment makes it possible to obtain percent-level errors in the prediction for the $\mu \to e$ conversion rate without unduly complicating the calculation. In general, however, inclusion of the lower component of the muon requires a significant extension of the formalism, and the impact of these relativistic corrections is not as immediate as in the coherent case.

As we shall demonstrate in this chapter, the lower component of the muon's Dirac wave function is effectively generated by the action of the muon velocity operator $\vec{v}_\mu$ on the upper component. Thus, the inclusion of the muon's lower component in the effective theory is (approximately) equivalent to the addition of the muon velocity operator. The effective theory describes the intrinsic interactions that result from removing the center-of-mass motion of the system by a phase-space integration [see Eq. (3.11) and subsequent discussion]. The initial system, assumed to be at rest, is described by $A-1$ inter-nucleon coordinates and one coordinate describing the muon's position relative to the nuclear center-of-mass. Consequently, there are $A-1$ inter-nucleon velocity operators and one muon velocity operator, which, again, is defined relative to the nuclear center-of-mass. From this perspective, the muon velocity operator is not privileged—it is one of A internal bound-state velocities. In fact, one may argue that it is more essential to retain the velocity operator of the nucleons than that of the muon: In ^{27}Al, $\sqrt{\langle v_\mu^2 \rangle} \approx 0.05$, whereas for a single unpaired $1d_{5/2}$ proton $\sqrt{\langle v_N^2 \rangle} \approx 0.21$. As the electron is ultra-relativistic, the muon's lower component always appears in combination with the upper component and therefore can be considered a correction. On the other hand, depending on the underlying CLFV operators, the $\mu \to e$ conversion response may be generated at leading order by $\vec{v}_N$.

As discussed at the end of Chapter 4, the most fundamental nuclear-scale effective theory is that of the point-like nucleus, which depends on three nuclear response functions. The point-like effective theory can then be extended to include first-order corrections in the nucleon velocity operator $\vec{v}_N$, generating three additional nuclear responses. Based on the above discussion, a final step in this program is to introduce operators that are first-order

in the muon velocity $\vec{v}_\mu$ (neglecting terms of order $v_\mu v_N \approx 1/100$). We will now undertake this construction, introducing the modifications of the nuclear-scale effective theory that are necessary in order to include the impact of the muon's lower component, leading to the introduction of six additional nuclear response functions.

7.1 Relationship between the Lower Component and the Velocity Operator

We begin by demonstrating how the muon's lower component can be obtained by action of the muon velocity operator on the corresponding upper component. (See Chapter 2, in particular Section 2.4, for complete details of the Dirac treatment of the muon wave function.) The muon is known to occupy the $1s$ orbital of the nuclear Coulomb field, and for $\kappa = -1$, the muon's Dirac solution has the form

$$\psi_m^{(\mu)}(\vec{r}) = \begin{pmatrix} \frac{G(r)}{r}\Omega_{\frac{1}{2}m}^0(\hat{r}) \\ i\frac{F(r)}{r}\Omega_{\frac{1}{2}m}^1(\hat{r}) \end{pmatrix}, \tag{7.1}$$

Using the fact that

$$\Omega_{\frac{1}{2}m}^1(\hat{r}) = -\vec{\sigma}\cdot\hat{r}\, Y_{00}(\hat{r})\xi_m, \tag{7.2}$$

we may write

$$\psi_m^{(\mu)}(\vec{r}) = \begin{pmatrix} \frac{G(r)}{r}\, Y_{00}(\hat{r})\xi_m \\ -i\frac{F(r)}{r}\vec{\sigma}\cdot\hat{r}\, Y_{0,0}(\hat{r})\xi_m \end{pmatrix}, \tag{7.3}$$

which makes manifest the two primary differences between the muon's upper and lower components: (1) The radial wave functions $G(r)$ and $F(r)$ are different. (2) The lower component carries an additional angular dependence through the operator $\vec{\sigma}\cdot\hat{r}$. The latter issue cannot be avoided and leads to a significant reorganization of the multipole decomposition, as we show in the next section. The difference between the radial wave functions can be addressed by noting that, for $\kappa = -1$, the radial Dirac equation implies that

$$\frac{d}{dr}\left(\frac{G(r)}{r}\right) = \left(2\bar{m} - E_\mu^{\text{bind}} - V(r)\right)\frac{F(r)}{r}. \tag{7.4}$$

In analogy with the effective momentum treatment of the electron (see Section 2.3), we may replace the Coulomb potential by an average value $\bar{V}_C$ and write

$$\frac{d}{dr}\left(\frac{G(r)}{r}\right) \approx 2m^*\frac{F(r)}{r}, \tag{7.5}$$

where

$$m^* \equiv \bar{m} - \left(E_\mu^{\text{bind}} + \bar{V}_C\right)/2, \tag{7.6}$$

is an effective muon mass, which varies from the physical reduced muon mass $\bar{m}$ by $\approx 2.6\%$ in ^{27}Al. We can now express both components of the muon wave function in terms of the
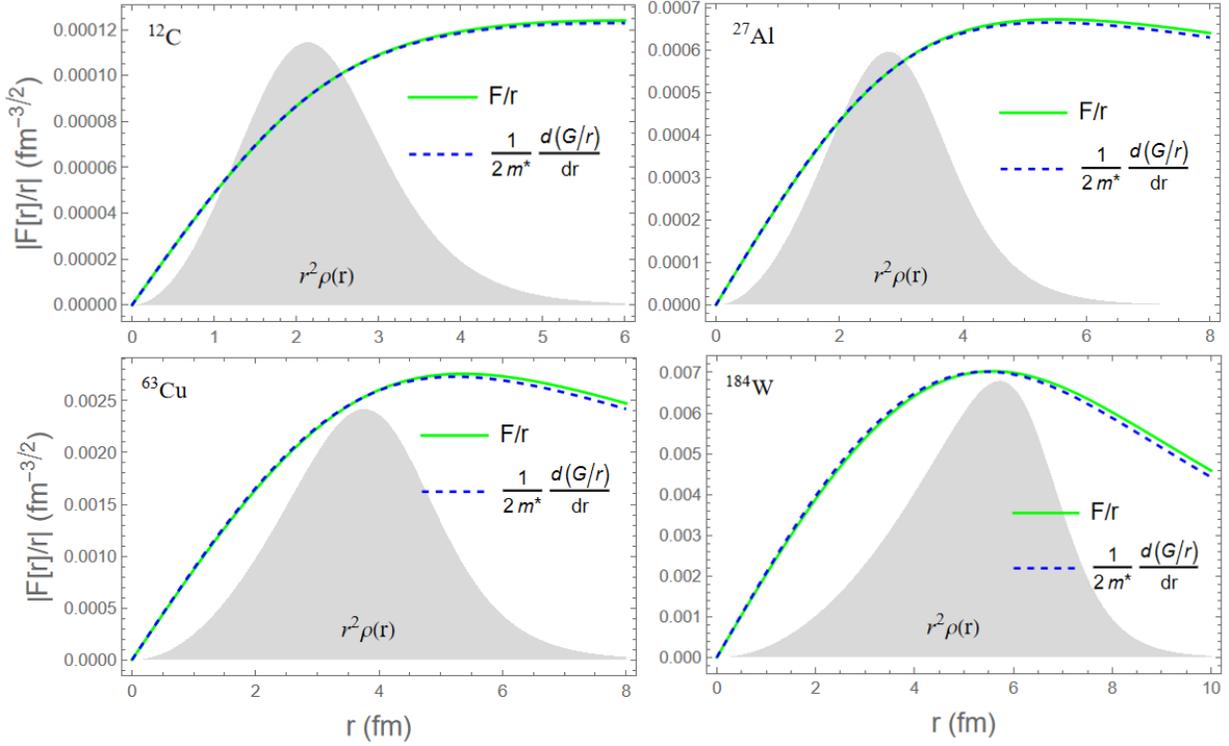
Figure 7.1: Comparison of the exact result (green line) for the absolute value of the muon wave function lower component $|F(r)/r|$ and the effective wave function (blue dashed line) given by Eq. (7.5) in four target nuclei: ^{12}C, ^{27}Al, ^{63}Cu, and ^{184}W. The grey shaded region shows the extent of the nuclear density $r^2\rho(r)$ (arbitrary normalization). Note that the scale of the plot is different across the four nuclei. In all cases, the effective wave function provides a good approximation of the muon's lower component.

radial function $G(r)$ as

$$
\begin{aligned}
\psi_m^{(\mu)}(\vec{r}) &\approx \begin{pmatrix} \xi_m \\ \frac{\vec{\sigma}\cdot\vec{p}_\mu}{2m^*}\xi_m \end{pmatrix} \frac{G(r)}{r} Y_{00}(\hat{r}) \\
&= \begin{pmatrix} \xi_m \\ \frac{\bar{m}}{m^*}\frac{\vec{\sigma}\cdot\vec{v}_\mu}{2}\xi_m \end{pmatrix} \frac{G(r)}{r} Y_{00}(\hat{r}),
\end{aligned}
\tag{7.7}
$$

where $\vec{p}_\mu = \bar{m}\vec{v}_\mu$ is the muon momentum operator. Figure 7.1 compares the numerically obtained Coulomb solution $F(r)$ to the effective lower-component wave function in Eq. (7.7) in four target nuclei. Across the range of targets, the effective form of the lower component accurately reproduces the reference solution; even in ^{184}W, the relative root-mean-square error, defined in analogy with Eq. (2.37), is $\approx 1\%$. In the next-generation target ^{27}Al, the RMS error is $\approx 0.5\%$.

7.2   Effective Theory Operators

We now construct all operators through first-order in the muon velocity operator $\vec{v}_\mu$. We ignore terms that depend on both the muon and nucleon velocities, as these terms are higher order. The new operators are

$$
\begin{aligned}
\mathcal{O}_2^{f'} &= i\hat{q} \cdot \frac{\vec{v}_\mu}{2}\, 1_N \\[4pt]
\mathcal{O}_3^{f} &= i\hat{q} \cdot \left[\frac{\vec{v}_\mu}{2} \times \vec{\sigma}_L\right]\, 1_N \\[4pt]
\mathcal{O}_5^{f} &= \left(i\hat{q} \times \frac{\vec{v}_\mu}{2}\right) \cdot \vec{\sigma}_N \\[4pt]
\mathcal{O}_7^{f} &= \frac{\vec{v}_\mu}{2} \cdot \vec{\sigma}_L\, 1_N \\[4pt]
\mathcal{O}_8^{f} &= \frac{\vec{v}_\mu}{2} \cdot \vec{\sigma}_N \\[4pt]
\mathcal{O}_{12}^{f} &= \left[\frac{\vec{v}_\mu}{2} \times \vec{\sigma}_L\right] \cdot \vec{\sigma}_N \\[4pt]
\mathcal{O}_{13}^{f'} &= \left(i\hat{q} \times \left[\frac{\vec{v}_\mu}{2} \times \vec{\sigma}_L\right]\right) \cdot \vec{\sigma}_N \\[4pt]
\mathcal{O}_{14}^{f} &= \frac{\vec{v}_\mu}{2} \cdot \vec{\sigma}_L\, i\hat{q} \cdot \vec{\sigma}_N \\[4pt]
\mathcal{O}_{15}^{f} &= i\hat{q} \cdot \left[\frac{\vec{v}_\mu}{2} \times \vec{\sigma}_L\right]\, i\hat{q} \cdot \vec{\sigma}_N \\[4pt]
\mathcal{O}_{16}^{f'} &= i\hat{q} \cdot \frac{\vec{v}_\mu}{2}\, i\hat{q} \cdot \vec{\sigma}_N,
\end{aligned}
\tag{7.8}
$$

where the superscript f indicates that these operators are paired with the muon lower-component wave function. The lower-component operators are related to their upper-component counterparts by exchanging $\vec{v}_N \leftrightarrow \vec{v}_\mu/2$ and $\vec{\sigma}_N \leftrightarrow \vec{\sigma}_L$. The operators that do not have a lower-component analogue, $\mathcal{O}_1$, $\mathcal{O}_4$, $\mathcal{O}_6$, $\mathcal{O}_9$, $\mathcal{O}_{10}$ and $\mathcal{O}_{11}$, transform among themselves under the lepton $\leftrightarrow$ nucleon interchange.

7.3   Connection to Relativistic Amplitudes

The operators $\mathcal{O}_i^f$ naturally arise from a Pauli reduction of the lepton-nucleon Dirac spinor currents. In Appendix A.2, the leptonic bilinears are expanded through first order in $\vec{v}_\mu$. The mappings between the relativistic amplitudes and the Pauli-reduced effective operators linear in $\vec{v}_\mu$ are shown in Table 7.1. These results should be added to the corresponding terms in Table 3.3 to obtain the complete expression. The fact that the upper and lower muon components are constrained by Lorentz covariance gives some advantage to the relativistic effective theory as a starting point over the Pauli-reduced form.

The 20 relativistic amplitudes that we consider correspond to scalar and vector couplings of the leptons to the nucleons. Originally, we found that operators that depend on the

j	$\mathcal{L}^j_{\text{int}}$	Pauli Reduction	$\sum_i c_i \mathcal{O}_i$
1	$\bar{\chi}_e \chi_\mu \bar{N} N$	$-\frac{1}{2}\hat{q}\cdot\vec{v}_\mu 1_N - \frac{i}{2}\hat{q}\cdot[\vec{v}_\mu\times\vec{\sigma}_L]1_N$	$i\mathcal{O}_2^{f'} - \mathcal{O}_3^f$
3	$\bar{\chi}_e i\gamma^5\chi_\mu\bar{N}N$	$\frac{i}{2}\vec{v}_\mu\cdot\vec{\sigma}_L 1_N$	$i\mathcal{O}_7^f$
5	$\bar{\chi}_e\gamma^\mu\chi_\mu\bar{N}\gamma_\mu N$	$\frac{1}{2}\hat{q}\cdot\vec{v}_\mu 1_N + \frac{i}{2}\hat{q}\cdot[\vec{v}_\mu\times\vec{\sigma}_L]1_N$	$-i\mathcal{O}_2^{f'} + \mathcal{O}_3^f$
7	$\bar{\chi}_e\gamma^\mu\chi_\mu\bar{N}\gamma_\mu\gamma^5 N$	$-\frac{1}{2}\vec{v}_\mu\cdot\vec{\sigma}_N - \frac{i}{2}[\vec{v}_\mu\times\vec{\sigma}_L]\cdot\vec{\sigma}_N$	$-\mathcal{O}_8^f - i\mathcal{O}_{12}^f$
9	$\bar{\chi}_e i\sigma^{\mu\nu}\frac{q_\nu}{m_L}\chi_\mu\bar{N}\gamma_\mu N$	$\frac{q}{2m_L}(\hat{q}\cdot\vec{v}_\mu + i\hat{q}\cdot[\vec{v}_\mu\times\vec{\sigma}_L])1_N$	$\frac{q}{m_L}\left(-i\mathcal{O}_2^{f'} + \mathcal{O}_3^f\right)$
11	$\bar{\chi}_e i\sigma^{\mu\nu}\frac{q_\nu}{m_L}\chi_\mu\bar{N}\gamma_\mu\gamma^5 N$	$\frac{q}{2m_L}(\vec{v}_\mu\cdot\vec{\sigma}_N + i[\vec{v}_\mu\times\vec{\sigma}_L]\cdot\vec{\sigma}_N$ $-i\hat{q}\cdot[\vec{v}_\mu\times\vec{\sigma}_L]\hat{q}\cdot\vec{\sigma}_N - \hat{q}\cdot\vec{v}_\mu\hat{q}\cdot\vec{\sigma}_N)$	$\frac{q}{m_L}\left(\mathcal{O}_8^f + i\mathcal{O}_{12}^f \right.$ $\left. +i\mathcal{O}_{15}^f + \mathcal{O}_{16}^{f'}\right)$
13	$\bar{\chi}_e\gamma^\mu\gamma^5\chi_\mu\bar{N}\gamma_\mu N$	$\frac{1}{2}\vec{v}_\mu\cdot\vec{\sigma}_L 1_N$	$\mathcal{O}_7^f$
15	$\bar{\chi}_e\gamma^\mu\gamma^5\chi_\mu\bar{N}\gamma_\mu\gamma^5 N$	$\frac{i}{2}[\hat{q}\times\vec{v}_\mu]\cdot\vec{\sigma}_N - \frac{1}{2}(\hat{q}\times[v_\mu\times\vec{\sigma}_L])\cdot\vec{\sigma}_N$ $-\frac{1}{2}\vec{v}_\mu\cdot\vec{\sigma}_L\,\hat{q}\cdot\vec{\sigma}_N$	$\mathcal{O}_5^f + i\mathcal{O}_{13}^{f'}$ $+i\mathcal{O}_{14}^f$
17	$\bar{\chi}_e\sigma^{\mu\nu}\frac{q_\nu}{m_L}\gamma^5\chi_\mu\bar{N}\gamma_\mu N$	$\frac{iq}{2m_L}\vec{v}_\mu\cdot\vec{\sigma}_L 1_N$	$\frac{iq}{m_L}\mathcal{O}_7^f$
19	$\bar{\chi}_e\sigma^{\mu\nu}\frac{q_\nu}{m_L}\gamma^5\chi_\mu\bar{N}\gamma_\mu\gamma^5 N$	$\frac{q}{2m_L}([\hat{q}\times\vec{v}_\mu]\cdot\vec{\sigma}_N + (i\hat{q}\times[\vec{v}_\mu\times\vec{\sigma}_L])\cdot\vec{\sigma}_N)$	$\frac{q}{m_L}\left(-i\mathcal{O}_5^f + \mathcal{O}_{13}^f\right)$

Table 7.1: As in Table 3.3 but listing the additional terms that are generated when the muon velocity operator $\vec{v}_\mu$ is retained to first order. The terms presented in this table should be combined with the corresponding results in Table 3.3 to obtain the full result.

nucleon spin-current $\vec{v}_N \times \vec{\sigma}_N$ cannot be obtained from these simple interactions but require more exotic mediators, such as the pseudo-tensor interaction $\bar{\chi}_e i\sigma^{\mu\nu}\gamma^5\chi_\mu\bar{N}i\sigma_{\mu\nu}\gamma^5 N$. The underlying reason for this is that the Pauli-reduced nucleon currents can be suppressed by factors of q/m_N and/or $\vec{v}_N$; indeed, the relativistic amplitudes that generate the nucleon spin-velocity current are suppressed by both of these factors and hence are neglected. In the leptonic case, the ultra-relativistic electron depends on the quantity $\hat{q}$, which removes the suppression penalty and allows one to obtain the lepton spin-velocity current $\vec{v}_\mu \times \vec{\sigma}_L$ from the scalar and vector interactions. As a result, all 10 of the lower component operators are generated by the set of 20 relativistic amplitudes.

7.4 Expression for the Decay Rate

The effective theory Lagrangian is now expanded to include the lower-component operators with corresponding low-energy constants b_i^τ. As we neglect terms that depend on both the muon and nucleon velocity operators, the resulting operators contain only the nucleon charge 1_N and spin-current $\vec{\sigma}_N$. Consequently, we modify the leptonic currents [originally defined in

Eq. (3.10)] as

$$
\begin{aligned}
l_0^\tau &\to l_0^\tau + b_2^\tau i\hat{q} \cdot \frac{\vec{v}_\mu}{2} + b_3^\tau i\hat{q} \cdot \left[\frac{\vec{v}_\mu}{2} \times \vec{\sigma}_L \right] + b_7^\tau \frac{\vec{v}_\mu}{2} \cdot \vec{\sigma}_L \\
&\equiv l_0^\tau + l_{0f}^\tau, \\
\vec{l}_5^\tau &\to \vec{l}_5^\tau + b_5^\tau i\hat{q} \times \frac{\vec{v}_\mu}{2} + b_8^\tau \frac{\vec{v}_\mu}{2} + b_{12}^\tau \frac{\vec{v}_\mu}{2} \times \vec{\sigma}_L + b_{13}^\tau i\hat{q} \times \left[\frac{\vec{v}_\mu}{2} \times \vec{\sigma}_L \right] \\
&\quad + b_{14}^\tau \frac{\vec{v}_\mu}{2} \cdot \vec{\sigma}_L \, i\hat{q} + b_{15}^\tau i\hat{q} \cdot \left[\frac{\vec{v}_\mu}{2} \times \vec{\sigma}_L \right] i\hat{q} + b_{16}^\tau i\hat{q} \cdot \frac{\vec{v}_\mu}{2} \, i\hat{q} \\
&\equiv \vec{l}_5^\tau + \vec{l}_{5f}^\tau,
\end{aligned}
\tag{7.9}
$$

with $l_0^{A\,\tau}$, $\vec{l}_M^\tau$, and $\vec{l}_E^\tau$ unchanged. The conversion amplitude is then given by

$$
\begin{aligned}
\mathcal{M} = &\sqrt{\frac{E_e}{2m_e}} \frac{q_{\text{eff}}}{q} \sum_{\tau=0,1} \langle \tfrac{1}{2} s_f; j_N m_f | \left[\sum_{i=1}^A e^{-i\vec{q}_{\text{eff}} \cdot \vec{x}_i} \left(l_0^\tau \frac{g(x_i)}{\sqrt{4\pi}} - l_{0f}^\tau(\hat{x}_i) \frac{if(x_i)}{\sqrt{4\pi}} \right) \right. \\
&+ l_0^{A\,\tau} \sum_{i=1}^A \frac{1}{2m_N} \left(-\frac{1}{i} \overleftarrow{\nabla}_i \cdot \vec{\sigma}_N(i) \, e^{-i\vec{q}_{\text{eff}} \cdot \vec{x}_i} \frac{g(x_i)}{\sqrt{4\pi}} + \frac{g(x_i)}{\sqrt{4\pi}} e^{-i\vec{q}_{\text{eff}} \cdot \vec{x}_i} \vec{\sigma}_N(i) \cdot \frac{1}{i} \overrightarrow{\nabla}_i \right) \\
&+ \sum_{i=1}^A \vec{\sigma}_N(i) \, e^{-i\vec{q}_{\text{eff}} \cdot \vec{x}_i} \cdot \left(\vec{l}_5^\tau \frac{g(x_i)}{\sqrt{4\pi}} - \vec{l}_{5f}^\tau(\hat{x}_i) \frac{if(x_i)}{\sqrt{4\pi}} \right) \\
&+ \vec{l}_M^\tau \cdot \sum_{i=1}^A \frac{1}{2m_N} \left(-\frac{1}{i} \overleftarrow{\nabla}_i \, e^{-i\vec{q}_{\text{eff}} \cdot \vec{x}_i} \frac{g(x_i)}{\sqrt{4\pi}} + \frac{g(x_i)}{\sqrt{4\pi}} e^{-i\vec{q}_{\text{eff}} \cdot \vec{x}_i} \frac{1}{i} \overrightarrow{\nabla}_i \right) \\
&\left. + \vec{l}_E^\tau \cdot \sum_{i=1}^A \frac{1}{2m_N} \left(\overleftarrow{\nabla}_i \times \vec{\sigma}_N(i) e^{-i\vec{q}_{\text{eff}} \cdot \vec{x}_i} \frac{g(x_i)}{\sqrt{4\pi}} + \frac{g(x_i)}{\sqrt{4\pi}} e^{-i\vec{q}_{\text{eff}} \cdot \vec{x}_i} \vec{\sigma}_N(i) \times \overrightarrow{\nabla}_i \right) \right]_{\text{int}} t^\tau(i) \, | \tfrac{1}{2} s_i; j_N m_i \rangle,
\end{aligned}
\tag{7.10}
$$

where $g(r) = G(r)/r$, $f(r) = F(r)/r$, and where the muon's p-wave lower component introduces an additional angular dependence through $\hat{x}_i$

$$
\begin{aligned}
l_{0f}^\tau(\hat{x}_i) &\equiv b_2^\tau i\hat{q} \cdot \hat{x}_i + b_3^\tau i\hat{q} \cdot [\hat{x}_i \times \vec{\sigma}_L] + b_7^\tau \hat{x}_i \cdot \vec{\sigma}_L \\
\vec{l}_{5f}^\tau(\hat{x}_i) &\equiv b_5^\tau i\hat{q} \times \vec{x}_i + b_8^\tau \hat{x}_i + b_{12}^\tau \hat{x}_i \times \vec{\sigma}_L + b_{13}^\tau i\hat{q} \times [\hat{x}_i \times \vec{\sigma}_L] \\
&\quad + b_{14}^\tau \hat{x}_i \cdot \vec{\sigma}_L i\hat{q} + b_{15}^\tau i\hat{q} \cdot [\hat{x}_i \times \vec{\sigma}_L] \, i\hat{q} + b_{16}^\tau i\hat{q} \cdot \hat{x}_i i\hat{q}.
\end{aligned}
\tag{7.11}
$$

When combined with the plane-wave factor $\exp(-i\vec{q}_{\text{eff}} \cdot \vec{x}_i)$, the operator $\hat{x}_i$ restructures the multipole expansion. Indeed, we identify eight new nuclear operators associated with the

muon lower component:

$$M_{JM;\tau}^{(1)}(q) \equiv \sum_{i=1}^{A} \sqrt{J(J+1)} \frac{1}{qx_i} j_J(qx_i) Y_{JM}(\hat{x}_i)\, t^\tau(i)$$

$$M_{JM;\tau}^{(2)}(q) \equiv \sum_{i=1}^{A} \frac{d}{dqx_i} j_J(qx_i) Y_{JM}(\hat{x}_i)\, t^\tau(i)$$

$$\Sigma_{JM;\tau}^{(1)}(q) \equiv \sum_{i=1}^{A} \sqrt{J(J+1)} \frac{1}{qx_i} j_J(qx_i) \vec{Y}_{JJM}(\hat{x}_i) \cdot \vec{\sigma}_N(i)\, t^\tau(i)$$

$$\Sigma_{JM;\tau}^{(2)}(q) \equiv \sum_{i=1}^{A} \frac{d}{dqx_i} j_J(qx_i) \vec{Y}_{JJM}(\hat{x}_i) \cdot \vec{\sigma}_N(i)\, t^\tau(i)$$

$$\Sigma_{JM;\tau}'^{(0)}(q) \equiv \sum_{i=1}^{A} j_J(qx_i) \left[\sqrt{\frac{J}{2J+1}} \vec{Y}_{JJ+1M}(\hat{x}_i) + \sqrt{\frac{J+1}{2J+1}} \vec{Y}_{JJ-1M}(\hat{x}_i) \right] \cdot \vec{\sigma}_N(i)\, t^\tau(i)$$

$$\Sigma_{JM;\tau}'^{(2)}(q) \equiv \sum_{i=1}^{A} \left[-\sqrt{\frac{J}{2J+1}} \frac{d}{dqx_i} j_{J+1}(qx_i) \vec{Y}_{JJ+1M}(\hat{x}_i) \right.$$
$$\left. + \sqrt{\frac{J+1}{2J+1}} \frac{d}{dqx_i} j_{J-1}(qx_i) \vec{Y}_{JJ-1M}(\hat{x}_i) \right] \cdot \vec{\sigma}_N(i)\, t^\tau(i)$$

$$\Sigma_{JM;\tau}''^{(0)}(q) \equiv \sum_{i=1}^{A} j_J(qx_i) \left[-\sqrt{\frac{J+1}{2J+1}} \vec{Y}_{JJ+1M}(\hat{x}_i) + \sqrt{\frac{J}{2J+1}} \vec{Y}_{JJ-1M}(\hat{x}_i) \right] \cdot \vec{\sigma}_N(i)\, t^\tau(i)$$

$$\Sigma_{JM;\tau}''^{(2)}(q) \equiv \sum_{i=1}^{A} \left[\sqrt{\frac{J+1}{2J+1}} \frac{d}{dqx_i} j_{J+1}(qx_i) \vec{Y}_{JJ+1M}(\hat{x}_i) \right.$$
$$\left. + \sqrt{\frac{J}{2J+1}} \frac{d}{dqx_i} j_{J-1}(qx_i) \vec{Y}_{JJ-1M}(\hat{x}_i) \right] \cdot \vec{\sigma}_N(i)\, t^\tau(i)$$

$$(7.12)$$

Table 7.2 summarizes the properties of these novel responses. Two of these operators, $\Sigma^{(1)}$ and $\Sigma^{(2)}$, have opposite P and T transformation properties and therefore cannot contribute to the elastic conversion process. Consequently, the lower-component operator $\mathcal{O}_5^f$, which is associated only with the response $\Sigma^{(1)}$, is not probed when the nucleus remains in the ground

state. The elastic conversion amplitude can then be expressed as

$$
\mathcal{M} = \sqrt{\frac{E_e}{2m_e}} \frac{q_{\text{eff}}}{q} \sum_{\tau=0,1} \langle \tfrac{1}{2} s_f; j_N m_f |
$$

$$
\left\{ \sum_{J=0,2,\dots}^{\infty} \sqrt{4\pi(2J+1)}(-i)^J \left[l_0^\tau M_{J0;\tau}^g(q_{\text{eff}}) - il_0^{\tau(2)} M_{J0;\tau}^{(2)f}(q_{\text{eff}}) + \frac{q_{\text{eff}}}{m_N} l_{E0}^\tau \Phi''^g_{J0;\tau}(q_{\text{eff}}) \right] \right.
$$

$$
+ \sum_{J=1,3,\dots}^{\infty} \sqrt{2\pi(2J+1)}(-i)^J \sum_{\lambda=\pm1} \left[-il_{5\lambda}^\tau \Sigma'^g_{J-\lambda;\tau}(q_{\text{eff}}) + l_{5\lambda}^{\tau(0)} \Sigma'^{(0)f}_{J-\lambda;\tau}(q_{\text{eff}}) + l_{5\lambda}^{\tau(2)} \Sigma'^{(2)f}_{J-\lambda;\tau}(q_{\text{eff}}) \right.
$$

$$
\left. + i\frac{q_{\text{eff}}}{m_N} l_{M\lambda}^\tau \lambda \Delta^g_{J-\lambda;\tau}(q_{\text{eff}}) \right]
$$

$$
+ \sum_{J=2,4,\dots}^{\infty} \sqrt{2\pi(2J+1)}(-i)^J \sum_{\lambda=\pm1} \left[-il_\lambda^{\tau(1)} M_{J-\lambda;\tau}^{(1)f}(q_{\text{eff}}) - \frac{q_{\text{eff}}}{m_N} l_{E\lambda}^\tau \tilde{\Phi}'^g_{J-\lambda;\tau}(q_{\text{eff}}) \right]
$$

$$
+ \sum_{J=1,3,\dots}^{\infty} \sqrt{4\pi(2J+1)}(-i)^J \left[il_{50}^\tau \Sigma''^g_{J0;\tau}(q_{\text{eff}}) + l_{50}^{\tau(0)} \Sigma''^{(0)f}_{J0;\tau}(q_{\text{eff}}) \right.
$$

$$
\left. \left. + l_{50}^{\tau(2)} \Sigma''^{(2)f}_{J0;\tau}(q_{\text{eff}}) \right] \right\} | \tfrac{1}{2} s_i; j_N m_i \rangle,
$$

$$
(7.13)
$$

where we have introduced the notation

$$
\hat{O}^g_{JM}(q) \equiv \sum_{i=1}^A \frac{g(x_i)}{\sqrt{4\pi}} \hat{O}_{JM}(qx_i)
$$

$$
\hat{O}^f_{JM}(q) \equiv \sum_{i=1}^A \frac{f(x_i)}{\sqrt{4\pi}} \hat{O}_{JM}(qx_i).
$$

$$
(7.14)
$$

The lower-component leptonic currents in Eq. (7.13) are

$$
\begin{aligned}
l_\lambda^{\tau(1)} &= -i\left(b_3^\tau \lambda + b_7^\tau\right)\sigma_{L\lambda}, & l_0^{\tau(2)} &= -b_2^\tau + ib_7^\tau \sigma_{L0}, \\
l_{5\lambda}^{\tau(0)} &= \left[\lambda\left(-b_{12}^\tau + b_{15}^\tau\right) + b_{14}^\tau\right]\sigma_{L\lambda}, & l_{5\lambda}^{\tau(2)} &= \left[-b_{13}^\tau + b_{14}^\tau + \lambda b_{15}^\tau\right]\sigma_{L\lambda}, \\
l_{50}^{\tau(0)} &= -ib_8^\tau + b_{13}^\tau \sigma_{L0}, & l_{50}^{\tau(2)} &= \left(b_{13}^\tau - b_{14}^\tau\right)\sigma_{L0} - ib_{16}^\tau.
\end{aligned}
$$

$$
(7.15)
$$

The nuclear-spin-averaged amplitude squared can be expressed as

$$
\frac{1}{2j_N+1} \sum_{m_f,m_i} |\langle \tfrac{1}{2} s_f; j_N m_f | \mathcal{M} | \tfrac{1}{2} s_i; j_N m_i \rangle|^2 = \frac{E_e}{2m_e} \frac{q_{\text{eff}}^2}{q^2} \frac{4\pi}{2j_N+1} \sum_{\tau=0,1} \sum_{\tau'=0,1}
$$

$$
\left\{ \sum_{J=0,2,\dots}^{\infty} \left(\langle l_0^\tau \rangle \langle l_0^{\tau'} \rangle^* \langle j_N || M_{J;\tau}^g(q_{\text{eff}}) || j_N \rangle \langle j_N || M_{J;\tau'}^g(q_{\text{eff}}) || j_N \rangle \right. \right.
$$

$$
+ 2\,\text{Re}\left[i\langle l_0^\tau \rangle \langle l_0^{\tau'(2)} \rangle^* \right] \langle j_N || M_{J;\tau}^g(q_{\text{eff}}) || j_N \rangle \langle j_N || M_{J;\tau'}^{(2)f}(q_{\text{eff}}) || j_N \rangle
$$

$$
+ \langle l_0^{\tau(2)} \rangle \langle l_0^{\tau'(2)} \rangle^* \langle j_N || M_{J;\tau}^{(2)f}(q_{\text{eff}}) || j_N \rangle \langle j_N || M_{J;\tau'}^{(2)f}(q_{\text{eff}}) || j_N \rangle
$$

Operator	Even J	Odd J	LECs Probed	Operator	Even J	Odd J	LECs Probed
$M^{(1)}_{JM}$	E-E	O-O	b_3, b_7	$M^{(2)}_{JM}$	E-E	O-O	b_2, b_7
$\Sigma^{(1)}_{JM}$	E-O	O-E	$b_5, b_{12}, b_{14}, b_{15}$	$\Sigma^{(2)}_{JM}$	E-O	O-E	b_{12}, b_{13}
$\Sigma'^{(0)}_{JM}$	O-O	E-E	b_{12}, b_{14}, b_{15}	$\Sigma'^{(2)}_{JM}$	O-O	E-E	b_{13}, b_{14}, b_{15}
$\Sigma''^{(0)}_{JM}$	O-O	E-E	b_8, b_{13}	$\Sigma''^{(2)}_{JM}$	O-O	E-E	b_{13}, b_{14}, b_{16}

Table 7.2: Multipole operators associated with the muon's lower component, their transformation properties under parity and time-reversal, and the LECs associated with each response.

$$+ \frac{\vec{q}_{\text{eff}}}{m_N} \cdot \langle \vec{l^\tau_E} \rangle \, \frac{\vec{q}_{\text{eff}}}{m_N} \cdot \langle \vec{l^{\tau'}_E} \rangle^* \, \langle j_N || \Phi''^g_{J;\tau}(q_{\text{eff}}) || j_N \rangle \, \langle j_N || \Phi''^g_{J;\tau'}(q_{\text{eff}}) || j_N \rangle$$

$$+ \frac{2\vec{q}_{\text{eff}}}{m_N} \cdot \text{Re} \left[\langle \vec{l^\tau_E} \rangle \langle l^{\tau'}_0 \rangle^* \right] \langle j_N || \Phi''^g_{J;\tau}(q_{\text{eff}}) || j_N \rangle \, \langle j_N || M^g_{J;\tau'}(q_{\text{eff}}) || j_N \rangle$$

$$+ \frac{2\vec{q}_{\text{eff}}}{m_N} \cdot \text{Re} \left[i \langle \vec{l^\tau_E} \rangle \langle l^{\tau'(2)}_0 \rangle^* \right] \langle j_N || \Phi''^g_{J;\tau}(q_{\text{eff}}) || j_N \rangle \, \langle j_N || M^{(2)f}_{J;\tau'}(q_{\text{eff}}) || j_N \rangle \Bigg)$$

$$+ \sum_{J=2,4,\dots} \Bigg(\frac{1}{2} \frac{q^2_{\text{eff}}}{m^2_N} \left(\langle \vec{l^\tau_E} \rangle \cdot \langle \vec{l^{\tau'}_E} \rangle^* - \hat{q} \cdot \langle \vec{l^\tau_E} \rangle \, \hat{q} \cdot \langle \vec{l^{\tau'}_E} \rangle^* \right) \langle j_N || \tilde{\Phi}'^g_{J;\tau}(q_{\text{eff}}) || j_N \rangle \, \langle j_N || \tilde{\Phi}'^g_{J;\tau'}(q_{\text{eff}}) || j_N \rangle$$

$$+ \frac{1}{2} \left(\langle \vec{l^{\tau(1)}} \rangle \cdot \langle \vec{l^{\tau'(1)}} \rangle^* - \hat{q} \cdot \langle \vec{l^{\tau(1)}} \rangle \, \hat{q} \cdot \langle \vec{l^{\tau'(1)}} \rangle^* \right) \langle j_N || M^{(1)f}_{J;\tau}(q_{\text{eff}}) || j_N \rangle \, \langle j_N || M^{(1)f}_{J;\tau'}(q_{\text{eff}}) || j_N \rangle$$

$$- \text{Re} \left[\frac{q_{\text{eff}}}{m_N} i \langle \vec{l^\tau_E} \rangle \cdot \langle \vec{l^{\tau'(1)}} \rangle^* - \frac{\vec{q}_{\text{eff}}}{m_N} \cdot i \langle \vec{l^\tau_E} \rangle \, \hat{q} \cdot \langle \vec{l^{\tau'(1)}} \rangle^* \right] \langle j_N || \tilde{\Phi}'^g_{J;\tau}(q_{\text{eff}}) || j_N \rangle \, \langle j_N || M^{(1)f}_{J;\tau'}(q_{\text{eff}}) || j_N \rangle \Bigg)$$

$$+ \sum_{J=1,3,\dots}^{\infty} \Bigg(\frac{1}{2} \left(\langle \vec{l^\tau_5} \rangle \cdot \langle \vec{l^{\tau'}_5} \rangle^* - \hat{q} \cdot \langle \vec{l^\tau_5} \rangle \, \hat{q} \cdot \langle \vec{l^{\tau'}_5} \rangle^* \right) \langle j_N || \Sigma'^g_{J;\tau}(q_{\text{eff}}) || j_N \rangle \, \langle j_N || \Sigma'^g_{J;\tau'}(q_{\text{eff}}) || j_N \rangle$$

$$+ \frac{1}{2} \left(\langle \vec{l^{\tau(0)}_5} \rangle \cdot \langle \vec{l^{\tau'(0)}_5} \rangle^* - \hat{q} \cdot \langle \vec{l^{\tau(0)}_5} \rangle \, \hat{q} \cdot \langle \vec{l^{\tau'(0)}_5} \rangle^* \right) \langle j_N || \Sigma'^{(0)f}_{J;\tau}(q_{\text{eff}}) || j_N \rangle \, \langle j_N || \Sigma'^{(0)f}_{J;\tau'}(q_{\text{eff}}) || j_N \rangle \quad (7.16)$$

$$+ \frac{1}{2} \left(\langle \vec{l^{\tau(2)}_5} \rangle \cdot \langle \vec{l^{\tau'(2)}_5} \rangle^* - \hat{q} \cdot \langle \vec{l^{\tau(2)}_5} \rangle \, \hat{q} \cdot \langle \vec{l^{\tau'(2)}_5} \rangle^* \right) \langle j_N || \Sigma'^{(2)f}_{J;\tau}(q_{\text{eff}}) || j_N \rangle \, \langle j_N || \Sigma'^{(2)f}_{J;\tau'}(q_{\text{eff}}) || j_N \rangle$$

$$- \text{Re} \left[\langle \vec{l^\tau_5} \rangle \cdot i \langle \vec{l^{\tau'(0)}_5} \rangle^* - \hat{q} \cdot \langle \vec{l^\tau_5} \rangle \, i\hat{q} \cdot \langle \vec{l^{\tau'(0)}_5} \rangle^* \right] \langle j_N || \Sigma'^g_{J;\tau}(q_{\text{eff}}) || j_N \rangle \, \langle j_N || \Sigma'^{(0)f}_{J;\tau'}(q_{\text{eff}}) || j_N \rangle$$

$$- \text{Re} \left[\langle \vec{l^\tau_5} \rangle \cdot i \langle \vec{l^{\tau'(2)}_5} \rangle^* - \hat{q} \cdot \langle \vec{l^\tau_5} \rangle \, i\hat{q} \cdot \langle \vec{l^{\tau'(2)}_5} \rangle^* \right] \langle j_N || \Sigma'^g_{J;\tau}(q_{\text{eff}}) || j_N \rangle \, \langle j_N || \Sigma'^{(2)f}_{J;\tau'}(q_{\text{eff}}) || j_N \rangle$$

$$+ \text{Re} \left[\langle \vec{l^{(0)\tau}_5} \rangle \cdot \langle \vec{l^{\tau'(2)}_5} \rangle^* - \hat{q} \cdot \langle \vec{l^{\tau(0)}_5} \rangle \, \hat{q} \cdot \langle \vec{l^{\tau'(2)}_5} \rangle^* \right] \langle j_N || \Sigma'^{(0)f}_{J;\tau}(q_{\text{eff}}) || j_N \rangle \, \langle j_N || \Sigma'^{(2)f}_{J;\tau'}(q_{\text{eff}}) || j_N \rangle$$

$$+ \frac{1}{2} \left(\frac{q^2_{\text{eff}}}{m^2_N} \langle \vec{l^\tau_M} \rangle \cdot \langle \vec{l^{\tau'}_M} \rangle^* - \frac{\vec{q}_{\text{eff}}}{m_N} \cdot \langle \vec{l^\tau_M} \rangle \, \frac{\vec{q}_{\text{eff}}}{m_N} \cdot \langle \vec{l^{\tau'}_M} \rangle^* \right) \langle j_N || \Delta^g_{J;\tau}(q_{\text{eff}}) || j_N \rangle \, \langle j_N || \Delta^g_{J;\tau'}(q_{\text{eff}}) || j_N \rangle$$

$$+ \frac{\vec{q}_{\text{eff}}}{m_N} \cdot \text{Re} \left[i \langle \vec{l^\tau_M} \rangle \times \langle \vec{l^{\tau'}_5} \rangle^* \right] \langle j_N || \Delta^g_{J;\tau}(q_{\text{eff}}) || j_N \rangle \, \langle j_N || \Sigma'^g_{J;\tau'}(q_{\text{eff}}) || j_N \rangle$$

$$+ \frac{\vec{q}_{\text{eff}}}{m_N} \cdot \text{Re} \left[\langle \vec{l^\tau_M} \rangle \times \langle \vec{l^{\tau'(0)}_5} \rangle^* \right] \langle j_N || \Delta^g_{J;\tau}(q_{\text{eff}}) || j_N \rangle \, \langle j_N || \Sigma'^{(0)f}_{J;\tau'}(q_{\text{eff}}) || j_N \rangle$$

$$
+ \frac{\vec{q}_{\text{eff}}}{m_N} \cdot \text{Re}\left[\langle \vec{l}_M^\tau \rangle \times \langle \vec{l}_5^{\tau'(2)} \rangle^*\right] \langle j_N || \Delta_{J;\tau}^g(q_{\text{eff}}) || j_N \rangle \langle j_N || \Sigma_{J;\tau'}^{\prime(2)f}(q_{\text{eff}}) || j_N \rangle
$$

$$
+ \hat{q} \cdot \langle \vec{l}_5^\tau \rangle \, \hat{q} \cdot \langle \vec{l}_5^{\tau'} \rangle^* \langle j_N || \Sigma_{J;\tau}^{\prime\prime g}(q_{\text{eff}}) || j_N \rangle \langle j_N || \Sigma_{J;\tau'}^{\prime\prime g}(q_{\text{eff}}) || j_N \rangle
$$

$$
+ \hat{q} \cdot \langle \vec{l}_5^{\tau(0)} \rangle \, \hat{q} \cdot \langle \vec{l}_5^{\tau'(0)} \rangle^* \langle j_N || \Sigma_{J;\tau}^{\prime\prime(0)f}(q_{\text{eff}}) || j_N \rangle \langle j_N || \Sigma_{J;\tau'}^{\prime\prime(0)f}(q_{\text{eff}}) || j_N \rangle
$$

$$
+ \hat{q} \cdot \langle \vec{l}_5^{\tau(2)} \rangle \, \hat{q} \cdot \langle \vec{l}_5^{\tau'(2)} \rangle^* \langle j_N || \Sigma_{J;\tau}^{\prime\prime(2)f}(q_{\text{eff}}) || j_N \rangle \langle j_N || \Sigma_{J;\tau'}^{\prime\prime(2)f}(q_{\text{eff}}) || j_N \rangle
$$

$$
+ 2\,\text{Re}\left[\hat{q} \cdot \langle \vec{l}_5^\tau \rangle \, i\hat{q} \cdot \langle \vec{l}_5^{\tau'(0)} \rangle^*\right] \langle j_N || \Sigma_{J;\tau}^{\prime\prime g}(q_{\text{eff}}) || j_N \rangle \langle j_N || \Sigma_{J;\tau'}^{\prime\prime(0)f}(q_{\text{eff}}) || j_N \rangle
$$

$$
+ 2\,\text{Re}\left[\hat{q} \cdot \langle \vec{l}_5^\tau \rangle \, i\hat{q} \cdot \langle \vec{l}_5^{\tau'(2)} \rangle^*\right] \langle j_N || \Sigma_{J;\tau}^{\prime\prime g}(q_{\text{eff}}) || j_N \rangle \langle j_N || \Sigma_{J;\tau'}^{\prime\prime(2)f}(q_{\text{eff}}) || j_N \rangle
$$

$$
+ 2\,\text{Re}\left[\hat{q} \cdot \langle \vec{l}_5^{\tau(0)} \rangle \, \hat{q} \cdot \langle \vec{l}_5^{\tau'(2)} \rangle^*\right] \langle j_N || \Sigma_{J;\tau}^{\prime\prime(0)f}(q_{\text{eff}}) || j_N \rangle \langle j_N || \Sigma_{J;\tau'}^{\prime\prime(2)f}(q_{\text{eff}}) || j_N \rangle \Bigg) \Bigg\}.
$$

In most practical calculations, we will replace both radial wave functions f and g by constant values. In order to exactly reproduce the leading coherent response, the upper-component wave function $g(r)$ is averaged over the isoscalar monopole operator $M_{00;0}(q_{\text{eff}}r)$

$$
\langle g \rangle \equiv |\phi_{1s}^{Z_{\text{eff}}}(\vec{0})| = \frac{1}{\sqrt{4\pi}} \frac{\int dr \; r^2 \rho(r) j_0(q_{\text{eff}}r) g(r)}{\int dr \; r^2 \rho(r) j_0(q_{\text{eff}}r)}. \tag{7.17}
$$

A suitable constant value for the muon's lower component $f(r)$ can be obtained by averaging over the corresponding lower-component operator $M_{00;0}^{(2)}(q_{\text{eff}}r)$

$$
\langle f \rangle \equiv \frac{1}{\sqrt{4\pi}} \frac{\int dr \; r^2 \rho(r) j_1(q_{\text{eff}}r) f(r)}{\int dr \; r^2 \rho(r) j_1(q_{\text{eff}}r)}. \tag{7.18}
$$

This choice of $\langle f \rangle$ exactly reproduces the leading lower-component correction to the coherent conversion amplitude. The constant approximation is then implemented via the replacements

$$
\hat{O}_{JM}^g(q) \to |\phi_{1s}^{Z_{\text{eff}}}(\vec{0})| \sum_{i=1}^{A} \hat{O}_{JM}(qx_i)
$$
$$
\hat{O}_{JM}^f(q) \to |\phi_{1s}^{Z_{\text{eff}}}(\vec{0})| \frac{\langle f \rangle}{\langle g \rangle} \sum_{i=1}^{A} \hat{O}_{JM}(qx_i). \tag{7.19}
$$

The values of the ratio $\langle f \rangle / \langle g \rangle$ for the nuclear targets of interest are reported in Table 7.3. It is not strictly necessary to employ the constant approximation: the radial wave functions of the muon may be retained inside the nuclear matrix elements, where they contribute an additional weight to the corresponding radial integrals. The downside of this approach is that nuclear matrix elements that include the muon wave function can no longer be evaluated analytically—each multipole operator requires a distinct radial integral that must be evaluated numerically. Nonetheless, the effective theory framework can be extended in this way to more accurately describe the muon physics, which may be particularly important in heavy nuclei where the curvature of the muon wave function over the nuclear size becomes significant. Throughout the remainder of this chapter, we will continue with the approximate constant values, having implemented the substitutions of Eq. (7.19).

The various contributions in Eq. (7.16) can be distinguished by their dependence on the muon lower component: there are terms that depend only on the upper component (no powers of f), terms that represent interference between the upper and lower components (one power of f), and terms that depend only on the lower component (two powers of f). To make this distinction manifest, we express the final decay rate as

$$\Gamma(\mu \to e) = \Gamma^{(0)} + 2\frac{\langle f \rangle}{\langle g \rangle}\Gamma^{(1)} + \left(\frac{\langle f \rangle}{\langle g \rangle}\right)^2 \Gamma^{(2)}, \tag{7.20}$$

where the factor of 2 in the coefficient of $\Gamma^{(1)}$ reflects the fact that these terms result from interference. The leading term $\Gamma^{(0)}$ is, of course, the result that we previously obtained in Eq. (3.33).

As we have incorporated the muon velocity (hence the lower component) to first order in the single-nucleon effective theory, we should technically only be concerned with the first-order relativistic correction $\Gamma^{(1)}$. The terms contained in $\Gamma^{(2)}$, although valid, are incomplete from an effective theory perspective, as we did not include any terms of order $\vec{v}_\mu^2 \propto \langle f \rangle^2$ in our basis of lower-component single-nucleon operators $\mathcal{O}_i^f$. Likewise, we neglect single-nucleon operators that contain both the muon and nucleon velocity operators. However, there are interference terms in Eq. (7.16) between muon-velocity-dependent lower-component responses, such as $M^{(2)}$, and nucleon-velocity-dependent upper-component responses, such as Φ''. These are genuine contributions to the CLFV rate, but the effective theory as constructed is not complete through the relevant order in power counting (first order in both $\vec{v}_N$ and $\vec{v}_\mu$). Therefore, the relativistic corrections that we are primarily interested in are those contained within $\Gamma^{(1)}$ and consisting of nucleon-velocity-independent response functions. Nonetheless, we will provide the complete expressions for $\Gamma^{(1)}$ and $\Gamma^{(2)}$.

Defining the leptonic response functions

$$\begin{aligned}
R_{MM^{(2)}}^{\tau\tau'} &\equiv \mathrm{Im}\left[c_1^\tau b_2^{\tau'*} - c_{11}^\tau b_7^{\tau'*}\right]\\
R_{\Sigma'\Sigma'^{(0)}}^{\tau\tau'} &\equiv \mathrm{Im}\left[c_4^\tau b_{14}^{\tau'*} + c_9^\tau(-b_{12}^{\tau'*} + b_{15}^{\tau'*})\right]\\
R_{\Sigma'\Sigma'^{(2)}}^{\tau\tau'} &\equiv \mathrm{Im}\left[c_4^\tau(-b_{13}^{\tau'*} + b_{14}^{\tau'*}) + c_9^\tau b_{15}^{\tau'*}\right]\\
R_{\Sigma''\Sigma''^{(0)}}^{\tau\tau'} &\equiv \mathrm{Im}\left[(c_6^\tau - c_4^\tau)b_{13}^{\tau'*} + c_{10}^\tau b_8^{\tau'*}\right]\\
R_{\Sigma''\Sigma''^{(2)}}^{\tau\tau'} &\equiv \mathrm{Im}\left[(c_6^\tau - c_4^\tau)(b_{13}^{\tau'*} - b_{14}^{\tau'*}) + c_{10}^\tau b_{16}^{\tau'*}\right]\\
R_{\Delta\Sigma'^{(0)}}^{\tau\tau'} &\equiv \mathrm{Im}\left[-c_5^\tau b_{14}^{\tau'*} + c_8^\tau(b_{12}^{\tau'*} - b_{15}^{\tau'*})\right]\\
R_{\Delta\Sigma'^{(2)}}^{\tau\tau'} &\equiv \mathrm{Im}\left[c_5^\tau(b_{13}^{\tau'*} - b_{14}^{\tau'*}) - c_8^\tau b_{15}^{\tau'*}\right]\\
R_{\tilde{\Phi}'M^{(1)}}^{\tau\tau'} &\equiv \mathrm{Im}\left[-c_{12}^\tau b_7^{\tau'*} - c_{13}^\tau b_3^{\tau'*}\right]\\
R_{\Phi''M^{(2)}}^{\tau\tau'} &\equiv \mathrm{Im}\left[-c_3^\tau b_2^{\tau'*} + (-c_{12}^\tau + c_{15}^\tau)b_7^{\tau'*}\right],
\end{aligned} \tag{7.21}$$

the leading lower-component corrections to the conversion rate can be expressed as

$$
\Gamma^{(1)} = \frac{G_F^2}{\pi} \frac{q_{\text{eff}}^2}{1 + \frac{q}{M_T}} |\phi_{1s}^{Z_{\text{eff}}}(\vec{0})|^2 \sum_{\tau=0,1} \sum_{\tau'=0,1} \left\{ \tilde{R}_{MM^{(2)}}^{\tau\tau'} W_{MM^{(2)}}^{\tau\tau'}(q_{\text{eff}}) \right.
$$
$$
+ \tilde{R}_{\Sigma'\Sigma'^{(0)}}^{\tau\tau'} W_{\Sigma'\Sigma'^{(0)}}^{\tau\tau'}(q_{\text{eff}}) + \tilde{R}_{\Sigma'\Sigma'^{(2)}}^{\tau\tau'} W_{\Sigma'\Sigma'^{(2)}}^{\tau\tau'}(q_{\text{eff}})
$$
$$
+ \tilde{R}_{\Sigma''\Sigma''^{(0)}}^{\tau\tau'} W_{\Sigma''\Sigma''^{(0)}}^{\tau\tau'}(q_{\text{eff}}) + \tilde{R}_{\Sigma''\Sigma''^{(2)}}^{\tau\tau'} W_{\Sigma''\Sigma''^{(2)}}^{\tau\tau'}(q_{\text{eff}}) \tag{7.22}
$$
$$
+ \frac{q_{\text{eff}}}{m_N} \left[\tilde{R}_{\Delta\Sigma'^{(0)}}^{\tau\tau'} W_{\Delta\Sigma'^{(0)}}^{\tau\tau'}(q_{\text{eff}}) + \tilde{R}_{\Delta\Sigma'^{(2)}}^{\tau\tau'} W_{\Delta\Sigma'^{(2)}}^{\tau\tau'}(q_{\text{eff}}) \right]
$$
$$
\left. + \frac{q_{\text{eff}}}{m_N} \left[\tilde{R}_{\Phi''M^{(2)}}^{\tau\tau'} W_{\Phi''M^{(2)}}^{\tau\tau'}(q_{\text{eff}}) + \tilde{R}_{\Phi'M^{(1)}}^{\tau\tau'} W_{\Phi'M^{(1)}}^{\tau\tau'}(q_{\text{eff}}) \right] \right\},
$$

where $\tilde{R}$ denotes that the leptonic tensors are composed of dimensionless LECs $\tilde{b}$ and $\tilde{c}$, defined with respect to the weak scale v. The corresponding nuclear response functions are

$$
W_{OM^{(2)}}^{\tau\tau'}(q) \equiv \frac{4\pi}{2j_N + 1} \sum_{J=0,2,\dots}^{\infty} \langle j_N || O_{J;\tau}(q) || j_N \rangle \langle j_N || M_{J;\tau'}^{(2)}(q) || j_N \rangle \text{ for } O = M, \Phi''
$$

$$
W_{O\Sigma'^{(i)}}^{\tau\tau'}(q) \equiv \frac{4\pi}{2j_N + 1} \sum_{J=1,3,\dots}^{\infty} \langle j_N || O_{J;\tau}(q) || j_N \rangle \langle j_N || \Sigma_{J;\tau'}'^{(i)}(q) || j_N \rangle \text{ for } O = \Delta, \Sigma',
$$

$$
\text{and } i = 0, 2 \tag{7.23}
$$

$$
W_{\Sigma''\Sigma''^{(i)}}^{\tau\tau'}(q) \equiv \frac{4\pi}{2j_N + 1} \sum_{J=1,3,\dots}^{\infty} \langle j_N || \Sigma_{J;\tau}''(q) || j_N \rangle \langle j_N || \Sigma_{J;\tau'}''^{(i)}(q) || j_N \rangle \text{ for } i = 0, 2
$$

$$
W_{\Phi'M^{(1)}}^{\tau\tau'}(q) \equiv \frac{4\pi}{2j_N + 1} \sum_{J=2,4,\dots}^{\infty} \langle j_N || \tilde{\Phi}_{J;\tau}'(q) || j_N \rangle \langle j_N || M_{J;\tau'}^{(1)}(q) || j_N \rangle
$$

Every single-nucleon lower-component operator contributes to $\Gamma^{(1)}$ except for $\mathcal{O}_5$. The upper-component responses M, Σ', Σ'', Δ, $\tilde{\Phi}'$, and Φ'' generically receive corrections (in the form of interference terms) from the lower component of the muon. The CLFV response functions that contribute to $\Gamma^{(1)}$ vanish if the LECs are strictly real. We see from Tables 3.3 and 7.1 that both the c_i and b_i coefficients are generically complex.

The leptonic response functions that contribute to the second-order relativistic correction $\Gamma^{(2)}$ are defined as

$$
\begin{aligned}
R_{M^{(1)}}^{\tau\tau'} &\equiv b_3^\tau b_3^{\tau'*} + b_7^\tau b_7^{\tau'*} \\
R_{M^{(2)}}^{\tau\tau'} &\equiv b_2^\tau b_2^{\tau'*} + b_7^\tau b_7^{\tau'*} \\
R_{\Sigma''^{(0)}}^{\tau\tau'} &\equiv b_8^\tau b_8^{\tau'*} + b_{13}^\tau b_{13}^{\tau'*} \\
R_{\Sigma''^{(2)}}^{\tau\tau'} &\equiv (b_{13}^\tau - b_{14}^\tau)(b_{13}^{\tau'*} - b_{14}^{\tau'*}) + b_{16}^\tau b_{16}^{\tau'*} \\
R_{\Sigma'^{(0)}}^{\tau\tau'} &\equiv (-b_{12}^\tau + b_{15}^\tau)(-b_{12}^{\tau'*} + b_{15}^{\tau'*}) + b_{14}^\tau b_{14}^{\tau'*} \\
R_{\Sigma'^{(2)}}^{\tau\tau'} &\equiv (-b_{13}^\tau + b_{14}^\tau)(-b_{13}^{\tau'*} + b_{14}^{\tau'*}) + b_{15}^\tau b_{15}^{\tau'*} \\
R_{\Sigma''^{(0)}\Sigma''^{(2)}}^{\tau\tau'} &\equiv \text{Re} \left[b_8^\tau b_{16}^{\tau'*} + b_{13}^\tau (b_{13}^{\tau'*} - b_{14}^{\tau'*}) \right] \\
R_{\Sigma'^{(0)}\Sigma'^{(2)}}^{\tau\tau'} &\equiv \text{Re} \left[(-b_{12}^\tau + b_{15}^\tau) b_{15}^{\tau'*} + b_{14}^\tau (-b_{13}^{\tau'*} + b_{14}^{\tau'*}) \right],
\end{aligned} \tag{7.24}
$$

and the corresponding decay rate is

$$\Gamma^{(2)} = \frac{G_F^2}{\pi} \frac{q_{\rm eff}^2}{1 + \frac{q}{M_T}} |\phi_{1s}^{Z_{\rm eff}}(\vec{0})|^2 \sum_{\tau=0,1} \sum_{\tau'=0,1} \left\{ \tilde{R}_{M^{(1)}}^{\tau\tau'} W_{M^{(1)}}^{\tau\tau'}(q_{\rm eff}) + \tilde{R}_{M^{(2)}}^{\tau\tau'} W_{M^{(2)}}^{\tau\tau'}(q_{\rm eff}) \right.$$
$$+ \tilde{R}_{\Sigma'(0)}^{\tau\tau'} W_{\Sigma'(0)}^{\tau\tau'}(q_{\rm eff}) + \tilde{R}_{\Sigma'(2)}^{\tau\tau'} W_{\Sigma'(2)}^{\tau\tau'}(q_{\rm eff})$$
$$+ \tilde{R}_{\Sigma''(0)}^{\tau\tau'} W_{\Sigma''(0)}^{\tau\tau'}(q_{\rm eff}) + \tilde{R}_{\Sigma''(2)}^{\tau\tau'} W_{\Sigma''(2)}^{\tau\tau'}(q_{\rm eff})$$
$$\left. + 2 \left[\tilde{R}_{\Sigma'(0)\Sigma'(2)}^{\tau\tau'} W_{\Sigma'(0)\Sigma'(2)}^{\tau\tau'}(q_{\rm eff}) + \tilde{R}_{\Sigma''(0)\Sigma''(2)}^{\tau\tau'} W_{\Sigma''(0)\Sigma''(2)}^{\tau\tau'}(q_{\rm eff}) \right] \right\},$$

$$(7.25)$$

where the nuclear response functions are

$$W_{M^{(1)}}^{\tau\tau'}(q) \equiv \frac{4\pi}{2j_N + 1} \sum_{J=2,4,\ldots}^{\infty} \langle j_N || M_{J;\tau}^{(1)}(q) || j_N \rangle \langle j_N || M_{J;\tau'}^{(1)}(q) || j_N \rangle$$

$$W_{M^{(2)}}^{\tau\tau'}(q) \equiv \frac{4\pi}{2j_N + 1} \sum_{J=0,2,\ldots}^{\infty} \langle j_N || M_{J;\tau}^{(2)}(q) || j_N \rangle \langle j_N || M_{J;\tau'}^{(2)}(q) || j_N \rangle$$

$$W_O^{\tau\tau'}(q) \equiv \frac{4\pi}{2j_N + 1} \sum_{J=1,3,\ldots}^{\infty} \langle j_N || O_{J;\tau}(q) || j_N \rangle \langle j_N || O_{J;\tau'}(q) || j_N \rangle, \text{ for } O = \Sigma'^{(0)}, \Sigma'^{(2)},$$

$$\Sigma''^{(0)}, \Sigma''^{(2)}$$

$$W_{\Sigma'(0)\Sigma'(2)}^{\tau\tau'}(q) \equiv \frac{4\pi}{2j_N + 1} \sum_{J=1,3,\ldots}^{\infty} \langle j_N || \Sigma_{J;\tau}'^{(0)}(q) || j_N \rangle \langle j_N || \Sigma_{J;\tau'}'^{(2)}(q) || j_N \rangle$$

$$W_{\Sigma''(0)\Sigma''(2)}^{\tau\tau'}(q) \equiv \frac{4\pi}{2j_N + 1} \sum_{J=1,3,\ldots}^{\infty} \langle j_N || \Sigma_{J;\tau}''^{(0)}(q) || j_N \rangle \langle j_N || \Sigma_{J;\tau'}''^{(2)}(q) || j_N \rangle.$$

$$(7.26)$$

7.5   The Rate in Terms of Lorentz-invariant Operators

In the preceding derivations, the low-energy constants associated with the muon's upper component c_i are assumed to be independent of those associated with the muon's lower component b_i. Of course, we know that the operators of the Galilean-invariant effective theory must ultimately embed into a Lorentz-invariant theory, and therefore certain constraints between the two sets of LECs b_i and c_i must be satisfied. Assuming that the CLFV interaction is generated by only scalar and/or vector mediators, we may use the results of Tables 3.3 and 7.1 in order to express the conversion rate in terms of the dimensionless coefficients $\tilde{d}_i$ of the

Lorentz-invariant interactions $\mathcal{L}_{\text{int}}^i$ (defined in the aforementioned tables). We find

$$\Gamma = \frac{G_F^2}{\pi} \, \frac{q_{\text{eff}}^2}{1 + \frac{q}{M_T}} \, \frac{4\pi}{2j_N + 1} \sum_{\tau=0,1} \sum_{\tau'=0,1}$$

$$\left\{ \sum_{J=0,2,\dots}^{\infty} \left[\left| (\tilde{d}_1^\tau - \frac{q}{m_L}\tilde{d}_9^\tau)\langle M_\tau^g - M_\tau^{(2)f}\rangle + \tilde{d}_5^\tau\langle M_\tau^g + M_\tau^{(2)f}\rangle \right|_{\tau\tau'}^2 \right.\right.$$

$$\left. + \left| (\tilde{d}_3^\tau + \frac{q}{m_L}\tilde{d}_{17}^\tau)\langle M_\tau^g - M_\tau^{(2)f}\rangle \right|_{\tau\tau'}^2 + \left| \tilde{d}_{13}^\tau\langle M_\tau^g + M_\tau^{(2)f}\rangle \right|_{\tau\tau'}^2 \right]$$

$$+ \sum_{J=1,3,\dots}^{\infty} \left[\left| \tilde{d}_{15}^\tau\langle \Sigma_\tau'^g + \Sigma_\tau'^{(0)f}\rangle - \frac{q_{\text{eff}}}{m_N}(\tilde{d}_5^\tau + \frac{q}{m_L}\tilde{d}_9^\tau)\langle \Delta_\tau^g\rangle \right.\right.$$

$$\left. + \frac{q}{2m_N}(\tilde{d}_5^\tau - 2\tilde{d}_6^\tau + \frac{q}{m_L}(\tilde{d}_9^\tau - 2\tilde{d}_{10}^\tau))\langle \Sigma_\tau'^g\rangle \right|_{\tau\tau'}^2 + \left| \frac{q}{m_L}\tilde{d}_{19}^\tau\langle \Sigma_\tau'^g + \Sigma_\tau'^{(2)f}\rangle \right|_{\tau\tau'}^2$$

$$+ \left| \tilde{d}_7^\tau\langle \Sigma_\tau'^g + \Sigma_\tau'^{(0)f}\rangle + \frac{q}{m_L}\tilde{d}_{11}^\tau\langle \Sigma_\tau'^g + \Sigma_\tau'^{(2)f}\rangle - \frac{q_{\text{eff}}}{m_N}\tilde{d}_{13}^\tau\langle \Delta_\tau^g\rangle + \frac{q}{2m_N}(\tilde{d}_{13}^\tau - 2\tilde{d}_{14}^\tau)\langle \Sigma_\tau'^g\rangle \right|_{\tau\tau'}^2$$

$$\left. + \left| \frac{q}{m_L}\frac{q_{\text{eff}}}{m_N}\tilde{d}_{17}^\tau\langle \Delta_\tau^g\rangle + \frac{q}{m_L}\frac{q}{2m_N}(2\tilde{d}_{18}^\tau - \tilde{d}_{17}^\tau)\langle \Sigma_\tau'^g\rangle \right|_{\tau\tau'}^2 \right]$$

$$+ \sum_{J=2,4,\dots}^{\infty} \left[\left| (\tilde{d}_3^\tau + \frac{q}{m_L}\tilde{d}_{17}^\tau)\langle M_\tau^{(1)f}\rangle \right|_{\tau\tau'}^2 + \left| \tilde{d}_{13}^\tau\langle M_\tau^{(1)f}\rangle \right|_{\tau\tau'}^2 + \left| (\tilde{d}_1^\tau - \tilde{d}_5^\tau - \frac{q}{m_L}\tilde{d}_9^\tau)\langle M_\tau^{(1)f}\rangle \right|_{\tau\tau'}^2 \right]$$

$$+ \sum_{J=1,3,\dots}^{\infty} \left[\left| \tilde{d}_{15}^\tau\langle \Sigma_\tau''^g - \Sigma_\tau''^{(0)f}\rangle - \frac{q}{2m_N}(\tilde{d}_4^\tau - \frac{2q}{m_L}\tilde{d}_{20}^\tau)\langle \Sigma_\tau''^g\rangle \right|_{\tau\tau'}^2 \right.$$

$$+ \left| \frac{q}{m_L}\tilde{d}_{19}^\tau\langle \Sigma_\tau''^{(0)f} + \Sigma_\tau''^{(2)f}\rangle + \frac{q}{m_N}\tilde{d}_{16}^\tau\langle \Sigma_\tau''^g\rangle \right|_{\tau\tau'}^2 + \left| \frac{q}{2m_N}(\tilde{d}_2^\tau - 2\tilde{d}_8^\tau + \frac{2q}{m_L}\tilde{d}_{12}^\tau)\langle \Sigma_\tau''^g\rangle \right|_{\tau\tau'}^2$$

$$\left.\left. + \left| \tilde{d}_7^\tau\langle \Sigma_\tau''^g - \Sigma_\tau''^{(0)f}\rangle + \frac{q}{m_L}\tilde{d}_{11}^\tau\langle \Sigma_\tau''^{(0)f} + \Sigma_\tau''^{(2)f}\rangle \right|_{\tau\tau'}^2 \right] \right\},$$

$$\tag{7.27}$$

where we have introduced the notation $\langle O\rangle \equiv \langle j_N||O(q_{\text{eff}})||j_N\rangle$ and $|A_\tau|_{\tau\tau'}^2 \equiv A_\tau A_{\tau'}^*$. Note that we have retained the radial muon wave functions $g(r)$ and $f(r)$ within the nuclear matrix elements. This is our most precise form of the effective theory decay rate, limited only by the accuracy of nuclear response function evaluations (and the typically very small error introduced through the effective momentum approximation). We reiterate that Eq. (7.27) is only applicable in the case that $\mu \to e$ conversion is mediated by a scalar or vector coupling of the leptons to the nucleons. In principle, an analogous expression could be derived for tensor or other exotic interactions.

7.6   Lower-component Response Functions

The muon's lower component generates eight additional nuclear response functions, those in Eq. (7.12), six of which contribute to the elastic conversion process. Like their namesake counterparts, the operators $M^{(1)}$, $M^{(2)}$, $\Sigma^{(1)}$, and $\Sigma^{(2)}$ are normal parity operators that transform with a phase $(-1)^J$ under parity, whereas the operators $\Sigma'^{(0)}$, $\Sigma'^{(2)}$, $\Sigma''^{(0)}$, and $\Sigma''^{(2)}$
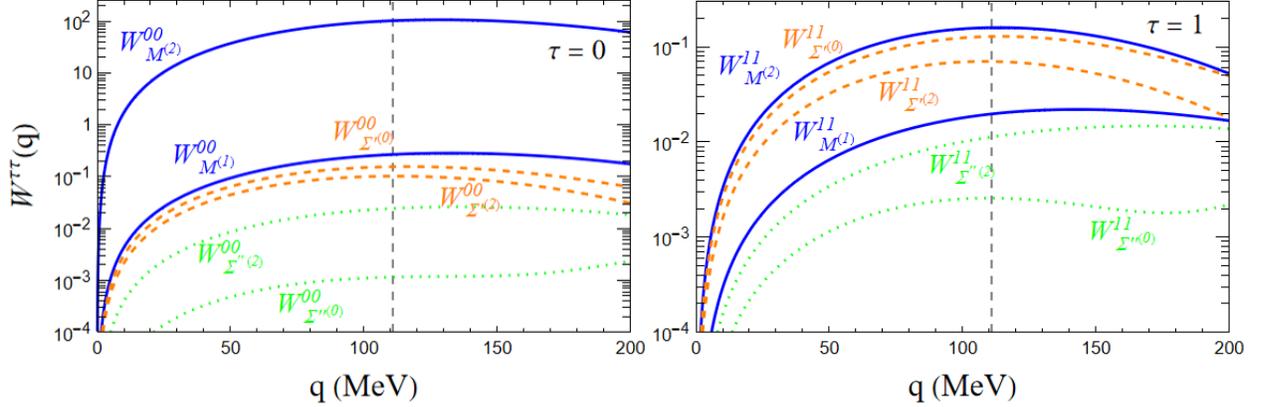
Figure 7.2: The nuclear response functions $W_{\mathcal{O}}^{\tau\tau}(q_{\mathrm{eff}})$ for the six operators generated by the muon's lower component in ^{27}Al. The left (right) panel gives the results for the isoscalar (isovector) coupling. The response functions are needed at the three-momentum transfer q_{eff} indicated by the dashed line. The blue solid curves correspond to the modified charge responses $M^{(1)}$ and $M^{(2)}$, the dashed orange curves correspond to the modified transverse-electric spin responses $\Sigma'(0)$ and $\Sigma'^{(2)}$, and the dotted green curves correspond to the modified longitudinal spin responses $\Sigma''^{(0)}$ and $\Sigma''^{(2)}$.

are abnormal parity operators that transform with a phase $(-1)^{J+1}$ under parity. Similarly, under exchange of initial and final single-particle states, these operators satisfy

$$\langle n(\ell\,1/2)j||T_J(q\vec{x})||n'(\ell'\,1/2)j'\rangle = (-1)^\lambda\,\langle n'(\ell'\,1/2)j'||T_J(q\vec{x})||n(\ell\,1/2)j\rangle, \qquad (7.28)$$

with $\lambda = j' - j$ for the operators $M^{(1)}$, $M^{(2)}$, $\Sigma'^{(0)}$, $\Sigma'^{(2)}$, $\Sigma''^{(0)}$, and $\Sigma''^{(2)}$, and $\lambda = j' + j$ for the operators $\Sigma^{(1)}$ and $\Sigma^{(2)}$. However, harmonic oscillator matrix elements of the novel lower-component response functions *cannot* be expressed in the usual way as

$$\langle n'\,(\ell'\,1/2)\,j'||T_J(q\vec{r})||n\,(\ell\,1/2)\,j\rangle = \frac{1}{\sqrt{4\pi}}y^{(J-K)/2}e^{-y}p(y), \qquad (7.29)$$

where $p(y)$ is a finite-order polynomial. See Appendix D.1 for the details of evaluating the lower-component operators between harmonic oscillator wave functions.

Figures 7.2 and 7.3 show the momentum dependence of the six allowed lower-component response functions evaluated in Al and Cu, respectively. All contributions from lower-component operators vanish in the long wavelength limit $q \to 0$. In this limit, the nucleus becomes point-like and all operators are evaluated at the origin—the muon's lower component is a p-wave and therefore $f(r)$ is required to vanish as $r \to 0$. The isoscalar charge response $W_{M^{(2)}}^{00}$ contains a leading $J = 0$ multipole component that sums coherently over the nuclear target and is consequently the strongest of the lower-component responses. However, the more important measure of the strength of the lower-component nuclear responses is the relative size of the correction that they yield. For example, the interference term $W_{MM^{(2)}}$ enters the decay rate at first-order in $\langle f \rangle / \langle g \rangle$ and acts as a relativistic correction to the upper-component charge response W_M.

The radial-weighting functions differ between the standard nuclear multipole operators and their lower-component counterparts. For example, $M_J^{(2)}$ is obtained from M_J by the
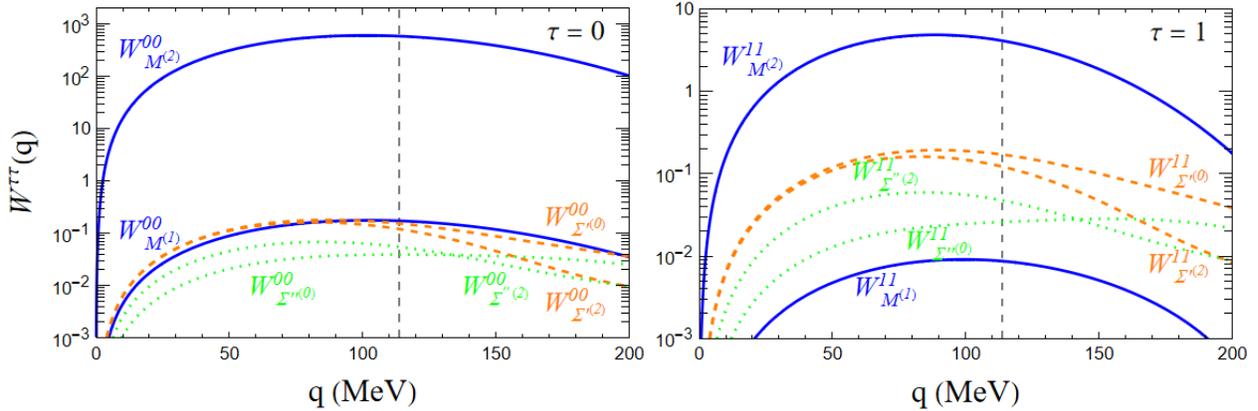
Figure 7.3: As in Fig. 7.2 but for Cu.

Target	$\dfrac{\langle f \rangle}{\langle g \rangle}$	$\dfrac{W^{00}_{MM^{(2)}}}{W^{00}_M}$	$\dfrac{W^{00}_{\Sigma'\Sigma'^{(0)}}}{W^{00}_{\Sigma'}}$	$\dfrac{W^{00}_{\Sigma'\Sigma'^{(2)}}}{W^{00}_{\Sigma'}}$	$\dfrac{W^{00}_{\Sigma''\Sigma''^{(0)}}}{W^{00}_{\Sigma''}}$	$\dfrac{W^{00}_{\Sigma''\Sigma''^{(2)}}}{W^{00}_{\Sigma''}}$
C	-0.015	-0.49	2.23	-1.31	-0.83	0.07
O	-0.019	-0.49	—	—	—	—
F	-0.021	-0.56	0.72	-0.72	0.69	-0.70
Na	-0.025	-0.58	0.90	-0.61	0.39	-0.35
Al	-0.029	-0.62	1.25	-0.95	0.10	-0.40
Si	-0.031	-0.63	1.15	-0.83	-0.16	-0.24
S	-0.035	-0.67	2.96	-1.77	-0.60	-0.07
Ca	-0.042	-0.73	—	—	—	—
Ti	-0.045	-0.81	2.04	-1.32	0.09	-0.45
Fe	-0.051	-0.89	1.33	-1.19	0.39	-0.81
Cu	-0.055	-0.95	0.95	-0.55	0.56	-0.39

Table 7.3: Importance of the relativistic muon corrections compared to the leading-order result. $\langle f \rangle / \langle g \rangle$ is the ratio of average lower and upper muon wave functions defined, respectively, in Eq. (7.18) and Eq. (7.17). In the remaining columns, the interference term $W^{00}_{OO^{(i)}}$ between upper- and lower-component isoscalar nuclear responses is compared to the corresponding upper-component response function W^{00}_O. All nuclear response functions are evaluated at the appropriate effective momentum q_{eff}.

Target	$\dfrac{\langle f \rangle}{\langle g \rangle}$	$\dfrac{W^{11}_{MM^{(2)}}}{W^{11}_M}$	$\dfrac{W^{11}_{\Sigma'\Sigma'^{(0)}}}{W^{11}_{\Sigma'}}$	$\dfrac{W^{11}_{\Sigma'\Sigma'^{(2)}}}{W^{11}_{\Sigma'}}$	$\dfrac{W^{11}_{\Sigma''\Sigma''^{(0)}}}{W^{11}_{\Sigma''}}$	$\dfrac{W^{11}_{\Sigma''\Sigma''^{(2)}}}{W^{11}_{\Sigma''}}$
C	-0.015	-0.55	2.42	-1.39	-0.89	0.10
O	-0.019	-0.68	—	—	—	—
F	-0.021	-0.73	0.73	-0.72	0.70	-0.71
Na	-0.025	-0.74	1.33	-0.89	-0.33	-0.15
Al	-0.029	-0.70	1.54	-1.02	-0.16	-0.25
Si	-0.031	-0.76	0.91	-0.50	0.30	-0.23
S	-0.035	-0.82	3.81	-2.10	-0.76	0.02
Ca	-0.042	-1.16	—	—	—	—
Ti	-0.045	-1.23	2.14	-1.30	0.01	-0.40
Fe	-0.051	-1.19	0.97	-0.97	2.65	-2.60
Cu	-0.055	-1.22	1.04	-0.54	0.46	-0.35

Table 7.4: As in Table 7.3 but for isovector responses.

replacement

$$j_J(qr) \to \frac{d}{dqr} j_J(qr). \tag{7.30}$$

Compared to the original upper-component operators, there is no guarantee that the nuclear responses associated with the muon's lower component will contribute with a similar magnitude. Tables 7.3 and 7.4 compare the size of the relativistic corrections to the corresponding leading order response in isoscalar and isovector channels, respectively[1]. In both isospin channels, the lower-component responses are generally comparable to the upper-component responses across the range of nuclei considered. The isoscalar charge interference term $W^{00}_{MM^{(2)}}$ contributes at roughly 50% of the strength of the leading charge response W^{00}_M in C and at roughly 90% in Cu, smoothly varying between these values for intermediate nuclei. We observe similar behavior in the isovector charge response. The spin-dependent responses do not show such a regular pattern, but the ratios are typically order one, with a maximum of 2.96 (3.81) and a minimum of 0.07 (0.01) in the pure isoscalar (isovector) case. Thus, there are scenarios where relativistic muon effects are moderately amplified, relative to the naïve power-counting in $\langle f \rangle / \langle g \rangle$, by a factor of roughly 3–4 and scenarios where these corrections are significantly suppressed, by as much as two orders of magnitude. The sign of the lower-component correction relative to the leading contribution appears to be consistent across all nuclei for the operators $M^{(2)}$, $\Sigma'^{(0)}$, and $\Sigma'^{(2)}$, whereas the sign of the contributions from $\Sigma''^{(0)}$ and $\Sigma''^{(2)}$ can vary depending on the target.

In computing the decay rate, the nuclear responses are weighted by different leptonic

---

[1]The reported ratios are meant only to assess the strength of the leading lower-component contributions vis-à-vis the nuclear response. In computing the decay rate, the lower-component interference terms are additionally suppressed by $\langle f \rangle / \langle g \rangle$, as in Eq. (7.22).

R factors. For example, let us consider the case of coherent conversion where, including relativistic muon effects to first order, the $\mu \to e$ decay rate is

$$\Gamma_{\text{coherent}} = \frac{G_F^2}{\pi} \frac{q_{\text{eff}}^2}{1 + \frac{q}{M_T}} |\phi_{1s}^{Z_{\text{eff}}}(\vec{0})|^2 \left[\tilde{R}_M^{00} W_M^{00}(q_{\text{eff}}) + 2\frac{\langle f \rangle}{\langle g \rangle} \tilde{R}_{MM^{(2)}}^{00} W_{MM^{(2)}}^{00}(q_{\text{eff}}) \right]. \qquad (7.31)$$

Assuming that the leptonic response functions are equal in magnitude, the inclusion of the muon's lower component corrects the rate obtained from the upper-component result by $\approx 3.6\%$ in ^{27}Al. We can make this scenario more concrete by assuming that the upper- and lower-component operators arise from a common Lorentz-invariant operator, as in Tables 3.3 and 7.1. For example, suppose that the sole CLFV operator is the relativistic scalar, isoscalar interaction $\bar{e}\mu\bar{N}N$. Then, the relevant LECs obey $\tilde{b}_2^0 = i\tilde{c}_1^0$, which implies that $\tilde{R}_M^{00} = -\tilde{R}_{MM^{(2)}}^{00}$. As a result, we are able to determine that the relativistic correction *reduces* the leading-order coherent rate by 3.6% in ^{27}Al.

In these evaluations, we have replaced both the upper $g(r)$ and lower $f(r)$ radial wave functions of the muon by constant approximations. The errors incurred in the relativistic corrections due to this procedure are summarized in Table 7.5. In particular, we report the variation that results when the exact response function

$$W_{O^g O^{(i)f}}^{\tau\tau'}(q_{\text{eff}}) \equiv \frac{4\pi}{2j_N + 1} \sum_J \langle j_N || O_{J;\tau}^g(q_{\text{eff}}) || j_N \rangle \langle j_N || O_{J;\tau'}^{(i)f}(q_{\text{eff}}) || j_N \rangle, \qquad (7.32)$$

is replaced by the constant approximation

$$\langle f \rangle \langle g \rangle W_{OO^{(i)}}^{\tau\tau'} = \langle f \rangle \langle g \rangle \frac{4\pi}{2j_N + 1} \sum_J \langle j_N || O_{J;\tau}(q_{\text{eff}}) || j_N \rangle \langle j_N || O_{J;\tau'}^{(i)}(q_{\text{eff}}) || j_N \rangle. \qquad (7.33)$$

In ^{27}Al and ^{63}Cu, the error incurred in the isoscalar charge response $W_{MM^{(2)}}^{00}$ is entirely negligible. Consequently, the relativistic correction to the coherent rate in Eq. (7.31) should accurately reproduce the exact result, up to terms of order $(\langle f \rangle / \langle g \rangle)^2$. This is not guaranteed by construction: the average values $\langle g \rangle$ and $\langle f \rangle$ are defined with respect to the lowest $J = 0$ multipoles of the operators M and $M^{(2)}$, respectively. The full response function evaluation includes all allowed multipoles. Contributions from multipoles with $J > 0$ are highly suppressed relative to the leading coherent response. In other isospin channels, errors $\lesssim 5\%$ are observed in ^{27}Al and ^{63}Cu. Similar errors result when one considers the spin-dependent responses, with variations as high as 22% in some cases. The typical deviations are $\approx 6.4\%$ in ^{27}Al and $\approx 5.5\%$ in ^{63}Cu. Thus, the constant approximations should provide a reasonable estimate of the conversion rate, though, in any case where greater precision is required, the full radial muon wave functions can be restored in the nuclear matrix elements, as in Eq. (7.32).

The consideration of relativistic corrections to the muon wave function is most sensible in a "top-down" approach to $\mu \to e$ conversion; that is, if one begins from a particular UV theory of CLFV and proceeds down to the nuclear scale. Then, it is straightforward—using the formalism developed here—to include the effect of the lower component of the muon, sharpening the prediction of the branching ratio by a few percent. (Of course, uncertainties arising elsewhere in the procedure, for example in the evaluation of nuclear responses, may,

Target	% variation			
	$W^{00}_{MM^{(2)}}$	$W^{11}_{MM^{(2)}}$	$W^{10}_{MM^{(2)}}$	$W^{01}_{MM^{(2)}}$
^{27}Al	0.00%	-5.19%	0.98%	-5.91%
^{63}Cu	0.00%	-4.05%	-1.27%	-2.83%
	$W^{00}_{\Sigma'\Sigma'^{(0)}}$	$W^{11}_{\Sigma'\Sigma'^{(0)}}$	$W^{10}_{\Sigma'\Sigma'^{(0)}}$	$W^{01}_{\Sigma'\Sigma'^{(0)}}$
^{27}Al	-5.58%	-6.78%	-6.20%	-6.17%
^{63}Cu	-3.26%	-4.16%	-2.69%	-4.76%
	$W^{00}_{\Sigma'\Sigma'^{(2)}}$	$W^{11}_{\Sigma'\Sigma'^{(2)}}$	$W^{10}_{\Sigma'\Sigma'^{(2)}}$	$W^{01}_{\Sigma'\Sigma'^{(2)}}$
^{27}Al	-5.61%	-6.47%	-6.38%	-5.68%
^{63}Cu	-10.29%	-13.03%	-11.04%	-12.27%
	$W^{00}_{\Sigma''\Sigma''^{(0)}}$	$W^{11}_{\Sigma''\Sigma''^{(0)}}$	$W^{10}_{\Sigma''\Sigma''^{(0)}}$	$W^{01}_{\Sigma''\Sigma''^{(0)}}$
^{27}Al	-2.70%	-22.12%	-2.59%	-22.11%
^{63}Cu	3.57%	3.27%	4.58%	2.37%
	$W^{00}_{\Sigma''\Sigma''^{(2)}}$	$W^{11}_{\Sigma''\Sigma''^{(2)}}$	$W^{10}_{\Sigma''\Sigma''^{(2)}}$	$W^{01}_{\Sigma''\Sigma''^{(2)}}$
^{27}Al	-5.33%	-3.79%	-5.29%	-3.82
^{63}Cu	-5.78%	-7.27%	-4.15%	-8.86%

Table 7.5: Error incurred when $W^{\tau\tau'}_{O^g O^{(i)} f}$ is replaced by $\langle g \rangle \langle f \rangle W^{\tau\tau'}_{OO^{(i)}}$, where $\langle g \rangle$ is obtained by averaging over the isoscalar monopole operator $M_{00;0}$ and $\langle f \rangle$ is obtained by averaging over the corresponding lower-component operator $M^{(2)}_{00;0}$. To some extent, this table can be considered as the analogue of Table 2.4, which describes the error incurred in the upper-component nuclear response functions when $g(r)$ is replaced by its average.

at least partially, negate the benefit of including these corrections.) In general, however, the quantities probed by $\mu \to e$ conversion experiments are not particularly sensitive to these relativistic effects: The muon's lower component always enters as a correction to the upper-component result, which is itself described by 12 independent response functions. Considerable experimental effort will be required to distinguish among these leading order responses. In light- and medium-mass nuclei, it is far more important to include in the effective theory the operators associated with the nucleon velocity, which heretofore have been completely ignored in the literature.

Any attempt to discern relativistic corrections would almost certainly require conversion experiments to be performed on very heavy nuclei. In ^{184}W, the inclusion of the muon's lower component reduces the expected coherent conversion rate by 50%. In ^{63}Cu, the corresponding effect is only at the level of 10%. If $\mu \to e$ conversion were to be observed in ^{27}Al at Mu2e and COMET, there would be little motivation to thereafter consider an exceedingly heavy target, aside from perhaps probing the isospin-dependence of CLFV operators with a neutron-rich target. The spin- and velocity-dependence can be investigated without resorting to heavy nuclei where relativistic muon corrections complicate the analysis. Nonetheless, the nucleon-scale effective theory is now equipped to describe heavy nuclei, which may play a role in determining the nature of CLFV.

Chapter 8

Scalar-mediated Coherent $\mu \to e$ Conversion

At present, there exist a wealth of possible extensions of the standard model that are not in tension with current limits on CLFV processes. Although any positive observation of CLFV is an unambiguous signal of BSM physics, an isolated measurement is not sufficient to distinguish between candidate UV theories. In this thesis, we have introduced the necessary formalism at the nuclear scale to extract all of the available information about CLFV operators from elastic $\mu \to e$ conversion experiments. Satisfied that we have constructed the most general effective theory at the single-nucleon level, our next aim is to connect constraints obtained on the low-energy constants of the nuclear effective theory to the coefficients of higher-scale effective theories through a successive matching procedure, eventually making contact with UV theories of CLFV.

Short of developing the general matching program, in this chapter we focus our attention on the case of coherent $\mu \to e$ conversion mediated by scalar quark operators. We map these operators to the nucleon-level effective theory, using chiral perturbation theory (with inputs from lattice QCD) to match the quark and nucleon degrees of freedom through next-to-leading order. Particular care is devoted to the treatment of the two-nucleon CLFV interaction, which—in contrast to the single-nucleon coherent operators—cannot be evaluated a priori using the scalar nuclear density.

We illustrate the advantages of this specialized, top-down approach by computing the $\mu \to e$ conversion branching ratio with quantified uncertainty, allowing one to translate limits on CLFV processes into rigorous constraints on the parameter space of candidate BSM theories. In the case that CLFV processes are observed, one may leverage complementary measurements of $\mu \to e\gamma$ and $\mu \to e$ (in multiple nuclear targets) to exclude altogether particular classes of UV models, including, as we consider, those in which CLFV is mediated by the standard model Higgs. Finally, we take the first steps toward the general effective theory matching program by connecting the single-nucleon operators of the nuclear-scale effective theory to the quark-level Lagrangian of scalar-mediated coherent conversion. The analysis and discussion in this chapter mirror that originally described in Ref. [57].

8.1 Quark-level Effective Theories: SM-EFT & LEFT

Augmenting the standard model with higher-dimensional $\mathrm{SU}(3)_c \times \mathrm{SU}(2)_L \times \mathrm{U}(1)_Y$ invariant operators constructed from standard-model fields, one obtains the so-called standard model effective field theory (SM-EFT) [109]. At dimension five, there is only one operator that obeys the SM gauge symmetries: the famous Weinberg operator [110], which violates lepton number L by two units and therefore permits processes such as neutrinoless double beta decay. The Weinberg operator is not relevant to the L-conserving CLFV processes that we consider in this work[1]; on the other hand, a variety of CLFV operators arise in SM-EFT at dimension six.

Below the scale of electroweak symmetry breaking, the $\mathrm{SU}(2)_L \times \mathrm{U}(1)_Y$ symmetry is broken to the electromagnetic gauge symmetry $\mathrm{U}(1)_{\mathrm{EM}}$. The gauge symmetry that governs the effective theory is now $\mathrm{SU}(3)_c \times \mathrm{U}(1)_{\mathrm{EM}}$, and the consistent set of higher-dimensional operators is known as low-energy effective field theory (LEFT). The complete set of LEFT operators up to and including dimension six is known [111], as is their anomalous dimension [112]. At the electroweak scale, the operators of LEFT can be matched to the operators of SM-EFT (at tree-level and one-loop [113]).

Thus, one envisions a general procedure, starting with a particular UV theory of CLFV characterized by some energy scale Λ above the electroweak scale. Below the scale of new physics, any heavy particles associated with CLFV can be integrated out, inducing higher dimensional SM-EFT operators. The SM-EFT operators can be renormalized down to the scale where the Higgs vacuum expectation value breaks electroweak symmetry; at this point, the SM-EFT operators are matched onto the operators of LEFT. This program of renormalization and matching was recently carried out for the full set of dimension-six operators mediating CLFV τ decays [33]. As the procedure is relatively straightforward, and the physics is well-understood, we shall begin our discussion below the electroweak scale. Short of considering the most general basis of CLFV LEFT operators, we will restrict our attention to those operators that arise when CLFV is mediated by a heavy scalar particle—including, as we consider in detail in Section 8.6, the standard-model Higgs boson. We take the effective Lagrangian below the electroweak scale to be given by

$$
\begin{aligned}
\mathcal{L}_{\mathrm{eff}} = -\frac{1}{\Lambda^2} \sum_{\alpha=L,R} \Big[& C_{D\alpha}\, m_\mu\, \bar{e}\sigma^{\lambda\nu} P_\alpha \mu\, F_{\lambda\nu} + \sum_{q=u,d,s,c,b,t} C_{S\alpha}^{(q)}\, G_F m_\mu m_q\, \bar{q}q\, \bar{e} P_\alpha \mu \\
& + C_{G\alpha}\, G_F m_\mu \alpha_s\, G_{\lambda\nu}^a G^{a\,\lambda\nu}\, \bar{e} P_\alpha \mu + \mathrm{h.c.} \Big],
\end{aligned}
\tag{8.1}
$$

where Λ is a mass scale associated with the CLFV physics, $P_{L/R} = \left(1 \mp \gamma_5\right)/2$ are the chiral projection operators, $F_{\mu\nu}$ and $G_{\mu\nu}^a$ are, respectively, the photon and gluon field strength tensors, and the Wilson coefficients $C_{D\alpha}$, $C_{S\alpha}^{(q)}$, and $C_{G\alpha}$ are dimensionless. The effective theory of scalar-mediated coherent conversion is therefore specified by 16 dimensionless Wilson coefficients.

The CLFV operators themselves carry the following mass dimension: the photon dipole operator is dimension five, the scalar quark operator is dimension six, and the gluonic operator

---

[1]One can consider processes that violate both lepton number and lepton flavor, such as $\mu^- \to e^+$ conversion in nuclei.

is dimension seven. We have included the factors of m_q and α_s in the quark and gluon operators, respectively, to ensure that the Wilson coefficients $C_{S\alpha}^{(q)}$ and $C_{G\alpha}$ do not run under QCD renormalization. When the heavy quarks are integrated out at the GeV scale, their scalar quark couplings generate contributions to the gluonic Wilson coefficients

$$C_{G\alpha} \to C_{G\alpha} - \frac{1}{12\pi} \sum_{q=c,b,t} C_{S\alpha}^{(q)}. \tag{8.2}$$

Otherwise, the effective Lagrangian remains unchanged, with the summation of q in Eq. (8.1) restricted to $q = (u, d, s)$. This is the reason for retaining the dimension-seven gluon operator in our treatment: it is induced by the dimension-six heavy quark operators.

The photon dipole term induces the $\mu \to e$ conversion process through the exchange of a virtual photon with the target nucleus, as in Fig. 6.1 (b). The dipole operator can also mediate the $\mu \to e\gamma$ process whereby an on-shell photon is produced, as in Fig. 6.1 (a). The branching ratio for this latter process has the simple form

$$B_{\mu \to e\gamma} = 96\pi^2 \left(\frac{v}{\Lambda}\right)^4 \left(|C_{DR}|^2 + |C_{DL}|^2\right). \tag{8.3}$$

Relating the dipole Wilson coefficients to the electric and magnetic dipole form factors defined in Eq. (6.1), we find

$$\begin{aligned}
\tilde{f}_M(0) &= \frac{1}{e} \left(C_{DL} + C_{DR}\right), \\
\tilde{f}_E(0) &= \frac{i}{e} \left(C_{DL} - C_{DR}\right),
\end{aligned} \tag{8.4}$$

where $e = \sqrt{4\pi\alpha}$ is the elementary electromagnetic charge. The on-shell process provides a valuable complementary constraint on CLFV, particularly when the $\mu \to e$ conversion branching ratio can be computed to high accuracy with known uncertainties.

8.2 Connecting Quarks to Nucleons with Chiral Effective Theory

To make contact with $\mu \to e$ conversion experiments, we must continue to run down in energy past the QCD scale where the quarks confine into hadrons. Beyond this point, QCD becomes strongly coupled, and a perturbative treatment in terms of quark degrees of freedom becomes intractable. In order to proceed, we must match the quark theory to one in which the degrees of freedom are protons, neutrons, and light mesons. Retaining only the up and down quark, in the limit that $m_u, m_d \to 0$, the QCD Lagrangian exhibits a chiral symmetry $\mathrm{SU}(2)_L \times \mathrm{SU}(2)_R$ that allows for separate isospin rotations of right-handed and left-handed up and down quark doublets

$$\begin{pmatrix} u_L \\ d_L \end{pmatrix} \to g_L \begin{pmatrix} u_L \\ d_L \end{pmatrix}, \quad \begin{pmatrix} u_R \\ d_R \end{pmatrix} \to g_R \begin{pmatrix} u_R \\ d_R \end{pmatrix}, \tag{8.5}$$
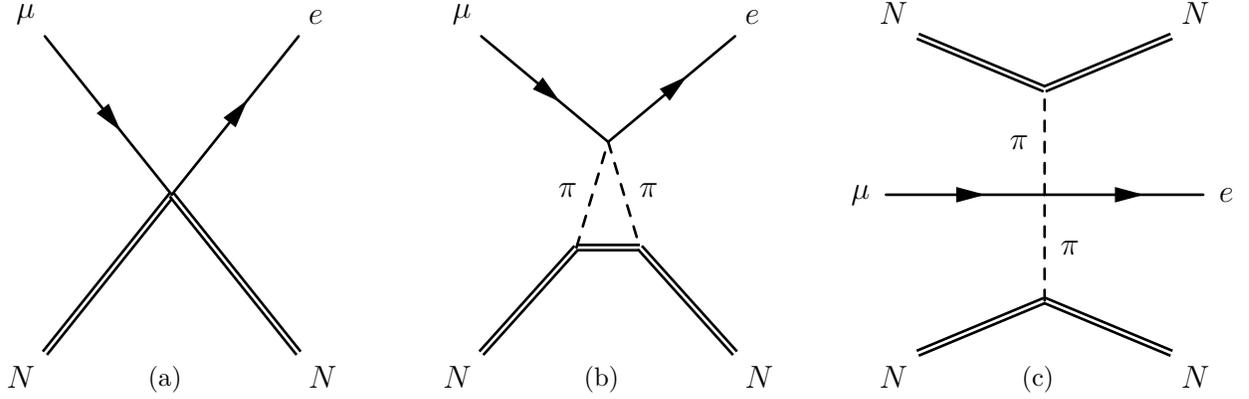
Figure 8.1: Diagrams in ChPT contributing to scalar-mediated $\mu \to e$ conversion through next-to-leading order: (a) LO $NNe\mu$ contact interaction. (b) NLO two-pion one-loop diagram with $\pi\pi e\mu$ vertex. (c) NLO two-nucleon two-pion-exchange diagram with $\pi\pi e\mu$ vertex.

where $g_L \in \mathrm{SU}(2)_L$ and $g_R \in \mathrm{SU}(2)_R$. Ultimately, the chiral symmetry is spontaneously broken to the vector subgroup $\mathrm{SU}(2)_L \times \mathrm{SU}(2)_R \to SU(2)_V$. (The chiral symmetry is also explicitly broken by the non-zero quark masses, leading to massive pions as the pseudo-Goldstone bosons.) Nonetheless, we may construct effective hadronic operators that transform under the broken chiral symmetry. The resulting effective field theory is known as SU(2) Chiral Perturbation Theory (ChPT).

In $\mu \to e$ conversion, the three-momentum transfer is roughly equal to the strange quark mass $|\vec{q}| \approx m_s$. Technically, one should retain the strange quark in the preceding analysis and consider the chiral symmetry $\mathrm{SU}(3)_L \times \mathrm{SU}(3)_R$ that rotates among the three lightest quarks. However, as the external nucleon states do not carry net strangeness and the momentum transfer is not significantly greater than the strange quark mass, one expects that the effect of the strange quark on CLFV processes will be suppressed relative to the contributions from up and down quarks. In that case, we may work in SU(2) ChPT with the strange quark treated as an additional singlet under the chiral symmetry.

The one- and two-nucleon operators arising in SU(2) ChPT through next-to-leading order (NLO) in chiral power-counting have been computed previously [56, 114–116]. The diagrams relevant to scalar-mediated coherent $\mu \to e$ conversion are shown in Fig. 8.1. The quark-level operators hadronize into nucleon-level operators as

$$\langle N(\vec{k}')| \left(C_{S\alpha}^{(u)} m_u \bar{u}u + C_{S\alpha}^{(d)} m_d \bar{d}d \right) |N(\vec{k})\rangle \to \bar{N}' J_{ud,\alpha}^{(1)}(\vec{q})N$$

$$\langle N(\vec{k_1}')N(\vec{k_2}')| \left(C_{S\alpha}^{(u)} m_u \bar{u}u + C_{S\alpha}^{(d)} m_d \bar{d}d \right) |N(\vec{k_1})N(\vec{k_2})\rangle \to \bar{N}_1' \bar{N}_2' J_{ud,\alpha}^{(2)}(\vec{q_1}, \vec{q_2})N_1 N_2$$

$$\langle N(\vec{k}')|C_{S\alpha}^{(s)} m_s \bar{s}s|N(\vec{k})\rangle \to \bar{N}' J_{s,\alpha}^{(1)}(\vec{q})N \tag{8.6}$$

$$\langle N(\vec{k}')|C_{G\alpha}\alpha_s G_{\lambda\nu}^a G^{a\ \lambda\nu}|N(\vec{k})\rangle \to \bar{N}' J_{G,\alpha}^{(1)}(\vec{q})N$$

$$\langle N(\vec{k_1}')N(\vec{k_2}')|C_{G\alpha}\alpha_s G_{\lambda\nu}^a G^{a\ \lambda\nu}|N(\vec{k_1})N(\vec{k_2})\rangle \to \bar{N}_1' \bar{N}_2' J_{G,\alpha}^{(2)}(\vec{q_1}, \vec{q_2})N_1 N_2,$$

where the corresponding nucleon currents are given by

$$J^{(1)}_{ud,\alpha}(q) = \left[\sigma_{\pi N} - \frac{3m_\pi^3 g_A^2}{64\pi f_\pi^2}F(q^2/m_\pi^2)\right] C^{(0)}_{S\alpha} - \frac{\delta m_N}{4}\tau_3 C^{(1)}_{S\alpha}$$

$$J^{(2)}_{ud,\alpha}(\vec{q}_1, \vec{q}_2) = -\frac{g_A^2 m_\pi^2}{4f_\pi^2}\frac{\vec{\sigma}(1)\cdot\vec{q}_1\,\vec{\sigma}(2)\cdot\vec{q}_2}{(q_1^2+m_\pi^2)(q_2^2+m_\pi^2)}\,\vec{\tau}_1\cdot\vec{\tau}_2\,C^{(0)}_{S\alpha}$$

$$J^{(1)}_{s,\alpha}(q) = \left(\sigma_s - \dot\sigma_s q^2\right)C^{(s)}_{S\alpha} \tag{8.7}$$

$$J^{(1)}_{G,\alpha}(q) = -\frac{8\pi}{9}C_{G\alpha}\left\{m_N - \left[\sigma_{\pi N} - \frac{3m_\pi^3 g_A^2}{64\pi f_\pi^2}F(q^2/m_\pi^2)\right] + \frac{\delta m_N}{2}\tau_3 - \left(\sigma_s - \dot\sigma_s q^2\right)\right\}$$

$$J^{(2)}_{G,\alpha}(\vec{q}_1, \vec{q}_2) = -\frac{8\pi}{9}C_{G\alpha}\frac{g_A^2 m_\pi^2}{4f_\pi^2}\frac{\vec{\sigma}(1)\cdot\vec{q}_1\,\vec{\sigma}(2)\cdot\vec{q}_2}{(q_1^2+m_\pi^2)(q_2^2+m_\pi^2)}\,\vec{\tau}_1\cdot\vec{\tau}_2.$$

The isoscalar and isovector combinations of scalar Wilson coefficients are

$$C^{(0)}_{S\alpha} = \frac{1-\epsilon}{2}C^{(u)}_{S\alpha} + \frac{1+\epsilon}{2}C^{(d)}_{S\alpha},$$

$$C^{(1)}_{S\alpha} = \left(1-\frac{1}{\epsilon}\right)C^{(u)}_{S\alpha} + \left(1+\frac{1}{\epsilon}\right)C^{(d)}_{S\alpha}, \tag{8.8}$$

where

$$\epsilon = \frac{m_d - m_u}{m_d + m_u}, \tag{8.9}$$

describes the mass difference between up- and down-type quarks. This quantity can be computed from lattice QCD, and we adopt the value $\epsilon = 0.365(23)$ from the Flavour Lattice Averaging Group (FLAG) [117]. The strong-force contribution to isospin violation is captured by the nucleon mass splitting

$$\delta m_N = (m_n - m_p)_{\text{strong}}, \tag{8.10}$$

which determines the strength of the isovector contributions. We adopt the lattice QCD determination $\delta m_N = 2.32(17)$ MeV [118]. The quark content of the nucleons is quantified by the so-called sigma terms

$$\sigma_{\pi N} = \frac{1}{2}\langle N|(m_u + m_d)(\bar{u}u + \bar{d}d)|N\rangle,$$

$$\sigma_s = \langle N|m_s \bar{s}s|N\rangle. \tag{8.11}$$

For the pion-nucleon sigma term, we employ the value $\sigma_{\pi N} = 59.1(3.5)$ MeV, obtained from the Roy-Steiner equations [119]. Lattice QCD calculations of this quantity indicate $\sigma_{\pi N} = 63(13)$ MeV (with dynamical charm quark [120]) and $\sigma_{\pi N} = 40(4)$ MeV (no dynamical charm quark [121–123]). A recent analysis [124] of the lattice results suggests that the inclusion of excited state effects can alleviate some of the tension between the (currently less precise) lattice QCD determinations and the Roy-Steiner value. For the strange sigma term, we adopt the FLAG value $\sigma_s = 41(9)$ MeV [117], while for the slope of this form factor we take $\dot\sigma_s = 0.3(2)$ GeV^{-1} [125]. Finally, we take $g_A = 1.2759 \pm 0.0045$ [126] as the value of the nucleon axial-vector coupling constant and $f_\pi = 92.2(1)$ MeV as the physical pion

decay constant [117]. Table 8.1 provides a summary of the values of the hadronic parameters adopted in this work.

The single-nucleon scalar form factor $F(x)$, corresponding to the one-loop diagram in Fig. 8.1, is given by

$$
\begin{aligned}
F(x) &= \frac{2+x}{\sqrt{x}} \operatorname{arccot}\left(\frac{2}{\sqrt{x}}\right) - 1 \\
&\approx \frac{5}{12}x - \frac{7}{240}x^2 + \frac{9}{2240}x^3 + ...
\end{aligned}
\tag{8.12}
$$

Although the typical momentum transfer[2] is comparable to the pion mass

$$
(q/m_\pi)^2 \approx (m_\mu/m_\pi)^2 \approx 0.6,
\tag{8.13}
$$

the dependence of the form factor on x is quite mild. (Higher order terms in the Taylor series are naturally suppressed.) The first-order term reproduces the full expression to 2% accuracy for $x \le 1$ and to 5% accuracy for $1 < x \le 2$. Therefore, we are justified in retaining only the linear term in our analysis.

8.3   Treatment of Two-Nucleon Operators

Having successfully traded the quark degrees of freedom for nucleons, the one- and two-nucleon CLFV amplitudes are

$$
\begin{aligned}
\mathcal{A}^{(1)} &= -\frac{G_F m_\mu}{\Lambda^2} \sum_{\alpha=L,R} \bar{N}' J_\alpha^{(1)} N \langle \bar{e} P_\alpha \mu \rangle , \\
\mathcal{A}^{(2)} &= -\frac{G_F m_\mu}{\Lambda^2} \sum_{\alpha=L,R} \bar{N}_1' \bar{N}_2' J_\alpha^{(2)} N_1 N_2 \langle \bar{e} P_\alpha \mu \rangle ,
\end{aligned}
\tag{8.14}
$$

where

$$
\begin{aligned}
J_\alpha^{(1)} &\equiv J_{ud,\alpha}^{(1)} + J_{s,\alpha}^{(1)} + J_{G,\alpha}^{(1)} \\
J_\alpha^{(2)} &\equiv J_{ud,\alpha}^{(2)} + J_{G,\alpha}^{(2)}.
\end{aligned}
\tag{8.15}
$$

The two-nucleon current $J_\alpha^{(2)}$ presents a significant theoretical challenge. First, the nuclear effective theory that we have developed throughout this thesis is based entirely on single-nucleon charges and currents. According to ChPT, however, two-nucleon operators can contribute to the coherent conversion amplitude at the 10% level. The fact that these terms are incompatible with the structure of the nuclear effective theory threatens to spoil our conclusion that $\mu \to e$ conversion is governed by six response functions (plus two interference terms) and to undermine the utility of the effective theory as a tool for constraining the most general set of CLFV operators.

---

[2]In contrast to the effective theory treatment, when we retain the full Dirac solutions for the leptons, the three-momentum transfer is not a well-defined quantity. Instead, the "typical" momentum transfer is determined by the electron wave function, which is peaked in momentum space near $q = m_\mu$.

Quantity	Accepted Value	Reference
$\sigma_{\pi N}$	59.1 ± 3.5 MeV	[119]
σ_s	41 ± 9 MeV	[117]
$\dot{\sigma}_s$	0.3 ± 0.2 GeV^{-1}	[125]
ϵ	0.365 ± 0.23	[117]
δm_N	2.32 ± 0.17 MeV	[118]
f_π	92.2 ± 0.1 MeV	[117]
g_A	1.2759 ± 0.0045	[126]

Table 8.1: Hadronic input parameters, their uncertainties, and references.

The two-nucleon operator also endangers the present top-down approach. In order to provide a clean prediction for the $\mu \to e$ conversion branching ratio $B_{\mu \to e}$ with a quantified error, we must be able to compute the strength of the two-nucleon term and understand the associated uncertainty. The difficulty with $J_\alpha^{(2)}$ arises because—unlike the single-nucleon current $J_\alpha^{(1)}$—total nuclear matrix elements of the two-nucleon current cannot be obtained using only the (experimentally measured) scalar nucleon density $\rho_N(r)$ but require knowledge of the two-nucleon correlation function. One can obtain the two-nucleon correlation function from a nuclear shell-model calculation, as described in detail in Chapter 9. Such a calculation, relying on a severely-truncated model space and a phenomenological Hamiltonian, can provide an estimate of the strength of the two-nucleon operator, but the error cannot be quantified in any rigorous way. To improve upon this situation somewhat, one would like an additional, independent determination of the size of the two-nucleon contribution.

Alternative to the shell-model approach, one may replace the two-nucleon operator by an effective one-body operator by averaging over a degenerate Fermi gas model of the target nucleus. The resulting single-nucleon operator can then be treated on the same footing as $J_\alpha^{(1)}$ and evaluated with the scalar nucleon density. More precisely, an effective one-body operator is obtained by performing a mean-field-like sum over direct and exchange terms

$$\langle \alpha | \mathcal{O}^{(1)} | \beta \rangle \equiv \sum_\gamma \langle \alpha \gamma | \mathcal{O}^{(2)} | \beta \gamma \rangle - \langle \alpha \gamma | \mathcal{O}^{(2)} | \gamma \beta \rangle \,, \tag{8.16}$$

where γ sums over occupied core states. In the degenerate Fermi gas model, each core state is a direct product of space, spin, and isospin components

$$|\alpha\rangle = |\vec{p}(\alpha)\rangle \otimes |\frac{1}{2} m_s(\alpha)\rangle \otimes |\frac{1}{2} m_t(\alpha)\rangle \,. \tag{8.17}$$

States of momentum $\vec{p}$ are occupied up to the nuclear Fermi momentum k_F. The details of the averaging procedure in the case that $\mathcal{O}^{(2)} = J_\alpha^{(2)}$ are relegated to Appendix E. The net effect of performing the Fermi gas average is a shift in the single-nucleon coupling parameter

$$\sigma_{\pi N} \to \sigma_{\pi N} - \frac{3 g_A^2 m_\pi^2 k_F}{64 \pi f_\pi^2} f_{\text{eff}}^{SI} \,, \tag{8.18}$$

where f_{eff}^{SI} is a (nucleus-dependent) constant that encodes the strength of the effective one-body operator.

Target	c_p (fm)	c_n (fm)	β (fm)	k_F (MeV)	q (MeV)	$f^{SI}_{\text{eff,FGA}}$	$f^{SI}_{\text{eff,NSM}}$
$^{27}_{13}\text{Al}$	3.05	3.18 ± 0.19	0.535	238	104.97	$0.43^{+0.03}_{-0.22}$	0.18
$^{48}_{22}\text{Ti}$	3.843	3.843	0.588	255	104.27	$0.49^{+0.03}_{-0.25}$	0.18
$^{197}_{79}\text{Au}$	6.55	6.83 ± 0.1	0.522	265	95.61	$0.55^{+0.03}_{-0.28}$	—
$^{208}_{82}\text{Pb}$	6.624	6.93 ± 0.09	0.549	265	95.10	$0.55^{+0.03}_{-0.28}$	—

Table 8.2: Input parameters and output values of the effective one-body coupling constant f^{SI}_{eff} for four nuclei of interest. c_p (c_n) and β are the parameters of the proton (neutron) density profile, $f^{SI}_{\text{eff,FGA}}$ is the value of the spin-independent form factor implied by the Fermi gas average, and $f^{SI}_{\text{eff,NSM}}$ is the value implied by the nuclear shell model (without additional correlation function).

Table 9.1 compares, in several nuclei of interest, two estimates of the effective single-nucleon coupling parameter: $f^{SI}_{\text{eff,FGA}}$, the value obtained by the Fermi gas average, and $f^{SI}_{\text{eff,NSM}}$, the value implied by a shell-model evaluation of the two-nucleon operator. We find that the FGA result exceeds the NSM result by a factor of $\approx$ 2–3 in those nuclei, ^{27}Al and ^{48}Ti, for which both calculations were performed. A similar overestimation has been observed previously in two-nucleon operators that generate nuclear anapole moments [127]. In that study, which focused on the relatively heavy nuclei ^{133}Cs and ^{205}Tl and considered a variety of two-body nuclear currents—none of them the operator of present concern—it was found that the Fermi gas average result was typically 2–3 times larger than the corresponding shell-model result. Although we did not perform shell-model calculations for the heavy nuclei ^{197}Au and ^{208}Pb, given that the anapole moment study observed this same effect in ^{133}Cs and ^{205}Tl, it seems likely that a similar result would be found for ^{197}Au and ^{208}Pb in the present case. (In Chapter 9, we compare $f^{SI}_{\text{eff,FGA}}$ and $f^{SI}_{\text{eff,NSM}}$ for a range of light- to medium-mass nuclei, from ^{12}C to ^{63}Cu, and observe the same trend.)

We assign to $f^{SI}_{\text{eff,FGA}}$ an upper uncertainty that accounts, primarily, for the uncertainty in the experimental determination of the nuclear Fermi momentum (± 5 MeV) and a lower uncertainty that reflects the expectation that the Fermi gas average tends to overestimate the shell-model result by approximately a factor of two. This is the value of the effective single-nucleon coupling constant that we employ in the top-down approach, propagating the corresponding uncertainty throughout the calculation. We have been rather conservative in assigning the error, but the lower end of this range may still represent an overestimation of the strength of the two-nucleon amplitude. The nuclear shell-model calculation is not rigorous; the two-nucleon correlation function is obtained in a soft Hilbert space that lacks the high-momentum modes required to resolve the strong repulsion of two nucleons at short range. Preliminary estimates suggest that the inclusion of the missing short-range physics tends to further depress the two-nucleon $\mu \to e$ conversion operator. (For a detailed discussion of this issue, see Section 9.2.)

The advantages of the Fermi gas average are twofold. First, it yields an estimate of the strength of the two-nucleon operator without the need for a computationally intensive nuclear shell-model calculation; the resulting effective operator can be readily evaluated using the

scalar nucleon density. Second, the averaging procedure provides additional justification for basing our nuclear effective theory of $\mu \to e$ conversion on single-nucleon currents: any two-nucleon current that might be relevant can be averaged to an effective one-body operator. The Fermi gas averaging procedure represents a concrete realization of a generic feature of nuclear systems: saturation implies that nucleons locally experience little variation in the nuclear medium with increasing A, and, as a result, density-dependent renormalization effects are, to a large extent, independent of the target nucleus. This fact is demonstrated empirically by the apparent constancy of the effective coupling $f_{\text{eff,NSM}}^{SI}$ derived from nuclear shell-model calculations (see Tables 8.2 and 9.1). Therefore, we can interpret the single-nucleon low-energy constants as already containing information about two-nucleon currents in the form of effective one-body operators.

In fact, the operator coefficients of the nuclear-scale effective theory should always be interpreted as effective couplings. In addition to the neglect of higher-body nuclear operators, the shell-model treatment itself, which typically relies on rather severe model-space truncations and phenomenological tuning of interactions, can introduce a significant shift in the effective coupling parameters when the single-nucleon operators are embedded in the target nuclear system. A famous example of this effect is the renormalization of the axial-vector coupling, which for a free nucleon has a measured value $g_A \approx 1.27$. In order for the nuclear shell model to accurately reproduce beta decay lifetimes of nuclei in the $2s1d$ valence, an effective coupling must be employed that reduces the strength of the Gamow-Teller operator by $\approx 20\%$ [128].

The truncation of the nuclear Hilbert space also induces the mixing of operators within the same symmetry class, permitting, for example, the axial-vector spin $\vec{\sigma}$ to mix with the orbital angular momentum $\vec{\ell}$ and the spin-tensor $[Y_2(\hat{r}) \otimes \vec{\sigma}]_1$. As the operator basis that we employ to describe $\mu \to e$ conversion is complete, the nuclear-scale effective theory should contain all candidate mixing partners, thereby faithfully encoding this effect into the renormalized coupling constants. Thus, it is natural to view the single-nucleon LECs as effective coupling parameters, capable of absorbing the effects of operator mixing and renormalization as well as contributions from two- and three-nucleon interactions (and momentum-dependent form factors, as discussed in Section 3.8).

Returning to the specific impact of higher-body operators, the general structure of the nuclear-scale effective theory—along with the conclusion that six response functions are probed in elastic $\mu \to e$ conversion—is unchanged, as long as the contributions from two-nucleon currents can be reliably captured by effective single-nucleon operators. At such time that $\mu \to e$ conversion is observed experimentally and detailed interpretation of the LECs is required, one may (in principle) disentangle the various one- and two-nucleon operators through detailed matching to ChPT, though one must simultaneously unwind the effects of operator mixing and renormalization induced by the nuclear embedding.

The aforementioned unraveling of the effective LECs is at present not explicitly realizable, primarily due to the fact that we are currently lacking a bona fide effective treatment of nuclear many-body systems rooted in the fundamental theory of QCD. (Work in this direction is ongoing; see Ref. [129] for a review of these efforts.) The first steps in a matching program capable of separating the various contributions to the effective couplings have only recently been undertaken in the related case of dark matter direction detection, and many significant challenges remain. Nonetheless, the fact that these complications—which should arise in any

general description of the $\mu \to e$ conversion process—are elegantly distilled into the effective single-nucleon LECs makes the nuclear-scale effective theory a useful phenomenology for understanding CLFV constraints obtained from experiments.

8.4 The Coherent Conversion Branching Ratio

We now proceed to the calculation of the branching ratio, having replaced the two-nucleon current $J_\alpha^{(2)}$ with an effective contribution to $J_\alpha^{(1)}$ via the substitution in Eq. (8.18). Writing the standard muon capture rate as $\Gamma_{\mathrm{capt}} = \kappa_{\mathrm{capt}} m_\mu^5 / v^4$, the branching ratio for scalar-mediated $\mu \to e$ conversion can be expressed simply as

$$B_{\mu \to e} = \left(\frac{v}{\Lambda}\right)^4 \frac{1}{\kappa_{\mathrm{capt}}} \left(\left|\tau^{(+1)}\right|^2 + \left|\tau^{(-1)}\right|^2\right), \tag{8.19}$$

where $\tau^{(\pm 1)}$ are the dimensionless overlap integrals

$$\begin{aligned}
\tau^{(-1)} &= (C_{DL} + C_{DR})\, \tau_D^{(-1)} + \tau_S^{(-1)}, \\
\tau^{(+1)} &= (C_{DL} - C_{DR})\, \tau_D^{(+1)} - \tau_D^{(+1)}.
\end{aligned} \tag{8.20}$$

The superscript (± 1) denotes the value of the Dirac eigenvalue κ of the electron solution. As we retain only the monopole nuclear operator, no angular momentum can be transferred between the leptons and the nucleus, and therefore the only allowed partial waves for the electron are those with total angular momentum $j = 1/2$. The overlap integrals for the dipole operator can be expressed in terms of the electric field produced by the nuclear charge

$$\begin{aligned}
\tau_D^{(-1)} &= -\frac{1}{m_\mu^{3/2}} \frac{1}{4\pi} \int_0^\infty dr\, \left(G_{-1}^{(e)} F_{-1}^{(\mu)} + F_{-1}^{(e)} G_{-1}^{(\mu)}\right) E(r), \\
\tau_D^{(+1)} &= -\frac{i}{m_\mu^{3/2}} \frac{1}{4\pi} \int_0^\infty dr\, \left(G_{+1}^{(e)} G_{-1}^{(\mu)} - F_{+1}^{(e)} F_{-1}^{(\mu)}\right) E(r).
\end{aligned} \tag{8.21}$$

Employing a two-parameter Fermi model of the nuclear charge density, the electric field can be expressed analytically as

$$\begin{aligned}
E(r) &= \frac{Ze}{r^2} \int_0^r dr'\, r'^2 \rho_p(r') \\
&= \frac{Ze}{r^2} + e\rho_0 r \left[\frac{\beta}{r} \mathrm{Li}_1\left(-e^{(c-r)/\beta}\right) + 2\frac{\beta^2}{r^2} \mathrm{Li}_2\left(-e^{(c-r)/\beta}\right) + 2\frac{\beta^3}{r^3} \mathrm{Li}_3\left(-e^{(c-r)/\beta}\right)\right],
\end{aligned} \tag{8.22}$$

where ρ_0 is the normalization constant defined in Eq. (2.12).

As we are striving to quantify all errors associated with the calculation of the coherent amplitude, in this chapter we adopt separate values of the nuclear density parameter c for the proton and neutron distributions, when available [61]. For ^{48}Ti, in the absence of an independent determination, we retain the assumption that the proton and neutron density profiles are identical, up to normalization. Table 8.2 summarizes that values that we adopt for the four nuclei considered in this chapter.

The scalar overlap integrals

$$
\begin{aligned}
\tau_S^{(-1)} &= \frac{1}{2} G_F m_\mu^2 \sum_{N=p,n} \left[\left(C_{NL}^\rho + C_{NR}^\rho \right) \tau_{\rho_N}^{(-1)} + \left(C_{NL}^f + C_{NR}^f \right) \tau_{f_N}^{(-1)} \right], \\
\tau_S^{(+1)} &= \frac{1}{2} G_F m_\mu^2 \sum_{N=p,n} \left[\left(C_{NL}^\rho - C_{NR}^\rho \right) \tau_{\rho_N}^{(+1)} + \left(C_{NL}^f - C_{NR}^f \right) \tau_{f_N}^{(+1)} \right],
\end{aligned}
\tag{8.23}
$$

have been decomposed into contributions that are momentum-*independent*

$$
\begin{aligned}
m_\mu C_{N\alpha}^\rho &= \left(\sigma_{\pi N} - \frac{3 g_A^2 m_\pi^2}{64 \pi f_\pi^2} k_F f_{\text{eff}}^{\text{SI}} \right) \left(C_{S\alpha}^{(0)} + \frac{8\pi}{9} C_{G\alpha} \right) \mp \frac{\delta m_N}{4} \left(C_{S\alpha}^{(1)} + \frac{16\pi}{9} C_{G\alpha} \right) \\
&\quad + \sigma_s \left(C_{S\alpha}^{(s)} + \frac{8\pi}{9} C_{G\alpha} \right) - \frac{8\pi}{9} C_{G\alpha} m_N,
\end{aligned}
\tag{8.24}
$$

and momentum-*dependent*

$$
m_\mu C_{N\alpha}^f = -\frac{3 g_A^2 m_\pi^3}{64 \pi f_\pi^2} \frac{5}{12} \left(C_{S\alpha}^{(0)} + \frac{8\pi}{9} C_{G\alpha} \right) - \dot{\sigma}_s m_\pi^2 \left(C_{S\alpha}^{(s)} + \frac{8\pi}{9} C_{G\alpha} \right).
\tag{8.25}
$$

In Eq. (8.24), the minus (plus) sign in the second term corresponds to the proton (neutron). The basic scalar overlap integrals are

$$
\begin{aligned}
\tau_{\rho_N}^{(-1)} &= \frac{1}{m_\mu^{5/2}} \frac{1}{4\pi} \int_0^\infty dr \, \left(G_{-1}^{(e)} G_{-1}^{(\mu)} - F_{-1}^{(e)} F_{-1}^{(\mu)} \right) \rho_N(r) \\
\tau_{f_N}^{(-1)} &= \frac{1}{m_\mu^{5/2}} \frac{1}{4\pi} \int_0^\infty dr \, \left(G_{-1}^{(e)} G_{-1}^{(\mu)} - F_{-1}^{(e)} F_{-1}^{(\mu)} \right) f_N(r) \\
\tau_{\rho_N}^{(+1)} &= \frac{i}{m_\mu^{5/2}} \frac{1}{4\pi} \int_0^\infty dr \, \left(F_{+1}^{(e)} G_{-1}^{(\mu)} + G_{+1}^{(e)} F_{-1}^{(\mu)} \right) \rho_N(r) \\
\tau_{f_N}^{(+1)} &= \frac{i}{m_\mu^{5/2}} \frac{1}{4\pi} \int_0^\infty dr \, \left(F_{+1}^{(e)} G_{-1}^{(\mu)} + G_{+1}^{(e)} F_{-1}^{(\mu)} \right) f_N(r),
\end{aligned}
\tag{8.26}
$$

where ρ_N is the usual scalar nucleon density and

$$
f_N(r) = -\frac{1}{m_\pi^2} \left(\frac{\partial^2}{\partial r^2} + \frac{2}{r} \frac{\partial}{\partial r} \right) \rho_N(r),
\tag{8.27}
$$

is the position-space representation of the linear term in the expansion of the single-nucleon scalar form factor $F(q^2/m_\pi^2)$.

The resulting values of the overlap integrals are shown in Table 8.3. In the limit that we neglect the electron mass, a symmetry emerges between the Dirac solutions: $F_{+1}^{(e)} = -G_{-1}^{(e)}$ and $G_{+1}^{(e)} = F_{-1}^{(e)}$. Consequently, the numerical difference between the $\kappa = \pm 1$ overlap integrals is almost negligible. Comparing the dipole, momentum-independent, and momentum-dependent overlap integrals directly is not particularly useful, as the scalar quantities $\tau_{\rho_N}^{(\pm 1)}$ and $\tau_{f_N}^{(\pm 1)}$ must be multiplied by various hadronic factors before being combined into the expression for the branching ratio. In order to assess the relative importance of the LO contact, NLO

Target	$\tau_D^{(-1)}$	$-i\tau_D^{(+1)}$	$\tau_{\rho_p}^{(-1)}$	$\tau_{\rho_n}^{(-1)}$	$\tau_{f_p}^{(-1)}$	$\tau_{f_n}^{(-1)}$	$-i\tau_{\rho_p}^{(+1)}$	$-i\tau_{\rho_n}^{(+1)}$	$-i\tau_{f_p}^{(+1)}$	$-i\tau_{f_n}^{(+1)}$
$^{27}_{13}$Al	0.013	0.013	0.043	0.045	0.029	0.030	-0.043	-0.045	-0.029	-0.030
$^{48}_{22}$Ti	0.029	0.029	0.099	0.117	0.067	0.079	-0.099	-0.116	-0.067	-0.079
$^{197}_{79}$Au	0.059	0.059	0.148	0.161	0.030	0.007	-0.147	-0.159	-0.029	-0.007
$^{208}_{82}$Pb	0.057	0.057	0.140	0.148	0.022	-0.006	-0.138	-0.147	-0.022	0.006

Table 8.3: Dimensionless overlap integrals computed for the target nuclei of interest.

Target	$I_p^{\text{LO}(-)}$	$I_{p,\text{loop}}^{\text{NLO}(-)}$	$I_{p,\text{2N}}^{\text{NLO}(-)}$	$I_n^{\text{LO}(-)}$	$I_{n,\text{loop}}^{\text{NLO}(-)}$	$I_{n,\text{2N}}^{\text{NLO}(-)}$
$^{27}_{13}$Al	268.49	-9.65	-25.2	280.16	-10.01	-26.30
$^{48}_{22}$Ti	618.10	-22.15	-70.84	730.48	-26.18	-83.72
$^{197}_{79}$Au	924.93	-9.79	-123.66	1003.3	-2.31	-134.13
$^{208}_{82}$Pb	871.15	-7.23	-116.47	923.59	2.00	-123.48

Table 8.4: Comparison of the LO and NLO contributions [defined in Eq. (8.28)] in units of MeV^2. Given the near degeneracy of the Dirac solutions, we report the results for $\kappa = -1$ only. In computing the two-nucleon contribution, we have adopted the value of the effective one-body coupling obtained from the Fermi gas average.

one-loop, and NLO two-nucleon contributions, we define

$$
\begin{aligned}
I_N^{\text{LO}(\pm)} &\equiv \sigma_{\pi N} m_\mu \tau_{\rho_N}^{(\pm 1)}, \\
I_{N,\text{loop}}^{\text{NLO}(\pm)} &\equiv -\frac{3 g_A^2 m_\pi^3 m_\mu}{64\pi f_\pi^2} \frac{5}{12} \tau_{f_N}^{(\pm 1)}, \\
I_{N,\text{2N}}^{\text{NLO}(\pm)} &\equiv -\frac{3 g_A^2 m_\pi^2 k_F m_\mu}{64\pi f_\pi^2} f_{\text{eff}}^{SI} \tau_{\rho_N}^{(\pm 1)}.
\end{aligned}
\tag{8.28}
$$

The corresponding values in the nuclei of interest are given in Table 8.4. The NLO contributions generically come with a minus sign relative to the LO result, thereby reducing the expected CLFV amplitude. In ^{27}Al, the one-loop correction amounts to $\approx 4\%$ of the LO result whereas the two-nucleon diagram contributes at the level of 10%. In very heavy nuclei, the momentum-dependent one-loop effect is suppressed while the two-nucleon operator still contributes a $\approx 10\%$ correction to the LO amplitude.

The above calculations were performed by adopting the central values of the relevant hadronic parameters (see Table 8.1). To assess the sensitivity of the overlap integrals to each input parameter, we vary one parameter at a time over its 1σ error range and compute the ratio of the resulting overlap integral $\tau_S^{(-1)}$ to the "central value" overlap integral $\tau_{S,c}^{(-1)}$. The outcome depends on the values of the quark Wilson coefficients, and so we consider two illustrative examples: (1) the case where only down-type right-handed quarks contribute, $C_{SR}^{(d,s,b)} \neq 0$, with all other couplings set to zero (2) the case where all right-handed quarks contribute, $C_{SR}^{q=\text{all}} \neq 0$. In both scenarios, all non-zero Wilson coefficients are assumed equal
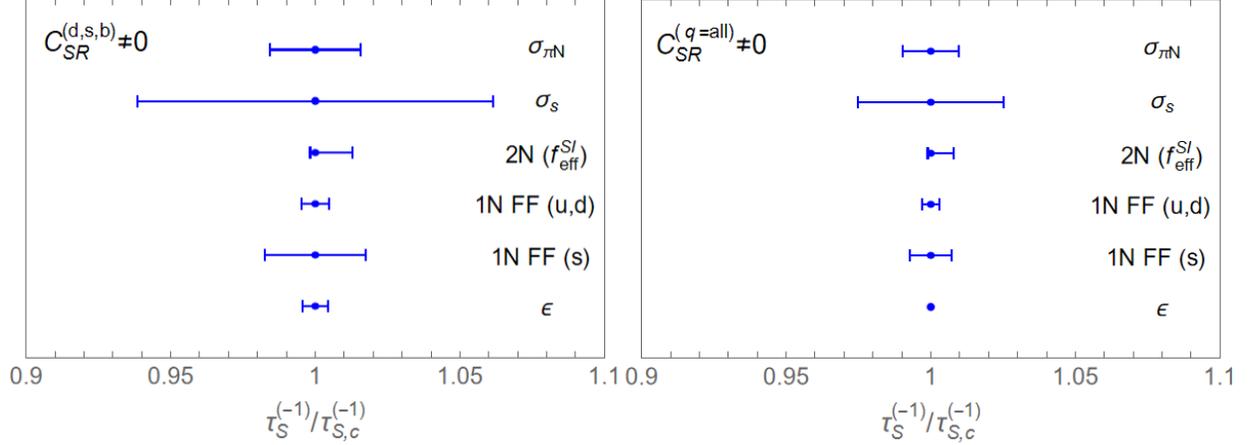
Figure 8.2: Dependence of the scalar overlap integrals $\tau_S^{(-1)}$ on the hadronic parameters $\sigma_{\pi N}$, σ_s, and ϵ, the two-nucleon contribution, represented by $2\mathrm{N}(f_{\mathrm{eff}}^{SI})$, and the NLO single-nucleon form factors, represented by 1N FF (u, d) and (s). In each case, the relevant parameter is varied over its 1σ range of uncertainty, and the resulting value of $\tau_S^{(-1)}$ is compared to that obtained when all parameters are set to their central values. In the left panel, only down-type right-handed quarks have non-zero Wilson coefficients. In the right panel, all right-handed quarks contribute.

(i.e., $C_{SR}^{(d)} = C_{SR}^{(s)} = C_{SR}^{(b)}$ in the former case).

Figure 8.2 shows the dependence of the scalar overlap integrals on the hadronic parameters $\sigma_{\pi N}$, σ_s, and ϵ, as well as the two-nucleon contribution, represented by the effective coupling f_{eff}^{SI}, and the single-nucleon form factors. The strange-quark form factor depends on the quantity $\dot{\sigma}_s$. We assign to the isoscalar form factor an uncertainty corresponding to $\pm 50\%$ of the central value. The parameters g_A, f_π, and δm_N are not included, as the impact of their uncertainty is too minor to be discerned on the scale of the figure. In both scenarios, the leading source of uncertainty is the strange quark sigma term. When only the down-type quarks are active, the uncertainty in σ_s translates to $\approx 10\%$ error on the scalar overlap integrals. This effect is somewhat diminished when the number of contributing quark flavors is increased from three to six. In fact, the inclusion of additional heavy quarks reduces the sensitivity of the overlap integrals to all of the input parameters, as the gluonic coupling $C_{G\alpha}$ contributes to τ_S primarily though the term proportional to m_N. The $\mu \to e$ conversion amplitude is fairly insensitive to the precise value of the two-nucleon effective coupling: reducing the value of f_{eff}^{SI} by a factor of 2 results in a ≈ 1–2% increase in the overlap integrals.

One important source of error that is not represented in Fig. 8.2 is the uncertainty in the determination of the neutron density profile. The error on the value of c_n determined from experiments on pionic atoms is $\approx 6\%$ in $^{27}\mathrm{Al}$, which propagates to $\approx 5\%$ error on the resulting neutron overlap integrals. In $^{48}\mathrm{Ti}$, we have assumed that the proton and neutron density profiles are equivalent, up to normalization. While these distributions are effectively the same in light systems with roughly equal numbers of protons and neutrons, in nuclei with an appreciable neutron excess the neutron density is peaked at a larger radius than the proton density, and one may incur significant error by assuming that $c_n = c_p$. For example, in

^{56}Fe—a nucleus close in mass to ^{48}Ti but for which a measurement of the neutron density is available—the difference between using a neutron density measured in pionic atoms compared to assuming that $c_n = c_p$ results in $\approx 7\%$ change in the neutron overlap integrals. Accounting for this discrepancy, as well as the underlying uncertainty in the neutron profile parameter, we assume an overall error of 8% on the Ti neutron overlap integrals. The proton density parameters, which are constrained by electron scattering experiments, are known to a much higher precision than their neutron analogues. Their error is neglected in this analysis.

The relative importance of the NLO contributions depends on the nature of the underlying CLFV physics. In scenarios where flavor-violation is driven primarily by the light quarks, the size of the NLO contribution can exceed the uncertainty on the LO result, implying that the NLO corrections are relevant to phenomenology. Consider the case in which only the two lightest quarks have non-zero couplings, $C_{S\alpha}^{(u)} \approx C_{S\alpha}^{(d)}$. Then the 1σ uncertainty on the LO result for $B_{\mu \to e}(\text{Al})$ is $\pm 13\%$, and the NLO contribution reduces the LO branching ratio by $\approx 25\%$. Including the strange quark, $C_{S\alpha}^{(u)} \approx C_{S\alpha}^{(d)} \approx C_{S\alpha}^{(s)}$, increases the LO uncertainty on the branching ratio to $\pm 19\%$ and decreases slightly the relative size of the NLO contribution to 23% of the LO rate. Still, the NLO correction exceeds the LO uncertainty. On the other hand, in scenarios with large contributions from either photon dipole operators or gluonic couplings (possibly induced by heavy quarks), the relative significance of the NLO contributions can be substantially diminished.

8.5   Dipole-Scalar Dominance Model

As an application of the top-down approach, we consider the dipole-scalar dominance model [130], where the only CLFV sources are the photon dipole and scalar quark operators. For simplicity, we limit to right-handed down-type quark operators and introduce a parameter r that describes the relative strength of the dipole and scalar operators

$$C_{DR} = \frac{r}{8e} C_{SR}, \tag{8.29}$$

with $C_{SR} = C_{SR}^{(d)} = C_{SR}^{(s)} = C_{SR}^{(b)}$. All other Wilson coefficients are set to zero. Although this setup may seem contrived, such a scenario may, in fact, be explicitly realized in some regions of the R-parity conserving SUSY seesaw parameter space [131] and within R-parity violating SUSY [132–134].

In addition to $\mu \to e$ conversion, the photon dipole operator mediates the on-shell $\mu \to e\gamma$ process. Applied to the dipole-scalar dominance model, the top-down formalism provides concrete predictions for the CLFV branching ratios $B_{\mu \to e\gamma}$ and $B_{\mu \to e}$ (in various target nuclei). By taking ratios of these quantities, we arrive at a result that depends only on the dipole-scalar ratio r. Figure 8.3 shows the behavior of the quotient $B_{\mu \to e}(\text{Al})/B_{\mu \to e\gamma}$, including the associated uncertainty, as r is varied. For $r \lesssim 10^{-5}$, the scalar quark operators dominate, the photon production rate becomes increasingly suppressed, and the result is sensitive to the uncertainty in the hadronic physics. For $r \gtrsim 10^{-5}$, the response is dictated by the dipole coupling, the relevant nuclear physics simplifies dramatically (depending only on the nuclear charge), and the overall error becomes negligible.

Figure 8.4 compares the ratio $B_{\mu \to e}(\text{Ti})/B_{\mu \to e}(\text{Al})$ as a function of r. As in the previous example, there is a clear transition (near $r = 10^{-5}$) between the scalar- and dipole-dominated regions. When the process is dipole-dominated, the uncertainty is, as before, negligibly small. In the scalar-dominated region, not only is the prediction sensitive to the uncertainty in the hadronic input parameters, but significant error—at the level of $\pm 10\%$—results from the uncertainty in the neutron density profile.

The width of the lines in Figs. 8.3 and 8.4 should only be used to compare the relative uncertainty (as r is varied) within each plot. It is misleading to compare the line width between the two figures, as the scale of the vertical axes is different. For example, at $r = 10^{-7}$, where the process is dominated by the scalar quark operators, the uncertainty stemming from hadronic parameters in $B_{\mu \to e}(\text{Al})/B_{\mu \to e\gamma}$ is $\pm 20\%$, whereas the corresponding uncertainty in $B_{\mu \to e}(\text{Ti})/B_{\mu \to e}(\text{Al})$ is $\pm 0.5\%$ ($\pm 15\%$ including the error in the neutron density parameter c_n). Variations in the hadronic input parameters have relatively little effect on the quantity $B_{\mu \to e}(\text{Ti})/B_{\mu \to e}(\text{Al})$, as any impact on the individual branching ratios largely cancels in their quotient. The opposite is true for $B_{\mu \to e}(\text{Al})/B_{\mu \to e\gamma}$, where the leading source of uncertainty is the hadronic parameters, especially σ_s, while the error in the neutron density has little effect on the overall result.

With these results, we have succeeded in our original ambition to produce testable predictions from a quark-level effective theory of CLFV. If experiments succeed in measuring the quantities $B_{\mu \to e}(\text{Ti})/B_{\mu \to e}(\text{Al})$ and $B_{\mu \to e}(\text{Al})/B_{\mu \to e\gamma}$, and the implied values of the dipole-scalar ratio r are not consistent with one another, then one can confidently exclude the dipole-scalar dominance model. Alternatively, if such measurements do yield a consistent value of r, then it would significantly restrict the parameter space of candidate UV theories. We now turn to the consideration of one such BSM model, in which flavor violation is mediated by the standard-model Higgs, generating both dipole and scalar operators.

8.6   Higgs-Mediated CLFV

As an explicit example of the top-down formalism that we have developed, let us consider the Higgs-mediated CLFV model with effective Lagrangian

$$\mathcal{L} = -Y_{e\mu}\bar{e}P_R\mu h - Y_{\mu e}\bar{\mu}P_R e h + \text{h.c.}, \tag{8.30}$$

specified by two Yukawa-like coupling parameters $Y_{e\mu}$, $Y_{\mu e}$. The tree-level Higgs exchange shown in Fig. 8.5 (a) induces the scalar quark couplings

$$
\begin{aligned}
\frac{1}{\Lambda^2}G_F m_\mu v C_{SR}^{(q)} &= -\frac{1}{m_h^2}Y_{e\mu}, \\
\frac{1}{\Lambda^2}G_F m_\mu v C_{SL}^{(q)} &= -\frac{1}{m_h^2}Y_{\mu e},
\end{aligned}
\tag{8.31}
$$

where $m_h = 125$ GeV is the Higgs boson mass. Thus, in the Higgs-mediated model, the scalar quark Wilson coefficients are independent of quark flavor.

The Yukawa-like CLFV interaction generates a coupling of the leptons to on-shell photons at one- and two-loop level. The one-loop diagrams are shown in Fig. 8.5 (b) and (c). Given
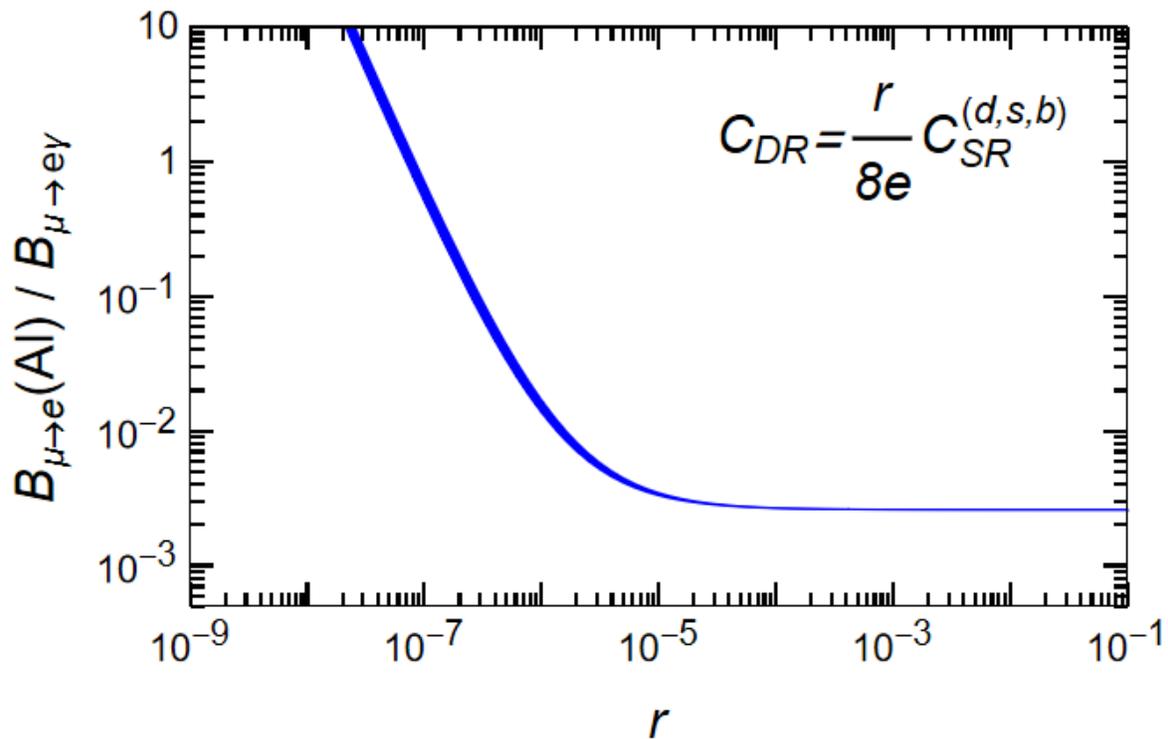
Figure 8.3: Comparison of the branching ratios for $\mu \to e$ conversion in ^{27}Al and $\mu \to e\gamma$ within the dipole-scalar dominance model, as the ratio of dipole and scalar Wilson coefficients r is varied. The width of the curve indicates the uncertainty obtained by varying each of the hadronic input parameters over its 1σ range.
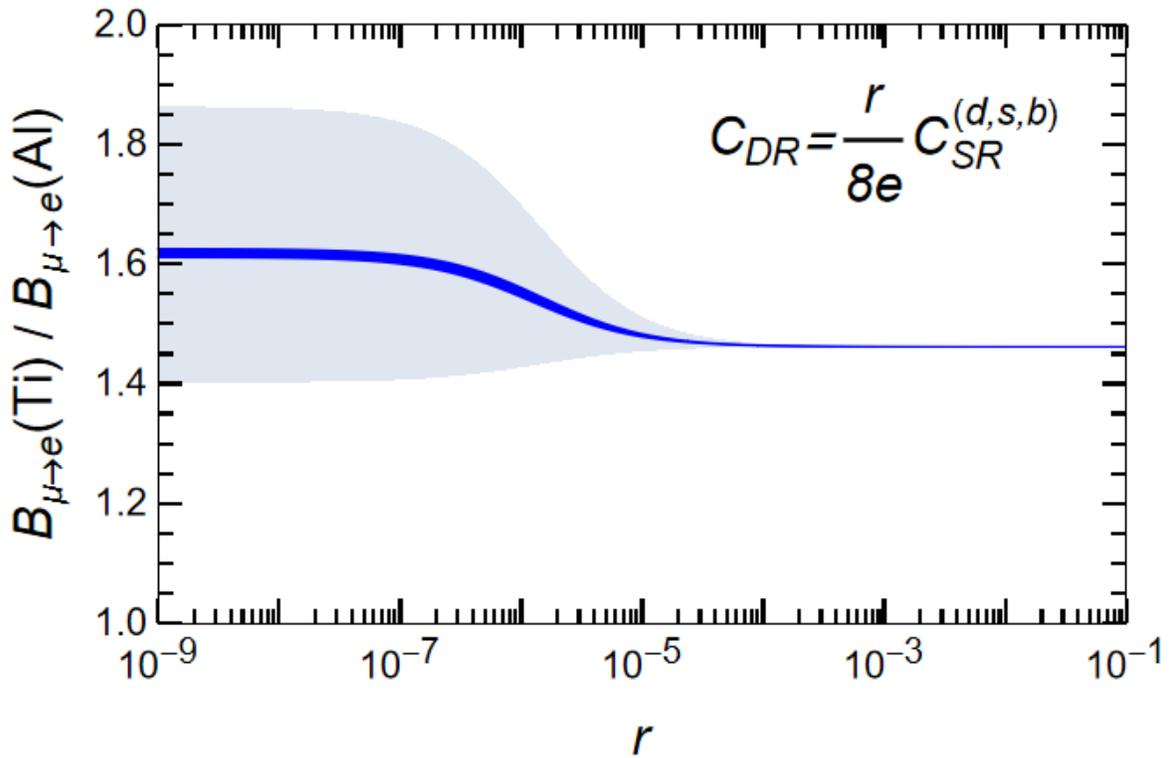
Figure 8.4: Comparison of the $\mu \to e$ conversion branching ratios in Ti and Al within the dipole-scalar dominance model, as the ratio of dipole and scalar Wilson coefficients r is varied. The width of the curve indicates the uncertainty obtained by varying each of the hadronic input parameters over their 1σ range. The light-blue shaded region shows the uncertainty when the error in the neutron density parameters is included in the analysis.
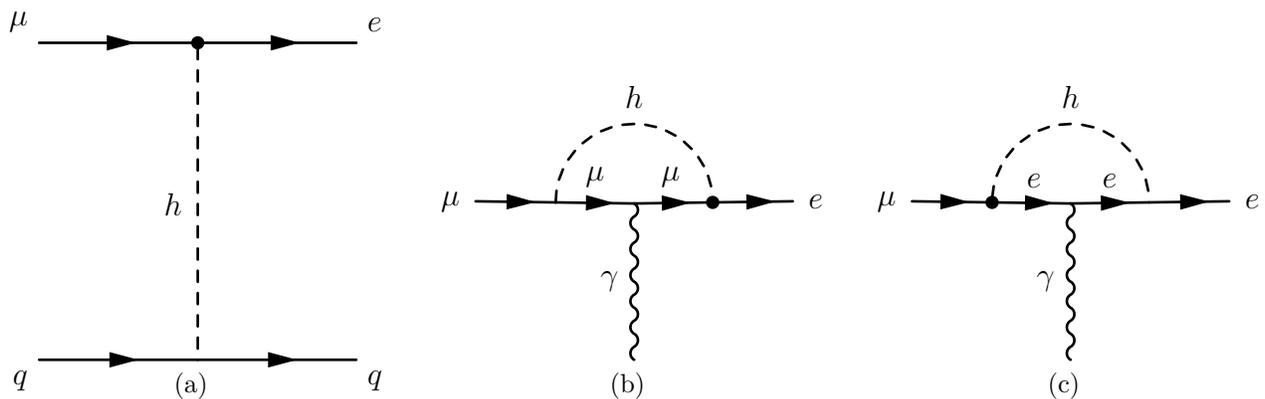
Figure 8.5: CLFV Higgs Diagrams. (a) Tree-level Higgs exchange that mediates $\mu \to e$ conversion (b) One-loop diagram that induces $\mu \to e\gamma$ with muon Yukawa coupling. (c) One-loop diagram that induces $\mu \to e\gamma$ with electron Yukawa coupling. The dotted vertex is the CLFV Higgs coupling.

the hierarchy of the lepton Yukawas, $Y_{\mu\mu} \gg Y_{ee}$, diagram (b) dominates, and the one-loop contributions to the CLFV dipole couplings are given approximately by [135]

$$\begin{aligned}
\frac{1}{\Lambda^2}C_{DR}^{\text{1loop}} &\approx -\frac{e}{32\pi^2}\frac{1}{m_h^2}Y_{\mu\mu}\left[\ln\frac{m_h^2}{m_\mu^2}-\frac{4}{3}\right]Y_{e\mu} \approx -5.27\times10^{-6}\frac{1}{m_h^2}Y_{e\mu}, \\
\frac{1}{\Lambda^2}C_{DL}^{\text{1loop}} &\approx -\frac{e}{32\pi^2}\frac{1}{m_h^2}Y_{\mu\mu}\left[\ln\frac{m_h^2}{m_\mu^2}-\frac{4}{3}\right]Y_{\mu e} \approx -5.27\times10^{-6}\frac{1}{m_h^2}Y_{\mu e}.
\end{aligned} \tag{8.32}$$

Thus, the leading one-loop diagram contributing to $\mu \to e\gamma$ is suppressed by the muon's standard-model Yukawa coupling to the Higgs, $Y_{\mu\mu}$. At two-loop order, this suppression can be avoided by the Bar-Zee type diagrams shown in Fig. 8.6, whose flavor-conserving analogues contribute to fermion electric dipole moments [136, 137]. We do not reproduce the full result for the two-loop amplitudes here—complete gauge-invariant expressions can be found in Ref. [33]. Numerically, the two-loop contributions to the dipole Wilson coefficients are roughly three orders of magnitude larger than the one-loop contributions

$$\begin{aligned}
\frac{1}{\Lambda^2}C_{DR}^{\text{2loop}} &\approx -4.67\times10^{-3}\frac{1}{m_h^2}Y_{e\mu}, \\
\frac{1}{\Lambda^2}C_{DL}^{\text{2loop}} &\approx -4.67\times10^{-3}\frac{1}{m_h^2}Y_{\mu e},
\end{aligned} \tag{8.33}$$

and therefore dominate the response. We now recognize that Higgs-mediated CLFV has the form of the dipole-scalar dominance model considered in the previous section with dipole-scalar ratio $r = 3.4 \times 10^{-6}$.

The $\mu \to e\gamma$ branching ratio can be expressed in terms of the unknown CLFV Yukawas as

$$B_{\mu\to e\gamma} \approx 0.312\left(|Y_{e\mu}|^2 + |Y_{\mu e}|^2\right), \tag{8.34}$$

from which one can immediately exclude regions of parameter space based on the existing limit from MEG, $B_{\mu\to e\gamma} < 4.2 \times 10^{-13}$, and the expected limit from MEG II, $B_{\mu\to e\gamma} < 6 \times 10^{-14}$. Using Eq. (8.19), the branching ratio for the coherent conversion process can also be used to restrict the values of $Y_{e\mu}$ and $Y_{\mu e}$. The resulting exclusion plot is shown in Fig. 8.7. The strongest limit on the CLFV Yukawas is currently provided by MEG. In the future, the conversion experiments, Mu2e and COMET, should provide a more sensitive probe of Higgs-mediated CLFV than MEG II. In addition to tree-level Higgs exchange, $\mu \to e$ is also induced by the dipole operator through exchange of a virtual photon with the nuclear charge. In fact, the contribution to the conversion rate in ^{27}Al from virtual photon exchange is roughly 4 times larger than the contribution from tree-level Higgs exchange—the quark Yukawa in the latter process introduces a suppression factor $m_N/v = o\left(10^{-3}\right)$, even for the heaviest quarks.

We now demonstrate the primary advantage of the top-down approach by computing the branching ratio for $\mu \to e$ conversion with a quantified uncertainty

$$\frac{B_{\mu\to e}(\text{Al})}{B_{\mu\to e\gamma}} = (8.7 \pm 0.3) \times 10^{-3}, \tag{8.35}$$

where we have divided by the branching ratio for the on-shell photon process to remove any dependence on the unknown CLFV parameters. Therefore, if these quantities were to be
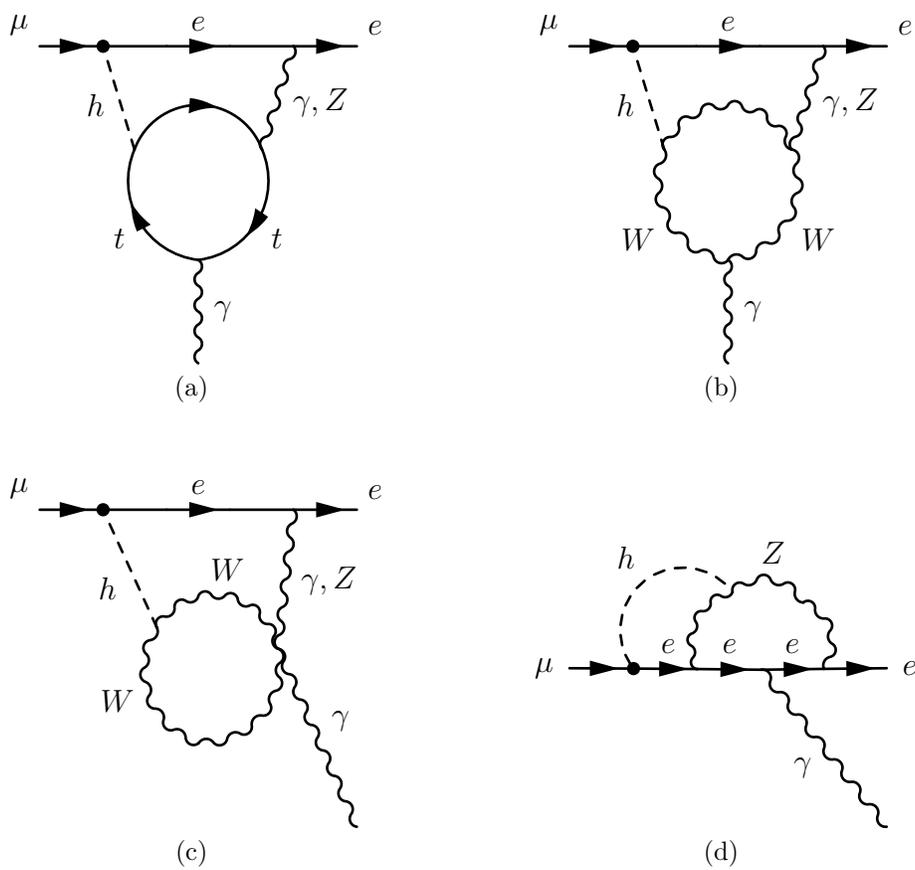
Figure 8.6: Two-loop diagrams that constitute the dominant contribution to $\mu \to e\gamma$ in Higgs-mediated CLFV. The dotted vertex is the CLFV Higgs coupling.

measured at Mu2e/COMET and MEG II, respectively, and their ratio fell significantly outside of the 1σ uncertainty window, then it would be good evidence to disfavor the Higgs-mediated CLFV model specified by Eq. (8.30). The same is true when comparing the conversion rate in different nuclei— the following ratio is predicted by the Higgs-mediated theory:

$$\frac{B_{\mu \to e}(\text{Ti})}{B_{\mu \to e}(\text{Al})} = 1.5 \pm 0.1. \tag{8.36}$$

The primary source of error in the ratio in Eq. (8.35) is the uncertainty in the hadronic input parameters, whereas the primary source of error in Eq. (8.36) is the uncertainty in the neutron overlap integrals. When computing the ratio of $\mu \to e$ conversion rates in two different targets, the hadronic uncertainties are common to both nuclei and therefore have a negligible impact on the overall error.

8.7 Matching to Nuclear Effective Theory

The top-down approach to $\mu \to e$ conversion that we have outlined in this chapter is a valuable tool for constraining certain classes of BSM models—particularly, as we have considered, theories in which flavor violation is mediated by a heavy scalar particle. Our grand objective, however, is to establish the complete chain of effective theories depicted in Fig. 1.2, spanning from the very high energies where the BSM physics originates, all the way down to the scale of $\mu \to e$ conversion experiments where the response is rooted in the simple, factorized form of the nuclear-scale effective theory developed in this work. The top-down treatment of scalar-mediated conversion represents the first steps in this program, connecting a limited set of UV operators to their nucleon-level counterparts. In particular, the isoscalar and isovector single-nucleon currents are related to the quark-level Wilson coefficients by

$$\begin{aligned}
J_\alpha^{(T=0)}(q^2) &= \left[\sigma_{\pi N} - \frac{3m_\pi^3 g_A^2}{64\pi f_\pi^2}\left(F\left(q^2/m_\pi^2\right) + \frac{k_F}{m_\pi}f_{\text{eff}}^{SI}\right)\right]\left(C_{S\alpha}^{(0)} + \frac{8\pi}{9}C_{G\alpha}\right) \\
&\quad + \left(\sigma_s - \dot{\sigma}_s q^2\right)\left(C_{S\alpha}^{(s)} + \frac{8\pi}{9}C_{G\alpha}\right) - \frac{8\pi}{9}C_{G\alpha}m_N \\
J_\alpha^{(T=1)}(q^2) &= -\frac{\delta m_N}{4}\left(C_{S\alpha}^{(1)} + \frac{16\pi}{9}C_{G\alpha}\right).
\end{aligned} \tag{8.37}$$

In the nuclear effective theory, the one-loop pion form factor $F(q^2/m_\pi^2)$ and the momentum-dependent correction to the strange quark sigma term $\dot{\sigma}_s q^2$ will be evaluated at the effective momentum transfer q_{eff}.

The low-energy coefficient c_1 corresponds to the scalar leptonic charge and therefore depends on the *sum* of right- and left-handed Wilson coefficients

$$\begin{aligned}
\tilde{c}_1^0 &= \frac{1}{2\sqrt{2}}\frac{m_\mu}{\Lambda^2}\Bigg\{\left[\sigma_{\pi N} - \frac{3g_A^2 m_\pi^3}{64\pi f_\pi^2}\left(F\left(q_{\text{eff}}^2/m_\pi^2\right) + \frac{k_F}{m_\pi}f_{\text{eff}}^{SI}\right)\right]\left[C_{SR}^{(0)} + C_{SL}^{(0)} + \frac{8\pi}{9}(C_{GR} + C_{GL})\right] \\
&\quad + \left(\sigma_s - \dot{\sigma}_s q_{\text{eff}}^2\right)\left[C_{SR}^{(s)} + C_{SL}^{(s)} + \frac{8\pi}{9}(C_{GR} + C_{GL})\right] - \frac{8\pi}{9}m_N(C_{GR} + C_{GL})\Bigg\} \\
&\quad + \sqrt{\alpha\pi}\frac{v^2}{\Lambda^2}(C_{DR} + C_{DL}),
\end{aligned}$$
$$\tag{8.38}$$
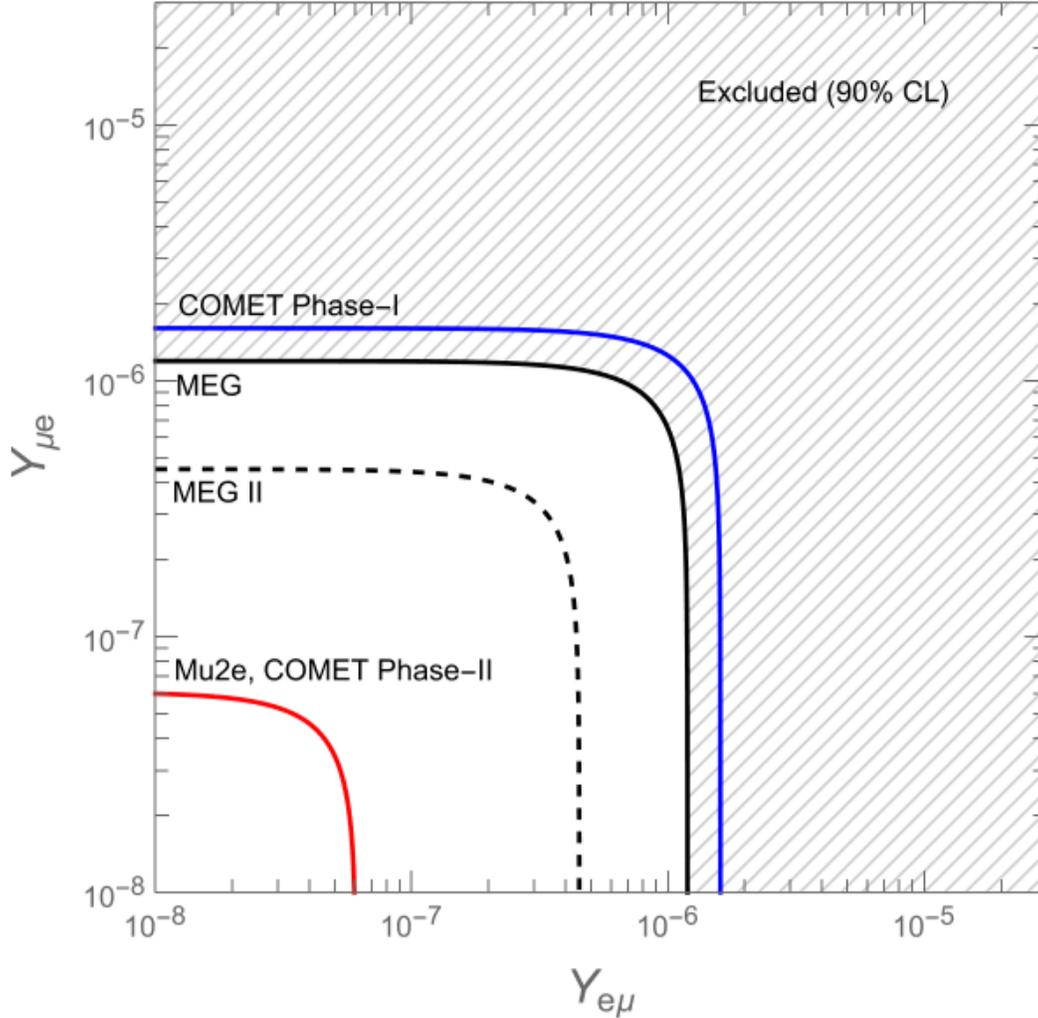
Figure 8.7: Exclusion curves for the Higgs-mediated CLFV model considered in Eq. (8.30). The dashed (solid) black curve shows the (expected) limit for on-shell $\mu \to e\gamma$ conversion obtained from MEG (MEG II). The branching ratio limits are $B_{\mu \to e\gamma} < 4.2 \times 10^{-13}$ for the MEG experiment and 6×10^{-14} for MEG II. The red (blue) curve corresponds to a $\mu \to e$ branching ratio limit $B_{\mu \to e}(\text{Al}) < 10^{-17}$ (7×10^{-15}).

whereas c_{11} corresponds to the lepton axial charge and depends on the *difference* of right- and left-handed Wilson coefficients

$$
\begin{aligned}
\tilde{c}_{11}^0 &= \frac{i}{2\sqrt{2}} \frac{m_\mu}{\Lambda^2} \Bigg\{ \left[\sigma_{\pi N} - \frac{3 g_A^2 m_\pi^3}{64\pi f_\pi^2} \left(F\left(q_{\text{eff}}^2 / m_\pi^2 \right) + \frac{k_F}{m_\pi} f_{\text{eff}}^{SI} \right) \right] \left[C_{SR}^{(0)} - C_{SL}^{(0)} + \frac{8\pi}{9} (C_{GR} - C_{GL}) \right] \\
&\quad + \left(\sigma_s - \dot{\sigma}_s q_{\text{eff}}^2 \right) \left[C_{SR}^{(s)} - C_{SL}^{(s)} + \frac{8\pi}{9} (C_{GR} - C_{GL}) \right] - \frac{8\pi}{9} m_N (C_{GR} - C_{GL}) \Bigg\} \\
&\quad + i\sqrt{\alpha\pi} \frac{v^2}{\Lambda^2} (C_{DR} - C_{DL}) \,.
\end{aligned}
\tag{8.39}
$$

Similarly, for the isovector operators

$$
\begin{aligned}
\tilde{c}_1^1 &= -\frac{1}{2\sqrt{2}} \frac{m_\mu}{\Lambda^2} \frac{\delta m_N}{4} \left[C_{SR}^{(1)} + C_{SL}^{(1)} + \frac{16\pi}{9} (C_{GR} + C_{GL}) \right] + \sqrt{\alpha\pi} \frac{v^2}{\Lambda^2} (C_{DR} + C_{DL}) \\
\tilde{c}_{11}^1 &= -\frac{i}{2\sqrt{2}} \frac{m_\mu}{\Lambda^2} \frac{\delta m_N}{4} \left[C_{SR}^{(1)} - C_{SL}^{(1)} + \frac{16\pi}{9} (C_{GR} - C_{GL}) \right] + i\sqrt{\alpha\pi} \frac{v^2}{\Lambda^2} (C_{DR} - C_{DL}) \,.
\end{aligned}
\tag{8.40}
$$

Chapter 9

Two-Nucleon Contribution to $\mu \to e$ Conversion

In the previous chapter, we identified a two-nucleon diagram [shown in Fig. 8.1 (c)] that contributes to scalar-mediated $\mu \to e$ conversion at next-to-leading order in the chiral power counting. Such operators have important consequences for the interpretation of experimental outcomes—in coherent conversion, the two-nucleon contribution can reduce the expected CLFV rate by $\approx 20\%$. Furthermore, the ability to fully utilize the single-nucleon effective theory that we have developed in this work depends on understanding the impact of higher-body operators and the degree to which they can be approximated by effective one-body operators.

Here, we demonstrate how the coherent two-nucleon operator is evaluated in the nuclear shell model, comparing the result to that obtained from the Fermi gas effective one-body operator. We discuss the limitations of the shell-model calculation. In particular, we identify a strong dependence on the two-nucleon correlation function, which has known deficiencies when obtained from the nuclear shell model. Despite these obstacles, the shell-model calculation provides decent evidence that the essential two-body physics can be well-described by an effective single-nucleon operator.

9.1   The Two-Nucleon Operator in Position Space

In Appendix F, we demonstrate that the total two-nucleon operator contributing to scalar-mediated $\mu \to e$ conversion can be expressed as

$$\mathcal{O}^{(2)}(q) = -\frac{g_A^2 m_\pi^2}{4 f_\pi^2} \frac{1}{2} \sum_{i \neq j} \sum_{k=1}^{7} \mathcal{O}_k(\vec{r}_{ij}, \vec{R}_{ij}, q) \; \vec{\tau}(i) \cdot \vec{\tau}(j), \tag{9.1}$$

where $\vec{r}_{ij} = \vec{r}_i - \vec{r}_j$, $\vec{R}_{ij} = (\vec{r}_i + \vec{r}_j)/2$, and the summation over i, j extends over all nucleons in the target nucleus. The seven independent operators are

$$\begin{aligned}
\mathcal{O}_1(\vec{r}, \vec{R}, q) = &-\frac{1}{12\sqrt{\pi}} \vec{\sigma}(1) \cdot \vec{\sigma}(2) \sum_{L=0,2,\ldots}^{\infty} Y_L(\hat{r}) \odot Y_L(\hat{R}) \, j_L(qR) \\
&\times \int_0^1 d\alpha \; e^{-r\Pi(q,\alpha)} j_L\left(qr(\alpha - 1/2)\right) \frac{2 - r\Pi(q,\alpha)}{r},
\end{aligned} \tag{9.2}$$

$$\mathcal{O}_2(\vec{r}, \vec{R}, q) = \frac{1}{12\sqrt{\pi}} \vec{\sigma}(1) \cdot \vec{\sigma}(2) \sum_{L=0,2,\ldots}^{\infty} Y_L(\hat{r}) \odot Y_L(\hat{R}) \, j_L(qR)$$
$$\times \int_0^1 d\alpha \, e^{-r\Pi(q,\alpha)} j_L(qr\,(\alpha - 1/2)) \frac{q^2\alpha(1-\alpha)}{\Pi(q,\alpha)}, \tag{9.3}$$

$$\mathcal{O}_3(\vec{r}, \vec{R}, q) = \frac{1}{5\sqrt{24\pi}} \sum_{L_1=0,2,\ldots}^{\infty} \sum_{L_2=0,2,\ldots}^{\infty} (-1)^{(L_1-L_2)/2} C_{L_10L_20}^{20} \sqrt{(2L_1+1)(2L_2+1)} j_{L_2}(qR)$$
$$\times \left[Y_{L_1}(\hat{r}) \otimes Y_{L_2}(\hat{R})\right]_2 \odot [\vec{\sigma}(1) \otimes \vec{\sigma}(2)]_2 \int_0^1 d\alpha \, e^{-r\Pi(q,\alpha)} j_{L_1}(qr(\alpha-1/2)) \frac{q^2\alpha(1-\alpha)}{\Pi(q,\alpha)}, \tag{9.4}$$

$$\mathcal{O}_4(\vec{r}, \vec{R}, q) = \frac{1}{5\sqrt{24\pi}} \sum_{L_1=0,2,\ldots}^{\infty} \sum_{L_2=0,2,\ldots}^{\infty} C_{L_10L_20}^{20} \sqrt{(2L_1+1)(2L_2+1)} j_{L_2}(qR)$$
$$\times \left[Y_{L_1}(\hat{r}) \otimes Y_{L_2}(\hat{R})\right]_2 \odot [\vec{\sigma}(1) \otimes \vec{\sigma}(2)]_2 \int_0^1 d\alpha \, e^{-r\Pi(q,\alpha)} j_{L_2}(qr(\alpha-1/2)) \frac{1}{r} [1 + r\Pi(q,\alpha)], \tag{9.5}$$

$$\mathcal{O}_5(\vec{r}, \vec{R}, q) = \frac{1}{12\sqrt{\pi}} \sum_{L_1=1,3,\ldots}^{\infty} \sum_{L_2=0,2,\ldots}^{\infty} (-1)^{(1+L_1-L_2)/2} \left(\frac{2L_1+1}{2L_2+1}\right) \left(C_{L_1010}^{L_20}\right)^2$$
$$\times j_{L_2}(qR) \, Y_{L_2}(\hat{r}) \odot Y_{L_2}(\hat{R}) \, \vec{\sigma}(1) \cdot \vec{\sigma}(2) \, q \int_0^1 d\alpha \, e^{-r\Pi(q,\alpha)}(1-2\alpha) j_{L_1}(qr(\alpha-1/2)), \tag{9.6}$$

$$\mathcal{O}_6(\vec{r}, \vec{R}, q) = -\frac{1}{4\sqrt{\pi}} \sum_{L_1=0,2,\ldots}^{\infty} \sum_{L_2=1,3,\ldots}^{\infty} \sum_{J=1,3,\ldots}^{\infty} (-1)^{(1+L_1-L_2)/2} C_{L_1010}^{L_20} C_{L_1010}^{J0} \left\{ \begin{matrix} L_1 & 1 & L_2 \\ 1 & J & 1 \end{matrix} \right\}$$
$$\times (2L_1+1) \left[Y_J(\hat{r}) \otimes Y_{L_2}(\hat{R})\right]_1 \odot [\vec{\sigma}(1) \otimes \vec{\sigma}(2)]_1 \, j_{L_2}(qR) \, q \int_0^1 d\alpha \, e^{-r\Pi(q,\alpha)} j_{L_1}(qr(\alpha-1/2)), \tag{9.7}$$

and

$$\mathcal{O}_7(\vec{r}, \vec{R}, q) = -\frac{1}{4\sqrt{\pi}} \sum_{L_1=1,3,\ldots}^{\infty} \sum_{L_2=0,2,\ldots}^{\infty} \sum_{J=0,2,\ldots}^{\infty} (-1)^{(1+L_1-L_2)/2} C_{L_1020}^{L_20} C_{L_1020}^{J0} \left\{ \begin{matrix} L_1 & 1 & L_2 \\ 2 & J & 1 \end{matrix} \right\}$$
$$\times (2L_1+1) \left[Y_J(\hat{r}) \otimes Y_{L_2}(\hat{R})\right]_2 \odot [\vec{\sigma}(1) \otimes \vec{\sigma}(2)]_2$$
$$\times j_{L_2}(qR) \, q \int_0^1 d\alpha \, e^{-r\Pi(q,\alpha)}(1-2\alpha) j_{L_1}(qr(\alpha-1/2)). \tag{9.8}$$

In the above operators, α is a Feynman parameter and

$$\Pi^2(q,\alpha) \equiv \alpha(1-\alpha)q^2 + m_\pi^2. \tag{9.9}$$

Total nuclear matrix elements of the two-nucleon operator can be computed in terms of the reduced two-body density matrix, as discussed in Appendix C.2. Each of the seven operator structures $\mathcal{O}_k(\vec{r}, \vec{R}, q)$ contains an infinite sum of tensor operators indexed by angular momenta L, (L_1, L_2), or (L_1, L_2, J). It is worth exploring whether these series can be truncated in practical calculations. Figure 9.1 shows the relative strength of various operator components in ^{27}Al, normalized by the strength of the leading contribution, the $L = 0$ component of
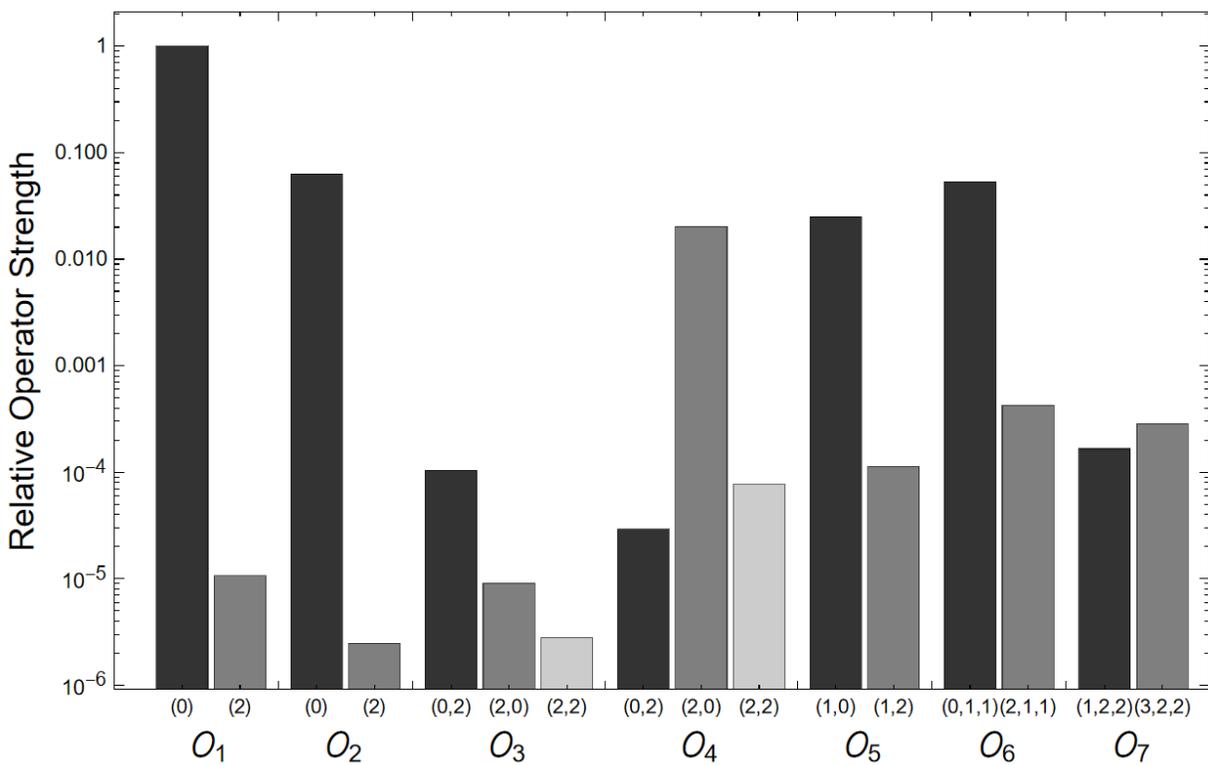
Figure 9.1: The relative strength of various tensor components of the two-nucleon operators evaluated in ^{27}Al with $q = 104.976$ MeV. Labels in parentheses indicate the angular momenta (L), (L_1, L_2), or (L_1, L_2, J) of the tensor operator. For this chart, we ignore the sign of the resulting matrix element and normalize by the leading operator, the $L = 0$ component of $\mathcal{O}_1$.
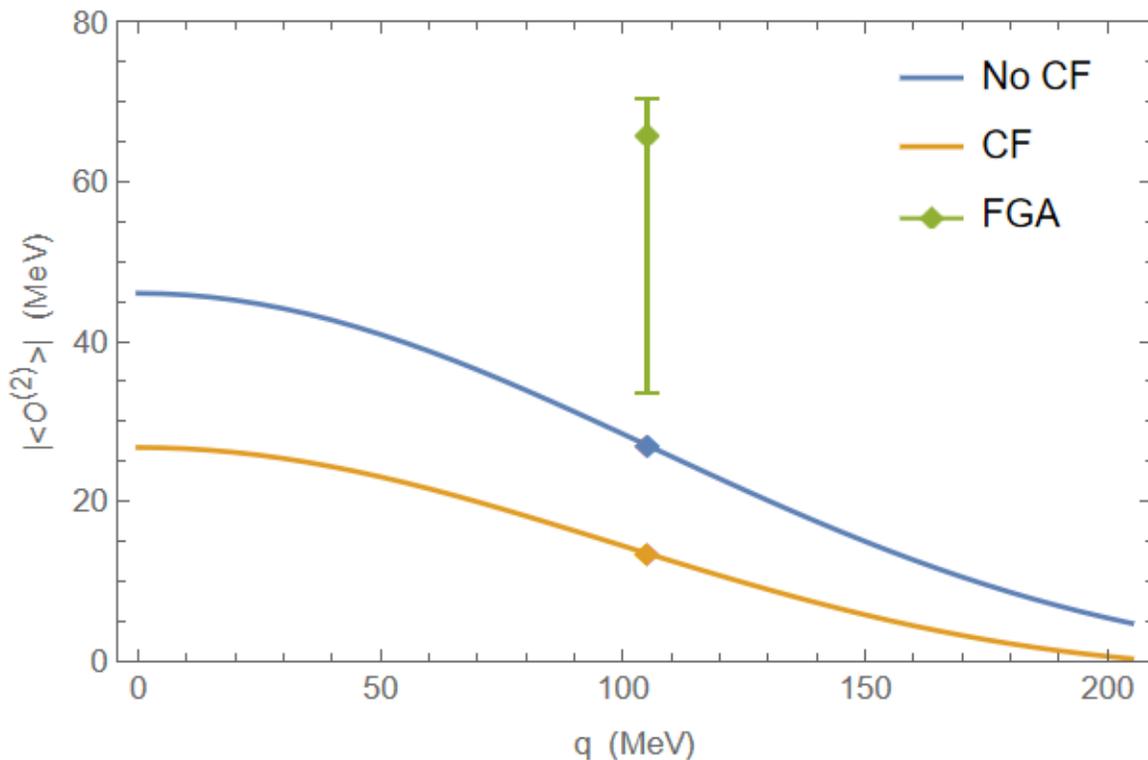
Figure 9.2: Total nuclear matrix element of the NLO coherent two-body operator contributing to $\mu \to e$ conversion as a function of three-momentum transfer q for the case of ^{27}Al. The orange and blue curves, respectively, show the matrix element computed from a nuclear shell-model wave function with and without the additional two-body correlation function of Eq. (9.17). The marked points denote the physically relevant value of the three-momentum transfer $q \approx m_\mu$. The green point and error bars indicate the value of the 1-body effective operator obtained via the Fermi gas average calculation.

$\mathcal{O}_1(\vec{r}, \vec{R}, q)$. We see that there are only five components that contribute above the level of 1%. Two of these operators, the dominant $L = 0$ mode of $\mathcal{O}_1$ and the $(L_1 = 2, L_2 = 0)$ mode of $\mathcal{O}_4$, correspond to the two distinct operator structures that survive in the $q \to 0$ limit [see Eq. (F.19)]. The three remaining operators that contribute significantly to the total two-body operator are the $L = 0$ mode of $\mathcal{O}_2$, the $(L_1 = 1, L_2 = 0)$ mode of $\mathcal{O}_5$, and the $(L_1 = 0, L_2 = 1, J = 1)$ mode of $\mathcal{O}_6$. These operators represent intrinsically finite-q corrections to the two-nucleon response.

We have retained the full q dependence of the two-nucleon operator based on the fact that the magnitude of the three-momentum transfer in $\mu \to e$ conversion is comparable to the pion mass, $q \approx m_\pi$. Figure 9.2 shows the value of the total two-body nuclear matrix element in ^{27}Al as a function of three-momentum transfer q. The strength of the operator at $q = m_\mu$ is reduced by roughly 40% from the value at $q = 0$. The finite-q corrections are significant and should not be neglected.

Figure 9.2 also compares the nuclear shell-model result to the Fermi gas average result at the physically relevant value of the momentum-transfer $q \approx m_\mu$. As discussed in Section 8.2,

the Fermi gas result is roughly a factor of two larger than the shell-model result. We can compute the value of the effective 1-body coupling implied by the shell-model calculation, $f^{SI}_{\text{eff,NSM}}$, by equating the matrix elements

$$\langle J_i||\mathcal{O}^{(2)}(q)||J_i\rangle = -\frac{3g_A^2 m_\pi^2 k_F}{64\pi f_\pi^2} f^{SI}_{\text{eff,NSM}} \langle J_i||M_0(q)||J_i\rangle, \tag{9.10}$$

where $M_{00}(q) = \sum_{i=1}^{A} j_0(qr_i)Y_{00}(\hat{r}_i)$ is the one-body isoscalar monopole charge operator. The resulting values of $f^{SI}_{\text{eff,NSM}}$ for the nuclear targets of interest are shown in Table 9.1. The effective coupling implied by the shell model is essentially constant across the range of nuclei from ^{12}C to ^{63}Cu, and the value is insensitive to the interaction employed to obtain the nuclear wave function.

The FGA result is consistently larger than the NSM result, by a factor that ranges from 2.0 for ^{12}C to 2.83 for ^{63}Cu. The effective one-body coupling implied by the NSM calculation $f^{SI}_{\text{eff,NSM}}$ is nearly constant across the range of nuclei considered in Table 9.1. The fact that the shell-model result does not depend strongly on the target isotope or the shell-model interaction is evidence that the two-nucleon physics can be well-described by an effective one-body operator. Unlike the shell-model calculations, the Fermi gas average does not include any correlations between nucleons. In principle, the two-nucleon operator can depend strongly on these correlations, in which case we would expect to observe significant variation in the value of $f^{SI}_{\text{eff,NSM}}$ as the target is varied. Fortunately, it appears that the two-nucleon operator depends primarily on the single-nucleon density, and therefore can be captured by a single-nucleon effective operator.

The one-body monopole operator can be evaluated using either measured proton and neutron densities or the same many-body wave function that is used to evaluate the two-body operator. Using the measured densities we find

$$\langle J_i||M_0(q)||J_i\rangle_\rho = 11.69 \pm 0.23, \tag{9.11}$$

whereas the NSM wave function yields

$$\langle J_i||M_0(q)||J_i\rangle_{\text{NSM}} = 11.81. \tag{9.12}$$

Thus the NSM value is consistent with the measured nuclear density result. The uncertainty in the value computed from proton and neutron densities is due entirely to the error in the determination of the neutron density.

Having identified the most important components of the two-nucleon operator, we may obtain a simplified form by expanding to first order in q/m_π. To this order, $\Pi(q,\alpha) \approx m_\pi$, and consequently the Feynman parameter integrals can be performed analytically. Combining the leading multipoles of $\mathcal{O}_1$, $\mathcal{O}_2$, $\mathcal{O}_4$, $\mathcal{O}_5$, and $\mathcal{O}_6$, we may express the total two-nucleon operator in terms of three unique tensor structures

$$\begin{aligned}
\mathcal{O}^{(2)}(q) = -\frac{g_A^2 m_\pi^2}{64\pi^{3/2} f_\pi^2}\frac{1}{2}\sum_{i\neq j}\frac{e^{-r_{ij}m_\pi}}{r_{ij}}&\left\{\frac{1}{3}\vec{\sigma}(i)\cdot\vec{\sigma}(j)\, j_0(qR_{ij})\left[F^{(0)}(qr_{ij}/2) + \frac{q}{m_\pi}F'^{(0)}(qr_{ij}/2)\right]\right.\\
&+ \hat{r}\cdot\vec{\sigma}(i)\,\hat{r}\cdot\vec{\sigma}(j)\, j_0(qR_{ij})F^{(1)}(qr_{ij}/2)\\
&\left.- \left[\hat{r}_{ij}\times\hat{R}_{ij}\right]\cdot\left[\vec{\sigma}(i)\times\vec{\sigma}(j)\right] j_1(qR_{ij})F^{(2)}(qr_{ij}/2)\right\}\vec{\tau}(i)\cdot\vec{\tau}(j).
\end{aligned} \tag{9.13}$$

Isotope	k_F (MeV)	q (MeV)	$f^{SI}_{\text{eff,FGA}}$	$f^{SI}_{\text{eff,NSM}}$	$f^{SD}_{\text{eff,FGA}}$
$^{12}_{6}$C	**221.0**	105.07	$0.36^{+0.03}_{-0.18}$	0.18	$0.38^{+0.04}_{-0.19}$
$^{16}_{8}$O	225.7	105.11	$0.38^{+0.03}_{-0.19}$	0.18	$0.40^{+0.04}_{-0.20}$
$^{19}_{9}$F	229.2	105.12	$0.40^{+0.03}_{-0.20}$	0.18, 0.18, 0.18	$0.41^{+0.04}_{-0.21}$
$^{23}_{11}$Na	233.8	105.07	$0.41^{+0.03}_{-0.21}$	0.18, 0.18, 0.18	$0.42^{+0.04}_{0.21}$
$^{27}_{13}$Al	238.0	104.98	$0.43^{+0.03}_{-0.22}$	0.18, 0.18, 0.18	$0.43^{+0.03}_{-0.22}$
$^{28}_{14}$Si	239.0	104.91	$0.43^{+0.03}_{-0.22}$	0.18, 0.18, 0.18	$0.44^{+0.03}_{-0.22}$
$^{32}_{16}$S	243.0	104.78	$0.45^{+0.03}_{-0.23}$	0.18, 0.18, 0.18	$0.45^{+0.03}_{-0.23}$
$^{40}_{20}$Ca	**251.0**	104.45	$0.48^{+0.03}_{-0.24}$	0.19	$0.47^{+0.03}_{-0.24}$
$^{48}_{22}$Ti	255.0	104.28	$0.49^{+0.03}_{-0.25}$	0.18, 0.18, 0.18	$0.48^{+0.03}_{-0.24}$
$^{56}_{26}$Fe	259.0	103.84	$0.51^{+0.03}_{-0.26}$	0.18, 0.18, 0.18	$0.48^{+0.03}_{-0.24}$
$^{63}_{29}$Cu	259.0	103.48	$0.51^{+0.03}_{-0.26}$	0.18, 0.18, 0.18	$0.48^{+0.03}_{-0.24}$

Table 9.1: Input parameters and outputs for the one-body averaging of the two-nucleon coherent operator: k_F is the nuclear Fermi momentum, obtained by linear interpolation between the values measured in Ref. [138], q is the value of the three-momentum transferred to the nucleus, $f^{SI}_{\text{eff,FGA}}$ is the value of the effective spin-independent coupling obtained from the Fermi gas average, $f^{SI}_{\text{eff,NSM}}$ is the value implied by the nuclear shell-model evaluation of the two-nucleon operator, $f^{SD}_{\text{eff,FGA}}$ is the value of the effective spin-dependent coupling obtained from the Fermi gas average (see Appendix E). Shell-model wave functions for ^{12}C, ^{16}O, and ^{40}Ca are taken to be an inert core. The nuclei ^{19}F, ^{23}Na, ^{27}Al, and ^{28}Si are modeled in the $2s$-$1d$ valence space above an inert ^{16}O core. The nuclei ^{48}Ti and ^{56}Fe are modeled in the $2p$-$1f$ valence space above an inert ^{40}Ca core. ^{63}Cu is modeled in the $1f_{5/2}$-$2p$-$1g_{9/2}$ valence space above an inert ^{56}Ni core. The interactions employed in the sd valence space are BW [93], USDA [92], USDB [92], in the fp valence space GXPF1 [96], KB3G [95], KB$'$ [97], and in the pfg valence space JUN45 [98], GCN2850 [100], jj44b [99]. Multiple entries of $f^{SI}_{\text{eff,NSM}}$ for a single target correspond to calculations performed with different shell-model interactions (ordered as they appear in this caption).

The form factors are given by

$$F^{(0)}(z) \equiv -\frac{1}{z}\mathrm{Si}(z) - 2j_0(z)$$
$$F'^{(0)}(z) \equiv \frac{1}{2}\mathrm{Si}(z) - 2j_1(z)$$
$$F^{(1)}(z) \equiv j_0(z)$$
$$F^{(2)}(z) \equiv \sin(z),$$

(9.14)

where

$$\mathrm{Si}(x) \equiv \int_0^x dt\,\frac{\sin t}{t}.$$

(9.15)

9.2   Correlation Function

The shell-model calculations that we have performed may still overestimate the strength of the two-nucleon contribution. The nuclear shell-model wave functions are obtained by diagonalizing a phenomenological interaction that has been tuned to reproduce low-energy nuclear observables, such as charge radii and low-lying spectra. The model spaces employed in these calculations are severely truncated. In ^{27}Al, the valence nucleons are restricted to the $2s$-$1d$ harmonic oscillator shells. Although this treatment is capable of accurately reproducing a range of nuclear observables, it is known to fail at capturing the following behavior: at short range, the two-nucleon potential is strongly repulsive, causing a hole to develop in the two-nucleon correlation function at very small separations.

Resolving this fine structure, however, requires high-momentum modes that are not included in the typically very soft Hilbert spaces of nuclear shell-model calculations. To demonstrate this concretely, we take the exact S-channel deuteron wave function obtained by solving the Schrödinger equation with potential given by the Argonne v_{18} (Av_{18}) potential [139] and project this solution into harmonic oscillator spaces of varying dimension, specified by a cutoff in harmonic oscillator quanta of $N = 100$ (101 states), $N = 50$ (51 states), $N = 10$ (6 states) and finally $N = 0$ (1 state). In Fig. 9.3, these model-space projections are compared to the exact wave function. Although the long-range behavior is faithfully reproduced by the projected wave functions, the "hole" in the exact wave function at small separations is removed when the higher momentum modes are integrated out. The closest analogue to the nuclear shell-model calculations that we employ in our $\mu \to e$ studies is the $N = 1$ curve. Thus, the two-nucleon correlation function obtained in our shell-model calculations is erroneously enhanced at short range.

In the present case, the induced error is of particular consequence because matrix elements of the two-nucleon $\mu \to e$ conversion operator strongly depend on the short-range behavior of the two-nucleon correlation function. As illustrated in Fig. 9.1, the leading contribution to the two-nucleon amplitude in ^{27}Al is the $L = 0$ multipole of the $\mathcal{O}_1$ operator, which has the following dependence on the relative radial coordinate:

$$V_1(r, q) \equiv \int_0^1 d\alpha\, e^{-r\Pi(q,\alpha)} j_0(qr(\alpha - 1/2))\frac{2 - r\Pi(q,\alpha)}{r}$$

(9.16)
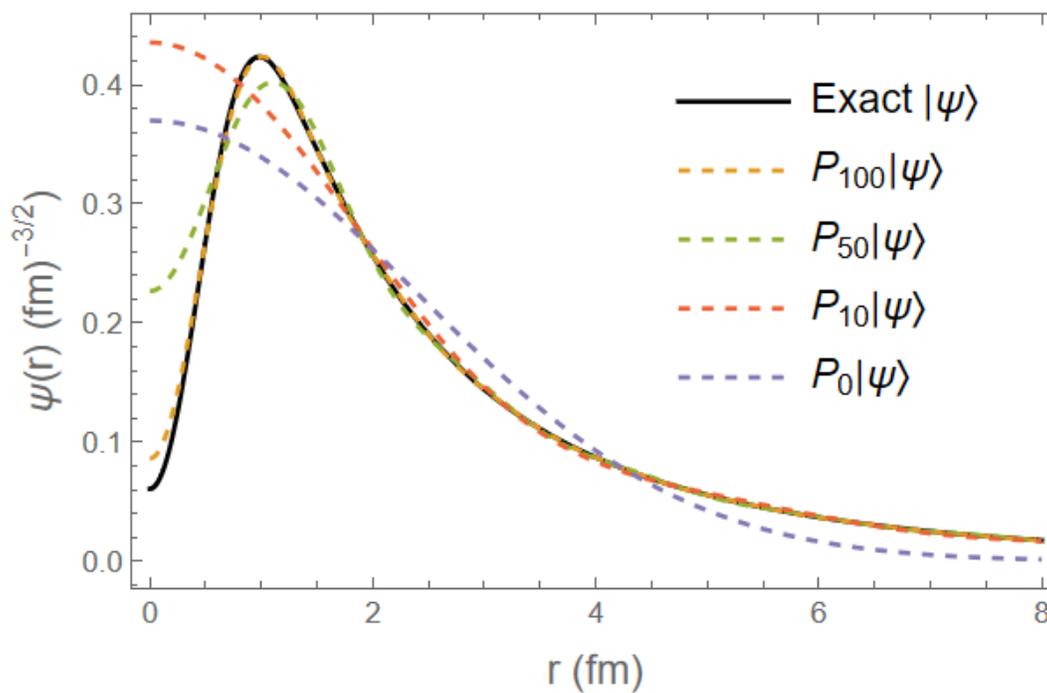
Figure 9.3: The $^3S_1$ component of the deuteron wave function projected into various harmonic oscillator spaces indexed by cutoff in oscillator quanta N. The coordinate r is the separation between the two nucleons. The exact solution is obtained from the potential Av_{18}. A value for the harmonic oscillator parameter $b = 1.7$ fm was employed in these calculations.
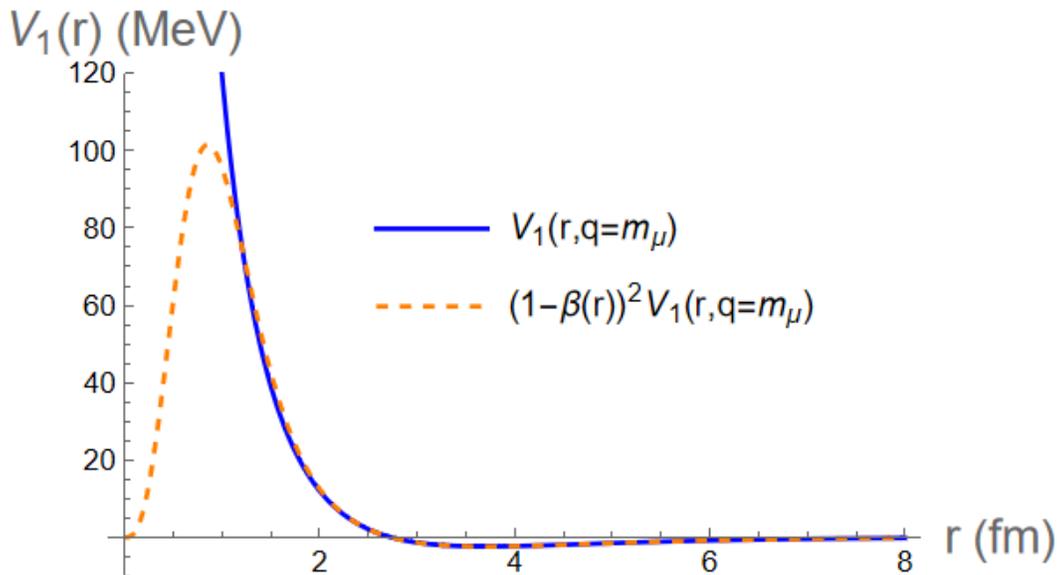
Figure 9.4: Dependence of the leading 2-body multipole on the relative radial coordinate r. The solid blue curve show the bare radial potential evaluated at the momentum transfer $q = m_\mu$. The dashed orange curve shows the same radial potential modified by an ad hoc correlation function that is intended to restore the hole in the two-nucleon density at short-range.

For small values of r, $V_1(r, q) \propto 1/r$, and the potential divergences. This behavior is illustrated in Fig. 9.4. In matrix elements, the divergence is regulated by the harmonic oscillator basis, yielding a finite result. Nonetheless, the matrix element is very sensitive to the behavior of the two-nucleon correlation function. We can see this explicitly by modifying the two-nucleon density with the addition of an ad hoc correlation function [140]

$$\psi(\vec{r}_i, \vec{r}_j) \to (1 - \beta(r_{ij})) \, \psi(\vec{r}_i, \vec{r}_j)$$
$$\beta(r) = e^{-ar^2} \left(1 - br^2\right), \tag{9.17}$$

where $a = 1.1$ fm^{-2} and $b = 0.68$ fm^{-2}. The radial coordinate here is $r_{ij} = |\vec{r}_i - \vec{r}_j|$. The effect of this modification is to add a hole to the two-nucleon density at separations $r \lesssim 1$ fm while leaving the long-distance behavior unchanged. We see this effect in Fig. 9.4, where the additional correlation function removes the divergence at $r = 0$. Compared to the bare result, the total two-body matrix element in ^{27}Al is reduced by $\approx 40\%$ by the additional correlation function, as in Fig. 9.2.

The shell-model wave functions that we obtain are not genuine effective wave functions. No attempt is made to properly normalize them in the model space (i.e., to account for the proportion of the total wave function that lies outside of the model space). Furthermore, when computing matrix elements with the shell-model wave functions, we (erroneously) evaluate only the bare operator. Having truncated the full Hilbert space down to a model space, the bare operator must be replaced by an effective operator that accounts for the physics that has been integrated out. Although a framework does exist for promoting the

nuclear-shell model to a bona fide effective theory [141–145], these considerations are beyond the scope of the current work. For now, it suffices to have some estimate of the strength of the two-nucleon operator in $\mu \to e$ conversion, particularly given that our estimates likely represent an upper limit, as evidenced by the significant reduction effected by the addition of the ad hoc correlation function.

Chapter 10

Conclusions

Before summarizing the work presented in this thesis, we discuss two directions for future endeavors: First, we generalize the effective theory to describe the inelastic process in which the nucleus transitions to an excited state. This result will enable new efforts, in close consultation with experimentalists, to identify the best opportunities for constraining the unique CLFV operators that are probed when $\mu \to e$ conversion proceeds via nuclear excitation. Second, we discuss the steps that remain in connecting the nuclear-scale theory to effective theories formulated at higher energy scales. Once completed, this program will allow us to leverage the full information extracted from $\mu \to e$ conversion experiments to constrain candidate BSM theories.

10.1   Next Step: Inelastic $\mu \to e$ Conversion

In Chapter 3, we identified 11 independent response functions arising from the multipole decomposition of the relevant nuclear charges and currents. Restricting our attention to the case of elastic conversion, we found that the approximate parity and time-reversal symmetries of the nuclear ground state permit only six allowed response functions to contribute to the CLFV amplitude (each response appearing in only even or odd multipoles). Consequently, we determined that 4 of the 16 single-nucleon CLFV operators are not probed in elastic $\mu \to e$ conversion. This apparent blind spot can be remedied by extending the effective theory formalism to the case of inelastic $\mu \to$ conversion, allowing the nucleus to transition to an excited state. Experimentally, it is a considerable challenge to distinguish outgoing electrons originating in the inelastic conversion process from background electrons. Nonetheless, one can likely set interesting limits on otherwise inaccessible regions of CLFV parameter space.

The energy required to excite the nucleus is subtracted from the energy of the outgoing electron

$$E_e = m_\mu - E_\mu^{\text{bind}} - \frac{\vec{q}^{\,2}}{2M_T} - \Delta E_{\text{nuc}}, \qquad (10.1)$$

where ΔE_{nuc} is the energy difference between the final and initial nuclear states. The case of elastic conversion ($\Delta E_{\text{nuc}} = 0$) is experimentally favorable because the energy of the conversion electron is at the exact endpoint of the spectrum of background electrons that originate in standard-model $\mu \to e + 2\nu$ decays. In the inelastic process, the outgoing electron

is shifted into a region with considerably larger backgrounds. Near the endpoint energy, the spectrum of background decay-in-orbit electrons may be approximated as [146]

$$\frac{1}{\Gamma_0}\frac{d\Gamma}{dE_e} \approx B\left(m_\mu - E_\mu^{\text{bind}} - E_e - \frac{E_e^2}{2M_T}\right)^5, \tag{10.2}$$

where

$$\Gamma_0 = \frac{G_F^2 m_\mu^5}{192\pi^3}, \tag{10.3}$$

is the free-muon decay rate and $B = 8.98 \times 10^{-17}$ MeV^{-6} in ^{27}Al. The $\mu \to e + 2\nu$ background increases dramatically as the electron energy decreases (as the fifth power of the energy difference from the endpoint). Sufficiently far from the endpoint energy, one begins to encounter an additional electron background from radiative muon capture (RMC)

$$\mu^- + A(Z, N) \to \nu_\mu + \gamma + A(Z - 1, N + 1), \tag{10.4}$$

where the emitted photon can subsequently undergo pair production $\gamma \to e^+ e^-$. The maximum energy of the emitted electron is limited by the mass difference between the initial and final nuclei. In ^{27}Al, with daughter nucleus ^{27}Mg, the endpoint of the RMC electron spectrum is 2.61 MeV below the conversion electron energy.

The spectrum of background electrons in ^{27}Al is shown in Fig. 10.1. The RMC background is indicated by a region, as the exact shape of this spectrum near the endpoint is not well known. There are four states of ^{27}Al that are capable of producing $\mu \to e$ conversion electrons with an energy above the endpoint of the RMC background: the ground state with spin $J = \frac{5}{2}^+$ and the first three excited states with spin $J = \frac{1}{2}^+$, $\frac{3}{2}^+$, and $\frac{7}{2}^+$, respectively, and excitation energies $\Delta E_{\text{nuc}} = 0.844$ MeV, 1.015 MeV, and 2.212 MeV. The design goal of the Mu2e experiment is to reconstruct the energy of the outgoing electron with full width at half maximum (FWHM) resolution ≈ 900 KeV for electrons near the endpoint of the spectrum. To assess the magnitude of the decay-in-orbit background relevant to each transition, we have marked resolution windows[1] around the energy of the electron produced when $\mu \to e$ conversion proceeds to each of the four final states. The decay-in-orbit background for the inelastic process is several orders of magnitude larger compared to the ground-state process. Even if they can be discerned above the background, given the substantial overlap of the $J = \frac{1}{2}^+$ and $J = \frac{3}{2}^+$ states, it will be quite difficult to distinguish the two energy levels. Despite these challenges, it is worthwhile to consider the limits that can be obtained, as the inelastic process is capable of probing CLFV operators to which the elastic process is completely insensitive.

The construction of the inelastic effective theory proceeds in a similar manner to the elastic case. As before, we employ the effective momentum approximation for the outgoing electron, now accounting for the energy lost to nuclear excitation

$$q_{\text{eff}}^2 = \frac{M_T}{m_\mu + M_T}\left[\left(m_\mu - E_\mu^{\text{bind}} - \Delta E^{\text{nuc}} - \bar{V}_c\right)^2 - m_e^2\right]. \tag{10.5}$$

---

[1]The actual energy response function of Mu2e is asymmetric, with a long low-energy tail. See Fig. 3.16 of Ref. [53].
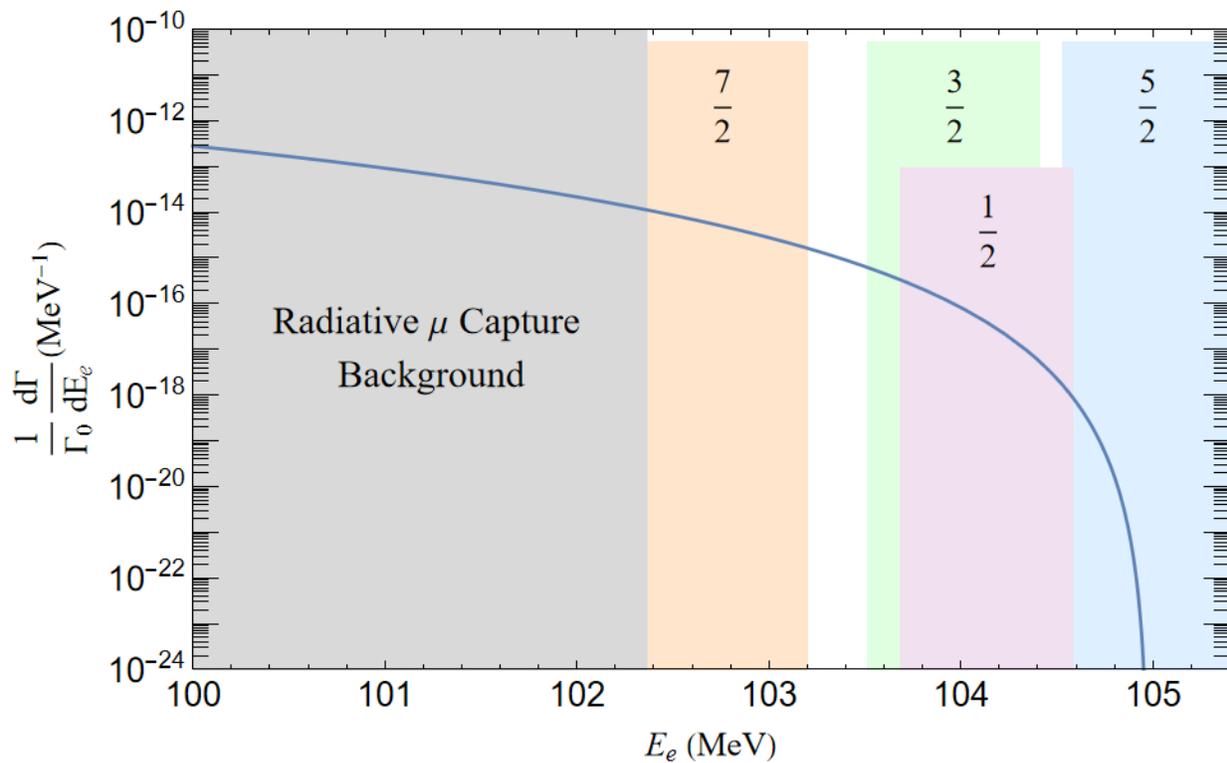
Figure 10.1: Comparison of the backgrounds for elastic and inelastic $\mu \to e$ conversion. The curve shows the differential decay rate for standard model $\mu \to e + 2\nu$ decays. The vertical bands represent the approximate energy resolution window of the Mu2e detector, centered on the energy of the outgoing conversion electron for the ground state $J = \frac{5}{2}^+$ and first three excited states $J = \frac{1}{2}^+$, $J = \frac{3}{2}^+$, and $J = \frac{7}{2}^+$ of ^{27}Al.

The 16 operators introduced in Section 3.4 still represent the most general basis of single-nucleon CLFV operators in the inelastic case. The $\mu \to e$ conversion amplitude is then expressed in terms of 11 independent nuclear response functions

$$
\mathcal{M} = \sqrt{\frac{E_e}{2m_e}} |\phi_{1s}^{Z_{\mathrm{eff}}}(\vec{0})| \frac{q_{\mathrm{eff}}}{q} \sum_{\tau=0,1} \langle \frac{1}{2} s_f; j_f m_f|
$$

$$
\left\{ \sum_{J=0}^{\infty} \sqrt{4\pi(2J+1)}(-i)^J \left[l_0^\tau M_{J0;\tau}(q_{\mathrm{eff}}) - i l_0^{A\,\tau} \frac{q_{\mathrm{eff}}}{m_N} \tilde{\Omega}_{J0;\tau}(q_{\mathrm{eff}}) \right] \right.
$$

$$
+ \sum_{J=1}^{\infty} \sqrt{2\pi(2J+1)}(-i)^J \sum_{\lambda=\pm1} \left[- l_{5\lambda}^\tau \left(\lambda \Sigma_{J-\lambda;\tau}(q_{\mathrm{eff}}) + i\Sigma'_{J-\lambda;\tau}(q_{\mathrm{eff}}) \right) \right.
$$

$$
+ i\frac{q_{\mathrm{eff}}}{m_N} l_{M\lambda}^\tau \left(\lambda \Delta_{J-\lambda;\tau}(q_{\mathrm{eff}}) + i\Delta'_{J-\lambda;\tau}(q_{\mathrm{eff}}) \right) + i\frac{q_{\mathrm{eff}}}{m_N} l_{E\lambda}^\tau \left(\lambda \tilde{\Phi}_{J-\lambda;\tau}(q_{\mathrm{eff}}) + i\tilde{\Phi}'_{J-\lambda;\tau}(q_{\mathrm{eff}}) \right) \right]
$$

$$
+ \sum_{J=0}^{\infty} \sqrt{4\pi(2J+1)}(-i)^J \left[i l_{50}^\tau \Sigma''_{J0;\tau}(q_{\mathrm{eff}}) + \frac{q_{\mathrm{eff}}}{m_N} l_{M0}^\tau \tilde{\Delta}''_{J0;\tau}(q_{\mathrm{eff}}) \right.
$$

$$
\left. \left. + \frac{q_{\mathrm{eff}}}{m_N} l_{E0}^\tau \Phi''_{J0;\tau}(q_{\mathrm{eff}}) \right] \right\} |\frac{1}{2} s_i; j_i m_i \rangle ,
$$

$$
(10.6)
$$

where j_i and j_f are, respectively, the total angular momentum of the initial and final nuclear states.

The inelastic process need not conserve parity, and as a result the summation over multipole angular momenta is not restricted to even or odd J. When we consider a particular nuclear final state, then the contributing operators will be limited based on their P transformation properties (see Table 3.1). The constraint of parity also determines the interference terms that can contribute to the overall conversion rate. For example, although Δ and Σ are both transverse-magnetic projections, they do not interfere because for fixed J they connect to states of opposite parity.

Let us assume that the nuclear transition conserves parity. We will also assume that the CP violation in the nuclear wave functions is negligible, so that all nuclear matrix elements are real. Then the $\mu \to e$ transition probability may be written as

$$
\frac{1}{2j_i+1} \sum_{m_f, m_i} |\langle \frac{1}{2} s_f; j_f m_f |\mathcal{M}| \frac{1}{2} s_i; j_i m_i \rangle|^2 = \frac{E_e}{2m_e} |\phi_{1s}^{Z_{\mathrm{eff}}}(\vec{0})|^2 \frac{q_{\mathrm{eff}}^2}{q^2} \frac{4\pi}{2j_i+1} \sum_{\tau=0,1} \sum_{\tau'=0,1}
$$

$$
\left\{ \sum_{J=0,2,\ldots}^{\infty} \left[\langle l_0^\tau \rangle \langle l_0^{\tau'} \rangle^* \langle j_f||M_{J,\tau}(q_{\mathrm{eff}})||j_i\rangle \langle j_f||M_{J,\tau'}(q_{\mathrm{eff}})||j_i\rangle \right. \right.
$$

$$
+ \frac{\vec{q}_{\mathrm{eff}}}{m_N} \cdot \langle \vec{l}_E^\tau \rangle \frac{\vec{q}_{\mathrm{eff}}}{m_N} \cdot \langle \vec{l}_E^{\tau'} \rangle^* \langle j_f||\Phi''_{J,\tau}(q_{\mathrm{eff}})||j_i\rangle \langle j_f||\Phi''_{J,\tau'}(q_{\mathrm{eff}})||j_i\rangle
$$

$$
+ \frac{\vec{q}_{\mathrm{eff}}}{m_N} \cdot \langle \vec{l}_M^\tau \rangle \frac{\vec{q}_{\mathrm{eff}}}{m_N} \cdot \langle \vec{l}_M^{\tau'} \rangle^* \langle j_f||\tilde{\Delta}''_{J,\tau}(q_{\mathrm{eff}})||j_i\rangle \langle j_f||\tilde{\Delta}''_{J,\tau'}(q_{\mathrm{eff}})||j_i\rangle
$$

$$
+ \frac{2\vec{q}_{\mathrm{eff}}}{m_N} \cdot \mathrm{Re}\left[\langle \vec{l}_E^\tau \rangle \langle l_0^{\tau'} \rangle^* \right] \langle j_f||\Phi''_{J,\tau}(q_{\mathrm{eff}})||j_i\rangle \langle j_f||M_{J,\tau'}(q_{\mathrm{eff}})||j_i\rangle
$$

$$+ \frac{2\vec{q}_{\text{eff}}}{m_N} \cdot \text{Re}\left[\langle \vec{l}_M^\tau \rangle \langle l_0^{\tau'} \rangle^*\right] \langle j_f || \tilde{\Delta}''_{J,\tau}(q_{\text{eff}}) || j_i \rangle \langle j_f || M_{J,\tau'}(q_{\text{eff}}) || j_i \rangle$$

$$+ 2\text{Re}\left[\frac{\vec{q}_{\text{eff}}}{m_N} \cdot \langle \vec{l}_E^\tau \rangle \frac{\vec{q}_{\text{eff}}}{m_N} \cdot \langle \vec{l}_M^{\tau'} \rangle^*\right] \langle j_f || \Phi''_{J,\tau}(q_{\text{eff}}) || j_i \rangle \langle j_f || \tilde{\Delta}''_{J,\tau'}(q_{\text{eff}}) || j_i \rangle \Bigg]$$

$$+ \sum_{J=2,4,\dots}^{\infty} \Bigg[\frac{1}{2} \left(\frac{q_{\text{eff}}^2}{m_N^2} \langle \vec{l}_E^\tau \rangle \cdot \langle \vec{l}_E^{\tau'} \rangle^* - \frac{\vec{q}_{\text{eff}}}{m_N} \cdot \langle \vec{l}_E^\tau \rangle \frac{\vec{q}_{\text{eff}}}{m_N} \cdot \langle \vec{l}_E^{\tau'} \rangle^* \right) \langle j_f || \tilde{\Phi}'_{J,\tau}(q_{\text{eff}}) || j_i \rangle \langle j_f || \tilde{\Phi}'_{J,\tau'}(q_{\text{eff}}) || j_i \rangle$$

$$+ \frac{1}{2} \left(\frac{q_{\text{eff}}^2}{m_N^2} \langle \vec{l}_M^\tau \rangle \cdot \langle \vec{l}_M^{\tau'} \rangle^* - \frac{\vec{q}_{\text{eff}}}{m_N} \cdot \langle \vec{l}_M^\tau \rangle \frac{\vec{q}_{\text{eff}}}{m_N} \cdot \langle \vec{l}_M^{\tau'} \rangle^* \right) \langle j_f || \Delta'_{J,\tau}(q_{\text{eff}}) || j_i \rangle \langle j_f || \Delta'_{J,\tau'}(q_{\text{eff}}) || j_i \rangle$$

$$+ \frac{1}{2} \left(\langle \vec{l}_5^\tau \rangle \cdot \langle \vec{l}_5^{\tau'} \rangle^* - \hat{q} \cdot \langle \vec{l}_5^\tau \rangle \hat{q} \cdot \langle \vec{l}_5^{\tau'} \rangle^* \right) \langle j_f || \Sigma_{J,\tau}(q_{\text{eff}}) || j_i \rangle \langle j_f || \Sigma_{J,\tau'}(q_{\text{eff}}) || j_i \rangle$$

$$- \frac{\vec{q}_{\text{eff}}}{m_N} \cdot \text{Re}\left[i \langle \vec{l}_5^\tau \rangle \times \langle \vec{l}_M^{\tau'} \rangle^* \right] \langle j_f || \Sigma_{J,\tau}(q_{\text{eff}}) || j_i \rangle \langle j_f || \Delta'_{J,\tau'}(q_{\text{eff}}) || j_i \rangle \tag{10.7}$$

$$- \frac{\vec{q}_{\text{eff}}}{m_N} \cdot \text{Re}\left[i \langle \vec{l}_5^\tau \rangle \times \langle \vec{l}_E^{\tau'} \rangle^* \right] \langle j_f || \Sigma_{J,\tau}(q_{\text{eff}}) || j_i \rangle \langle j_f || \tilde{\Phi}'_{J,\tau'}(q_{\text{eff}}) || j_i \rangle$$

$$+ \text{Re}\left[\frac{q_{\text{eff}}^2}{m_N^2} \langle \vec{l}_M^\tau \rangle \cdot \langle \vec{l}_E^{\tau'} \rangle^* - \frac{\vec{q}_{\text{eff}}}{m_N} \cdot \langle \vec{l}_M^\tau \rangle \frac{\vec{q}_{\text{eff}}}{m_N} \cdot \langle \vec{l}_E^{\tau'} \rangle^* \right] \langle j_f || \Delta'_{J,\tau}(q_{\text{eff}}) || j_i \rangle \langle j_f || \tilde{\Phi}'_{J,\tau'}(q_{\text{eff}}) || j_i \rangle \Bigg]$$

$$+ \sum_{J=1,3,\dots}^{\infty} \Bigg[\frac{q_{\text{eff}}^2}{m_N^2} \langle l_0^{A\,\tau} \rangle \langle l_0^{A\,\tau'} \rangle^* \langle j_f || \tilde{\Omega}_{J,\tau}(q_{\text{eff}}) || j_i \rangle \langle j_f || \tilde{\Omega}_{J,\tau'}(q_{\text{eff}}) || j_i \rangle$$

$$+ \hat{q} \cdot \langle \vec{l}_5^\tau \rangle \hat{q} \cdot \langle \vec{l}_5^{\tau'} \rangle^* \langle j_f || \Sigma''_{J,\tau}(q_{\text{eff}}) || j_i \rangle \langle j_f || \Sigma''_{J,\tau'}(q_{\text{eff}}) || j_i \rangle$$

$$+ \frac{1}{2} \left(\langle \vec{l}_5^\tau \rangle \cdot \langle \vec{l}_5^{\tau'} \rangle^* - \hat{q} \cdot \langle \vec{l}_5^\tau \rangle \hat{q} \cdot \langle \vec{l}_5^{\tau'} \rangle^* \right) \langle j_f || \Sigma'_{J,\tau}(q_{\text{eff}}) || j_i \rangle \langle j_f || \Sigma'_{J,\tau'}(q_{\text{eff}}) || j_i \rangle$$

$$+ \frac{1}{2} \left(\frac{q_{\text{eff}}^2}{m_N^2} \langle \vec{l}_M^\tau \rangle \cdot \langle \vec{l}_M^{\tau'} \rangle^* - \frac{\vec{q}_{\text{eff}}}{m_N} \cdot \langle \vec{l}_M^\tau \rangle \frac{\vec{q}_{\text{eff}}}{m_N} \cdot \langle \vec{l}_M^{\tau'} \rangle^* \right) \langle j_f || \Delta_{J,\tau}(q_{\text{eff}}) || j_i \rangle \langle j_f || \Delta_{J,\tau'}(q_{\text{eff}}) || j_i \rangle$$

$$+ \frac{1}{2} \left(\frac{q_{\text{eff}}^2}{m_N^2} \langle \vec{l}_E^\tau \rangle \cdot \langle \vec{l}_E^{\tau'} \rangle^* - \frac{\vec{q}_{\text{eff}}}{m_N} \cdot \langle \vec{l}_E^\tau \rangle \frac{\vec{q}_{\text{eff}}}{m_N} \cdot \langle \vec{l}_E^{\tau'} \rangle^* \right) \langle j_f || \tilde{\Phi}_{J,\tau}(q_{\text{eff}}) || j_i \rangle \langle j_f || \tilde{\Phi}_{J,\tau'}(q_{\text{eff}}) || j_i \rangle$$

$$+ \frac{\vec{q}_{\text{eff}}}{m_N} \cdot \text{Re}\left[i \langle \vec{l}_M^\tau \rangle \times \langle \vec{l}_5^{\tau'} \rangle^* \right] \langle j_f || \Delta_{J,\tau}(q_{\text{eff}}) || j_i \rangle \langle j_f || \Sigma'_{J,\tau'}(q_{\text{eff}}) || j_i \rangle$$

$$+ \frac{\vec{q}_{\text{eff}}}{m_N} \cdot \text{Re}\left[i \langle \vec{l}_E^\tau \rangle \times \langle \vec{l}_5^{\tau'} \rangle^* \right] \langle j_f || \tilde{\Phi}_{J,\tau}(q_{\text{eff}}) || j_i \rangle \langle j_f || \Sigma'_{J,\tau'}(q_{\text{eff}}) || j_i \rangle$$

$$- \frac{2\vec{q}_{\text{eff}}}{m_N} \cdot \text{Re}\left[\langle \vec{l}_5^\tau \rangle \langle l_0^{A\,\tau'} \rangle^* \right] \langle j_f || \Sigma''_{J,\tau}(q_{\text{eff}}) || j_i \rangle \langle j_f || \tilde{\Omega}_{J,\tau'}(q_{\text{eff}}) || j_i \rangle$$

$$+ \text{Re}\left[\frac{q_{\text{eff}}^2}{m_N^2} \langle \vec{l}_M^\tau \rangle \cdot \langle \vec{l}_E^{\tau'} \rangle^* - \frac{\vec{q}_{\text{eff}}}{m_N} \cdot \langle \vec{l}_M^\tau \rangle \frac{\vec{q}_{\text{eff}}}{m_N} \cdot \langle \vec{l}_E^{\tau'} \rangle^* \right] \langle j_f || \Delta_{J,\tau}(q_{\text{eff}}) || j_i \rangle \langle j_f || \tilde{\Phi}_{J,\tau'}(q_{\text{eff}}) || j_i \rangle \Bigg] \Bigg\}.$$

We see that all 11 nuclear response functions—and various interference terms—contribute to this process. Many of the leptonic factors are not unique. We recover eight familiar leptonic

response functions, unchanged from the elastic effective theory:

$$
\begin{aligned}
R_M^{\tau\tau'} &\equiv c_1^\tau c_1^{\tau'*} + c_{11}^\tau c_{11}^{\tau'*} \\
R_{\Phi''}^{\tau\tau'*} &\equiv c_3^\tau c_3^{\tau'*} + (c_{12}^\tau - c_{15}^\tau)(c_{12}^{\tau'*} - c_{15}^{\tau'*}) \\
R_{\Sigma''}^{\tau\tau'} &\equiv (c_4^\tau - c_6^\tau)(c_4^{\tau'*} - c_6^{\tau'*}) + c_{10}^\tau c_{10}^{\tau'*} \\
R_{\tilde{\Phi}}^{\tau\tau'} = R_{\tilde{\Phi}'}^{\tau\tau'} &\equiv c_{12}^\tau c_{12}^{\tau'*} + c_{13}^\tau c_{13}^{\tau'*} \\
R_{\Sigma}^{\tau\tau'} = R_{\Sigma'}^{\tau\tau'} &\equiv c_4^\tau c_4^{\tau'*} + c_9^\tau c_9^{\tau'*} \\
R_{\Delta}^{\tau\tau'} = R_{\Delta'}^{\tau\tau'} &\equiv c_5^\tau c_5^{\tau'*} + c_8^\tau c_8^{\tau'*} \\
R_{\Phi''M}^{\tau\tau'} &\equiv \mathrm{Re}\left[c_3^\tau c_1^{\tau'*} - (c_{12}^\tau - c_{15}^\tau)c_{11}^{\tau'*} \right] \\
R_{\Delta'\Sigma}^{\tau\tau'} = R_{\Delta\Sigma'}^{\tau\tau'} &\equiv \mathrm{Re}\left[c_5^\tau c_4^{\tau'*} + c_8^\tau c_9^{\tau'*} \right],
\end{aligned}
\tag{10.8}
$$

and seven new leptonic response functions, unique to the inelastic case:

$$
\begin{aligned}
R_{\tilde{\Omega}}^{\tau\tau'} &\equiv c_7^\tau c_7^{\tau'*} + c_{14}^\tau c_{14}^{\tau'*} \\
R_{\tilde{\Delta}''}^{\tau\tau'} &\equiv c_2^\tau c_2^{\tau'*} + (c_8^\tau - c_{16}^\tau)(c_8^{\tau'*} - c_{16}^{\tau'*}) \\
R_{\tilde{\Delta}''M}^{\tau\tau'} &\equiv \mathrm{Im}\left[-c_2^\tau c_1^{\tau'*} + (c_8^\tau - c_{16}^\tau)c_{11}^{\tau'*} \right] \\
R_{\Phi''\tilde{\Delta}''}^{\tau\tau'} &\equiv \mathrm{Im}\left[-c_3^\tau c_2^{\tau'*} - (c_{12}^\tau - c_{15}^\tau)(c_8^{\tau'*} - c_{16}^{\tau'*}) \right] \\
R_{\Sigma''\tilde{\Omega}}^{\tau\tau'} &\equiv \mathrm{Im}\left[(c_4^\tau - c_6^\tau)c_{14}^{\tau'*} - c_{10}^\tau c_7^{\tau'*} \right] \\
R_{\Delta\tilde{\Phi}}^{\tau\tau'} = R_{\Delta'\tilde{\Phi}'}^{\tau\tau'} &\equiv \mathrm{Im}\left[c_5^\tau c_{13}^{\tau'*} + c_8^\tau c_{12}^{\tau'*} \right] \\
R_{\Sigma'\tilde{\Phi}}^{\tau\tau'} = R_{\Sigma\tilde{\Phi}'}^{\tau\tau'} &\equiv \mathrm{Im}\left[-\left(c_4^\tau c_{13}^{\tau'*} + c_9^\tau c_{12}^{\tau'*} \right) \right].
\end{aligned}
\tag{10.9}
$$

The first two novel terms are direct contributions, whereas the remaining five are interference terms. The direct terms correspond to multipoles of the axial charge $\tilde{\Omega}$ and the longitudinal projection of the convection current $\tilde{\Delta}''$. Together, these responses provide sensitivity to the four LECs to which the elastic theory is blind: c_2, c_7, c_{14}, and c_{16}. The five new interference terms depend on the LECs containing an imaginary component. In general, these coefficients are complex. (Table 3.3 demonstrates that imaginary components arise naturally from the relativistic matching.)

In total, we identify 15 unique CLFV response functions, allowing one to probe 15 independent combinations of the underlying LECs, compared to 8 independent combinations probed by the elastic process. The transverse-electric and transverse-magnetic projections of a given current are always paired with the same leptonic response, reducing the number of unique LEC combinations that can be constrained.

The rate for inelastic $\mu \to e$ conversion can then be expressed as

$$\Gamma = \frac{G_F^2}{\pi} \frac{q_{\text{eff}}^2}{1 + \frac{q}{M_T}} |\phi_{1s}^{Z_{\text{eff}}}(\vec{0})|^2 \sum_{\tau=0,1} \sum_{\tau'=0,1} \left\{ \tilde{R}_M^{\tau\tau'} W_M^{\tau\tau'}(q_{\text{eff}}) + \frac{q_{\text{eff}}^2}{m_N^2} \tilde{R}_{\tilde{\Omega}}^{\tau\tau'} W_{\tilde{\Omega}}^{\tau\tau'}(q_{\text{eff}}) \right.$$

$$+ \tilde{R}_{\Sigma''}^{\tau\tau'} W_{\Sigma''}^{\tau\tau'}(q_{\text{eff}}) + \tilde{R}_{\Sigma'}^{\tau\tau'} \left(W_{\Sigma'}^{\tau\tau'}(q_{\text{eff}}) + W_{\Sigma}^{\tau\tau'}(q_{\text{eff}}) \right)$$

$$+ \frac{q_{\text{eff}}^2}{m_N^2} \left[\tilde{R}_{\tilde{\Delta}''}^{\tau\tau'} W_{\tilde{\Delta}''}^{\tau\tau'}(q_{\text{eff}}) + \tilde{R}_{\tilde{\Delta}'}^{\tau\tau'} \left(W_{\tilde{\Delta}'}^{\tau\tau'}(q_{\text{eff}}) + W_{\tilde{\Delta}}^{\tau\tau'}(q_{\text{eff}}) \right) \right]$$

$$+ \frac{q_{\text{eff}}^2}{m_N^2} \left[\tilde{R}_{\Phi''}^{\tau\tau'} W_{\Phi''}^{\tau\tau'}(q_{\text{eff}}) + \tilde{R}_{\Phi'}^{\tau\tau'} \left(W_{\Phi'}^{\tau\tau'}(q_{\text{eff}}) + W_{\tilde{\Phi}}^{\tau\tau'}(q_{\text{eff}}) \right) \right] \quad (10.10)$$

$$- \frac{2q_{\text{eff}}}{m_N} \left[\tilde{R}_{\Phi'' M}^{\tau\tau'} W_{\Phi'' M}^{\tau\tau'}(q_{\text{eff}}) + \tilde{R}_{\Delta\Sigma'}^{\tau\tau'} \left(W_{\Delta\Sigma'}^{\tau\tau'}(q_{\text{eff}}) - W_{\Delta'\Sigma}^{\tau\tau'}(q_{\text{eff}}) \right) \right]$$

$$+ \frac{2q_{\text{eff}}}{m_N} \left[\tilde{R}_{M\tilde{\Delta}''}^{\tau\tau'} W_{M\tilde{\Delta}''}^{\tau\tau'}(q_{\text{eff}}) - \tilde{R}_{\Sigma''\tilde{\Omega}}^{\tau\tau'} W_{\Sigma''\tilde{\Omega}}^{\tau\tau'}(q_{\text{eff}}) \right] + \frac{2q_{\text{eff}}^2}{m_N^2} \tilde{R}_{\Phi''\tilde{\Delta}''}^{\tau\tau'} W_{\Phi''\tilde{\Delta}''}^{\tau\tau'}(q_{\text{eff}})$$

$$\left. + \frac{2q_{\text{eff}}}{m_N} \tilde{R}_{\Sigma'\tilde{\Phi}}^{\tau\tau'} \left(W_{\Sigma'\tilde{\Phi}}^{\tau\tau'}(q_{\text{eff}}) - W_{\Sigma\tilde{\Phi}'}^{\tau\tau'}(q_{\text{eff}}) \right) + \frac{2q_{\text{eff}}^2}{m_N^2} \tilde{R}_{\Delta\tilde{\Phi}}^{\tau\tau'} \left(W_{\Delta\tilde{\Phi}}^{\tau\tau'}(q_{\text{eff}}) + W_{\Delta'\tilde{\Phi}'}^{\tau\tau'}(q_{\text{eff}}) \right) \right\}.$$

As usual, the notation $\tilde{R}$ indicates that the leptonic responses have been expressed in terms of dimensionless LECs, defined relative to the weak scale v. For transitions that conserve parity, the nuclear response functions are

$$W_O^{\tau\tau'}(q) \equiv \frac{4\pi}{2j_i+1} \sum_{J=0,2,\dots}^{\infty} \langle j_f||O_{J;\tau}(q)||j_i\rangle \langle j_f||O_{J;\tau'}(q)||j_i\rangle \text{ for } O = M, \Phi'', \tilde{\Delta}''$$

$$W_O^{\tau\tau'}(q) \equiv \frac{4\pi}{2j_i+1} \sum_{J=1,3,\dots}^{\infty} \langle j_f||O_{J;\tau}(q)||j_i\rangle \langle j_f||O_{J;\tau'}(q)||j_i\rangle \text{ for } O = \Sigma', \Sigma'', \Delta, \tilde{\Omega}, \tilde{\Phi}$$

$$W_O^{\tau\tau'}(q) \equiv \frac{4\pi}{2j_i+1} \sum_{J=2,4,\dots}^{\infty} \langle j_f||O_{J;\tau}(q)||j_i\rangle \langle j_f||O_{J;\tau'}(q)||j_i\rangle \text{ for } O = \tilde{\Phi}', \Delta', \Sigma$$

$$W_{\Phi'' M}^{\tau\tau'}(q) \equiv \frac{4\pi}{2j_i+1} \sum_{J=0,2,\dots}^{\infty} \langle j_f||\Phi''_{J;\tau}(q)||j_i\rangle \langle j_f||M_{J;\tau'}(q)||j_i\rangle$$

$$W_{\Delta\Sigma'}^{\tau\tau'}(q) \equiv \frac{4\pi}{2j_i+1} \sum_{J=1,3,\dots}^{\infty} \langle j_f||\Delta_{J;\tau}(q)||j_i\rangle \langle j_f||\Sigma'_{J;\tau'}(q)||j_i\rangle$$

$$W_{\Delta'\Sigma}^{\tau\tau'}(q) \equiv \frac{4\pi}{2j_i+1} \sum_{J=2,4,\dots}^{\infty} \langle j_f||\Delta'_{J;\tau}(q)||j_i\rangle \langle j_f||\Sigma_{J;\tau'}(q)||j_i\rangle \quad (10.11)$$

$$W_{O\tilde{\Delta}''}^{\tau\tau'}(q) \equiv \frac{4\pi}{2j_i+1} \sum_{J=0,2,\dots}^{\infty} \langle j_f||O_{J;\tau}(q)||j_i\rangle \langle j_f||\tilde{\Delta}_{J;\tau'}(q)||j_i\rangle, \text{ for } O = M, \tilde{\Phi}''$$

$$W_{\Sigma''\tilde{\Omega}}^{\tau\tau'}(q) \equiv \frac{4\pi}{2j_i+1} \sum_{J=1,3,\dots}^{\infty} \langle j_f||\Sigma''_{J;\tau}(q)||j_i\rangle \langle j_f||\tilde{\Omega}_{J;\tau'}(q)||j_i\rangle$$

$$W_{\Delta\tilde{\Phi}}^{\tau\tau'}(q) \equiv \frac{4\pi}{2j_i+1} \sum_{J=1,3,\dots}^{\infty} \langle j_f||\Delta_{J;\tau}(q)||j_i\rangle \langle j_f||\tilde{\Phi}_{J;\tau'}(q)||j_i\rangle$$

$$W_{\Delta'\tilde{\Phi}'}^{\tau\tau'}(q) \equiv \frac{4\pi}{2j_i+1} \sum_{J=2,4,\dots}^{\infty} \langle j_f||\Delta'_{J;\tau}(q)||j_i\rangle \langle j_f||\tilde{\Phi}'_{J;\tau'}(q)||j_i\rangle$$

$$W_{\Sigma'\tilde{\Phi}}^{\tau\tau'}(q) \equiv \frac{4\pi}{2j_i+1} \sum_{J=1,3,\dots}^{\infty} \langle j_f||\Sigma'_{J;\tau}(q)||j_i\rangle \langle j_f||\tilde{\Phi}_{J;\tau'}(q)||j_i\rangle$$

$$W_{\Sigma\tilde{\Phi}'}^{\tau\tau'}(q) \equiv \frac{4\pi}{2j_i+1} \sum_{J=2,4,\dots}^{\infty} \langle j_f||\Sigma_{J;\tau}(q)||j_i\rangle \langle j_f||\tilde{\Phi}'_{J;\tau'}(q)||j_i\rangle .$$

If the nucleus transitions to a state of opposite parity, then the nuclear response functions must change to opposite parity. In this case, the conversion rate is still described by Eq. (10.10), the leptonic response functions R are unchanged, but the nuclear response functions are given by

$$W_O^{\tau\tau'}(q) \equiv \frac{4\pi}{2j_i+1} \sum_{J=1,3,\dots}^{\infty} \langle j_f||O_{J;\tau}(q)||j_i\rangle \langle j_f||O_{J;\tau'}(q)||j_i\rangle \text{ for } O = M, \Phi'', \tilde{\Delta}'', \tilde{\Phi}', \Delta', \Sigma$$

$$W_O^{\tau\tau'}(q) \equiv \frac{4\pi}{2j_i+1} \sum_{J=0,2,\dots}^{\infty} \langle j_f||O_{J;\tau}(q)||j_i\rangle \langle j_f||O_{J;\tau'}(q)||j_i\rangle \text{ for } O = \Sigma'', \tilde{\Omega}$$

$$W_O^{\tau\tau'}(q) \equiv \frac{4\pi}{2j_i+1} \sum_{J=2,4,\dots}^{\infty} \langle j_f||O_{J;\tau}(q)||j_i\rangle \langle j_f||O_{J;\tau'}(q)||j_i\rangle \text{ for } O = \tilde{\Phi}, \Delta, \Sigma'$$

$$W_{\Phi''M}^{\tau\tau'}(q) \equiv \frac{4\pi}{2j_i+1} \sum_{J=1,3,\dots}^{\infty} \langle j_f||\Phi''_{J;\tau}(q)||j_i\rangle \langle j_f||M_{J;\tau'}(q)||j_i\rangle$$

$$W_{\Delta\Sigma'}^{\tau\tau'}(q) \equiv \frac{4\pi}{2j_i+1} \sum_{J=2,4,\dots}^{\infty} \langle j_f||\Delta_{J;\tau}(q)||j_i\rangle \langle j_f||\Sigma'_{J;\tau'}(q)||j_i\rangle$$

$$W_{\Delta'\Sigma}^{\tau\tau'}(q) \equiv \frac{4\pi}{2j_i+1} \sum_{J=1,3,\dots}^{\infty} \langle j_f||\Delta'_{J;\tau}(q)||j_i\rangle \langle j_f||\Sigma_{J;\tau'}(q)||j_i\rangle \tag{10.12}$$

$$W_{O\tilde{\Delta}''}^{\tau\tau'}(q) \equiv \frac{4\pi}{2j_i+1} \sum_{J=1,3,\dots}^{\infty} \langle j_f||O_{J;\tau}(q)||j_i\rangle \langle j_f||\tilde{\Delta}_{J;\tau'}(q)||j_i\rangle , \text{ for } O = M, \tilde{\Phi}''$$

$$W_{\Sigma''\tilde{\Omega}}^{\tau\tau'}(q) \equiv \frac{4\pi}{2j_i+1} \sum_{J=0,2,\dots}^{\infty} \langle j_f||\Sigma''_{J;\tau}(q)||j_i\rangle \langle j_f||\tilde{\Omega}_{J;\tau'}(q)||j_i\rangle$$

$$W_{\Delta\tilde{\Phi}}^{\tau\tau'}(q) \equiv \frac{4\pi}{2j_i+1} \sum_{J=1,3,\dots}^{\infty} \langle j_f||\Delta_{J;\tau}(q)||j_i\rangle \langle j_f||\tilde{\Phi}_{J;\tau'}(q)||j_i\rangle$$

$$W_{\Delta'\tilde{\Phi}'}^{\tau\tau'}(q) \equiv \frac{4\pi}{2j_i+1} \sum_{J=1,3,\dots}^{\infty} \langle j_f||\Delta'_{J;\tau}(q)||j_i\rangle \langle j_f||\tilde{\Phi}'_{J;\tau'}(q)||j_i\rangle$$

$$W_{\Sigma'\tilde{\Phi}}^{\tau\tau'}(q) \equiv \frac{4\pi}{2j_i+1} \sum_{J=2,4,\dots}^{\infty} \langle j_f||\Sigma'_{J;\tau}(q)||j_i\rangle \langle j_f||\tilde{\Phi}_{J;\tau'}(q)||j_i\rangle$$

$$W_{\Sigma\tilde{\Phi}'}^{\tau\tau'}(q) \equiv \frac{4\pi}{2j_i+1} \sum_{J=1,3,\dots}^{\infty} \langle j_f||\Sigma_{J;\tau}(q)||j_i\rangle \langle j_f||\tilde{\Phi}'_{J;\tau'}(q)||j_i\rangle .$$

Having obtained the expression for the inelastic $\mu \to e$ conversion rate, significant work remains in fully utilizing this formalism. In order to determine the most suitable targets for constraining CLFV-induced transitions to excited nuclear states, we must work with experimentalists to carefully consider the impacts of various backgrounds and detector limitations. In addition, further study of the novel inelastic nuclear response functions $\tilde{\Delta}''$

and $\tilde{\Omega}$ must undertaken in hopes of identifying nuclear targets with enhanced sensitivity to inelastic CLFV operators. To this end, additional nuclear shell-model calculations must be performed in order to obtain wave functions that accurately describe the low-lying excited states of interest.

Finally, we note that special attention must be devoted to the operators $\mathcal{O}'_2$ and $\mathcal{O}'_{16}$, which contain the longitudinal projection of the nuclear convection current $\hat{q} \cdot \vec{v}_N$, a quantity constrained by current conservation through Siegert's theorem [147]. The continuity equation in position space takes the form

$$\vec{\nabla} \cdot \vec{J}(\vec{x}) = \dot{\rho}(\vec{x}) = -i \left[H_0, \rho(\vec{x}) \right], \tag{10.13}$$

where ρ is the charge and H_0 is the nuclear Hamiltonian. Equation 10.13 implies that the longitudinal projection of the convection current is related to the standard charge operator. Explicitly,

$$
\begin{aligned}
\mathcal{L}(\vec{J}_c) &= \frac{i}{q} \int d^3x \, \left[\vec{\nabla} \left(j_J(qx) Y_{JM}(\hat{x}) \right) \right] \cdot \vec{J}_c(\vec{x}) \\
&= -\frac{i}{q} \int d^3x \, j_J(qx) Y_{JM}(\hat{x}) \, \vec{\nabla} \cdot \vec{J}_c(\vec{x}) \\
&= \frac{1}{q} \int d^3x \, j_J(qx) Y_{JM}(\hat{x}) \, \left[H_0, \, \rho(\vec{x}) \right] \\
&= \frac{q_0}{q} M_{JM}(q),
\end{aligned}
\tag{10.14}
$$

where $q_0 = E_f - E_i$ is the time component of the four-momentum transfer. Therefore the constraint of current conservation implies the existence of a redundancy between the operators $\tilde{\Delta}''$ and M_{JM}.

In practice, the situation is more subtle. For free nucleons, one reasonably expects that the nuclear convective current and charge density will obey the continuity equation. When the nucleons are embedded in the nucleus, however, the relevant degrees of freedom are the $A - 1$ inter-nucleon Jacobi coordinates, which are unconstrained by external kinematics. Thus, further study is required to determine the impact that current conservation has on the form of the inelastic nuclear response.

10.2   Next Step: Effective Theory Matching

The nuclear scale is a natural setting for an effective theory treatment of the low-energy $\mu \to e$ conversion process, allowing us to factorize the CLFV leptonic physics from the nuclear physics, each described in terms of response functions that are directly probed by experiments. Understanding the interplay between the various nuclear response functions—depending on both macroscopic nuclear quantities and details of nuclear structure—provides us with a pathway to extracting all of the information about CLFV operators that $\mu \to e$ conversion experiments (performed across a range of nuclear targets) can provide. Whether or not flavor violation is ultimately observed, the constraints obtained from $\mu \to e$ conversion experiments provide information about the potential form of BSM physics. Of course, the nuclear-scale

theory alone is not a complete tool for distinguishing among candidate UV theories. In order to translate limits obtained at low energies into constraints on the parameter space of CLFV BSM models, one must construct the full tower of effective theories illustrated in Fig. 1.2, with the nuclear-scale effective theory as the low-energy base that interfaces directly with experiment.

In Chapter 8, we implemented a portion of this matching program, for the limited case of coherent $\mu \to e$ conversion mediated by heavy scalar particles, allowing us to connect limits on CLFV branching ratios directly to constraints on parameters of candidate UV theories. In order for this formalism to apply to any extension of the standard model, we must undertake the full matching program, wherein a complete basis of CLFV operators is constructed at each relevant energy scale in terms of appropriate degrees of freedom. At the boundaries between these energy domains, the operators in neighboring theories can be matched. Specifically, below the scale of new CLFV physics and above the scale of electroweak symmetry breaking, the effect of BSM operators can be described within standard model effective field theory (SM-EFT). When the Higgs boson acquires a vacuum expectation value, electroweak symmetry is spontaneously broken, and the relevant description is the so-called low-energy effective field theory (LEFT). (See Section 8.1 for a brief review of SM-EFT and LEFT). These effective theories have already been employed in the study of CLFV τ decays at the Electron-Ion Collider [33], including the one-loop renormalization and tree-level matching of operators. Adapting these results for $\mu \to e$ conversion should be relatively straightforward.

We anticipate that the most significant effort will be required in matching the LEFT operators, which describe quark degrees of freedom, to nucleon-level operators through chiral perturbation theory. Fortunately, we are not without a guide, as the analogous matching has been performed for the effective theory of dark matter direct detection [148–152]. When we considered scalar-mediated conversion in Chapter 8, the only relevant hadronic matrix elements were those of the scalar quark bilinear

$$\langle N'|m_q\bar{q}q|N\rangle \, , \tag{10.15}$$

and trace of the gluon field strength tensor

$$\langle N'|\frac{\alpha_s}{12\pi}G^{a\,\mu\nu}G^a_{\mu\nu}|N\rangle \, . \tag{10.16}$$

In the general case, we must also compute nuclear matrix elements of the pseudoscalar

$$\langle N'|m_q\bar{q}i\gamma^5 q|N\rangle \, , \tag{10.17}$$

vector

$$\langle N'|\bar{q}\gamma^\mu q|N\rangle \, , \tag{10.18}$$

axial-vector

$$\langle N'|\bar{q}\gamma^\mu\gamma^5 q|N\rangle \, , \tag{10.19}$$

and tensor quark operators

$$\langle N'|m_q\bar{q}\sigma^{\mu\nu}q|N\rangle \, , \tag{10.20}$$

and the contraction of the gluon field strength tensor with its dual

$$\langle N' | \frac{\alpha_s}{8\pi} G^{a\,\mu\nu} \tilde{G}^a_{\mu\nu} | N \rangle . \tag{10.21}$$

Each hadronic matrix element can be expanded in terms of a momentum-dependent form factor, and the various low-energy constants that determine the behavior of the form factors can be obtained from lattice QCD calculations. As written, the above matrix elements are specified between single-nucleon states, but in the hadronization of the scalar quark operator $m_q \bar{q} q$, we encountered two-nucleon contributions at next-to-leading order in the chiral power counting. One crucial aspect of the matching program is to understand the order at which two-nucleon contributions become relevant in each form factor. Although this classification has already been performed in the case of dark matter effective theory, we have to verify if the same behavior persists in $\mu \to e$ conversion. Given the differing nature of the external fields (non-relativistic dark matter vs. bound muon and ultra-relativistic electron), it remains to be seen whether the power-counting is modified in any way. Once we have specified the complete matching procedure, our ultimate goal is to make available a computer program—analogous to the dark matter effective theory code DIRECTDM [150] —that will automate the process of connecting high-energy CLFV theories to the low-energy constraints obtained from $\mu \to e$ conversion experiments.

10.3 Summary

Inspired by previous work on dark matter direct detection and spurred by the looming promise of exceptional experimental progress in searches for charged lepton flavor violation, we have developed a nuclear effective theory of $\mu \to e$ conversion. Whereas previous works in the literature have either focused on the narrow—though exceptionally interesting—case of coherent conversion or retained only the relatively simple nuclear charge and spin operators, we have, for the first time, identified the most general set of response functions that can be probed through measurements of elastic $\mu \to e$ conversion in nuclei. As the nature of possible CLFV operators is yet entirely undetermined, one should consider a complete basis of effective operators (through a given order in some small power-counting parameter). Such a construction can be performed at a variety of energy scales in terms of different degrees of freedom, but the nuclear-scale effective theory is the most natural in the sense that it interfaces directly with experiments. Moreover, by constructing the effective theory directly at the nuclear scale, we are able to achieve a factorization between the underlying CLFV physics—which must be independent of the choice of target—and the nuclear physics. This separation provides a clean path for constraining the underlying CLFV response functions through an ensemble of $\mu \to e$ conversion measurements on various nuclear targets.

Crucial to obtaining the simple yet general form of our effective theory are the approximations that we have employed for the leptonic fields. In particular, the effective momentum approximation allows us to accurately model the outgoing electron as a Dirac plane wave, thereby permitting a straightforward multipole decomposition of the nuclear charges and currents. Our novel application of this technique yields a powerful compromise between the numerical solution, which is highly-accurate but extremely cumbersome to employ in the general case, and the uncorrected plane-wave solution, which allows for a simplified treatment but is a rather poor model of the outgoing electron. In ^{27}Al, the effective momentum solution introduces $\lesssim 1\%$ deviations from the numerical solution while retaining all the advantages of the plane wave.

The muon wave function can be treated exactly in the effective theory while maintaining a reasonably simple expression for the conversion rate. An even more transparent form for the effective theory can be obtained by neglecting entirely the muon's lower component and/or replacing the muon's slowly-varying (compared to the nuclear extent) radial wave function by a constant value. Applying both of these approximations, performing the multipole decomposition of the nuclear charges and currents, and appealing to the approximately good parity and time-reversal symmetries of the nuclear ground state, we find that the most general $\mu \to e$ conversion response is governed by six response functions and two interference terms. Restoring the muon's lower component supplements the effective theory with six additional response functions, which are proportional to the muon velocity and always subleading.

The form of the effective theory dictates what can and cannot be learned about CLFV operators from measurements of elastic $\mu \to e$ conversion: in principle, one can determine the values of the leptonic response functions but one cannot parse out the values of the individual low-energy constants of the nucleon-level effective theory. Only the particular bilinear combinations of LECs specified by the CLFV response functions can be constrained by experiment. The nuclear effective theory provides a blueprint for a program of $\mu \to e$ conversion measurements on an ensemble of nuclear targets that would allow one to probe

the various CLFV response functions.

As the ultimate goal of this experimental program is to constrain and/or determine the nature of beyond-standard-model CLFV physics, one must be able to relate any information obtained in the nuclear-level effective theory to candidate UV theories. These apparently disparate descriptions can be connected through a program of effective theory renormalization and matching that relates physics at different energy scales, beginning from the very low nuclear scale of $\mu \to e$ conversion experiments, past the scale where quarks deconfine, past the scale of electroweak symmetry breaking, and eventually to the scale of new CLFV physics. In fact, this matching program has already been explicitly realized in the special case of scalar-mediated coherent conversion. Work is now underway to extend the matching to the general effective theory. An analogous matching program has already been completed for the closely related case of dark matter direct detection, connecting UV models of dark matter to the corresponding nuclear scale effective theory.

Having successfully modeled our effective theory of $\mu \to e$ conversion after its dark matter predecessor, we can begin to think of nuclear effective theory as a general approach, applicable to a variety of problems where the nucleus acts as a low-energy laboratory in which to search for new physics. In order for these experimental programs to be successful, one must be able to systematically disentangle the nuclear physics, which is not the primary object of interest, from the desired observable. As nuclear many-body theory progresses to the level of a genuine effective theory with controlled approximations and well-understood uncertainties, we expect that formalisms like the one developed in this work will play a key role in utilizing low-energy measurements to probe physics at energy scales far beyond the reach of direct searches.

And so we await the results of the next-generation experiments in eager anticipation that, in probing ten thousand times deeper than ever before, we might bear incontrovertible witness to a 1-in-100-quadrillion event—a physical miracle, indisputable evidence of a law of nature beyond our current understanding. Equipped with the nuclear effective theory of $\mu \to e$ conversion, we are confident in our ability to isolate and interpret any signal of new physics that we might receive.

Bibliography

[1]G. Feinberg, "Decays of the μ meson in the intermediate-meson theory", Phys. Rev. **110**, 1482–1483 (1958).

[2]G. Lokanathan and J. Steinberger, Phys. Rev. **98**, 240 (A) (1955).

[3]B. Pontecorvo, "Electron and Muon Neutrinos", Zh. Eksp. Teor. Fiz. **37**, 1751–1757 (1959).

[4]G. Danby, J.-M. Gaillard, K. Goulianos, L. M. Lederman, N. Mistry, M. Schwartz, and J. Steinberger, "Observation of high-energy neutrino reactions and the existence of two kinds of neutrinos", Phys. Rev. Lett. **9**, 36–44 (1962).

[5]M. Koshiba, "Nobel lecture: birth of neutrino astrophysics", Rev. Mod. Phys. **75**, 1011–1020 (2003).

[6]A. B. McDonald, "Nobel lecture: the sudbury neutrino observatory: observation of flavor change for solar neutrinos", Rev. Mod. Phys. **88**, 030502 (2016).

[7]K. S. Babu, B. Dutta, and R. N. Mohapatra, "Lepton flavor violation and the origin of the seesaw mechanism", Phys. Rev. D **67**, 076006 (2003).

[8]A. Abada, V. De Romeri, and A. M. Teixeira, "Impact of sterile neutrinos on nuclear-assisted cLFV processes", JHEP **02**, 083 (2016).

[9]M. Lindner, M. Platscher, and F. S. Queiroz, "A Call for New Physics : The Muon Anomalous Magnetic Moment and Lepton Flavor Violation", Phys. Rept. **731**, 1–82 (2018).

[10]T. Li, M. A. Schmidt, C.-Y. Yao, and M. Yuan, "Charged lepton flavor violation in light of the muon magnetic moment anomaly and colliders", Eur. Phys. J. C **81**, 811 (2021).

[11]D. F. Carvalho, M. E. Gomez, and J. C. Romao, "Charged lepton flavor violation in supersymmetry with bilinear R-parity violation", Phys. Rev. D **65**, 093013 (2002).

[12]L. Calibbi, A. Faccia, A. Masiero, and S. K. Vempati, "Lepton flavor violation from supersymmetric grand unified theories: where do we stand for meg, prism/prime, and a super flavor factory", Phys. Rev. D **74**, 116002 (2006).

[13]A. J. R. Figueiredo and A. M. Teixeira, "Slepton mass splittings and cLFV in the SUSY seesaw in the light of recent experimental results", JHEP **01**, 015 (2014).

[14]M. E. Gomez, S. Heinemeyer, and M. Rehman, "Lepton flavor violating Higgs Boson Decays in Supersymmetric High Scale Seesaw Models", J. Part. Phys. **1**, 30–50 (2017).

[15]P. Ciafaloni, A. Romanino, and A. Strumia, "Lepton flavor violations in SO(10) with large tan beta", Nucl. Phys. B **458**, 3–22 (1996).

[16]R. Benbrik, M. Chabab, and G. Faisel, "Lepton Flavour Violating τ and μ decays induced by scalar leptoquark", `10.48550/ARXIV.1009.3886` (2010).

[17]T. Feldmann, C. Luhn, and P. Moch, "Lepton-flavour violation in a Pati-Salam model with gauged flavour symmetry", JHEP **11**, 078 (2016).

[18]F. F. Deppisch and A. Pilaftsis, "Lepton flavor violation and θ_{13} in minimal resonant leptogenesis", Phys. Rev. D **83**, 076007 (2011).

[19]L. Merlo and S. Rosauro-Alcaraz, "Predictive Leptogenesis from Minimal Lepton Flavour Violation", JHEP **07**, 036 (2018).

[20]G. Aad et al., "Search for charged-lepton-flavour violation in Z-boson decays with the ATLAS detector", Nature Phys. **17**, 819–825 (2021).

[21]G. Aad et al., "Search for lepton-flavor-violation in Z-boson decays with τ-leptons with the ATLAS detector", Phys. Rev. Lett. **127**, 271801 (2022).

[22]G. Aad et al., "Search for lepton-flavour-violating decays of the Higgs and Z bosons with the ATLAS detector", Eur. Phys. J. C **77**, 70 (2017).

[23]A. M. Sirunyan et al., "Search for lepton flavour violating decays of the Higgs boson to $\mu\tau$ and eτ in proton-proton collisions at $\sqrt{s} = 13$ TeV", JHEP **06**, 001 (2018).

[24]A. M. Sirunyan et al., "Search for lepton-flavor violating decays of the Higgs boson in the $\mu\tau$ and eτ final states in proton-proton collisions at $\sqrt{s} = 13$ TeV", Phys. Rev. D **104**, 032013 (2021).

[25]R. Aaij et al., "Search for the lepton flavour violating decay $B^+ \to K^+\mu^-\tau^+$ using B_{s2}^{*0} decays", JHEP **06**, 129 (2020).

[26]R. Aaij et al., "Search for Lepton-Flavor Violating Decays $B^+ \to K^+\mu^\pm e^\mp$", Phys. Rev. Lett. **123**, 241802 (2019).

[27]R. Aaij et al., "Search for the lepton-flavour-violating decays $B_s^0 \to \tau^\pm\mu^\mp$ and $B^0 \to \tau^\pm\mu^\mp$", Phys. Rev. Lett. **123**, 211801 (2019).

[28]R. Aaij et al., "Search for the lepton flavour violating decay $\tau^- \to \mu^-\ \mu^+\ \mu^-$", JHEP **02**, 121 (2015).

[29]G. Aad et al., "Probing lepton flavour violation via neutrinoless $\tau \longrightarrow 3\mu$ decays with the ATLAS detector", Eur. Phys. J. C **76**, 232 (2016).

[30]A. M. Sirunyan et al., "Search for the lepton flavor violating decay $\tau \to 3\mu$ in proton-proton collisions at $\sqrt{s} = 13$ TeV", JHEP **01**, 163 (2021).

[31]W. Altmannshofer et al., "The Belle II Physics Book", PTEP **2019**, edited by E. Kou and P. Urquijo, [Erratum: PTEP 2020, 029201 (2020)], 123C01 (2019).

[32]R. Abdul Khalek et al., "Snowmass 2021 White Paper: Electron Ion Collider for High Energy Physics", in 2022 Snowmass Summer Study (Mar. 2022).

[33]V. Cirigliano, K. Fuyuto, C. Lee, E. Mereghetti, and B. Yan, "Charged Lepton Flavor Violation at the EIC", JHEP **03**, 256 (2021).

[34]J. R. Ellis, M. E. Gomez, G. K. Leontaris, S. Lola, and D. V. Nanopoulos, "Charged lepton flavor violation in the light of the Super-Kamiokande data", Eur. Phys. J. C **14**, 319–334 (2000).

[35]R. Aaij et al., "Test of lepton universality in beauty-quark decays", Nature Phys. **18**, 277–282 (2022).

[36]B. Abi et al., "Measurement of the Positive Muon Anomalous Magnetic Moment to 0.46 ppm", Phys. Rev. Lett. **126**, 141801 (2021).

[37]R. Barbieri and L. Hall, "Signals for supersymmetric unification", Physics Letters B **338**, 212–218 (1994).

[38]A. Lagarrigue and C. Peyrou, Compt. rend. **234**, 1873 (1952).

[39]J. Steinberger and H. B. Wolfe, "Electrons from Muon Capture", Phys. Rev. **100**, 1490 (1955).

[40]W. Bertl, R. Engfer, E. Hermes, G. Kurz, T. Kozlowski, J. Kuth, G. Otter, F. Rosenbaum, N. Ryskulov, A. van der Schaaf, P. Wintz, I. Zychor, and The SINDRUM II Collaboration, "A search for μ-e conversion in muonic gold", The European Physical Journal C - Particles and Fields **47**, 337–346 (2006).

[41]R. H. Bernstein, "The mu2e experiment", Frontiers in Physics **7**, 1 (2019).

[42]M. Lee, "Comet muon conversion experiment in j-parc", Frontiers in Physics **6**, 133 (2018).

[43]R. M. Dzhilkibaev and V. M. Lobashev, "On the Search for $\mu \to e$ Conversion on Nuclei. (In Russian)", Sov. J. Nucl. Phys. **49**, 384–385 (1989).

[44]V. S. Abadzhev et al., "MELC experiment to search for the mu- A —> e- A process", (1992).

[45]F. Abusalma et al., "Expression of Interest for Evolution of the Mu2e Experiment", 10.48550/ARXIV.1802.02599 (2018).

[46]D. A. Bryman, M. Blecher, K. Gotow, and R. J. Powers, "Search for the reaction $\mu^- + \mathrm{Cu} \to e^+ + \mathrm{Co}$", Phys. Rev. Lett. **28**, 1469–1471 (1972).

[47]A. Badertscher, K. Borer, G. Czapek, A. Flückiger, H. Hänni, B. Hahn, E. Hugentobler, A. Markees, T. Marti, U. Moser, E. Ramseyer, J. Schacher, H. Scheidiger, P. Schlatter, G. Viertel, and W. Zeller, "A search for muon-electron and muon-positron conversion in sulfur", Nuclear Physics A **377**, 406–440 (1982).

[48]W. Honecker, C. Dohmen, H. Haan, D. Junker, G. Otter, M. Starlinger, P. Wintz, J. Hofmann, W. Bertl, J. Egger, B. Krause, S. Eggli, R. Engfer, C. Findeisen, E. A. Hermes, T. Kozlowski, C. B. Niebuhr, H. S. Pruys, and A. van der Schaaf, "Improved limit on the branching ratio of $\mu \to e$ conversion on lead", Phys. Rev. Lett. **76**, 200–203 (1996).

[49]P. Wintz, in Proc. 1st int. symp. on lepton and baryon number violation, edited by H. V. Klapdor-Kleingrothaus and I. V. Krivosheina (1999), p. 534.

[50]W. H. Bertl et al., "A Search for muon to electron conversion in muonic gold", Eur. Phys. J. C **47**, 337–346 (2006).

[51] A. M. Baldini et al., "Search for the lepton flavour violating decay $\mu^+ \to e^+\gamma$ with the full dataset of the MEG experiment", Eur. Phys. J. C **76**, 434 (2016).

[52] U. Bellgardt et al., "Search for the Decay $\mu^+ \to e^+e^+e^-$", Nucl. Phys. B **299**, 1–6 (1988).

[53] L. Bartoszek et al., "Mu2e Technical Design Report", 10.2172/1172555 (2014).

[54] A. M. Baldini et al., "The design of the MEG II experiment", Eur. Phys. J. C **78**, 380 (2018).

[55] F. W. on behalf of the Mu3e collaboration, "The Mu3e experiment", SciPost Phys. Proc., 20 (2021).

[56] A. Bartolotta and M. J. Ramsey-Musolf, "Coherent μ -e conversion at next-to-leading order", Phys. Rev. C **98**, 015208, 015208 (2018).

[57] V. Cirigliano, K. Fuyuto, M. J. Ramsey-Musolf, and E. Rule, "Next-to-leading order scalar contributions to $\mu \to e$ conversion", Phys. Rev. C **105**, 055504 (2022).

[58] E. Rule, W. C. Haxton, and K. McElvain, *Nucleon-level effective theory of $\mu \to e$ conversion*, 2021.

[59] W. C. Haxton, E. Rule, K. McElvain, and M. J. Ramsey-Musolf, "Nucleon-level effective theory of $\mu \to e$ conversion in the nuclear field", In Preparation (2022).

[60] H. De Vries, C. De Jager, and C. De Vries, "Nuclear charge-density-distribution parameters from elastic electron scattering", Atomic Data and Nuclear Data Tables **36**, 495–536 (1987).

[61] C. Garcia-Recio, J. Nieves, and E. Oset, "Neutron distributions from pionic atoms", Nucl. Phys. A **547**, 473–487 (1992).

[62] J. D. Bjorken and S. D. Drell, *Relativistic Quantum Mechanics*, International Series In Pure and Applied Physics (McGraw-Hill, New York, 1965).

[63] J. Knoll, "An analytic description of inelastic electron scattering on nuclei", Nuclear Physics A **223**, 462–476 (1974).

[64] F. Lenz and R. Rosenfelder, "Nuclear radii in the high-energy limit of elastic electron scattering", Nuclear Physics A **176**, 513–525 (1971).

[65] J. D. Walecka, "Semileptonic Weak Interactions in Nuclei", in Muon physics, volume ii: weak interactions, edited by V. W. Hughes and C. S. Wu (Jan. 1975), p. 114.

[66] S. Weinberg and G. Feinberg, "Electromagnetic transitions between μ meson and electron", Phys. Rev. Lett. **3**, 111–114 (1959).

[67] J. A. Wheeler, "Some consequences of the electromagnetic interaction between μ^--mesons and nuclei", Rev. Mod. Phys. **21**, 133–143 (1949).

[68] H. Primakoff, "Theory of muon capture", Rev. Mod. Phys. **31**, 802–822 (1959).

[69] G. Do Dang, "On the closure approximation in the study of muon capture by nuclei", Phys. Lett. B **38**, 397–400 (1972).

[70] W. J. Marciano and A. I. Sanda, "Reaction $\mu^- +$ Nucleus $\to e^- +$ Nucleus in gauge theories", Phys. Rev. Lett. **38**, 1512–1515 (1977).

[71]O. Shanker, "*Z* Dependence of coherent μe conversion rate in anomalous neutrinoless muon capture", Phys. Rev. D **20**, 1608–1615 (1979).

[72]T. Kosmas and J. Vergados, "Study of the flavour violating (μ^-, e^-) conversion in nuclei", Nuclear Physics A **510**, 641–670 (1990).

[73]H. Chiang, E. Oset, T. Kosmas, A. Faessler, and J. Vergados, "Coherent and incoherent (μ^-, e^-) conversion in nuclei", Nuclear Physics A **559**, 526–542 (1993).

[74]T. Kosmas, J. Vergados, O. Civitarese, and A. Faessler, "Study of the muon number violating (μ^-, e^-) conversion in a nucleus by using quasi-particle rpa", Nuclear Physics A **570**, 637–656 (1994).

[75]A. Czarnecki, W. J. Marciano, and K. Melnikov, "Coherent muon-electron conversion in muonic atoms", The workshop on physics at the first muon collider and at the front end of a muon collider, `10.1063/1.56214` (1998).

[76]T. Siiskonen, J. Suhonen, and T. S. Kosmas, "Realistic nuclear matrix elements for the lepton-flavor violating $\mu^- \rightarrow e^-$ conversion in ^{27}Al and ^{48}Ti", Phys. Rev. C **62**, 035502 (2000).

[77]T. Kosmas, "Exotic $\mu^- \rightarrow e^-$ conversion in nuclei: energy moments of the transition strength and average energy of the outgoing e^-", Nuclear Physics A **683**, 443–462 (2001).

[78]R. Kitano, M. Koike, and Y. Okada, "Detailed calculation of lepton flavor violating muon-electron conversion rate for various nuclei", Phys. Rev. D **66**, 096002 (2002).

[79]T. Kosmas, "On the nuclear dependence of the $\mu^- \rightarrow e^-$ conversion branching ratio", Nuclear Instruments and Methods in Physics Research Section A: Accelerators, Spectrometers, Detectors and Associated Equipment **503**, 247–251 (2003).

[80]V. Cirigliano, R. Kitano, Y. Okada, and P. Tuzon, "Model discriminating power of $\mu \rightarrow e$ conversion in nuclei", Physical Review D **80**, `10.1103/physrevd.80.013002` (2009).

[81]A. Crivellin, S. Davidson, G. M. Pruna, and A. Signer, "Renormalisation-group improved analysis of $\mu \rightarrow e$ processes in a systematic effective-field-theory approach", JHEP **05**, 117 (2017).

[82]V. Cirigliano, S. Davidson, and Y. Kuno, "Spin-dependent $\mu \rightarrow e$ conversion", Physics Letters B **771**, 242–246 (2017).

[83]S. Davidson, Y. Kuno, and A. Saporta, ""spin-dependent" $\mu \rightarrow e$ conversion on light nuclei", Eur. Phys. J. C **78**, 109 (2018).

[84]O. Civitarese and T. Tarutina, "Multipole decomposition of the rate of muon-to-electron $(\mu^- \longrightarrow e^-)$ conversion in ^{208}Pb", Phys. Rev. C **99**, 065504 (2019).

[85]J. Heeck, R. Szafron, and Y. Uesaka, "Isotope dependence of muon-to-electron conversion", Nucl. Phys. B **980**, 115833 (2022).

[86]B. D. Serot, "Semileptonic Weak and Electromagnetic Interactions with Nuclei: Nuclear Current Operators Through Order (v/c)**2 (Nucleon)", Nucl. Phys. A **308**, 457–499 (1978).

[87]T. Donnelly and W. Haxton, "Multipole operators in semileptonic weak and electromagnetic interactions with nuclei: harmonic oscillator single-particle matrix elements", Atomic Data and Nuclear Data Tables **23**, 103 –176 (1979).

[88]B. D. Serot, "Semileptonic weak and electromagnetic interactions with nuclei: parity violations in electron scattering and abnormal-parity admixtures in nuclear states", Nuclear Physics A **322**, 408–438 (1979).

[89]C. W. Johnson, W. E. Ormand, and P. G. Krastev, "Factorization in large-scale many-body calculations", Computer Physics Communications **184**, 2761–2774 (2013).

[90]C. W. Johnson, W. E. Ormand, K. S. McElvain, and H. Shan, "BIGSTICK: A flexible configuration-interaction shell-model code", arXiv e-prints, arXiv:1801.08432, `10.48550/ARXIV.1801.08432` (2018).

[91]S. Cohen and D. Kurath, "Effective interactions for the 1p shell", Nuclear Physics **73**, 1–24 (1965).

[92]B. A. Brown and W. A. Richter, "New "usd" hamiltonians for the *sd* shell", Phys. Rev. C **74**, 034315 (2006).

[93]B. A. Brown and B. H. Wildenthal, "Status of the nuclear shell model", Annual Review of Nuclear and Particle Science **38**, 29–66 (1988).

[94]W. C. Haxton and C. Johnson, "Weak-interaction rates in ^{16}O", Phys. Rev. Lett. **65**, 1325–1328 (1990).

[95]A. Poves, J. Sánchez-Solano, E. Caurier, and F. Nowacki, "Shell model study of the isobaric chains a=50, a=51 and a=52", Nuclear Physics A **694**, 157–198 (2001).

[96]M. Honma, T. Otsuka, B. A. Brown, and T. Mizusaki, "New effective interaction for pf-shell nuclei and its implications for the stability of the $N = Z = 28$ closed core", Phys. Rev. C **69**, 034335 (2004).

[97]J. B. McGrory, B. H. Wildenthal, and E. C. Halbert, "Shell-model structure of $^{42-50}$Ca", Phys. Rev. C **2**, 186–212 (1970).

[98]M. Honma, T. Otsuka, T. Mizusaki, and M. Hjorth-Jensen, "New effective interaction for f_5pg_9-shell nuclei", Phys. Rev. C **80**, 064323 (2009).

[99]B. A. Brown, (Unpublished; See B. Cheal et al., Phys. Rev. Lett. 104 (2010) 252502.)

[100]A. Gniady, E. Caurier, and F. Nowacki, (Unpublished).

[101]A. Czarnecki, W. J. Marciano, and K. Melnikov, "Coherent muon-electron conversion in muonic atoms", The workshop on physics at the first muon collider and at the front end of a muon collider, `10.1063/1.56214` (1998).

[102]N. Teshima, "Status of the DeeMe Experiment, an Experimental Search for *μ-e* Conversion at J-PARC MLF", PoS **NuFact2019**, 082 (2020).

[103]T. Suzuki, D. F. Measday, and J. P. Roalsvig, "Total nuclear capture rates for negative muons", Phys. Rev. C **35**, 2212–2224 (1987).

[104]E. Fermi and E. Teller, "The capture of negative mesotrons in matter", Phys. Rev. **72**, 399–408 (1947).

[105]M. Raidal and A. Santamaria, "Muon electron conversion in nuclei versus mu —> e gamma: An Effective field theory point of view", Phys. Lett. B **421**, 250–258 (1998).

[106]V. Cirigliano, A. Kurylov, M. J. Ramsey-Musolf, and P. Vogel, "Lepton flavor violation without supersymmetry", Phys. Rev. D **70**, 075007 (2004).

[107]V. Cirigliano, A. Kurylov, M. J. Ramsey-Musolf, and P. Vogel, "Neutrinoless double beta decay and lepton flavor violation", Phys. Rev. Lett. **93**, 231802 (2004).

[108]J. Hisano, T. Moroi, K. Tobe, and M. Yamaguchi, "Lepton-flavor violation via right-handed neutrino yukawa couplings in the supersymmetric standard model", Phys. Rev. D **53**, 2442–2459 (1996).

[109]I. Brivio and M. Trott, "The Standard Model as an Effective Field Theory", Phys. Rept. **793**, 1–98 (2019).

[110]S. Weinberg, "Baryon- and lepton-nonconserving processes", Phys. Rev. Lett. **43**, 1566–1570 (1979).

[111]E. E. Jenkins, A. V. Manohar, and P. Stoffer, "Low-Energy Effective Field Theory below the Electroweak Scale: Operators and Matching", JHEP **03**, 016 (2018).

[112]E. E. Jenkins, A. V. Manohar, and P. Stoffer, "Low-Energy Effective Field Theory below the Electroweak Scale: Anomalous Dimensions", JHEP **01**, 084 (2018).

[113]W. Dekens and P. Stoffer, "Low-energy effective field theory below the electroweak scale: matching at one loop", JHEP **10**, 197 (2019).

[114]A. Crivellin, M. Hoferichter, and M. Procura, "Improved predictions for $\mu \to e$ conversion in nuclei and Higgs-induced lepton flavor violation", Phys. Rev. D **89**, 093024 (2014).

[115]A. Crivellin, M. Hoferichter, and M. Procura, "Accurate evaluation of hadronic uncertainties in spin-independent WIMP-nucleon scattering: Disentangling two- and three-flavor effects", Phys. Rev. D **89**, 054021 (2014).

[116]C. Körber, A. Nogga, and J. de Vries, "First-principle calculations of Dark Matter scattering off light nuclei", Phys. Rev. C **96**, 035805 (2017).

[117]Y. Aoki et al., "FLAG Review 2021", `10.48550/ARXIV.2111.09849` (2021).

[118]D. A. Brantley, B. Joo, E. V. Mastropas, E. Mereghetti, H. Monge-Camacho, B. C. Tiburzi, and A. Walker-Loud, "Strong isospin violation and chiral logarithms in the baryon spectrum", `10.48550/ARXIV.1612.07733` (2016).

[119]M. Hoferichter, J. Ruiz de Elvira, B. Kubis, and U.-G. Meißner, "High-Precision Determination of the Pion-Nucleon σ Term from Roy-Steiner Equations", Phys. Rev. Lett. **115**, 092301 (2015).

[120]C. Alexandrou, V. Drach, K. Jansen, C. Kallidonis, and G. Koutsou, "Baryon spectrum with $N_f = 2 + 1 + 1$ twisted mass fermions", Phys. Rev. D **90**, 074501 (2014).

[121]S. Durr et al., "Sigma term and strangeness content of octet baryons", Phys. Rev. D **85**, [Erratum: Phys.Rev.D 93, 039905 (2016)], 014509 (2012).

[122]S. Durr et al., "Lattice computation of the nucleon scalar quark contents at the physical point", Phys. Rev. Lett. **116**, 172001 (2016).

[123]Y.-B. Yang, A. Alexandru, T. Draper, J. Liang, and K.-F. Liu, "πN and strangeness sigma terms at the physical point with chiral fermions", Phys. Rev. D **94**, 054503 (2016).

[124]R. Gupta, S. Park, M. Hoferichter, E. Mereghetti, B. Yoon, and T. Bhattacharya, "Pion–Nucleon Sigma Term from Lattice QCD", Phys. Rev. Lett. **127**, 242002 (2021).

[125]M. Hoferichter, C. Ditsche, B. Kubis, and U. G. Meissner, "Dispersive analysis of the scalar form factor of the nucleon", JHEP **06**, 063 (2012).

[126]J. Liu et al., "Determination of the Axial-Vector Weak Coupling Constant with Ultracold Neutrons", Phys. Rev. Lett. **105**, 181803 (2010).

[127]W. C. Haxton, C.-P. Liu, and M. J. Ramsey-Musolf, "Nuclear anapole moments", Phys. Rev. C **65**, 045502, 045502 (2002).

[128]B. A. Brown, W. Chung, and B. H. Wildenthal, "Empirical Renormalization of the One-Body Gamow-Teller beta-Decay Matrix Elements in the 1s-0d Shell", Phys. Rev. Lett. **40**, 1631–1635 (1978).

[129]C. Drischler, W. Haxton, K. McElvain, E. Mereghetti, A. Nicholson, P. Vranas, and A. Walker-Loud, "Towards grounding nuclear physics in QCD", Prog. Part. Nucl. Phys. **121**, 103888 (2021).

[130]V. Cirigliano, R. Kitano, Y. Okada, and P. Tuzon, "On the model discriminating power of mu —> e conversion in nuclei", Phys. Rev. D **80**, 013002 (2009).

[131]R. Kitano, M. Koike, S. Komine, and Y. Okada, "Higgs-mediated muon–electron conversion process in supersymmetric see-saw model", Physics Letters B **575**, 300–308 (2003).

[132]J. E. Kim, P. Ko, and D.-G. Lee, "More on $R-$parity- and lepton-family-number-violating couplings from muon(ium) conversion, and τ and π^0 decays", Phys. Rev. D **56**, 100–106 (1997).

[133]K. Huitu, J. Maalampi, M. Raidal, and A. Santamaria, "New constraints on r-parity violation from μ–e conversion in nuclei", Physics Letters B **430**, 355–362 (1998).

[134]A. Faessler, T. Kosmas, S. Kovalenko, and J. Vergados, "Exotic μ^--e^- conversion in nuclei and r-parity violating supersymmetry", Nuclear Physics B **587**, 25–44 (2000).

[135]R. Harnik, J. Kopp, and J. Zupan, "Flavor Violating Higgs Decays", JHEP **03**, 026 (2013).

[136]S. M. Barr and A. Zee, "Electric dipole moment of the electron and of the neutron", Phys. Rev. Lett. **65**, 21–24 (1990).

[137]T. Abe, J. Hisano, T. Kitahara, and K. Tobioka, "Gauge invariant Barr-Zee type contributions to fermionic EDMs in the two-Higgs doublet models", JHEP **01**, [Erratum: JHEP 04, 161 (2016)], 106 (2014).

[138]E. J. Moniz, I. Sick, R. R. Whitney, J. R. Ficenec, R. D. Kephart, and W. P. Trower, "Nuclear fermi momenta from quasielastic electron scattering", Phys. Rev. Lett. **26**, 445–448 (1971).

[139]R. B. Wiringa, V. G. J. Stoks, and R. Schiavilla, "Accurate nucleon-nucleon potential with charge-independence breaking", Phys. Rev. C **51**, 38–51 (1995).

[140] G. A. Miller and J. E. Spencer, "A survey of pion charge-exchange reactions with nuclei", Annals of Physics **100**, 562 –606 (1976).

[141] W. C. Haxton and C.-L. Song, "Morphing the shell model into an effective theory", Phys. Rev. Lett. **84**, 5484–5487 (2000).

[142] W. Haxton and T. Luu, "The canonical nuclear many-body problem as an effective theory", Nuclear Physics A **690**, Proc. Int. Symp. on Nuclei and Nucleons, 15–28 (2001).

[143] W. C. Haxton and T. Luu, "Perturbative effective theory in an oscillator basis?", Phys. Rev. Lett. **89**, 182503 (2002).

[144] W. C. Haxton, "Form of the effective interaction in harmonic-oscillator-based effective theory", Phys. Rev. C **77**, 034005 (2008).

[145] K. McElvain and W. Haxton, "Nuclear physics without high-momentum potentials: constructing the nuclear effective interaction directly from scattering observables", Physics Letters B **797**, 134880 (2019).

[146] A. Czarnecki, X. Garcia i Tormo, and W. J. Marciano, "Muon decay in orbit: spectrum of high-energy electrons", Phys. Rev. D **84**, 013006 (2011).

[147] A. J. F. Siegert, "Note on the interaction between nuclei and electromagnetic radiation", Phys. Rev. **52**, 787–789 (1937).

[148] F. Bishara, J. Brod, B. Grinstein, and J. Zupan, "Chiral effective theory of dark matter direct detection", Journal of Cosmology and Astroparticle Physics **2017**, 009–009 (2017).

[149] F. Bishara, J. Brod, B. Grinstein, and J. Zupan, "From quarks to nucleons in dark matter direct detection", JHEP **11**, 059 (2017).

[150] F. Bishara, J. Brod, B. Grinstein, and J. Zupan, "DirectDM: a tool for dark matter direct detection", `10.48550/ARXIV.1708.02678` (2017).

[151] J. Brod, A. Gootjes-Dreesbach, M. Tammaro, and J. Zupan, "Effective Field Theory for Dark Matter Direct Detection up to Dimension Seven", JHEP **10**, 065 (2018).

[152] F. Bishara, J. Brod, B. Grinstein, and J. Zupan, "Renormalization Group Effects in Dark Matter Interactions", JHEP **03**, 089 (2020).

[153] A. Edmonds, *Angular momentum in quantum mechanics*, Investigations in Physics Series (Princeton University Press, 1996).

[154] G. Prézeau, M. Ramsey-Musolf, and P. Vogel, "Neutrinoless double β decay and effective field theory", Phys. Rev. D **68**, 034016, 034016 (2003).

Appendix A

Treatment of Spinor Currents

Following Bjorken & Drell [62], we work in the Dirac representation of the γ matrices and employ the following normalization convention for spinors:

$$u(p) = \sqrt{\frac{E+m}{2m}} \left(\begin{array}{c} \xi \\ \frac{\vec{\sigma}\cdot\vec{p}}{E+m}\xi \end{array} \right), \tag{A.1}$$

so that

$$\bar{u}(p)u(p) = 1. \tag{A.2}$$

The γ matrices in the Dirac basis are

$$\gamma^0 = \left(\begin{array}{cc} I_2 & 0 \\ 0 & -I_2 \end{array} \right), \ \gamma^k = \left(\begin{array}{cc} 0 & \sigma^k \\ -\sigma^k & 0 \end{array} \right), \ \gamma^5 = \left(\begin{array}{cc} 0 & I_2 \\ I_2 & 0 \end{array} \right) \tag{A.3}$$

The basis for Dirac spinors is then furnished by the scalar 1, pseudoscalar γ^5, vector γ^μ, axial-vector $\gamma^\mu\gamma^5$ and tensor $\sigma^{\mu\nu} \equiv \frac{i}{2}\left[\gamma^\mu,\gamma^\nu\right]$ matrices. Explicitly, in the Dirac basis, the tensor operator can be written as

$$\sigma^{0i} = \frac{i}{2}\left[\gamma^0,\gamma^i\right] = i\left(\begin{array}{cc} 0 & \sigma^i \\ \sigma^i & 0 \end{array} \right)$$
$$\sigma^{ij} = \frac{i}{2}\left[\gamma^i,\gamma^j\right] = \epsilon^{ijk}\left(\begin{array}{cc} \sigma^k & 0 \\ 0 & \sigma^k \end{array} \right). \tag{A.4}$$

The left and right projections of a Dirac spinor are defined by

$$P_L \equiv \frac{1}{2}\left(1-\gamma_5\right), \ P_R \equiv \frac{1}{2}\left(1+\gamma_5\right) \tag{A.5}$$

Using the fact that

$$\left(\gamma_5\right)^2 = 1, \tag{A.6}$$

it follows that

$$\gamma_5 P_L = -P_L, \ \gamma_5 P_R = P_R \tag{A.7}$$

Using the fact that the fifth gamma matrix anticommutes with the other four

$$\left\{\gamma^{\mu}, \gamma^{5}\right\} = 0, \tag{A.8}$$

we have

$$\gamma^{\mu} P_L = P_R \gamma^{\mu}, \ \gamma^{\mu} P_R = P_L \gamma^{\mu}. \tag{A.9}$$

Then we may compute

$$
\begin{aligned}
\bar{u}u &= \bar{u}_R u_L + \bar{u}_L u_R \\
\bar{u}\gamma^5 u &= \bar{u}_L u_R - \bar{u}_R u_L \\
\bar{u}\gamma^{\mu} u &= \bar{u}_L \gamma^{\mu} u_L + \bar{u}_R \gamma^{\mu} u_R \\
\bar{u}\gamma^{\mu}\gamma^5 u &= -\bar{u}_L \gamma^{\mu} u_L + \bar{u}_R \gamma^{\mu} u_R \\
\bar{u}\sigma^{\mu\nu} u &= \bar{u}_R \sigma^{\mu\nu} u_L + \bar{u}_L \sigma^{\mu\nu} u_R.
\end{aligned}
\tag{A.10}
$$

A.1 Non-relativistic Expansion of Nucleon Spinor Currents

In the non-relativistic limit, the nucleon spinors can be written as

$$N(k) = \begin{pmatrix} \xi \\ \frac{1}{2m_N}\vec{k}\cdot\vec{\sigma}_N \xi \end{pmatrix} \tag{A.11}$$

Then the leading Lorentz-covariant nucleon spinor currents can be reduced in terms of Pauli spinors as

$$
\begin{aligned}
\bar{N}(k')N(k) &\approx \xi'^{\dagger} \left[1_N \right] \xi \\
\bar{N}(k')i\gamma^5 N(k) &\approx \xi'^{\dagger} \left[i\frac{\vec{q}}{2m_N}\cdot\vec{\sigma}_N \right] \xi \\
\bar{N}(k')\gamma^0 N(k) &\approx \xi'^{\dagger} \left[1_N \right] \xi \\
\bar{N}(k')\gamma^i N(k) &\approx \xi'^{\dagger} \left[\vec{v}_N + i\frac{\vec{q}}{2m_N}\times\vec{\sigma}_N \right]^i \xi \\
\bar{N}(k')\gamma^0\gamma^5 N(k) &\approx \xi'^{\dagger} \left[\vec{v}_N\cdot\vec{\sigma}_N \right] \xi \\
\bar{N}(k')\gamma^i\gamma^0 N(k) &\approx \xi'^{\dagger} \left[\vec{\sigma}_N \right]^i \xi \\
\bar{N}(k')i\sigma^{0i}\frac{q_i}{m_N} N(k) &\approx 0 \\
\bar{N}(k')i\sigma^{ij}\frac{q_j}{m_N} N(k) &\approx \xi^{\dagger'} \left[-i\frac{\vec{q}}{m_N}\times\vec{\sigma}_N \right]^i \xi \\
\bar{N}(k')\sigma^{0i}\gamma_5\frac{q_i}{m_N} N(k) &\approx \xi^{\dagger'} \left[-i\frac{\vec{q}}{m_N}\cdot\vec{\sigma}_N \right] \xi \\
\bar{N}(k')\sigma^{ij}\gamma_5\frac{q_j}{m_N} N(k) &\approx 0
\end{aligned}
\tag{A.12}
$$

Thus we see that only four unique Hermitian operators arise in the reduction of the single-nucleon currents: 1_N, $i\vec{q}$, $\vec{v}_N$, and $\vec{\sigma}_N$. This fact is crucial to the formulation of the single-nucleon effective theory.

A.2 Expansion of Leptonic Spinor Currents

For the purpose of deriving the Pauli operator form of the leptonic Dirac currents, we define the electron and muon Dirac spinors, respectively, as

$$\chi_e \equiv \begin{pmatrix} \xi \\ \hat{q} \cdot \vec{\sigma}_L \xi \end{pmatrix}, \quad \chi_\mu \equiv \begin{pmatrix} \xi \\ \frac{1}{2}\vec{v}_\mu \cdot \vec{\sigma}_L \xi \end{pmatrix}. \tag{A.13}$$

It is a straightforward exercise in vector and spinor algebra to derive the following reductions of the Lorentz-covariant lepton currents:

$$\bar{\chi}_e \chi_\mu \approx \xi^{\dagger'} \left[1_L - \frac{1}{2}\hat{q} \cdot \vec{v}_\mu - \frac{i}{2}\hat{q} \cdot (\vec{v}_\mu \times \vec{\sigma}_L) \right] \xi$$

$$\bar{\chi}_e i\gamma_5 \chi_\mu \approx \xi^{\dagger'} \left[-i\hat{q} \cdot \vec{\sigma}_L + \frac{i}{2}\vec{v}_\mu \cdot \vec{\sigma}_L \right] \xi$$

$$\bar{\chi}_e \gamma^0 \chi_\mu \approx \xi^{\dagger'} \left[1_L + \frac{1}{2}\hat{q} \cdot \vec{v}_\mu + \frac{i}{2}\hat{q} \cdot (\vec{v}_\mu \times \vec{\sigma}_L) \right] \xi$$

$$\bar{\chi}_e \gamma^i \chi_\mu \approx \xi^{\dagger'} \left[\hat{q} - i\hat{q} \times \vec{\sigma}_L + \frac{1}{2}\vec{v}_\mu + \frac{i}{2}\vec{v}_\mu \times \vec{\sigma}_L \right]^i \xi$$

$$\bar{\chi}_e \gamma^0 \gamma_5 \chi_\mu \approx \xi^{\dagger'} \left[\hat{q} \cdot \vec{\sigma}_L + \frac{1}{2}\vec{v}_\mu \cdot \vec{\sigma}_L \right] \xi$$

$$\bar{\chi}_e \gamma^i \gamma_5 \chi_\mu \approx \xi^{\dagger'} \left[\vec{\sigma}_L - \frac{1}{2}i\hat{q} \times \vec{v}_\mu + \frac{1}{2}\hat{q} \times (\vec{v}_\mu \times \vec{\sigma}_L) + \frac{1}{2}(\vec{v}_\mu \cdot \vec{\sigma}_L)\hat{q} \right]^i \xi$$

$$\bar{\chi}_e i\sigma^{0i}\frac{q_i}{m_L}\chi_\mu \approx \frac{q}{m_L}\xi^{\dagger'} \left[-1_L + \frac{1}{2}\hat{q} \cdot \vec{v}_\mu + \frac{i}{2}\hat{q} \cdot (\vec{v}_\mu \times \vec{\sigma}_L) \right] \xi$$

$$\bar{\chi}_e i\sigma^{ij}\frac{q_j}{m_L}\chi_\mu \approx -\frac{q}{m_L}\xi^{\dagger'} \left[i\hat{q} \times \vec{\sigma}_L + \frac{1}{2}\vec{v}_\mu - \frac{1}{2}(\hat{q} \cdot \vec{v}_\mu)\hat{q} - \frac{i}{2}\hat{q} \cdot (\vec{v}_\mu \times \vec{\sigma}_L)\hat{q} + \frac{i}{2}\vec{v}_\mu \times \vec{\sigma}_L \right]^i \xi$$

$$\bar{\chi}_e \sigma^{0i}\gamma_5 \frac{q_i}{m_L}\chi_\mu \approx \frac{q}{m_L}\xi^{\dagger'} \left[-i\hat{q} \cdot \vec{\sigma}_L + \frac{i}{2}\vec{v} \cdot \vec{\sigma}_L \right] \xi$$

$$\bar{\chi}_e \sigma^{ij}\gamma_5 \frac{q_j}{m_L}\chi_\mu \approx \frac{q}{m_L} \left[i\vec{\sigma}_L - i(\hat{q} \cdot \vec{\sigma}_L)\hat{q} - \frac{1}{2}\hat{q} \times \vec{v}_\mu - \frac{i}{2}\hat{q} \times (\vec{v}_\mu \times \vec{\sigma}_L) \right]^i \xi \tag{A.14}$$

Combining these results with the analogous expressions for the reduction of the nucleon currents, one can arrive at the expressions given in Tables 3.3 and 7.1. Just as we found in the case of the nucleons, there are four unique Hermitian operators that appear in the reduction of the leptonic currents: 1_L, $i\hat{q}$, $\vec{v}_\mu$, and $\vec{\sigma}_L$.

A.3 Isospin Matrices

The isospin matrices $\vec{\tau}$ are exactly the Pauli matrices

$$\tau_1 = \begin{pmatrix} 0 & 1 \\ 1 & 0 \end{pmatrix}, \quad \tau_2 = \begin{pmatrix} 0 & -i \\ i & 0 \end{pmatrix}, \quad \tau_3 = \begin{pmatrix} 1 & 0 \\ 0 & -1 \end{pmatrix}. \tag{A.15}$$

We define the isospin raising and lowering operators

$$\tau_\pm \equiv \frac{1}{2} \left(\tau_1 \pm i\tau_2 \right), \tag{A.16}$$

so that

$$\tau_+ = \begin{pmatrix} 0 & 1 \\ 0 & 0 \end{pmatrix}, \ \tau_- = \begin{pmatrix} 0 & 0 \\ 1 & 0 \end{pmatrix} \tag{A.17}$$

We note the following useful relations

$$\begin{aligned} [\tau_+, \tau_-] &= \tau_3 \\ [\tau_3, \tau_\pm] &= \pm 2\tau_\pm \\ \{\tau_+, \tau_-\} &= \mathbf{1} \\ \{\tau_3, \tau_\pm\} &= 0 \end{aligned} \tag{A.18}$$

Appendix B

Spherical Tensor Operators

Many calculations performed in this thesis are greatly simplified by working in terms of mathematical objects with well-defined angular momentum that transform in a prescribed manner under rotations of the coordinate system. Not only can one decompose scalar-valued functions in this way but also vector fields and more general tensor- and spinor-valued functions as well. In this appendix, we introduce the basic machinery required in such a treatment. We follow the conventions of Edmonds [153].

B.1   The Spherical Basis

Consider a three-dimensional coordinate system where $\hat{e}_x$, $\hat{e}_y$, and $\hat{e}_z$ are unit vectors along the x, y, and z axes respectively. The generators of rotations about these three axes are the operators

$$S_x = i\hat{e}_x\times, \quad S_y = i\hat{e}_y\times, \quad S_z = i\hat{e}_z\times, \tag{B.1}$$

where $\times$ indicates the vector cross product. The operators $\vec{S}$ satisfy the usual commutation relations of angular momentum operators

$$[S_i, S_j] = i\epsilon_{ijk}S_k. \tag{B.2}$$

We identify simultaneous eigenvectors of $\vec{S}^2$ and S_z by taking appropriate linear combinations of the spherical basis vectors

$$\begin{aligned}
\hat{e}_{+1} &= -\frac{1}{\sqrt{2}}\left(\hat{e}_x + i\hat{e}_y\right) \\
\hat{e}_0 &= \hat{e}_z \\
\hat{e}_{-1} &= \frac{1}{\sqrt{2}}\left(\hat{e}_x - i\hat{e}_y\right),
\end{aligned} \tag{B.3}$$

which satisfy

$$\begin{aligned}
\vec{S}^2\hat{e}_\lambda &= 2\hat{e}_\lambda \\
S_z\hat{e}_\lambda &= \lambda\hat{e}_\lambda,
\end{aligned} \tag{B.4}$$

where $\lambda = 0, \pm 1$. The eigenvalue of the total spin operator $\vec{S}^2$ indicates that the representation is spin 1. The spherical unit vectors $\hat{e}_\lambda$ have the following useful properties: Under complex conjugation

$$\hat{e}_\lambda^* = (-1)^\lambda \hat{e}_{-\lambda}, \text{ for } \lambda = 0, \pm 1 \tag{B.5}$$

The scalar product of two spherical unit vectors is given by

$$\hat{e}_\lambda^* \cdot \hat{e}_{\lambda'} = (-1)^\lambda \hat{e}_\lambda \cdot \hat{e}_{-\lambda} = \delta_{\lambda\lambda'}. \tag{B.6}$$

Any vector may be expanded in the spherical basis as

$$\vec{V} = \sum_\lambda V_\lambda \hat{e}_\lambda^* = \sum_\lambda (-1)^\lambda V_\lambda \hat{e}_{-\lambda} \tag{B.7}$$

where the vector components are given by

$$\begin{aligned} V_{\pm 1} &= \mp \frac{1}{\sqrt{2}} \left(V_x \pm i V_y \right), \\ V_0 &= V_z. \end{aligned} \tag{B.8}$$

These vector components can be obtained by projecting along the spherical basis vectors

$$V_\lambda = \hat{e}_\lambda \cdot \vec{V}. \tag{B.9}$$

Taking cross products of the spherical basis vectors yields

$$\begin{aligned} \hat{e}_\lambda \times \hat{e}_\lambda &= 0 \\ \hat{e}_\pm \times \hat{e}_\mp &= \pm i \hat{e}_0 \\ \hat{e}_\pm \times \hat{e}_0 &= \pm i \hat{e}_\pm. \end{aligned} \tag{B.10}$$

B.2   Vector Spherical Harmonics

The ordinary spherical harmonics $Y_{\ell m}(\theta, \phi) = Y_{\ell m}(\hat{r})$ form a basis of scalar functions on the sphere; that is, any (well-behaved) smooth function $f(\theta, \phi)$ can be decomposed as

$$f(\theta, \phi) = \sum_{\ell=0}^{\infty} \sum_{m=-\ell}^{\ell} f_{\ell m} Y_{\ell m}(\theta, \phi) \tag{B.11}$$

where

$$f_{\ell m} = \int d\Omega \, f(\theta, \phi) Y_{\ell m}^*(\theta, \phi). \tag{B.12}$$

The spherical harmonics are a privileged basis in that they are eigenfunctions of orbital angular momentum

$$\begin{aligned} \vec{L}^2 Y_{\ell m} &= \ell(\ell+1) Y_{\ell m} \\ L_z Y_{\ell m} &= m Y_{\ell m}. \end{aligned} \tag{B.13}$$

One would like to find an analogous basis for vector-valued functions on the sphere $\vec{V}(\theta, \phi)$. Of course, if we expand in the spherical basis $\vec{V} = \sum_\lambda (-1)^\lambda V_{-\lambda} \hat{e}_\lambda$, then each component $V_{-\lambda}(\theta, \phi)$ is a scalar function that can be decomposed in terms of ordinary spherical harmonics

$$\vec{V}(\theta, \phi) = \sum_\lambda (-1)^\lambda \hat{e}_\lambda \sum_{\ell=0}^\infty \sum_{m=-\ell}^\ell (V_{-\lambda})_{\ell m} \, Y_{\ell m}(\theta, \phi), \tag{B.14}$$

where we see that $\hat{e}_\lambda$ and $Y_{\ell m}$ carry angular momentum under the operators $\vec{S}$ and $\vec{L}$, respectively. Therefore, we may combine these two objects into a tensor of definite total angular momentum $\vec{J} = \vec{L} + \vec{S}$

$$\begin{aligned}
\vec{Y}_{J \, \ell \, M}(\hat{r}) &\equiv [Y_\ell(\hat{r}) \otimes \hat{e}]_{JM} \\
&= \sum_{m\lambda} Y_{\ell \, m}(\hat{r}) \hat{e}_\lambda \, \langle \ell \, m \, 1 \, \lambda | J \, M \rangle,
\end{aligned} \tag{B.15}$$

where $J = \ell, \ell \pm 1$. The resulting objects, the vector spherical harmonics, satisfy the orthogonality condition

$$\int d\Omega \, \vec{Y}^*_{J \, \ell \, M}(\hat{r}) \cdot \vec{Y}_{J' \, \ell' \, M'}(\hat{r}) = \delta_{JJ'} \delta_{\ell\ell'} \delta_{MM'} \tag{B.16}$$

and are eigenfunctions of total angular momentum

$$\begin{aligned}
\vec{J}^2 \vec{Y}_{J \, \ell \, M} &= J(J+1) \vec{Y}_{J \, \ell \, M} \\
J_z \vec{Y}_{J \, \ell \, M} &= M \vec{Y}_{J \, \ell \, M}.
\end{aligned} \tag{B.17}$$

Indeed they furnish a basis of vector-valued functions on the sphere

$$\vec{V}(\theta, \phi) = \sum_{\ell=0}^\infty \sum_J \sum_{M=-J}^J V_{J \, \ell \, M} \vec{Y}_{J \, \ell \, M}(\theta, \phi), \tag{B.18}$$

where the coefficients are given by

$$V_{J \, \ell \, M} = \int d\Omega \, \vec{V}(\theta, \phi) \cdot \vec{Y}^*_{J \, \ell \, M}(\theta, \phi). \tag{B.19}$$

The vector spherical harmonics have several other properties that make them an effective tool for, among other uses, performing a multipole expansion of three-current operators. First, they inherit the parity transformation of the ordinary spherical harmonics

$$Y_{\ell m}(-\hat{r}) = (-1)^\ell Y_{\ell m}(\hat{r}), \tag{B.20}$$

and therefore $\vec{Y}_{J \, \ell \, M}$ has parity $(-1)^\ell$. Next, as one may expect, there are many close relationships between the scalar and vector spherical harmonics. For example, the vector spherical harmonics can be obtained from the ordinary spherical harmonics by application of the unit vector $\hat{r}$

$$\hat{r} Y_{\ell M}(\hat{r}) = -\sqrt{\frac{\ell+1}{2\ell+1}} \vec{Y}_{\ell \, \ell+1 \, M}(\hat{r}) + \sqrt{\frac{\ell}{2\ell+1}} \vec{Y}_{\ell \, \ell-1 \, M}(\hat{r}), \tag{B.21}$$

or the gradient operator

$$\vec{\nabla}\left(f(r)Y_{\ell M}(\hat{r})\right) = -\sqrt{\frac{\ell+1}{2\ell+1}}\left(\frac{d}{dr}-\frac{\ell}{r}\right)f(r)\vec{Y}_{\ell\,\ell+1\,M}(\hat{r})$$
$$+\sqrt{\frac{\ell}{2\ell+1}}\left(\frac{d}{dr}+\frac{\ell+1}{r}\right)f(r)\vec{Y}_{\ell\,\ell-1\,M}(\hat{r}),$$

(B.22)

where $f(r)$ is any (well-behaved) scalar function. Conversely, the ordinary spherical harmonics arise through application of the divergence operator to the vector spherical harmonics

$$\vec{\nabla}\cdot\left(f(r)\vec{Y}_{\ell\,\ell+1\,M}(\hat{r})\right) = -\sqrt{\frac{\ell+1}{2\ell+1}}\left(\frac{d}{dr}+\frac{\ell+2}{r}\right)f(r)Y_{\ell M}(\hat{r})$$
$$\vec{\nabla}\cdot\left(f(r)\vec{Y}_{\ell\,\ell\,M}(\hat{r})\right) = 0,\ \text{for any}\ f(r)$$
$$\vec{\nabla}\cdot\left(f(r)\vec{Y}_{\ell\,\ell-1\,M}(\hat{r})\right) = \sqrt{\frac{\ell}{2\ell+1}}\left(\frac{d}{dr}-\frac{\ell-1}{r}\right)f(r)\ Y_{\ell M}(\hat{r}),$$

(B.23)

as well as the unit vector

$$\hat{r}\cdot\vec{Y}_{\ell\,\ell+1\,M}(\hat{r}) = -\sqrt{\frac{\ell+1}{2\ell+1}}Y_{\ell M}(\hat{r})$$
$$\hat{r}\cdot\vec{Y}_{\ell\,\ell\,M}(\hat{r}) = 0$$
$$\hat{r}\cdot\vec{Y}_{\ell\,\ell-1\,M}(\hat{r}) = \sqrt{\frac{\ell}{2\ell+1}}Y_{\ell M}(\hat{r}).$$

(B.24)

Finally, as the curl operator $\vec{\nabla}\times$ maps vector fields to vector fields, so it transforms the vector spherical harmonics among themselves:

$$\vec{\nabla}\times\left(f(r)\vec{Y}_{\ell\,\ell+1\,M}(\hat{r})\right) = i\sqrt{\frac{\ell}{2\ell+1}}\left(\frac{d}{dr}+\frac{\ell+2}{r}\right)f(r)\vec{Y}_{\ell\,\ell\,M}(\hat{r}),$$
$$\vec{\nabla}\times\left(f(r)\vec{Y}_{\ell\,\ell\,M}(\hat{r})\right) = i\sqrt{\frac{\ell}{2\ell+1}}\left(\frac{d}{dr}-\frac{\ell}{r}\right)f(r)\vec{Y}_{\ell\,\ell+1\,M}(\hat{r})$$
$$+i\sqrt{\frac{\ell+1}{2\ell+1}}\left(\frac{d}{dr}+\frac{\ell+1}{r}\right)f(r)\vec{Y}_{\ell\,\ell-1\,M}(\hat{r}),$$
$$\vec{\nabla}\times\left(f(r)\vec{Y}_{\ell\,\ell-1\,M}(\hat{r})\right) = i\sqrt{\frac{\ell+1}{2\ell+1}}\left(\frac{d}{dr}-\frac{\ell-1}{r}\right)f(r)\vec{Y}_{\ell\,\ell\,M}(\hat{r}).$$

(B.25)

Similarly,

$$\hat{r}\times\vec{Y}_{\ell\,\ell+1\,M}(\hat{r}) = i\sqrt{\frac{\ell}{2\ell+1}}\vec{Y}_{\ell\,\ell\,M}(\hat{r})$$
$$\hat{r}\times\vec{Y}_{\ell\,\ell\,M}(\hat{r}) = i\sqrt{\frac{\ell+1}{2\ell+1}}\vec{Y}_{\ell\,\ell-1\,M}(\hat{r})+i\sqrt{\frac{\ell}{2\ell+1}}\vec{Y}_{\ell\,\ell+1\,M}(\hat{r})$$
$$\hat{r}\times\vec{Y}_{\ell\,\ell-1\,M}(\hat{r}) = i\sqrt{\frac{\ell+1}{2\ell+1}}\vec{Y}_{\ell\,\ell\,M}(\hat{r}).$$

(B.26)

In this work, we often find that the scalar function is the regular spherical Bessel function of order ℓ, $f(r) = j_\ell(qr)$. It is useful to know the raising and lowering operators for the spherical Bessel functions

$$
\begin{aligned}
\left(\frac{d}{dr} - \frac{\ell}{r}\right) j_\ell(qr) &= -q j_{\ell+1}(qr), \\
\left(\frac{d}{dr} + \frac{\ell+1}{r}\right) j_\ell(qr) &= q j_{\ell-1}(qr).
\end{aligned}
\tag{B.27}
$$

Using these relations, we obtain the following expressions for the gradient and curl, specialized to the case $f(r) = j_\ell(qr)$:

$$
\begin{aligned}
\vec{\nabla}\left(j_\ell(qy) Y_{\ell\,M}(\hat{r})\right) &= q\left[\sqrt{\frac{\ell+1}{2\ell+1}} j_{\ell+1}(qr)\vec{Y}_{\ell\,\ell+1\,M}(\hat{r})\right. \\
&\qquad\left. + \sqrt{\frac{\ell}{2\ell+1}} j_{\ell-1}(qr)\vec{Y}_{\ell\,\ell-1\,M}(\hat{r})\right] \\
\vec{\nabla}\times\left(j_\ell(qr)\vec{Y}_{\ell\,\ell\,M}(\hat{r})\right) &= iq\left[-\sqrt{\frac{\ell}{2\ell+1}} j_{\ell+1}(qr)\vec{Y}_{\ell\,\ell+1\,M}(\hat{r})\right. \\
&\qquad\left. + \sqrt{\frac{\ell+1}{2\ell+1}} j_{\ell-1}(qr)\vec{Y}_{\ell\,\ell-1\,M}(\hat{r})\right].
\end{aligned}
\tag{B.28}
$$

We can invert these expressions to obtain

$$
\begin{aligned}
j_{\ell+1}(qr)\vec{Y}_{\ell\,\ell+1\,M}(\hat{r}) &= \frac{1}{q}\left[\sqrt{\frac{\ell+1}{2\ell+1}}\vec{\nabla}\left(j_\ell(qr)Y_{\ell\,M}(\hat{r})\right)\right. \\
&\qquad\left. + i\sqrt{\frac{\ell}{2\ell+1}}\vec{\nabla}\times\left(j_\ell(qr)\vec{Y}_{\ell\,\ell\,M}(\hat{r})\right)\right] \\
j_{\ell-1}(qr)\vec{Y}_{\ell\,\ell-1\,M}(\hat{r}) &= \frac{1}{q}\left[\sqrt{\frac{\ell}{2\ell+1}}\vec{\nabla}\left(j_\ell(qr)Y_{\ell\,M}(\hat{r})\right)\right. \\
&\qquad\left. - i\sqrt{\frac{\ell+1}{2\ell+1}}\vec{\nabla}\times\left(j_\ell(qr)\vec{Y}_{\ell\,\ell\,M}(\hat{r})\right)\right],
\end{aligned}
\tag{B.29}
$$

or equivalently

$$
\begin{aligned}
j_\ell(qr)\vec{Y}_{\ell-1\,\ell\,M}(\hat{r}) = \frac{1}{q}\Bigg[&\sqrt{\frac{\ell}{2\ell-1}}\vec{\nabla}\left(j_{\ell-1}(qr)Y_{\ell-1\,M}(\hat{r})\right) \\
&+ i\sqrt{\frac{\ell-1}{2\ell-1}}\vec{\nabla}\times\left(j_{\ell-1}(qr)\vec{Y}_{\ell-1\,\ell-1\,M}(\hat{r})\right)\Bigg] \\
j_\ell(qr)\vec{Y}_{\ell+1\,\ell\,M}(\hat{r}) = \frac{1}{q}\Bigg[&\sqrt{\frac{\ell+1}{2\ell+3}}\vec{\nabla}\left(j_{\ell+1}(qr)Y_{\ell+1\,M}(\hat{r})\right) \\
&- i\sqrt{\frac{\ell+2}{2\ell+3}}\vec{\nabla}\times\left(j_{\ell+1}(qr)\vec{Y}_{\ell+1\,\ell+1\,M}(\hat{r})\right)\Bigg],
\end{aligned}
\tag{B.30}
$$

The utility of these expressions is that the two vector fields $j_\ell(qr)\vec{Y}_{\ell\pm1\,\ell\,M}$ have been decomposed into longitudinal (curl-free) and transverse (divergence-free) components. The vector field $j_\ell(qr)\vec{Y}_{\ell\,\ell\,M}$ is inherently transverse [see Eq. (B.23)].

In general, a plane wave can be expanded in partial waves as

$$
e^{i\vec{q}\cdot\vec{r}} = 4\pi\sum_{L=0}^{\infty}i^L j_L(qr)Y_L(\hat{q})\odot Y_L(\hat{r}).
\tag{B.31}
$$

If we define our basis so that $\hat{z}$ is along the direction of $\hat{q}$, then the plane wave expansion takes the form

$$
e^{i\vec{q}\cdot\vec{r}} = \sum_{L=0}^{\infty}\sqrt{4\pi(2L+1)}i^L j_L(qr)Y_{L0}(\hat{r}).
\tag{B.32}
$$

Defining the multipole projection functions

$$
\begin{aligned}
M_{JM}(q\vec{r}) &\equiv j_J(qr)Y_{JM}(\hat{r}) \\
\vec{M}_{JLM}(q\vec{r}) &\equiv j_L(qr)\vec{Y}_{JLM}(\hat{r})
\end{aligned}
\tag{B.33}
$$

we find that the expansion of a plane wave times a vector field can be written as

$$
e^{i\vec{q}\cdot\vec{r}}\hat{e}_\lambda = -\sum_{L=1}^{\infty}\sqrt{2\pi(2L+1)}i^L\left[\lambda\vec{M}_{LL\lambda}(q\vec{r}) + \frac{1}{q}\vec{\nabla}\times\vec{M}_{LL\lambda}(q\vec{r})\right]
\tag{B.34}
$$

for $\lambda = \pm1$, whereas when $\lambda = 0$ we have

$$
e^{i\vec{q}\cdot\vec{r}}\hat{e}_0 = -\frac{i}{q}\sum_{L=0}^{\infty}\sqrt{4\pi(2L+1)}i^L\vec{\nabla}M_{J0}(q\vec{r}).
\tag{B.35}
$$

We identify the basic multipole projections: an arbitrary charge $\rho(\vec{r})$ can be decomposed into component with good angular momentum

$$
\mathcal{M}_{JM}(q) = \int d^3r\, M_{JM}(q\vec{r})\rho(\vec{r})
\tag{B.36}
$$

whereas an arbitrary three-current $\vec{J}(\vec{r})$ admits three independent projections

$$
\begin{aligned}
\mathcal{L}_{JM}(q) &= \frac{i}{q} \int d^3r \, \left[\vec{\nabla} M_{JM}(q\vec{r}) \right] \cdot \vec{J}(\vec{r}) \\
\mathcal{T}_{JM}^{\text{el}}(q) &= \frac{1}{q} \int d^3r \, \left[\vec{\nabla} \times \vec{M}_{JJM}(q\vec{r}) \right] \cdot \vec{J}(\vec{r}) \\
\mathcal{T}_{JM}^{\text{mag}}(q) &= \int d^3r \, \vec{M}_{JJM}(q\vec{r}) \cdot \vec{J}(\vec{r}).
\end{aligned}
\tag{B.37}
$$

Appendix C

Nuclear Matrix Elements of Few-body Operators

In order to make contact with $\mu \to e$ conversion experiments, the underlying nuclear operators must be evaluated between many-body wave functions that accurately capture the detailed structure of the target nucleus. Although many competing methods for these evaluations exist, our preferred paradigm is that of the nuclear shell model. In the shell-model approach, the total nuclear wave function is composed of linear combinations of Slater determinant basis elements. Each Slater determinant is a totally anti-symmetric combination of single-particle harmonic oscillator states labeled by nodal quantum number n, orbital angular momentum ℓ, spin $s = 1/2$, total angular momentum $j = \ell \pm 1/2$, and corresponding magnetic quantum number m. Separate Slater determinants are constructed for neutron and proton degrees of freedom, which are distinguished by the isospin quantum number $m_t = +1/2$ ($-1/2$) for protons (neutrons).

Having specified the basis, the required wave functions are obtained by diagonalizing a suitable Hamiltonian that describes the interactions among the nucleons. One encounters several difficulties in this construction: first, the exact form of these interactions—which contains two-body, three-body, and higher contributions—is not known precisely; the proper theory is that specified by quantum chromodynamics (QCD), which does not lend itself to a simple description in the strongly-coupled regime of nuclear physics. Second, the shell-model space that we have adopted must be severely truncated in practical calculations, requiring one to perform a program of operator and wave function renormalization. These complications can be avoided by abandoning efforts to root the calculation of the nuclear wave function in the first-principles of QCD and instead adopting a phenomenological interaction that has been tuned in the model space to reproduce low-energy nuclear observables such as charge radii and low-lying spectra. This is the strategy that we apply in work. The interactions and shell-model spaces that we employ are given in Table 3.2.

Having thus obtained the nuclear wave functions, there remains a significant computational task in evaluating matrix elements of few-body operators. A well-organized approach is required to avoid unnecessary effort and potential confusion. By formulating the problem in terms of irreducible tensor operators and exploiting the good angular momentum J and (approximate) isospin T quantum numbers of the nuclear ground state, we are able to factorize many-body matrix elements of few-body operators in terms of few-body matrix elements,

extracting from the total nuclear wave function only that nuclear structure information that is required to evaluate the few-body operators under consideration. In this appendix, we will demonstrate how this factorization is performed for one- and two-body operators.

C.1 One-body Density Matrices

The total one-body tensor operator for a system of A nucleons can be written in the coordinate representation as

$$\mathcal{O}_{JM} = \sum_{i=1}^{A} \mathcal{O}_{JM}(\vec{x}_i), \tag{C.1}$$

or in the second-quantized form as

$$\mathcal{O}_{JM} = \sum_{\alpha,\beta} \mathcal{O}_{JM}^{\alpha\beta} c_\alpha^\dagger c_\beta, \tag{C.2}$$

with

$$\mathcal{O}_{JM}^{\alpha\beta} \equiv \langle \alpha | \mathcal{O}_{JM} | \beta \rangle = \int d^3x \; \phi_\alpha^\dagger(\vec{x}) \mathcal{O}_{JM}(\vec{x}) \phi_\beta(\vec{x}). \tag{C.3}$$

The summation α extends to all single-particle states; for harmonic oscillator states, $\alpha = (n_\alpha, \ell_\alpha, j_\alpha, m_\alpha)$. The operators and the states may carry additional isospin quantum numbers, which we suppress here for brevity (the generalization to include isospin is straightforward).

Our aim is to evaluate the given operator for a total nuclear wave function. The nuclear response can be factorized into a piece that describes how the operator acts on single-particle states and a piece that encodes how the single-particle states are embedded in the initial and final nuclear wave functions. The latter quantity is known as the one-body density matrix. An expression for the one-body density matrix can be obtained directly from the second-quantized form of a one-body operator operator:

$$\begin{aligned} \langle J_f || \mathcal{O}_J || J_i \rangle &= \sum_{a,b} \frac{1}{\sqrt{2J+1}} \langle J_f || \left[c_a^\dagger \otimes \tilde{c}_b \right]_J || J_i \rangle \langle a || \mathcal{O}_J || b \rangle \\ &\equiv \sum_{a,b} \rho_{ab}^{f,i;J} \langle a || \mathcal{O}_J || b \rangle, \end{aligned} \tag{C.4}$$

where we have defined the reduced one-body density matrix

$$\rho_{ab}^{f,i;J} \equiv \frac{1}{\sqrt{2J+1}} \langle J_f || \left[c_a^\dagger \otimes \tilde{c}_b \right]_J || J_i \rangle, \tag{C.5}$$

and introduced the time-reversed annihilation operator

$$\tilde{c}_b = \tilde{c}_{j_b,m_b} = (-1)^{j_b+m_b} c_{j_b,-m_b}. \tag{C.6}$$

The summation in Eq. (C.4) is over single-particle orbits a, b, which do not carry magnetic angular momentum quantum numbers, as all of the matrix elements have been reduced. Thus the problem of computing many-body matrix elements of single-nucleon operators has been

reduced in terms of single-nucleon matrix elements. Assuming that one has obtained the initial and final nuclear wave functions in a Slater-determinant basis, it is straightforward— though perhaps computationally intensive—to obtain the desired one-body density matrix. No approximation has been made in deriving Eq. (C.4); when summed over a complete basis of single-particle states, the product of the one-body density matrix and the corresponding single-particle matrix element exactly reproduces the many-body matrix element of any one-body operator. In practical computations, the single-particle basis is truncated, introducing some error (that is typically difficult to quantify).

Restoring the isospin quantum numbers, we may define the doubly-reduced one-body density matrix by

$$\rho_{ab}^{f,i;J,T} \equiv \frac{1}{\sqrt{2J+1}}\frac{1}{\sqrt{2T+1}} \langle J_f; T_f \; \vdots\vdots \; \left[c_a^\dagger \otimes \tilde{c}_b \right]_{J,T} \; \vdots\vdots \; J_i; T_i \rangle , \tag{C.7}$$

where the time-reversed annihilation operator now satisfies

$$\tilde{c}_b = \tilde{c}_{j_b, m_b; \frac{1}{2}, m_{tb}} = (-1)^{j_b + m_b + 1/2 + m_{tb}} c_{j_b, -m_b; \frac{1}{2}, -m_{tb}}. \tag{C.8}$$

The doubly-reduced density matrix allows for efficient calculation of the doubly-reduced matrix element

$$\langle J_f; T_f \; \vdots\vdots \; \mathcal{O}_{J,T} \; \vdots\vdots \; J_i; T_i \rangle = \sum_{a,b} \rho_{ab}^{f,i;J,T} \langle a \; \vdots\vdots \; \mathcal{O}_{J,T} \; \vdots\vdots \; b \rangle . \tag{C.9}$$

C.2 Two-body Density Matrices

The total two-body operator for a nuclear system can be written in the coordinate representation as

$$\mathcal{O}_{J,M} = \sum_{i<j} \mathcal{O}_{J,M} (\vec{x}_i, \vec{x}_j) = \frac{1}{2} \sum_{i \neq j} \mathcal{O}_{J,M}(\vec{x}_i, \vec{x}_j), \tag{C.10}$$

or in the occupation number representation as

$$\mathcal{O}_{J,M} = \frac{1}{2} \sum_{\alpha\beta\gamma\delta} \mathcal{O}_{J,M}^{\alpha\beta\gamma\delta} c_\alpha^\dagger c_\beta^\dagger c_\delta c_\gamma, \tag{C.11}$$

where

$$\mathcal{O}_{J,M}^{\alpha\beta\gamma\delta} \equiv \int d^3\vec{x}_1 d^3\vec{x}_2 \; \phi_\alpha^\dagger(\vec{x}_1)\phi_\beta^\dagger(\vec{x}_2)\mathcal{O}_{J,M}(\vec{x}_1, \vec{x}_2) \phi_\gamma(\vec{x}_1)\phi_\delta(\vec{x}_2). \tag{C.12}$$

In the occupation number representation, the operator can also be written in terms of anti-symmetrized matrix elements

$$\mathcal{O}_{J,M} = \frac{1}{4} \sum_{abcd} \bar{\mathcal{O}}_{J,M}^{\alpha\beta\gamma\delta} c_\alpha^\dagger c_\beta^\dagger c_\delta c_\gamma, \tag{C.13}$$

where

$$\bar{\mathcal{O}}_{J,M}^{\alpha\beta\gamma\delta} \equiv \mathcal{O}_{J,M}^{\alpha\beta\gamma\delta} - \mathcal{O}_{J,M}^{\alpha\beta\delta\gamma}. \tag{C.14}$$

Defining two-particle states by

$$|\alpha\beta\rangle = c_\alpha^\dagger c_\beta^\dagger |0\rangle , \tag{C.15}$$

we write

$$\bar{\mathcal{O}}_{J,M}^{\alpha\beta\gamma\delta} = \langle\alpha\beta|\mathcal{O}_{J,M}|\gamma\delta\rangle . \tag{C.16}$$

We wish to compute many-body expectation values in terms of two-particle states coupled to good total angular momentum; that is, we define the two-body density matrix by

$$\langle J_f||\mathcal{O}_J||J_i\rangle = \sum_{abcd}\sum_{J_{ab}J_{cd}} \rho_{abcd}^{f,i,J;J_{ab},J_{cd}} \langle ab; J_{ab}||\mathcal{O}_J||cd; J_{cd}\rangle , \tag{C.17}$$

where the normalized two-particle coupled states are defined as

$$|a\,b; J, M\rangle = \mathcal{N}_{ab}(J) \left[c_a^\dagger c_b^\dagger\right]_{J,M} |0\rangle , \tag{C.18}$$

where $|0\rangle$ is a suitable vacuum state and the normalization factor is given by

$$\mathcal{N}_{ab}(J) \equiv \frac{\sqrt{1 - \delta_{ab}(-1)^J}}{1 + \delta_{ab}} . \tag{C.19}$$

The form of the coupled, reduced two-body density matrix follows from inserting the second-quantized form of the operator into Eq. (C.17):

$$\rho_{abcd}^{f,i,J;J_{ab}J_{cd}} = \frac{1}{4} \frac{(-1)^{J_c+J_d-J_{cd}}}{\sqrt{2J+1}} \langle J_f|| \left[[c_a^\dagger \otimes c_b^\dagger]_{J_{ab}} \otimes [\tilde{c}_d \otimes \tilde{c}_c]_{J_{cd}} \right]_J ||J_i\rangle . \tag{C.20}$$

As in the one-body case, prior to truncating the summation over single-particle states, Eq. (C.17) exactly reproduces the many-body matrix element of any two-body operator. The preceding section can be generalized in a straightforward manner to include isospin.

Appendix D

Single-nucleon Response Functions

The 11 single-nucleon response functions through order $1/m_N^2$ are given in Eq. (3.19). One would like to evaluate matrix elements of these operators between nuclear wave functions corresponding to the chosen nuclear target. In Appendix C, we demonstrated how total nuclear matrix elements of one-body operators can be factorized in terms of single-particle matrix elements multiplied by the relevant one-body density matrix. In this section, we discuss how to evaluate the single-particle matrix elements of the 11 multipole operators when the single-particle states are elements of a harmonic oscillator basis.

The basic operators from which the multipole responses are constructed are $M_{JM}(q\vec{r})$, $\vec{M}_{J\,L\,M}(q\vec{r})$, $\vec{M}_{J\,L\,M}(q\vec{r}) \cdot \frac{1}{q}\vec{\nabla}$, $M_{JM}(q\vec{r})\,\vec{\sigma} \cdot \frac{1}{q}\vec{\nabla}$, and $\vec{M}_{J\,L\,M}(q\vec{r}) \cdot \left(\vec{\sigma} \times \frac{1}{q}\vec{\nabla}\right)$. Matrix elements of the standard charge multipole and the projections of the spin current are relatively straightforward

$$
\begin{aligned}
\langle n'\,(\ell'\,1/2)\,j'||M_J(q\vec{r})||n\,(\ell\,1/2)\,j\rangle = {} & \frac{1}{\sqrt{4\pi}}(-1)^{J+j+1/2}[\ell'][\ell][j'][j][J] \\
& \times \left\{ \begin{array}{ccc} \ell' & j' & \frac{1}{2} \\ j & \ell & J \end{array} \right\} \left(\begin{array}{ccc} \ell' & J & \ell \\ 0 & 0 & 0 \end{array} \right) \langle n'\ell'|j_J(\rho)|n\ell\rangle ,
\end{aligned}
\tag{D.1}
$$

and

$$
\begin{aligned}
\langle n'\,(\ell'\,1/2)\,j'||\vec{M}_{J\,L}(q\vec{r}) \cdot \vec{\sigma}||n\,(\ell\,1/2)\,j\rangle = {} & \frac{\sqrt{6}}{\sqrt{4\pi}}(-1)^{\ell'}[\ell'][\ell][j'][j][L][J] \\
& \times \left\{ \begin{array}{ccc} \ell' & \ell & L \\ \frac{1}{2} & \frac{1}{2} & 1 \\ j' & j & J \end{array} \right\} \left(\begin{array}{ccc} \ell' & L & \ell \\ 0 & 0 & 0 \end{array} \right) \langle n'\ell'|j_L(\rho)|n\ell\rangle ,
\end{aligned}
\tag{D.2}
$$

where $[J] = \sqrt{2J+1}$ and $\rho = qr$. The radial matrix elements are computed in terms of radial harmonic oscillator wave functions

$$
\langle n'\ell'|j_L(\rho)|n\ell\rangle = \int_0^\infty dr \; r^2 H_{n'\ell'}(r) j_L(qr) H_{n\ell}(r).
\tag{D.3}
$$

We note that in Eq. (D.1), the 3-j symbol implies that $(-1)^{J+\ell'+\ell} = +1$ or equivalently $J + \ell' + \ell$ is even. Similarly in Eq. (D.2), $L + \ell' + \ell$ must be even. This constraint is

imposed by the parity transformation of the underlying multipole operator. The fact that $L + \ell' + \ell$ is even for these operators is crucial to demonstrating that the radial matrix element $\langle n'\ell'|j_L(\rho)|n\ell\rangle$ is a polynomial in $y = (qb/2)^2$. Next we consider the projections of the convection current

$$
\langle n'\,(\ell'\,1/2)\,j'||\vec{M}_{J\,L}(q\vec{r}) \cdot \frac{1}{q}\vec{\nabla}||n\,(\ell\,1/2)\,j\rangle = \frac{1}{\sqrt{4\pi}}(-1)^{L+j+1/2}[\ell'][j'][j][L][J]\begin{Bmatrix} \ell' & j' & \frac{1}{2} \\ j & \ell & J \end{Bmatrix}
$$

$$
\times \left[-\sqrt{\ell+1}[\ell+1]\begin{Bmatrix} L & 1 & J \\ \ell & \ell' & \ell+1 \end{Bmatrix}\begin{pmatrix} \ell' & L & \ell+1 \\ 0 & 0 & 0 \end{pmatrix} \langle n'\ell'|j_L(\rho)\left(\frac{d}{d\rho} - \frac{\ell}{\rho}\right)|n\ell\rangle \right.
$$

$$
\left. + \sqrt{\ell}[\ell-1]\begin{Bmatrix} L & 1 & J \\ \ell & \ell' & \ell-1 \end{Bmatrix}\begin{pmatrix} \ell' & L & \ell-1 \\ 0 & 0 & 0 \end{pmatrix} \langle n'\ell'|j_L(\rho)\left(\frac{d}{d\rho} + \frac{\ell+1}{\rho}\right)|n\ell\rangle \right]
$$

$$
(D.4)
$$

Here the 3-j symbols imply that $L + \ell' + \ell$ must be odd. The Coulomb multipoles of the axial charge operator can be evaluated as

$$
\langle n'\,(\ell'\,1/2)\,j'||M_J(q\vec{r})\vec{\sigma} \cdot \frac{1}{q}\vec{\nabla}||n\,(\ell\,1/2)\,j\rangle
$$

$$
= \frac{1}{\sqrt{4\pi}}(-1)^{\ell'}[\ell'][j'][j][2j-\ell][J]\begin{Bmatrix} \ell' & j' & \frac{1}{2} \\ j & 2j-\ell & J \end{Bmatrix}\begin{pmatrix} \ell' & J & 2j-\ell \\ 0 & 0 & 0 \end{pmatrix}
$$

$$
\times \left[-\delta_{j,\ell+1/2}\langle n'\ell'|j_J(\rho)\left(\frac{d}{d\rho} - \frac{\ell}{\rho}\right)|n\ell\rangle + \delta_{j,\ell-1/2}\langle n'\ell'|j_J(\rho)\left(\frac{d}{d\rho} + \frac{\ell+1}{\rho}\right)|n\ell\rangle \right],
$$

$$
(D.5)
$$

where again we find $J + \ell' + \ell$ is odd. For the multipoles Φ_J, Φ'_J, and Φ''_J, we reorganize

$$
\vec{M}_{J\,L\,M} \cdot \left(\vec{\sigma} \times \vec{\nabla}\right) = -i\sqrt{6}\sum_K (-1)^{K+L}\sqrt{2K+1}\begin{Bmatrix} 1 & 1 & 1 \\ J & K & L \end{Bmatrix}\left[\vec{\sigma} \otimes \left[Y_L \otimes \vec{\nabla}\right]_K\right]_{J,M} \quad (D.6)
$$

Then the projections of the spin-velocity current are

$$
\langle n'\,(\ell\,1/2)\,j'||\vec{M}_{J\,L}(q\vec{r}) \cdot \left(\vec{\sigma} \times \frac{1}{q}\vec{\nabla}\right)||n\,(\ell\,1/2)\,j\rangle
$$

$$
= \frac{i}{\sqrt{4\pi}}(-1)^{L+J+\ell}6[l'][j'][j][L][J] \sum_{K=J-1}^{J+1} (-1)^K[K]\begin{Bmatrix} \ell' & \ell & K \\ \frac{1}{2} & \frac{1}{2} & 1 \\ j' & j & J \end{Bmatrix}\begin{Bmatrix} 1 & 1 & 1 \\ J & K & L \end{Bmatrix}
$$

$$
\times \left[\sqrt{\ell+1}[\ell+1]\begin{Bmatrix} L & 1 & K \\ \ell & \ell' & \ell+1 \end{Bmatrix}\begin{pmatrix} \ell' & L & \ell+1 \\ 0 & 0 & 0 \end{pmatrix} \langle n'\ell'|j_L(\rho)\left(\frac{d}{d\rho} - \frac{\ell}{\rho}\right)|n\ell\rangle \right.
$$

$$
\left. - \sqrt{\ell}[\ell-1]\begin{Bmatrix} L & 1 & K \\ \ell & \ell' & \ell-1 \end{Bmatrix}\begin{pmatrix} \ell' & L & \ell-1 \\ 0 & 0 & 0 \end{pmatrix} \langle n'\ell'|j_L(\rho)\left(\frac{d}{d\rho} + \frac{\ell+1}{\rho}\right)|n\ell\rangle \right]
$$

$$
(D.7)
$$

and $L + \ell' + \ell$ is odd. Therefore, each of the 11 single-nucleon multipole operators can be computed in terms of a product of angular momentum factors and one of three radial matrix

elements

$$\langle n'\ell'|j_L(\rho)|n\ell\rangle,$$

$$\langle n'\ell'|j_L(\rho)\left(\frac{d}{d\rho}-\frac{\ell}{\rho}\right)|n\ell\rangle,$$

$$\langle n'\ell'|j_L(\rho)\left(\frac{d}{d\rho}+\frac{\ell+1}{\rho}\right)|n\ell\rangle \qquad (D.8)$$

The radial harmonic oscillator wave functions are given in terms of generalized Laguerre polynomials as

$$H_{n,\ell}(x) = \sqrt{\frac{2\Gamma(n)}{\Gamma(n+\ell+1/2)}}e^{-x^2/2}x^\ell L_{n-1}^{\ell+1/2}(x^2), \qquad (D.9)$$

where the coordinate $x = r/b$ is dimensionless. The harmonic oscillator radial wave functions satisfy recurrence relations that can be used to express states with $n > 1$ in terms of states with $n = 1$ and various ℓ. Explicitly, for $n = 2$ and $n = 3$ we have

$$H_{2\ell}(x) = \frac{1}{\sqrt{2}}\left\{[\ell+1]H_{1\ell}(x) - [\ell+2]H_{1\ell+2}(x)\right\}$$

$$H_{3\ell}(x) = \frac{1}{\sqrt{8}}\left\{[\ell+1][\ell+2]R_{1\ell}(x) - 2[\ell+2]^2 R_{1\ell+2}(x) + [\ell+3][\ell+4]R_{1\ell+4}(x)\right\} \qquad (D.10)$$

Note that the recurrence relation conserves the parity of ℓ. After using the recurrence relation to obtain $n = 1$ states, we can apply the derivative operators as

$$\left(\frac{d}{d\rho}-\frac{\ell}{\rho}\right)R_{1\ell}(x) = -\frac{1}{\sqrt{8y}}[\ell+1]R_{1\ell+1}(x)$$

$$\left(\frac{d}{d\rho}+\frac{\ell+1}{\rho}\right)R_{1\ell}(x) = \frac{1}{\sqrt{8y}}\left\{2[\ell]R_{1\ell-1}(x) - [\ell+1]R_{1\ell+1}(x)\right\}, \qquad (D.11)$$

where the parity of the state is now changed as $\ell \to \ell \pm 1$. With these relations in hand, the only matrix element that we need to explicitly compute is

$$\langle 1\ell'|j_L(\rho)|1\ell\rangle = \frac{(2y)^{L/2}e^{-y}(L+\ell'+\ell+1)!!}{(2L+1)!!\left[(2\ell'+1)!!(2\ell+1)!!\right]^{1/2}}\,_1F_1\left(\frac{L-\ell'-\ell}{2};L+\frac{3}{2};y\right) \qquad (D.12)$$

The crucial observation is that the confluent hypergeometric function

$$_1F_1(\alpha;\beta;y) = 1 + \frac{\alpha}{\beta}y + \frac{\alpha(\alpha+1)}{\beta(\beta+1)}\frac{y^2}{2!} + \dots \qquad (D.13)$$

terminates at finite order whenever $\alpha = (L-\ell'-\ell)/2$ is a non-positive integer. Therefore, letting $T_J(q\vec{r})$ represent any of the 11 single-particle multipole operators,

$$\langle n'\,(\ell'\,1/2)\,j'||T_J(q\vec{r})||n\,(\ell\,1/2)\,j\rangle = \frac{1}{\sqrt{4\pi}}y^{(J-K)/2}e^{-y}p(y), \qquad (D.14)$$

where $K = 2$ for the normal parity operators M, Δ', Σ, Φ', and Φ'', and where $K = 1$ for the abnormal parity operators Δ, Σ', Σ'', Ω, and Φ.

In addition to the recurrence relations, we can derive closed-form expressions for the matrix elements. The Laguerre polynomial can be expanded as

$$L_{n-1}^{\ell+1/2}(x^2) = \sum_{i=0}^{n-1} \begin{pmatrix} n + \ell - 1/2 \\ n - i - 1 \end{pmatrix} \frac{(-1)^i}{i!} x^{2i} \tag{D.15}$$

The required radial integrals are of the form

$$I_L(m, y) \equiv \int_0^\infty dx\, x^m e^{-x^2} j_L(qbx)$$
$$= \frac{\sqrt{\pi}}{4} y^{L/2} e^{-y} \frac{\Gamma\left(\frac{1}{2}(L + m + 1)\right)}{\Gamma(L + 3/2)} \,{}_1F_1\left(1 + \frac{L - m}{2}; L + \frac{3}{2}; y\right), \tag{D.16}$$

which converges for $L + m > -1$. Here the confluent hypergeometric function appears with parameter $\alpha = 1 + (L - m)/2$. As we see below, for the physically relevant values of m, α is always a non-positive integer and therefore the summation terminates at order α. The radial matrix elements can then be expressed in terms of the basic integral $I_L(m, y)$ as

$$\langle n'\ell'|j_L(\rho)|n\ell\rangle = \sqrt{\frac{2\Gamma(n')}{\Gamma(n' + \ell' + 1/2)} \frac{2\Gamma(n)}{\Gamma(n + \ell + 1/2)}} \sum_{i=0}^{n'-1} \sum_{j=0}^{n-1} \begin{pmatrix} n' + \ell' - 1/2 \\ n' - i - 1 \end{pmatrix}$$
$$\times \begin{pmatrix} n + \ell - 1/2 \\ n - j - 1 \end{pmatrix} \frac{(-1)^{i+j}}{i!j!} I_L\left(2 + 2i + 2j + \ell' + \ell, y\right), \tag{D.17}$$

$$\langle n'\ell'|j_L(\rho)\left(\frac{d}{d\rho} - \frac{\ell}{\rho}\right)|n\ell\rangle = \sqrt{\frac{2\Gamma(n')}{\Gamma(n' + \ell' + 1/2)} \frac{2\Gamma(n)}{\Gamma(n + \ell + 1/2)}} \sum_{i=0}^{n'-1} \sum_{j=0}^{n-1} \begin{pmatrix} n' + \ell' - 1/2 \\ n' - i - 1 \end{pmatrix}$$
$$\times \begin{pmatrix} n + \ell - 1/2 \\ n - j - 1 \end{pmatrix} \frac{(-1)^{i+j}}{i!j!} [2j I_L\left(1 + 2i + 2j + \ell' + \ell, y\right) - I_L\left(3 + 2i + 2j + \ell' + \ell, y\right)], \tag{D.18}$$

$$\langle n'\ell'|j_L(\rho)\left(\frac{d}{d\rho} + \frac{\ell + 1}{\rho}\right)|n\ell\rangle = \sqrt{\frac{2\Gamma(n')}{\Gamma(n' + \ell' + 1/2)} \frac{2\Gamma(n)}{\Gamma(n + \ell + 1/2)}} \sum_{i=0}^{n'-1} \sum_{j=0}^{n-1} \begin{pmatrix} n' + \ell' - 1/2 \\ n' - i - 1 \end{pmatrix}$$
$$\times \begin{pmatrix} n + \ell - 1/2 \\ n - j - 1 \end{pmatrix} \frac{(-1)^{i+j}}{i!j!} \Bigg[(2j + 2\ell + 1) I_L\left(1 + 2i + 2j + \ell' + \ell, y\right)$$
$$- I_L\left(3 + 2i + 2j + \ell' + \ell, y\right) \Bigg]. \tag{D.19}$$

D.1 Operators Generated by the Muon's Lower Component

In Chapter 7, we found that the inclusion of the muon's lower Dirac component leads to the introduction of new nuclear multipole operators. We will now discuss how single-particle

matrix elements of these operators can be evaluated in a harmonic oscillator basis. Matrix elements of the modified charge multipoles are relatively straightforward to compute, only the radial matrix element differs from the standard result:

$$
\langle n'\,(\ell'\,1/2)\,j'||M_J^{(1)}(q\vec{r})||n\,(\ell\,1/2)\,j\rangle = \frac{1}{\sqrt{4\pi}}(-1)^{J+j+1/2}[\ell'][\ell][j'][j][J]\sqrt{J(J+1)}
$$
$$
\times \begin{Bmatrix} \ell' & j' & \frac{1}{2} \\ j & \ell & J \end{Bmatrix} \begin{pmatrix} \ell' & J & \ell \\ 0 & 0 & 0 \end{pmatrix} \langle n'\ell'|\frac{1}{\rho}j_J(\rho)|n\ell\rangle,
$$

(D.20)

$$
\langle n'\,(\ell'\,1/2)\,j'||M_J^{(2)}(q\vec{r})||n\,(\ell\,1/2)\,j\rangle = \frac{1}{\sqrt{4\pi}}(-1)^{J+j+1/2}[\ell'][\ell][j'][j][J]
$$
$$
\times \begin{Bmatrix} \ell' & j' & \frac{1}{2} \\ j & \ell & J \end{Bmatrix} \begin{pmatrix} \ell' & J & \ell \\ 0 & 0 & 0 \end{pmatrix} \langle n'\ell'|\frac{dj_J(\rho)}{d\rho}|n\ell\rangle.
$$

(D.21)

In both cases, the 3-j symbols imply that $J + \ell' + \ell$ is even. In order to compute matrix elements of the modified spin projections $\Sigma'^{(0)}$ and $\Sigma''^{(0)}$, we define the operator

$$
\vec{M}^{(0)}_{J\,L\,M}(q\vec{r}) \equiv j_J(qr)\vec{Y}_{J\,L\,M}(\hat{r}),
$$

(D.22)

which differs from the familiar operator $\vec{M}_{J\,L\,M}$ in that the order of the Bessel function is J rather than L. The matrix elements are modified accordingly

$$
\langle n'\,(\ell'\,1/2)\,j'||\vec{M}^{(0)}_{J\,L}(q\vec{r})\cdot\vec{\sigma}||n\,(\ell\,1/2)\,j\rangle = \frac{\sqrt{6}}{\sqrt{4\pi}}(-1)^{\ell'}[\ell'][\ell][j'][j][L][J]
$$
$$
\times \begin{Bmatrix} \ell' & \ell & L \\ \frac{1}{2} & \frac{1}{2} & 1 \\ j' & j & J \end{Bmatrix} \begin{pmatrix} \ell' & L & \ell \\ 0 & 0 & 0 \end{pmatrix} \langle n'\ell'|j_J(\rho)|n\ell\rangle,
$$

(D.23)

where the 3-j symbol implies that $L + \ell' + \ell$ is even. In order to compute matrix elements of the modified spin projections $\Sigma'^{(2)}$ and $\Sigma''^{(2)}$, we define

$$
\vec{M}^{(2)}_{J\,L\,M}(q\vec{r}) \equiv \frac{dj_L(qr)}{dqr}\,\vec{Y}_{J\,L\,M}(\hat{r}).
$$

(D.24)

Again, only the radial matrix element is altered

$$
\langle n'\,(\ell'\,1/2)\,j'||\vec{M}^{(2)}_{J\,L}(q\vec{r})\cdot\vec{\sigma}||n\,(\ell\,1/2)\,j\rangle = \frac{\sqrt{6}}{\sqrt{4\pi}}(-1)^{\ell'}[\ell'][\ell][j'][j][L][J]
$$
$$
\times \begin{Bmatrix} \ell' & \ell & L \\ \frac{1}{2} & \frac{1}{2} & 1 \\ j' & j & J \end{Bmatrix} \begin{pmatrix} \ell' & L & \ell \\ 0 & 0 & 0 \end{pmatrix} \langle n'\ell'|\frac{dj_L(\rho)}{d\rho}|n\ell\rangle,
$$

(D.25)

and $L + \ell' + \ell$ is even. We find that two new radial matrix elements are needed in the evaluation of the lower-component operators. They can be expressed in terms of the quantity $I_L(m, y)$ [see Eq. (D.16)]

$$
\begin{aligned}
\langle n'\ell'|\frac{1}{\rho}j_L(\rho)|n\ell\rangle &= \sqrt{\frac{2\Gamma(n')}{\Gamma(n'+\ell'+1/2)}\frac{2\Gamma(n)}{\Gamma(n+\ell+1/2)}} \sum_{i=0}^{n'-1}\sum_{j=0}^{n-1} \begin{pmatrix} n'+\ell'-1/2 \\ n'-i-1 \end{pmatrix} \\
&\times \begin{pmatrix} n+\ell-1/2 \\ n-j-1 \end{pmatrix} \frac{(-1)^{i+j}}{i!j!}\frac{1}{2\sqrt{y}}I_L\left(1+2i+2j+\ell'+\ell,y\right),
\end{aligned}
\tag{D.26}
$$

$$
\begin{aligned}
\langle n'\ell'|\frac{dj_L(\rho)}{d\rho}|n\ell\rangle &= \sqrt{\frac{2\Gamma(n')}{\Gamma(n'+\ell'+1/2)}\frac{2\Gamma(n)}{\Gamma(n+\ell+1/2)}} \sum_{i=0}^{n'-1}\sum_{j=0}^{n-1} \begin{pmatrix} n'+\ell'-1/2 \\ n'-i-1 \end{pmatrix} \\
&\times \begin{pmatrix} n+\ell-1/2 \\ n-j-1 \end{pmatrix} \frac{(-1)^{i+j}}{i!j!}\frac{1}{2L+1}\Bigg[LI_{L-1}\left(2+2i+2j+\ell'+\ell,y\right) \\
&\qquad - (L+1)I_{L+1}\left(2+2i+2j+\ell'+\ell,y\right)\Bigg].
\end{aligned}
\tag{D.27}
$$

In the previous section, we found that, for all physically-allowed values of ℓ, ℓ', and L, the argument α of the hypergeometric function ${}_1F_1(\alpha; \beta; y)$ is a non-positive integer, yielding a finite polynomial in y. In the present case, this is no longer true. In fact, we find that, for all relevant values of the angular momenta, $\alpha = 1/2 - k$ for some $k \geq 0$. As a result, the hypergeometric sum in Eq. (D.13) does not terminate at any finite order. Therefore, matrix elements of the lower-component operators do not admit a simplified expression of the form in Eq. (D.14). Nonetheless, the hypergeometric function can be numerically evaluated to high precision.

Appendix E

Fermi Gas Average

In the Fermi Gas Average (FGA) approach, we choose a target nucleon and sum over its interaction with a spin and isospin symmetric core. The core nucleons occupy momentum states up to the nuclear Fermi momentum k_F. Starting from a two-nucleon operator $\mathcal{O}^{(2)}$, an effective one-body operator is obtained by performing a mean-field-like sum over direct and exchange terms

$$\langle \alpha | \mathcal{O}^{(1)} | \beta \rangle \equiv \sum_{\gamma} \langle \alpha\gamma | \mathcal{O}^{(2)} | \beta\gamma \rangle - \langle \alpha\gamma | \mathcal{O}^{(2)} | \gamma\beta \rangle \,, \tag{E.1}$$

where γ sums over occupied core states. Each core state is a direct product of space, spin, and isospin components

$$|\alpha\rangle = |\vec{p}(\alpha)\rangle \otimes |\frac{1}{2}m_s(\alpha)\rangle \otimes |\frac{1}{2}m_t(\alpha)\rangle \,. \tag{E.2}$$

Therefore, the summations over space, spin, and isospin components can be performed independently. The two-nucleon operator that arises in scalar-mediated coherent $\mu \to e$ conversion has the form

$$\mathcal{O}^{(2)} = \frac{\vec{q}_1 \cdot \vec{\sigma}(1)}{|\vec{q}_1|^2 + m_\pi^2} \frac{\vec{q}_2 \cdot \vec{\sigma}(2)}{|\vec{q}_2|^2 + m_\pi^2} \vec{\tau}(1) \cdot \vec{\tau}(2) \tag{E.3}$$

We begin by decomposing $\mathcal{O}^{(2)}$ into irreducible tensor operators

$$\vec{q}_1 \cdot \vec{\sigma}(1)\vec{q}_2 \cdot \vec{\sigma}(2) = \sum_{J=0}^{2} (-1)^J \left[\vec{q}_1 \otimes \vec{q}_2 \right]_J \odot \left[\vec{\sigma}(1) \otimes \vec{\sigma}(2) \right]_J$$
$$= \frac{1}{3}\vec{q}_1 \cdot \vec{q}_2 \vec{\sigma}(1) \cdot \vec{\sigma}(2) + \frac{1}{2} (\vec{q}_1 \times \vec{q}_2) \cdot (\vec{\sigma}(1) \times \vec{\sigma}(2)) + \left[\vec{q}_1 \otimes \vec{q}_2 \right]_2 \odot \left[\vec{\sigma}(1) \otimes \vec{\sigma}(2) \right]_2 \tag{E.4}$$

Computing the average over the spin operators (see Table E.1) we find that all direct contributions vanish. We have only to compute the exchange terms, where we find that the scalar spin operator $\vec{\sigma}(1) \cdot \vec{\sigma}(2)$ averages to the spin-independent operator I_2 whereas the vector operator $\vec{\sigma}(1) \times \vec{\sigma}(2)$ averages to the spin-dependent operator $\vec{\sigma}$.

In the exchange term, the momentum transfers are $\vec{q}_1 = \vec{p}_\alpha - \vec{p}_\gamma$, $\vec{q}_2 = \vec{p}_\gamma - \vec{p}_\beta$, $\vec{q} = \vec{p}_\alpha - \vec{p}_\beta$. Let us introduce the average momentum of the single nucleon $\vec{k} = \frac{1}{2} (\vec{p}_\alpha + \vec{p}_\beta)$. We will write the effective one-body operator as

$$\mathcal{O}^{(1)}(\vec{p}_\alpha, \vec{p}_\beta) = \frac{3}{16\pi} \left[f^{\text{SI}}(\vec{q}, \vec{k})I_2 - f^{\text{SD}}(\vec{q}, \vec{k})i\vec{\sigma} \cdot \left(\vec{q} \times \vec{k} \right) \right] \,, \tag{E.5}$$

	2-body	1-body direct	1-body exchange
$\vec{\sigma}(1) \cdot \vec{\sigma}(2)$		0	$3I_2$
$\vec{\sigma}(1) \times \vec{\sigma}(2)$		0	$2i\vec{\sigma}$
$3\sigma_z(1)\sigma_z(2) - \vec{\sigma}(1) \cdot \vec{\sigma}(2)$		0	0
$\vec{\tau}(1) \cdot \vec{\tau}(2)$		0	$3I_2$

Table E.1: One-body average of two-body spin and isospin operators for direct and exchange contributions. We assume that the Fermi distributions for the protons and neutrons are identical. This assumption may be violated in very heavy nuclei.

where $f^{\text{SI}}(\vec{q}, \vec{k})$ and $f^{\text{SD}}(\vec{q}, \vec{k})$ are, respectively, the spin-independent and spin-dependent effective one-body form factors to be computed. Let us begin by considering the spin-independent form factor, which we express as an integral over the Fermi sphere

$$
f^{\text{SI}}(\vec{q}, \vec{k}) = -16\pi \int \frac{d^3\vec{p}_\gamma}{(2\pi)^3} \frac{(\vec{p}_\alpha - \vec{p}_\gamma) \cdot (\vec{p}_\gamma - \vec{p}_\beta)}{\left[(\vec{p}_\alpha - \vec{p}_\gamma)^2 + m_\pi^2\right]\left[(\vec{p}_\gamma - \vec{p}_\beta)^2 + m_\pi^2\right]}
$$
$$
= -\frac{2}{\pi^2} \int_0^{K_F} d|\vec{p}_\gamma| \, |\vec{p}_\gamma|^2 \int d\Omega_{p_\gamma} \frac{\left(\vec{k} + \frac{1}{2}\vec{q} - \vec{p}_\gamma\right) \cdot \left(\vec{p}_\gamma - \vec{k} + \frac{1}{2}\vec{q}\right)}{\left[\left(\vec{k} + \frac{1}{2}\vec{q} - \vec{p}_\gamma\right)^2 + m_\pi^2\right]\left[\left(\vec{p}_\gamma - \vec{k} + \frac{1}{2}\vec{q}\right)^2 + m_\pi^2\right]}
$$
(E.6)

We introduce the Feynman parameter representation

$$
\frac{1}{AB} = \int_{-1/2}^{1/2} d\beta \frac{1}{[(1/2 - \beta)A + (1/2 + \beta)B]^2},
$$
(E.7)

with

$$
A = \left(\vec{k} + \frac{1}{2}\vec{q} - \vec{p}_\gamma\right)^2 + m_\pi^2, \quad B = \left(\vec{p}_\gamma - \vec{k} + \frac{1}{2}\vec{q}\right)^2 + m_\pi^2
$$
(E.8)

which yields

$$
f^{\text{SI}}(\vec{q}, \vec{k}) = -\frac{2}{\pi^2} \int_{-1/2}^{1/2} d\beta \int_0^{K_F} d|\vec{p}_\gamma| \, |\vec{p}_\gamma|^2 \int d\Omega_{p_\gamma} \frac{2\vec{p}_\gamma \cdot \vec{k} + \frac{1}{4}|\vec{q}|^2 - |\vec{k}|^2 - |\vec{p}_\gamma|^2}{\left[|\vec{p}_\gamma|^2 - 2\vec{p}_\gamma \cdot \left(\vec{k} - \beta\vec{q}\right) + \Delta\right]^2},
$$
(E.9)

where we have defined

$$
\Delta \equiv -2\beta\vec{k} \cdot \vec{q} + \frac{1}{4}|\vec{q}|^2 + |\vec{k}|^2 + m_\pi^2.
$$
(E.10)

Now we need to compute the angular Ω_{p_γ} integral. Let us orient our coordinate system so that $\hat{z}$ is along $\vec{k} - \beta\vec{q}$. Then

$$
\vec{p}_\gamma \cdot \left(\vec{k} - \beta\vec{q}\right) = |\vec{p}_\gamma||\vec{k} - \beta\vec{q}| \cos\theta.
$$
(E.11)

We also have to consider the angular dependence of $\vec{p}_\gamma \cdot \vec{k}$. The azimuthal ϕ-dependence of this dot product must integrate to zero so we are left with only the $\hat{z}$ component

$$
\vec{p}_\gamma \cdot \vec{k} \rightarrow |\vec{p}_\gamma| \cos\theta \frac{\vec{k} \cdot (\vec{k} - \beta\vec{q})}{|\vec{k} - \beta\vec{q}|}
$$
(E.12)

Therefore

$$
f^{\text{SI}}(\vec{q}, \vec{k}) = -\frac{4}{\pi} \int_{-1/2}^{1/2} d\beta \int_0^{K_F} dp \, p^2
$$
$$
\times \int_{-1}^1 d\mu \left(2p \frac{\vec{k} \cdot (\vec{k} - \beta \vec{q})}{Q} \mu + \frac{1}{4}|\vec{q}|^2 - |\vec{k}|^2 - p^2 \right) \frac{1}{[p^2 - 2pQ\mu + \Delta]^2}, \tag{E.13}
$$

where we have defined $Q = |\vec{k} - \beta \vec{q}|$ and $p = |\vec{p}_\gamma|$.

Before proceeding with the angular integration, let us pause to consider the spin-dependent term $f^{\text{SD}}(\vec{q}, \vec{k})$. We begin with the fact that

$$
\vec{q}_1 \times \vec{q}_2 = -\vec{q} \times \vec{k} + \vec{q} \times \vec{p}_\gamma \tag{E.14}
$$

and introduce the same Feynman parameter representation as in the spin-independent case. In the angular integration, the only non-vanishing part of $\vec{q} \times \vec{p}_\gamma$ is the $\hat{z}$ component of p_γ, so we may write

$$
-\vec{q} \times \vec{k} + \vec{q} \times \vec{p} \to \vec{q} \times \vec{k} \left(\frac{p}{Q} \cos\theta - 1 \right) \tag{E.15}
$$

leading to

$$
f^{\text{SD}}(\vec{q}, \vec{k}) = \frac{4}{\pi} \int_{-1/2}^{1/2} d\beta \int_0^{K_F} dp \, p^2 \int_{-1}^1 d\mu \left(1 - \frac{p}{Q}\mu \right) \frac{1}{[p^2 - 2pQ\mu + \Delta]^2}, \tag{E.16}
$$

Both of the required angular integrals can be computed analytically

$$
\int_{-1}^1 d\mu \, \frac{1}{[p^2 - 2pQ\mu + \Delta]^2} = \frac{2}{(p^2 + \Delta)^2 - 4p^2Q^2}
$$
$$
\int_{-1}^1 d\mu \, \frac{\mu}{[p^2 - 2pQ\mu + \Delta]^2} = \frac{p^2 + \Delta}{pQ} \frac{1}{(p^2 + \Delta)^2 - 4p^2Q^2} - \frac{1}{2Q^2} \text{arctanh}\left(\frac{2pQ}{p^2 + \Delta} \right). \tag{E.17}
$$

Introducing dimensionless quantities $\bar{p} = p/k_F$, $\bar{k} = \vec{k}/k_F$, $\bar{q} = \vec{k}/k_F$, $\bar{m} = m_\pi/k_F$, $\bar{Q} = Q/k_F$, and $\bar{\Delta} = \Delta/k_F^2$, allows us to write the form factors as

$$
f^{\text{SI}}(\vec{q}, \vec{k}) = -\frac{4}{\pi} k_F \int_{-1/2}^{1/2} d\beta \int_0^1 d\bar{p} \left\{ 2 \left(\frac{\bar{k} \cdot (\bar{k} - \beta \bar{q})}{\bar{Q}^2} \bar{\Delta} + \frac{1}{4}\bar{q}^2 - \bar{k}^2 \right) \frac{\bar{p}^2}{(\bar{p}^2 + \bar{\Delta})^2 - 4\bar{p}^2\bar{Q}^2} \right.
$$
$$
+ 2 \left(\frac{\bar{k} \cdot (\bar{k} - \beta \bar{q})}{\bar{Q}^2} - 1 \right) \frac{\bar{p}^4}{(\bar{p}^2 + \Delta)^2 - 4\bar{p}^2Q^2} - \frac{\bar{k} \cdot (\bar{k} - \beta \bar{q})}{\bar{Q}^3} \bar{p} \, \text{arctanh}\left(\frac{2\bar{p}\bar{Q}}{\bar{p}^2 + \bar{\Delta}} \right) \right\}
$$
$$
f^{\text{SD}}(\vec{q}, \vec{k}) = \frac{4}{\pi} k_F \int_{-1/2}^{1/2} d\beta \int_0^1 d\bar{p} \left\{ \left(2 - \frac{\bar{\Delta}}{\bar{Q}^2} \right) \frac{\bar{p}^2}{(\bar{p}^2 + \bar{\Delta})^2 - 4\bar{p}^2\bar{Q}^2} \right.
$$
$$
\left. - \frac{1}{\bar{Q}^2} \frac{\bar{p}^4}{(\bar{p}^2 + \bar{\Delta})^2 - 4\bar{p}^2\bar{Q}^2} + \frac{1}{2\bar{Q}^3} \bar{p} \, \text{arctanh}\left(\frac{2\bar{p}\bar{Q}}{\bar{p}^2 + \bar{\Delta}} \right) \right\}. \tag{E.18}
$$

The following three integrals necessary to compute the form factors can be performed analytically:

$$\int_0^1 d\bar{p}\, \frac{\bar{p}^2}{(\bar{p}^2 + \bar{\Delta})^2 - 4\bar{p}^2\bar{Q}^2} = \frac{1}{4}\frac{1}{\sqrt{\bar{\Delta} - \bar{Q}^2}}\left[\arctan\left(\frac{1 - \bar{Q}}{\sqrt{\bar{\Delta} - \bar{Q}^2}}\right) + \arctan\left(\frac{1 + \bar{Q}}{\sqrt{\bar{\Delta} - \bar{Q}^2}}\right)\right]$$
$$- \frac{1}{8\bar{Q}}\ln\left(\frac{1 + \bar{\Delta} + 2\bar{Q}}{1 + \bar{\Delta} - 2\bar{Q}}\right)$$

$$\int_0^1 d\bar{p}\, \frac{\bar{p}^4}{(\bar{p}^2 + \bar{\Delta})^2 - 4\bar{p}^2\bar{Q}^2} = -\frac{1}{4}\frac{3\bar{\Delta} - 4\bar{Q}^2}{\sqrt{\bar{\Delta} - \bar{Q}^2}}\left[\arctan\left(\frac{1 - \bar{Q}}{\sqrt{\bar{\Delta} - \bar{Q}^2}}\right) + \arctan\left(\frac{1 + \bar{Q}}{\sqrt{\bar{\Delta} - \bar{Q}^2}}\right)\right]$$
$$+ 1 + \frac{\bar{\Delta} - 4\bar{Q}^2}{8\bar{Q}}\ln\left(\frac{1 + \bar{\Delta} + 2\bar{Q}}{1 + \bar{\Delta} - 2\bar{Q}}\right)$$

$$\int_0^1 d\bar{p}\, \bar{p}\arctanh\left(\frac{2\bar{p}\bar{Q}}{\bar{p}^2 + \bar{\Delta}}\right) = \bar{Q}\sqrt{\bar{\Delta} - \bar{Q}^2}\left[\arctan\left(\frac{1 - \bar{Q}}{\sqrt{\bar{\Delta} - \bar{Q}^2}}\right) + \arctan\left(\frac{1 + \bar{Q}}{\sqrt{\bar{\Delta} - \bar{Q}^2}}\right)\right]$$
$$+ \bar{Q} - \frac{1}{4}\left(1 - 2\bar{Q}^2 + \Delta\right)\ln\left(\frac{1 + 2\bar{Q} + \bar{\Delta}}{1 - 2\bar{Q} + \bar{\Delta}}\right)$$
$$\tag{E.19}$$

Combining these results with the proper prefactors in Eq. (E.18), the resulting spin-independent and spin-dependent form factors are

$$f^{SI}(\bar{q}, \bar{k}) = \frac{2}{\pi}\int_{-1/2}^{1/2} d\beta \left\{ 2\left(1 + \frac{-\beta\bar{k}\cdot\bar{q} + \beta^2\bar{q}^2}{\bar{k}^2 - 2\beta\bar{k}\cdot\bar{q} + \beta^2\bar{q}^2}\right) - \left(\frac{4(\frac{1}{4} - \beta^2)\bar{q}^2 + 3\bar{m}^2}{\sqrt{(\frac{1}{4} - \beta^2)\bar{q}^2 + \bar{m}^2}}\right) \right.$$
$$\times \left[\arctan\left(\frac{1 + \sqrt{\bar{k}^2 - 2\beta\bar{k}\cdot\bar{q} + \beta^2\bar{q}^2}}{\sqrt{(\frac{1}{4} - \beta^2)\bar{q}^2 + \bar{m}^2}}\right) + \arctan\left(\frac{1 - \sqrt{\bar{k}^2 - 2\beta\bar{k}\cdot\bar{q} + \beta^2\bar{q}^2}}{\sqrt{(\frac{1}{4} - \beta^2)\bar{q}^2 + \bar{m}^2}}\right)\right]$$
$$+ \frac{1}{2\sqrt{\bar{k}^2 - 2\beta\bar{k}\cdot\bar{q} + \beta^2\bar{q}^2}}\ln\left(\frac{1 + 2\sqrt{\bar{k}^2 - 2\beta\bar{k}\cdot\bar{q} + \beta^2\bar{q}^2} + \bar{k}^2 - 2\beta\bar{k}\cdot\bar{q} + \frac{1}{4}\bar{q}^2 + \bar{m}^2}{1 - 2\sqrt{\bar{k}^2 - 2\beta\bar{k}\cdot\bar{q} + \beta^2\bar{q}^2} + \bar{k}^2 - 2\beta\bar{k}\cdot\bar{q} + \frac{1}{4}\bar{q}^2 + \bar{m}^2}\right) \times$$
$$\left[1 + 2\bar{m}^2 + \left(\frac{3}{4} - 4\beta^2\right)\bar{q}^2 - \bar{k}^2 + 2\beta\bar{k}\cdot\bar{q} + \beta\frac{\left(1 + \frac{1}{4}\bar{q}^2 + \bar{m}^2 + \bar{k}^2 - 2\beta\bar{k}\cdot\bar{q}\right)\left(\bar{k}\cdot\bar{q} - \beta\bar{q}^2\right)}{\bar{k}^2 - 2\beta\bar{k}\cdot\bar{q} + \beta^2\bar{q}^2}\right]\right\}$$
$$\tag{E.20}$$

$$f^{SD}(\bar{q}, \bar{k}) = -\frac{2}{\pi}\int_{-1/2}^{1/2} d\beta \frac{1}{\sqrt{\bar{k}^2 - 2\beta\bar{k}\cdot\bar{q} + \beta^2\bar{q}^2}}\left[\frac{1}{\sqrt{\bar{k}^2 - 2\beta\bar{k}\cdot\bar{q} + \beta^2\bar{q}^2}}\right.$$
$$-\frac{1 + \bar{m}^2 + \bar{k}^2 - 2\beta\bar{k}\cdot\bar{q} + \frac{1}{4}\bar{q}^2}{4\left(\bar{k}^2 - 2\beta\bar{k}\cdot\bar{q} + \beta^2\bar{q}^2\right)}\ln\left(\frac{1 + 2\sqrt{\bar{k}^2 - 2\beta\bar{k}\cdot\bar{q} + \beta^2\bar{q}^2} + \bar{k}^2 - 2\beta\bar{k}\cdot\bar{q} + \frac{1}{4}\bar{q}^2 + \bar{m}^2}{1 - 2\sqrt{\bar{k}^2 - 2\beta\bar{k}\cdot\bar{q} + \beta^2\bar{q}^2} + \bar{k}^2 - 2\beta\bar{k}\cdot\bar{q} + \frac{1}{4}\bar{q}^2 + \bar{m}^2}\right)\right]$$
$$\tag{E.21}$$

Note that these functions depend on not only the magnitude of the dimensionless momentum transfer $\bar{q}$ and average momentum $\bar{k}$, but on their relative angle. Fortunately, for the physically

relevant values of these momenta, f^{SI} and f^{SD} do not vary significantly over the range of possible angular values. Therefore we may replace each function by its angular average. The angle-averaged functions then depend only on the magnitude of the momentum transfer and the average momentum. For $\mu^- \to e^-$ conversion in ^{27}Al, $|\vec{q}| \approx m_\mu$. Fixing the magnitude of the momentum transfer, f^{SI} and f^{SD} are now functions of the dimensionless average nucleon momentum $\bar{k}$, as shown in Fig. E.1. In order to recover a local one-body effective operator, we now wish to replace these slowly-varying functions of $\bar{k}$ by a constant. We can weight our average by the nucleon momentum probability distribution obtained from the measured nucleon density. The resulting constant values f^{SI}_{eff} and f^{SD}_{eff} are compared to their respective $\bar{k}$-dependent form factors in Fig. E.1.

This calculation was first performed in Ref. [56], but several errors were committed that resulted in incorrect expressions for the form factors $f^{\text{SI}}(\bar{q}, \bar{k}$ and $f^{\text{SD}}(\bar{q}, \bar{k})$ and all quantities derived from them.
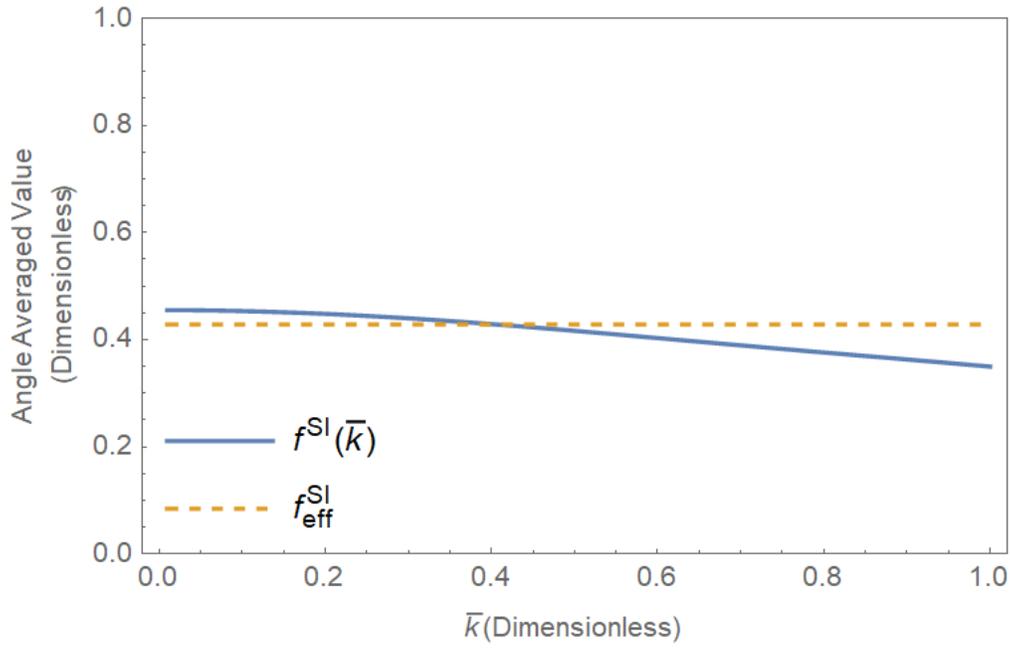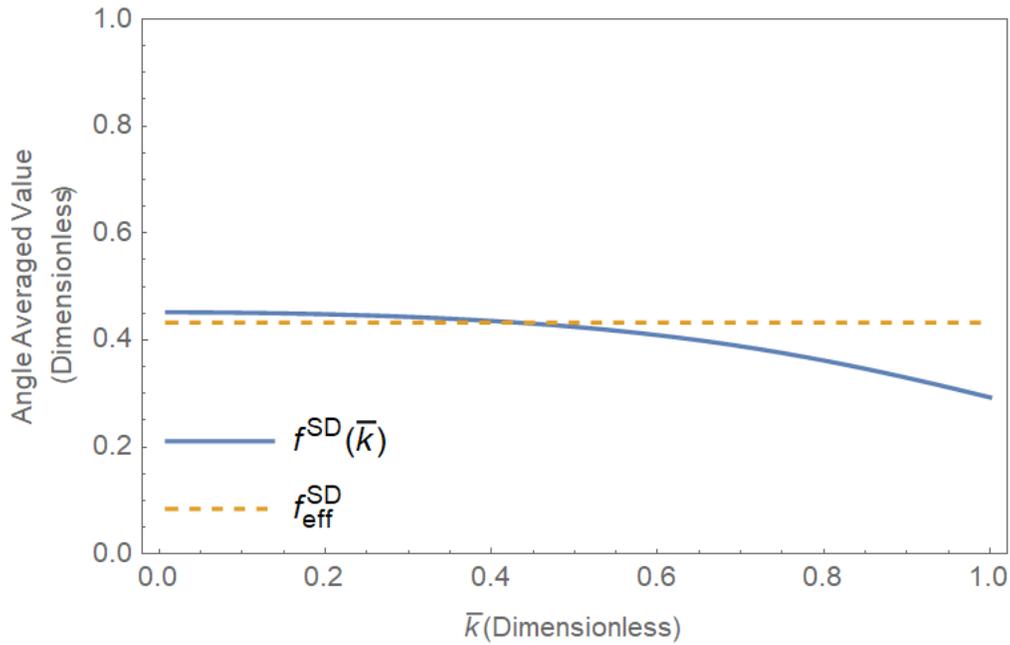
Figure E.1: (a) Angle averaged value of f^{SI} at $|\vec{q}| = m_\mu$ and its constant approximation f^{SI}_{eff} as a function of the dimensionless average momentum $\overline{k}$.
(b) Angle averaged value of f^{SD} at $|\vec{q}| = m_\mu$ and its constant approximation f^{SD}_{eff} as a function of the dimensionless average momentum $\overline{k}$.

Appendix F

Fourier Transform of Two-Nucleon Operator

The two-nucleon current that contributes to $\mu \to e$ conversion has the form

$$J_{ud,\alpha}^{(2)}(\vec{q}_1, \vec{q}_2) = -\frac{g_A^2 m_\pi^2}{4 f_\pi^2} \rho\left(\vec{k}_1, \vec{k}'_1, \vec{k}_2, \vec{k}'_2\right) \vec{\tau}(1) \cdot \vec{\tau}(2) \, C_{S\alpha}^{(0)}, \tag{F.1}$$

where we have defined the two-nucleon density

$$\rho\left(\vec{k}_1, \vec{k}'_1, \vec{k}_2, \vec{k}'_2\right) \equiv \frac{\vec{q}_1 \cdot \vec{\sigma}(1) \, \vec{q}_2 \cdot \vec{\sigma}(2)}{(q_1^2 + m_\pi^2)(q_2^2 + m_\pi^2)}. \tag{F.2}$$

The three-momentum transfers are defined to be

$$\vec{q}_1 \equiv \vec{p}_1 - \vec{p}'_1, \quad \vec{q}_2 \equiv \vec{p}_2 - \vec{p}'_2, \tag{F.3}$$

and we use the notation $q_i = |\vec{q}_i|$ to denote the length of the three-vectors. Then to transform to coordinate space and enforce momentum conservation, we have

$$\begin{aligned} \rho(\vec{x}_1, \vec{x}'_1, \vec{x}_2, \vec{x}'_2, \vec{q}) &= \frac{1}{(2\pi)^{12}} \int d^3p_1 \, d^3p'_1 \, d^3p_2 \, d^3p'_2 \, \tilde{J}_2(\vec{q}_1, \vec{q}_2, \vec{q}) \\ &\times (2\pi)^3 \delta(\vec{p}_1 + \vec{p}_2 - \vec{p}'_1 - \vec{p}'_2 - \vec{q}) e^{i\left(\vec{p}'_1 \cdot \vec{x}'_1 + \vec{p}'_2 \cdot \vec{x}'_2 - \vec{p}_1 \cdot \vec{x}_1 - \vec{p}_2 \cdot \vec{x}_2\right)}. \end{aligned} \tag{F.4}$$

We transform our integration variables to

$$\begin{aligned} \vec{q}_1 &= \vec{p}_1 - \vec{p}'_1, \ \vec{P}_1 = \frac{1}{2}\left(\vec{p}_1 + \vec{p}'_1\right) \\ \vec{q}_2 &= \vec{p}_2 - \vec{p}'_2, \ \vec{P}_2 = \frac{1}{2}\left(\vec{p}_2 + \vec{p}'_2\right), \end{aligned} \tag{F.5}$$

so that

$$\begin{aligned} &\rho(\vec{x}_1, \vec{x}'_1, \vec{x}_2, \vec{x}'_2, \vec{q}) \\ &= \frac{1}{(2\pi)^3} \delta(\vec{x}_1 - \vec{x}'_1) \delta(\vec{x}_2 - \vec{x}'_2) \int d^3q_1 \, \rho(\vec{q}_1, \vec{q} - \vec{q}_1, \vec{q}) e^{-\frac{i}{2}\left[\vec{q}_1 \cdot (\vec{x}_1 + \vec{x}'_1) + (\vec{q} - \vec{q}_1) \cdot (\vec{x}_2 + \vec{x}'_2)\right]}. \end{aligned} \tag{F.6}$$

Next we employ the Feynman parameter representation

$$\frac{1}{AB} = \int_0^1 d\alpha \frac{1}{[\alpha A + (1-\alpha)B]^2}, \tag{F.7}$$

with

$$A = q_1^2 + m_\pi^2, \ B = (\vec{q} - \vec{q}_1)^2 + m_\pi^2. \tag{F.8}$$

Then

$$\alpha A + (1-\alpha)B = [\vec{q}_1 - (1-\alpha)\vec{q}]^2 + \alpha(1-\alpha)q^2 + m_\pi^2. \tag{F.9}$$

Now let us shift the integration variable

$$\vec{q}_1 \to \vec{q}_1 + (1-\alpha)\vec{q}, \tag{F.10}$$

so that

$$\rho(\vec{x}_1, \vec{x}'_1, \vec{x}_2, \vec{x}'_2, \vec{q}) = \frac{1}{(2\pi)^3} \delta(\vec{x}_1 - \vec{x}'_1)\delta(\vec{x}_2 - \vec{x}'_2)e^{-\frac{i}{2}\vec{q}\cdot(\vec{x}_1+\vec{x}'_1)} \int_0^1 d\alpha \, e^{i\alpha\vec{q}\cdot\vec{r}}$$
$$\times \int d^3q_1 \frac{[\vec{q}_1 + (1-\alpha)\vec{q}\,] \cdot \vec{\sigma}(1) \, [\alpha\vec{q} - \vec{q}_1] \cdot \vec{\sigma}(2)}{[q_1^2 + \Pi^2(q,\alpha)]^2} e^{-i\vec{q}_1\cdot\vec{r}}, \tag{F.11}$$

where we have defined

$$\Pi^2(q,\alpha) \equiv \alpha(1-\alpha)q^2 + m_\pi^2, \tag{F.12}$$

and introduced the relative coordinate

$$\vec{r} \equiv \frac{1}{2}\left(\vec{x}_1 + \vec{x}'_1 - \vec{x}_2 - \vec{x}'_2\right)$$
$$= \vec{x}_1 - \vec{x}_2. \tag{F.13}$$

The quantity $\Pi(q,\alpha)$ can be interpreted as an effective pion mass arising from the finite momentum-transfer. Indeed, $\Pi(q,\alpha) \to m_\pi$ when $q \to 0$. Now we can perform the final momentum integral. There are three distinct integrands. First, with a trivial angular integrand:

$$\int d^3q_1 \frac{e^{-i\vec{q}_1\cdot\vec{r}}}{[q_1^2 + \Pi^2(q,\alpha)]^2} = \pi^2 \frac{e^{-r\Pi(q,\alpha)}}{\Pi(q,\alpha)}, \tag{F.14}$$

then with one factor of $\hat{q}_1$ in the angular integrand:

$$\int d^3q_1 \frac{\vec{q}_1 \cdot \vec{\sigma}(i)e^{-i\vec{q}_1\cdot\vec{r}}}{[q_1^2 + \Pi^2(q,\alpha)]^2} = -i\pi^2\hat{r} \cdot \vec{\sigma}(i)e^{-r\Pi(q,\alpha)}, \tag{F.15}$$

and finally with two factors of $\hat{q}_1$:

$$\int d^3q_1 \frac{\vec{q}_1 \cdot \vec{\sigma}(1)\vec{q}_1 \cdot \vec{\sigma}(2)e^{-i\vec{q}_1\cdot\vec{r}}}{[q_1^2 + \Pi^2(q,\alpha)]^2} = \frac{\pi^2}{3}\vec{\sigma}(1) \cdot \vec{\sigma}(2)\frac{e^{-r\Pi(q,\alpha)}}{r}\left[2 - r\Pi(q,\alpha)\right]$$
$$- \pi^2\sqrt{\frac{8\pi}{15}}[\vec{\sigma}(1) \otimes \vec{\sigma}(2)]_2 \odot Y_2(\hat{r})\frac{e^{-r\Pi(q,\alpha)}}{r}\left[1 + \Pi(q,\alpha)r\right]. \tag{F.16}$$

For this last integration we have employed the identity

$$(\hat{q} \cdot \vec{\sigma}(1))(\hat{q} \cdot \vec{\sigma}(2)) = \frac{1}{3}\vec{\sigma}(1) \cdot \vec{\sigma}(2) + \sqrt{\frac{8\pi}{15}}Y_2(\hat{q}) \odot [\vec{\sigma}(1) \otimes \vec{\sigma}(2)]_2. \tag{F.17}$$

Putting these pieces together yields

$$\rho(\vec{x}_1, \vec{x}'_1, \vec{x}_2, \vec{x}'_2, \vec{q}) = \frac{1}{8\pi}\delta(\vec{x}_1 - \vec{x}'_1)\delta(\vec{x}_2 - \vec{x}'_2)e^{-i\vec{q}\cdot\vec{x}_1}\int_0^1 d\alpha \; e^{i\alpha\vec{q}\cdot\vec{r}-\Pi(q,\alpha)r}$$

$$\left\{ -i\alpha\hat{r}\cdot\vec{\sigma}(1)\vec{q}\cdot\vec{\sigma}(2) + i(1-\alpha)\vec{q}\cdot\vec{\sigma}(1)\hat{r}\cdot\vec{\sigma}(2) - \frac{1}{3}\vec{\sigma}(1)\cdot\vec{\sigma}(2)\frac{1}{r}[2 - r\Pi(q,\alpha)] \right. \tag{F.18}$$

$$\left. + \alpha(1-\alpha)\frac{1}{\Pi(q,\alpha)}\vec{q}\cdot\vec{\sigma}(1)\vec{q}\cdot\vec{\sigma}(2) + \sqrt{\frac{8\pi}{15}}\frac{1}{r}[\vec{\sigma}(1) \otimes \vec{\sigma}(2)]_2 \odot Y_2(\hat{r})[1 + r\Pi(q,\alpha)] \right\}.$$

In the $\vec{q} \to 0$ limit, the Feynman parameter integral becomes trivial, $\Pi(q,\alpha) \to m_\pi$, and the two-body current becomes

$$\rho(\vec{x}_1, \vec{x}'_1, \vec{x}_2, \vec{x}'_2, 0) = \frac{1}{8\pi}\delta(\vec{x}_1 - \vec{x}'_1)\delta(\vec{x}_2 - \vec{x}'_2)\frac{1}{r}\left\{ \frac{1}{3}F_1(r/m_\pi)\vec{\sigma}(1) \cdot \vec{\sigma}(2) \right.$$

$$\left. + \sqrt{\frac{8\pi}{15}}F_2(r/m_\pi)Y_2(\hat{r}) \odot [\vec{\sigma}(1) \otimes \vec{\sigma}(2)]_2 \right\}, \tag{F.19}$$

where the form factors are given by

$$F_1(x) \equiv e^{-x}(x - 2), \; F_2(x) \equiv e^{-x}(x + 1). \tag{F.20}$$

This is a familiar result from studies of $0\nu\beta\beta$-decay (e.g., Ref. [154]), where the leading long-range contribution is due to two-pion exchange. Here, rather than relying on the long-wavelength limit, we will work at finite q.

If we were to Fourier transform the two-body current in Eq. (F.18) with respect to the momentum transfer $\vec{q}$

$$\rho(\vec{x}_1, \vec{x}'_1, \vec{x}_2, \vec{x}'_2, \vec{x}) = \int \frac{d^3q}{(2\pi)^3} \; e^{i\vec{q}\cdot\vec{x}}\rho(\vec{x}_1, \vec{x}'_1, \vec{x}_2, \vec{x}'_2, \vec{q}), \tag{F.21}$$

then the resulting position space current will exhibit a complicated dependence on the Fourier transform coordinate $\vec{x}$. The dominant piece will be the $J = 0$ component of this current and so we must project the spatial two-body current onto charge multipoles

$$\mathcal{M}_{J,M}(\kappa) = \int d^3x \; j_J(\kappa x)Y_{J,M}(\hat{x})\rho(\vec{x}_1, \vec{x}'_1, \vec{x}_2, \vec{x}'_2, \vec{x})$$

$$= \frac{1}{4\pi}i^J\delta(\kappa - q)\int d\Omega_q \; Y_{J,M}(\hat{q})\rho(\vec{x}_1, \vec{x}'_1, \vec{x}_2, \vec{x}'_2, \vec{q}). \tag{F.22}$$

Our focus is then the $J = M = 0$ contribution. We begin by considering the first term in the second line of Eq. (F.18). The only angular dependence on $\hat{q}$ in this term is in the exponentials, so we compute

$$\int d\Omega_q \; Y_{0,0}(\hat{q})e^{-i\vec{q}\cdot\vec{R}}e^{i(\alpha-1/2)\vec{q}\cdot\vec{r}} = (4\pi)^{3/2}\sum_{l=0}^{\infty} j_l(qR)j_l\left(qr(\alpha - 1/2)\right)Y_l(\hat{R}) \odot Y_l(\hat{r}), \tag{F.23}$$

where we have defined the center-of-mass coordinate

$$\vec{R} \equiv \frac{1}{2} \left(\vec{x}_1 + \vec{x}_2 \right). \tag{F.24}$$

Thus we have the two-body operator

$$
\begin{aligned}
\mathcal{O}_1(\vec{r}, \vec{R}, q) = & -\frac{1}{12\sqrt{\pi}} \vec{\sigma}(1) \cdot \vec{\sigma}(2) \sum_{L=0}^{\infty} Y_L(\hat{r}) \odot \ Y_L(\hat{R}) j_L(qR) \\
& \times \int_0^1 d\alpha \ e^{-r\Pi(q,\alpha)} j_L \left(qr(\alpha - 1/2) \right) \frac{2 - r\Pi(q,\alpha)}{r}.
\end{aligned}
\tag{F.25}
$$

The Feynman parameter integral vanishes unless L is even. This can be seen by shifting the Feynman parameter $\beta = \alpha - 1/2$ and noting that $\Pi(q,\beta)$ (and thus the entire Feynman parameter integrand) is an even function of β. Therefore

$$
\begin{aligned}
\mathcal{O}_1(\vec{r}, \vec{R}, q) = & -\frac{1}{12\sqrt{\pi}} \vec{\sigma}(1) \cdot \vec{\sigma}(2) \sum_{L=0,2,\dots}^{\infty} Y_L(\hat{r}) \odot \ Y_L(\hat{R}) \ j_L(qR) \\
& \times \int_0^1 d\alpha \ e^{-r\Pi(q,\alpha)} j_L \left(qr(\alpha - 1/2) \right) \frac{2 - r\Pi(q,\alpha)}{r}
\end{aligned}
\tag{F.26}
$$

Now let's look at the second term in the second line of Eq. (F.18) and apply the identity of Eq. (F.17). We find one term that has the same tensor structure as $\mathcal{O}_1$; that is

$$
\begin{aligned}
\mathcal{O}_2(\vec{r}, \vec{R}, q) = & \frac{1}{12\sqrt{\pi}} \vec{\sigma}(1) \cdot \vec{\sigma}(2) \sum_{L=0,2,\dots}^{\infty} Y_L(\hat{r}) \odot Y_L(\hat{R}) \ j_L(qR) \\
& \times \int_0^1 d\alpha \ e^{-r\Pi(q,\alpha)} j_L(qr \left(\alpha - 1/2 \right)) \frac{q^2\alpha(1 - \alpha)}{\Pi(q,\alpha)},
\end{aligned}
\tag{F.27}
$$

where again the Feynman parameter integral vanishes unless L is even.

The second term that we get from applying the tensor decomposition of Eq. (F.17) has a quadrupole dependence on $\hat{q}$:

$$
\begin{aligned}
& \int d\Omega_q \ Y_{0,0}(\hat{q}) e^{-i\vec{q}\cdot\vec{R}} e^{i(\alpha - 1/2)\vec{q}\cdot\vec{r}} Y_2(\hat{q}) \odot [\vec{\sigma}(1) \otimes \vec{\sigma}(2)]_2 \\
& = 4\pi \sum_{L_1, L_2} (i)^{L_1 - L_2} (-1)^{L_1 + L_2} C_{L_1 0 L_2 0}^{20} \sqrt{\frac{(2L_1 + 1)(2L_2 + 1)}{5}} j_{L_1} \left(qr(\alpha - 1/2) \right) j_{l_2}(qR) \\
& \times \left[Y_{L_1}(\hat{r}) \otimes Y_{L_2}(\hat{R}) \right]_2 \odot [\vec{\sigma}(1) \otimes \vec{\sigma}(2)]_2.
\end{aligned}
\tag{F.28}
$$

Therefore we have the operator

$$
\begin{aligned}
\mathcal{O}_3(\vec{r}, \vec{R}, q) = & \frac{1}{5\sqrt{24\pi}} \sum_{L_1, L_2} i^{L_1 - L_2} (-1)^{L_1 + L_2} C_{L_1 0 L_2 0}^{20} \sqrt{(2L_1 + 1)(2L_2 + 1)} j_{L_2}(qR) \\
& \times \left[Y_{L_1}(\hat{r}) \otimes Y_{L_2}(\hat{R}) \right]_2 \odot [\vec{\sigma}(1) \otimes \vec{\sigma}(2)]_2 \int_0^1 d\alpha \ e^{-r\Pi(q,\alpha)} j_{L_1} \left(qr(\alpha - 1/2) \right) \frac{q^2\alpha(1 - \alpha)}{\Pi(q,\alpha)}
\end{aligned}
\tag{F.29}
$$

As before, the Feynman parameter integral vanishes unless L_1 is even. The Clebsch-Gordan coefficient then implies that L_2 must be even as well. Thus

$$
\mathcal{O}_3(\vec{r}, \vec{R}, q) = \frac{1}{5\sqrt{24\pi}} \sum_{L_1=0,2,\dots}^{\infty} \sum_{L_2=0,2,\dots}^{\infty} (-1)^{(L_1-L_2)/2} C^{20}_{L_1 0 L_2 0} \sqrt{(2L_1+1)(2L_2+1)} j_{L_2}(qR)
$$
$$
\times \left[Y_{L_1}(\hat{r}) \otimes Y_{L_2}(\hat{R})\right]_2 \odot [\vec{\sigma}(1) \otimes \vec{\sigma}(2)]_2 \int_0^1 d\alpha\, e^{-r\Pi(q,\alpha)} j_{L_1}\left(qr(\alpha-1/2)\right) \frac{q^2\alpha(1-\alpha)}{\Pi(q,\alpha)}.
$$
$$(F.30)$$

Now we turn our attention to the term in the third line of Eq. (F.18). The only angular dependence on $\hat{q}$ is in the exponentials but after completing the angular integral we must recouple the resulting two $\hat{r}$ spherical harmonics. For this task we need the identity

$$
Y_{l_2}(\hat{r}) \odot Y_{l_2}(\hat{R})\, Y_2(\hat{r}) \odot [\vec{\sigma}(1) \otimes \vec{\sigma}(2)]_2
$$
$$
= (-1)^{l_2} \sqrt{\frac{2l_2+1}{4\pi}} \sum_{l_1} C^{l_1 0}_{l_2 0 2 0} \left[Y_{l_1}(\hat{r}) \otimes Y_{l_2}(\hat{R})\right]_2 \odot [\vec{\sigma}(1) \otimes \vec{\sigma}(2)]_2 .
$$
$$(F.31)$$

As before, we find that the integrand vanishes unless L_2 is even and the Clebsch-Gordon coefficient then requires that L_1 be even as well. Thus

$$
\mathcal{O}_4(\vec{r}, \vec{R}, q) = \frac{1}{5\sqrt{24\pi}} \sum_{L_1, L_2 \text{ even}} C^{20}_{L_1 0 L_2 0} \sqrt{(2L_1+1)(2L_2+1)} j_{L_2}(qR)
$$
$$
\times \left[Y_{L_1}(\hat{r}) \otimes Y_{L_2}(\hat{R})\right]_2 \odot [\vec{\sigma}(1) \otimes \vec{\sigma}(2)]_2 \int_0^1 d\alpha\, e^{-r\Pi(q,\alpha)} j_{L_2}\left(qr(\alpha-1/2)\right) \frac{1}{r}\left[1 + r\Pi(q,\alpha)\right].
$$
$$(F.32)$$

Now we turn our attention to the final set of terms, the first line of Eq. (F.18). First we decompose the tensor structure as

$$
-\alpha\hat{r} \cdot \vec{\sigma}(1)\hat{q} \cdot \vec{\sigma}(2) + (1-\alpha)\hat{q} \cdot \vec{\sigma}(1)\hat{r} \cdot \vec{\sigma}(2)
$$
$$
= \frac{4\pi}{3} \sum_{K=0}^{2} [Y_1(\hat{q}) \otimes Y_1(\hat{r})]_K \odot [\vec{\sigma}(1) \otimes \vec{\sigma}(2)]_K \left[-\alpha + (1-\alpha)(-1)^K\right].
$$
$$(F.33)$$

Next we must perform a more complicated angular integral: the $Y_1(\hat{q})$-dependence is non-trivially coupled to the $Y_1(\hat{r})$. After integrating and re-coupling (using an identity to rewrite a sum of three Clebsch-Gordon coefficients as a single Clebsch-Gordon coefficient and a Wigner 6-j symbol), we find

$$
\int d\Omega_q\, Y_{00}(\hat{q}) e^{-i\vec{q}\cdot\vec{R}} e^{i(\alpha-1/2)\vec{q}\cdot\vec{r}} [Y_1(\hat{q}) \otimes Y_1(\hat{r})]_K \odot [\vec{\sigma}(1) \otimes \vec{\sigma}(2)]_K
$$
$$
= 3\sqrt{4\pi} \sum_{L_1, L_2} (i)^{L_1-L_2} (2L_1+1) C^{L_2 0}_{L_1 0 1 0} \sum_J (-1)^{1+J} C^{J0}_{L_1 0 1 0} \begin{Bmatrix} L_1 & 1 & L_2 \\ K & J & 1 \end{Bmatrix}
$$
$$
\times \left[Y_J(\hat{r}) \otimes Y_{L_2}(\hat{R})\right]_K \odot [\vec{\sigma}(1) \otimes \vec{\sigma}(2)]_K j_{L_1}\left(qr(\alpha-1/2)\right) j_{L_2}(qR)
$$
$$(F.34)$$

Now let us consider the three cases: $K = 0, 1, 2$. When $K = 0$, then $J = L_2$ and many of the angular momentum factors simplify. In particular,

$$\begin{Bmatrix} L_1 & 1 & L_2 \\ 0 & L_2 & 1 \end{Bmatrix} = \frac{(-1)^{1+L_1+L_2}}{\sqrt{3(2L_2+1)}}, \tag{F.35}$$

$$\left[Y_{L_2}(\hat{r}) \otimes Y_{L_2}(\hat{R})\right]_{0,0} = \frac{(-1)^{L_2}}{\sqrt{2L_2+1}} Y_{L_2}(\hat{r}) \odot Y_{L_2}(\hat{R}), \tag{F.36}$$

and

$$\left[\vec{\sigma}(1) \otimes \vec{\sigma}(2)\right]_{0,0} = -\frac{1}{\sqrt{3}}\vec{\sigma}(1) \cdot \vec{\sigma}(2). \tag{F.37}$$

Therefore we have the operator

$$\mathcal{O}_5(\vec{r}, \vec{R}, q) = \frac{1}{12\sqrt{\pi}} \sum_{L_1, L_2} (i)^{1+L_1-L_2} \left(\frac{2L_1+1}{2L_2+1}\right) \left(C_{L_1010}^{L_20}\right)^2$$
$$\times j_{L_2}(qR) Y_{L_2}(\hat{r}) \odot Y_{L_2}(\hat{R}) \vec{\sigma}(1) \cdot \vec{\sigma}(2) q \int_0^1 d\alpha \, e^{-r\Pi(q,\alpha)}(1-2\alpha)j_{L_1}(qr(\alpha-1/2)). \tag{F.38}$$

The integral with respect to α vanishes unless L_1 is odd, and the Clebsch-Gordon coefficient then implies that L_2 must be even. Therefore

$$\mathcal{O}_5(\vec{r}, \vec{R}, q) = \frac{1}{12\sqrt{\pi}} \sum_{L_1=1,3,\dots}^{\infty} \sum_{L_2=0,2,\dots}^{\infty} (-1)^{(1+L_1-L_2)/2} \left(\frac{2L_1+1}{2L_2+1}\right) \left(C_{L_1010}^{L_20}\right)^2$$
$$\times j_{L_2}(qR) Y_{L_2}(\hat{r}) \odot Y_{L_2}(\hat{R}) \vec{\sigma}(1) \cdot \vec{\sigma}(2) q \int_0^1 d\alpha \, e^{-r\Pi(q,\alpha)}(1-2\alpha)j_{L_1}(qr(\alpha-1/2)) \tag{F.39}$$

Similarly when $K = 1$, we have

$$\mathcal{O}_6(\vec{r}, \vec{R}, q) = -\frac{1}{4\sqrt{\pi}} \sum_{L_1=0,2,\dots}^{\infty} \sum_{L_2=1,3,\dots}^{\infty} \sum_{J=1,3,\dots}^{\infty} (-1)^{(1+L_1-L_2)/2} C_{L_1010}^{L_20} C_{L_1010}^{J0} \begin{Bmatrix} L_1 & 1 & L_2 \\ 1 & J & 1 \end{Bmatrix}$$
$$\times (2L_1+1) \left[Y_J(\hat{r}) \otimes Y_{L_2}(\hat{R})\right]_1 \odot \left[\vec{\sigma}(1) \otimes \vec{\sigma}(2)\right]_1 j_{L_2}(qR) q \int_0^1 d\alpha \, e^{-r\Pi(q,\alpha)} j_{L_1}(qr(\alpha-1/2)). \tag{F.40}$$

Finally when $K = 2$,

$$\mathcal{O}_7(\vec{r}, \vec{R}, q) = -\frac{1}{4\sqrt{\pi}} \sum_{L_1=1,3,\dots}^{\infty} \sum_{L_2=0,2,\dots}^{\infty} \sum_{J=0,2,\dots}^{\infty} (-1)^{(1+L_1-L_2)/2} C_{L_1020}^{L_20} C_{L_1020}^{J0} \begin{Bmatrix} L_1 & 1 & L_2 \\ 2 & J & 1 \end{Bmatrix}$$
$$\times (2L_1+1) \left[Y_J(\hat{r}) \otimes Y_{L_2}(\hat{R})\right]_2 \odot \left[\vec{\sigma}(1) \otimes \vec{\sigma}(2)\right]_2$$
$$\times j_{L_2}(qR) q \int_0^1 d\alpha \, e^{-r\Pi(q,\alpha)}(1-2\alpha)j_{L_1}(qr(\alpha-1/2)). \tag{F.41}$$

The total two-body operator can then be expressed as

$$\mathcal{O}^{(2)}(q) = -\frac{g_A^2 m_\pi^2}{4f_\pi^2} \frac{1}{2} \sum_{i \neq j} \sum_{k=1}^{7} \mathcal{O}_k(\vec{r}_{ij}, \vec{R}_{ij}, q) \, \vec{\tau}(i) \cdot \vec{\tau}(j), \tag{F.42}$$

where the summation over i, j extends over all nucleons in the target nucleus.